AMPLIFIED EXTERNAL-CAVITY MODE-LOCKED SEMICONDUCTOR LASERS

ULTRASHORT-PULSE LASER SYSTEMS BASED ON EXTERNAL-CAVITY MODE-LOCKED InGaAs-GaAs SEMICONDUCTOR OSCILLATORS AND SEMICONDUCTOR OR Yb:FIBRE AMPLIFIERS

By

ANDREW JOHN BUDZ, B.Eng.

A Thesis

Submitted to the School of Graduate Studies

In Partial Fulfilment of the Requirements

for the Degree

Doctor of Philosophy

McMaster University

DOCTOR OF PHILOSOPHY (2008) McMaster University
(Engineering Physics) Hamilton, Ontario

TITLE: Ultrashort-Pulse Laser Systems Based on External-Cavity Mode-Locked InGaAs-GaAs Semiconductor Oscillators and Semiconductor or Yb:Fibre Amplifiers

AUTHOR: Andrew John Budz, B.Eng. (McMaster University)

SUPERVISOR: Professor Harold K. Haugen

NUMBER OF PAGES: xix, 157

Abstract

This thesis describes the development of a tunable, ultrashort-pulse semiconductor-based laser system operating in the 1 μm wavelength region. The design of the oscillator is based on a two-contact long-wavelength InGaAs-GaAs quantum-well semiconductor device containing integrated gain and saturable absorber sections. A key design component of the oscillator is the fabrication of a curved ridge-waveguide in the gain section of the device, which allows the laser to be operated in a compact, linear external cavity. Under conditions of passive or hybrid mode-locking, the semiconductor oscillator can generate pulses of 1 to 10 ps in duration, which are tunable from 1030 to 1090 nm. The oscillator is also capable of being passively mode-locked at harmonics of the cavity round-trip frequency, allowing tuning of the pulse repetition rate from 0.5 to over 5 GHz. Noise measurements on two independently hybridly mode-locked semiconductor lasers reveal that the absolute noise of each laser is dominated by phase noise at frequencies below 10^5 Hz, while amplitude noise dominates at higher frequencies.

Semiconductor and fibre optical amplifiers are used to scale the average power level of the mode-locked pulses. Semiconductor optical amplifiers consisting of narrow-stripe and flared-waveguide designs have been fabricated using the same material structure as that of the mode-locked semiconductor oscillator. Narrow-stripe devices with a length of 800 μm have produced amplified average signal powers of 13 mW, while 1700-μm-long, 2° flared-waveguide devices have produced amplified average signal powers of 50 mW. A fibre-based system consisting of a single-mode double-clad Yb-doped fibre has been constructed to investigate the suitability of a mode-locked diode laser as a seed-source for a Yb:fibre amplifier. Amplified average signal powers of up to 1.4 W have been obtained at the output of the fibre for a launched pump power of 2.1 W. Compression of the amplified pulses using a modified dual-grating compressor yields pulse durations as low as 500 fs and a peak power of up to 1.5 kW.

Preliminary work is reported on the development of a novel dual-wavelength optical source consisting of two synchronized mode-locked diode lasers and a polarization-maintaining Yb:fibre amplifier. Numerical simulations based on a rate-equation model for the amplifier gain are conducted to investigate the performance characteristics of a Yb:fibre amplifier when operated under dual-wavelength signal amplification. The simulations are used to predict and optimize the performance of the fibre amplifier for two mode-locked semiconductor-seed-oscillators operating at wavelengths of 1040 and 1079 nm. Good agreement is obtained between the simulations and experimental results.

Preface

The work presented in this thesis has been previously published in the form of four refereed journal articles and one manuscript accepted for publication (permission for the reproduction of published work is given in Appendix C).

Paper 1:
M. J. Brennan, A. J. Budz, B. J. Robinson, P. Mascher, and H. K. Haugen, "Ultrashort optical pulse generation with a mode-locked long-wavelength (1075–1085 nm) InGaAs-GaAs semiconductor laser," *IEEE Photon. Technol. Lett.*, vol. 16, pp. 1798–1800, Aug. 2004.

Paper 2:
A. J. Budz and H. K. Haugen, "Ultrashort pulse amplification at 1080 nm with a long-wavelength InGaAs-GaAs flared amplifier," *J. Lightwave Technol.*, vol. 25, pp. 3766–3769, Dec. 2007.

Paper 3:
A. J. Budz, A. S. Logan, D. Strickland, and H. K. Haugen, "Ultrashort pulses from a mode-locked diode-oscillator Yb-fiber-amplifier system," *IEEE Photon. Technol. Lett.*, vol. 19, pp. 94–96, Jan. 2007.

Paper 4:
A. J. Budz and H. K. Haugen, "Wavelength and repetition-rate tunable mode-locked semiconductor-seed-source for Yb-fiber-amplifier systems," *IEEE Photon. Technol. Lett.*, vol. 19, pp. 1412–1414, Oct. 2007.

Paper 5:
A. J. Budz, J. Waisman, H. F. Tiedje, and H. K. Haugen, "Short-pulse dual-wavelength system based on mode-locked diode lasers with a single polarization-maintaining Yb:fiber amplifier," accepted for publication in *J. Lightwave Technol.*, Nov. 12, 2008.

Note: A list of other contributions, including conferences and meetings, is given in Appendix A.

Acknowledgements

I would first like to thank my supervisor, Dr. Harold Haugen, for his insight, support, and guidance during the course of this thesis work. Harold first became my supervisor when I was an undergraduate summer student eager to gain research experience in an optics laboratory. Since then, I have learned a great deal from him about science and life. Harold's patience, scientific rigor, and attention to detail have been truly inspiring. Harold has also given me the opportunity to present my work at several prominent international conferences for which I am extremely grateful. I could not have asked for a better supervisor.

I would like to acknowledge several former graduate students that were intimately involved with the diode laser project. In particular, I thank Mike Brennan for the knowledge and skills he passed on to me during my first two years as a graduate student, as well as for his instruction on the art of processing lasers. Thanks extend to Joel Milgram, Andrew Logan, Jonathan Waisman, and Sarah Golin for their research contributions to the diode laser project, as well as for the many hours of technical discussions, assistance, and entertainment. I would also like to thank Henry Tiedje for the countless number of hours we spent discussing technical issues and for his willingness to help troubleshoot anything experimental. I also owe thanks to all the other group members, both current and former, including Andrzej Borowiec, Ben Doyle, Travis Crawford, and Eugene Hsu, for the many hours of technical discussions, assistance, and entertainment. I would particularly like to thank Eugene for the immeasurable amount of time that we spent engaging in activities unrelated to science.

I would like to thank my supervisory committee members, Dr. Cassidy and Dr. Preston, for their insight and advice. I would also like to thank Brad Robinson for the growth of all the semiconductor structures used in this thesis.

I would like to thank CIPI research collaborators, Michel Piché and Donna Strickland, for their many insightful suggestions during the course of this work. I would also like to thank Bertrand Morasse of CorActive Inc. for assistance with the benchmarking of my numerical simulations. Thanks are also due to the various funding agencies that supported this research either through grants or scholarships, including the Canadian Institute for Photonics Innovations and the Natural Sciences and Engineering Research Council of Canada.

I would also like to thank my parents for their unconditional love and support. Without their assistance, I would not have had the opportunity to pursue a higher education.

Finally, I would like to thank my wife, Hanna, for her love and support. She has steadily encouraged me throughout my graduate work and has always supported me in all of my endeavors. For that, I am forever grateful.

Contents

List of Figures

List of Tables

Chapter 1 Introduction

1.1 Outline

This section provides an overview of the content presented in this thesis. Chapter 1 provides the motivation behind the research, a brief review of the literature relevant to mode-locked semiconductor laser systems, and a discussion of the contributions made to the research by other individuals involved with the project.

The main background material of the work is presented in Chapter 2. Details on the theory, design, and development of the mode-locked semiconductor oscillator, narrow-stripe and flared-waveguide semiconductor optical amplifiers, and Yb-doped fibre amplifier are included.

Chapter 3 summarizes the various components that comprise the experimental setup used for the generation and amplification of short optical pulses. Experimental techniques, device mounting, and the characterization equipment are described in detail.

Chapter 4 presents the results of this thesis. Most of the experimental results are provided in the form of five journal articles. The pulse generation characteristics of the mode-locked semiconductor oscillators are described first, followed by the short-pulse amplification experiments using semiconductor- and fibre-based optical amplifiers. Subsequently, the noise properties and synchronization characteristics of two model-locked diode lasers are presented. Finally, the last section of the chapter focuses on the development of a dual-wavelength source consisting of two synchronized mode-locked diode lasers and a Yb:fibre amplifier. A numerical model describing the amplification characteristics of a dual-wavelength Yb:fibre amplifier is also included towards the end of the chapter.

Chapter 5 offers a summary of the key findings of the work, as well as the overall conclusions. A number of suggestions are also made for future research.

1.2 Motivation

The motivation behind this work is the development of a compact, tunable, ultrafast semiconductor-based optical source. Ultrafast optical sources generate pulses with picosecond or shorter durations and are interesting for many applications, including materials processing, biomedical imaging, and applied nonlinear optics. Conventional ultrafast systems are typically based on solid-state crystal lasers, which are large and costly. A semiconductor-based ultrashort-pulse laser could be an attractive replacement for a large table-top laser in applications requiring moderate pulse durations and energies. The advantages offered by a semiconductor-based oscillator compared to the conventional sources are significant: higher efficiency, much lower cost, smaller footprint, and better reliability. However, as the average output power of a short-pulse semiconductor laser is typically only a few milliwatts, the oscillator must be combined with a suitable external optical amplifier for the system to be a viable alternative to other laser sources. In this thesis, optical amplifiers based on semiconductor and fibre technologies are investigated.

Although there are many potential applications that could benefit from a compact semiconductor-based short-pulse source, one of the intended applications is that of two-photon fluorescence microscopy. Two-photon fluorescence is a process whereby a fluorescent dye is optically excited using two-photon absorption. The nonlinear nature of the optical interaction implies that an intense optical source is required for excitation. Therefore, a short-pulse laser system is typically employed due to its high peak intensity. Microscopy based on two-photon excitation has a number of advantages over single-photon methods [1], [2]. Included amongst these are improved spatial resolution and the ability to easily separate the pump (2λ) and fluorescence (λ) signals. An improvement in spatial resolution is achieved since only the most intense portion of the focused beam generates fluorescence. Given that a number of fluorescent dyes have broad absorption bands near ~500 nm [3], a tunable short-pulse semiconductor-based laser system operating in the wavelength region of 1 μm could represent an attractive two-photon excitation source. Wavelength tunability would allow for the investigation of a wide selection of dyes and could also be used to eliminate experimental artifacts in the measured fluorescence signals.

With the above application in mind, an external-cavity mode-locked semiconductor laser operating at a wavelength of around 1070 nm was fabricated. An external-cavity approach permits the operating wavelength of the system to be easily tuned using a diffraction grating. The choice of the operating wavelength allows the system to be combined with a Yb-doped fibre amplifier (YDFA), which typically operates in the wavelength range of ~975–1100 nm. The recent development of Yb:fibre amplifiers has permitted the development of novel optical sources in the 1 μm wavelength region. Since most of the reported Yb:fibre systems utilize a solid-state laser as the seed-source (e.g., [4]), an additional goal of this work is to investigate the suitability of a mode-locked diode laser as a seed-source for a Yb:fibre amplifier. Semiconductor optical amplifiers (SOAs) based on narrow-stripe and flared-waveguide geometries are also investigated as a means of scaling the average power of the mode-locked laser pulses. Since both the SOA and YDFA exhibit attractive features similar to that of a semiconductor oscillator, such as high efficiency, compact size, and low cost, a short-pulse laser system based on all-semiconductor technology or hybrid semiconductor-fibre technology could represent an attractive alternative for much larger and more costly mode-locked laser systems.

1.3 Literature Review

The study of mode-locked semiconductor lasers has been an area of intense research for several decades [5]. This section provides a brief overview of the experimental work on the development of mode-locked diode laser systems. Results are presented for actively and passively mode-locked semiconductor oscillators, followed by results for oscillator-amplifier systems consisting of either SOAs or fibre amplifiers.

1.3.1 Mode-Locked Semiconductor Oscillators

One of the first successful demonstrations of short-pulse generation using a mode-locked semiconductor laser was reported by Ho *et al.* [6]. The system consisted of an actively mode-locked AlGaAs laser with uncoated facets operating in an external cavity with a spherical mirror. Pulses with a duration of 20 ps were obtained at 800 nm and a repetition frequency of 3 GHz. Further work by Olsson and Tang demonstrated that improvements to the external-cavity system could be obtained by depositing an anti-reflection (AR) coating on the facets of the laser [7]. Their system consisted of an external-cavity actively mode-locked AlGaAs semiconductor laser operating at a repetition rate of 250 MHz. Both facets of the semiconductor device were AR-coated, allowing the laser to be mode-locked in both linear and ring external cavities. Pulse durations of 6–8 ps were obtained for the linear cavity and a duration of 16 ps was achieved for the ring cavity. By mode-locking in an external cavity containing a diffraction grating, Vasil'ev *et al.* were able to generate bandwidth-limited pulses using an actively mode-locked external-cavity AlGaAs laser [8]. The system produced 3-ps-pulses at a repetition rate of 660 MHz and a wavelength of 870 nm. More recently, Hofmann *et al.* demonstrated that broadly-tunable short pulses could be generated using an actively mode-locked InGaAsP laser containing a multiple quantum-well active region [9]. Tuning of the operating wavelength was achieved by rotating a diffraction grating in the external cavity. Short pulses at a wavelength of 1.55 μm were generated over a 115 nm tuning range, with a repetition frequency of 300 MHz.

Early studies on passive mode-locking of semiconductor lasers were performed with devices that were purposely aged to the point where there was a noticeable increase in lasing threshold (>10 %). The aging process induced defects in the laser which exhibited saturable absorption. Ippen *et al.* reported on the passive mode-locking characteristics of such aged devices [10]. Although pulses as short as 5 ps could be generated, the lasers could not be easily controlled and were prone to failure. Controllable saturable absorption was demonstrated by Silberberg *et al.* using an external-cavity GaAs laser [11]. The saturable absorber consisted of a multiple quantum-well sample attached to an external mirror. Passive mode-locking of the oscillator resulted in the generation of pulses as short as 1.6 ps with an average power of 1 mW and a repetition rate of 500 MHz. Sub-picosecond pulse generation was achieved by Chen *et al.* using a passive colliding-pulse monolithic mode-locked InGaAsP laser [12]. The mode-locking characteristics of the oscillator were studied as a function of the pulse repetition rate. Transform-limited pulses with durations of 1.1, 0.83, 1.0, and 0.64 ps were obtained at repetition rates of 40, 80, 160, and 350 GHz, respectively. To achieve lower pulse repetition rates using a monolithic-cavity approach, Hansen *et al.* reported on the development of an extended-cavity laser operating at a wavelength of 1560 nm and a repetition rate of 8.6 GHz [13]. The laser structure consisted of integrated gain, saturable absorber, and passive waveguide sections. The performance of the laser was studied under different mode-locking conditions. Pulse durations of 6.2 ps were obtained for active mode-locking, 4.2 ps for hybrid mode-locking, and 5.5 ps for passive mode-locking. More recently, Kunimatsu *et al.* studied the performance of a passively mode-locked two-contact laser containing a bandgap-detuned saturable absorber [14]. By increasing the bandgap energy of the absorber section relative to the bandgap of the gain section, the mode-locked pulse width was reduced from 2.6 ps to 1.2 ps. The laser operated in the wavelength region of 1.5 μm at a repetition frequency of 37 GHz.

The mode-locking results presented above were all obtained for edge-emitting semiconductor lasers. There has also been very recent work on the development of mode-locked surface-emitting diode lasers. Hoogland *et al.* have demonstrated mode-locking of a vertical-external-cavity surface-emitting-laser (VECSEL) [15]. A multiple quantum-well gain structure was optically pumped using an external diode laser and passive mode-locking was achieved using an external semiconductor saturable absorber mirror (SESAM). A 10 GHz train of 500 fs transform-limited pulses was generated with 30 mW of average power. One of the attractive features of a VECSEL is the nearly symmetric beam profile that can be obtained for the laser output.

1.3.2 Amplified Systems

Early work on the development of amplified mode-locked diode laser systems was conducted using narrow-stripe SOAs. Eisenstein *et al.* reported on a short-pulse laser system consisting of a wavelength-tunable external-cavity actively mode-locked diode laser and a 250-μm-long SOA operating at a wavelength of 1.3 μm and a repetition rate of 4 GHz [16]. Pulses generated by the oscillator (12 ps duration with an average power of 500 μW) were amplified in the SOA to an average power of 12 mW with no distortion to the amplified pulse width. Delfyett *et al.* reported on a similar short-pulse diode laser system operating at a wavelength of 870 nm [17]. Active mode-locking of the external-cavity oscillator at the third harmonic of the cavity round-trip frequency produced 15-ps-pulses at a repetition rate of 930 MHz and an average power of 800 μW. Subsequent amplification of the mode-locked pulses using an SOA biased with both direct-current (DC) and radio-frequency (RF) signals produced an amplified average power of 46 mW and a peak power of around 3 W. This system was further improved upon by Delfyett *et al.* [18] using a hybridly mode-locked semiconductor oscillator containing a multiple quantum-well saturable absorber mirror. Pulses 5 ps in duration at a repetition rate of 302 MHz were amplified to an average power of 32 mW, yielding an improvement in the peak power of 20 W. Subsequent compression of the amplified pulses resulted in a duration of 460 fs and a peak power of 72 W.

To improve upon the gain saturation characteristics of narrow-stripe SOAs, broad-area or flared-waveguide SOA structures were developed, which allowed further power scaling of mode-locked semiconductor laser systems. Mar *et al.* reported on the development of a high-power short-pulse diode laser system operating at 940 nm [19]. A two-section external-cavity oscillator was passively mode-locked at a repetition frequency of 2.5 GHz, producing 3.7-ps-pulses with an average power of 9 mW. Subsequent amplification of the mode-locked pulses in a flared-waveguide SOA having input and output lateral dimensions of 4 μm and 130 μm, respectively, yielded an amplified average power of 296 mW and a peak power of 28 W. A similar laser system was described by Xiong *et al.* operating at a wavelength of 800 nm [20]. An external-cavity diode laser was actively mode-locked at a repetition rate of 843 MHz, producing 8-ps-pulses with an average power of 0.75 mW. Amplification of the pulses in a 2°, 2.75-mm-long flared-SOA resulted in an average output power of 80 mW.

A comprehensive, all-semiconductor ultrafast optical source capable of generating record-high peak power was recently reported by Kim *et al.* [21]. The system consisted of a mode-locked semiconductor oscillator, two SOAs, and dispersion-control components to provide chirped pulse amplification. A colliding-pulse hybridly mode-locked semiconductor oscillator generated 38-ps-pulses at a repetition rate of 285 MHz, center wavelength of 974 nm, and an average power of 11 mW. After passing through a 'pulse-picker' SOA, which reduced the pulse repetition rate to 95 MHz, the pulses were stretched to 9.6 ns using a chirped-fibre-Bragg-grating. Amplification in a narrow-stripe SOA, followed by a flared-waveguide SOA, provided an average power of 1 W. The amplified pulses were sent back through the chirped-fibre-Bragg-grating and an external pulse compressor to obtain a pulse duration of 600 fs and a peak power of 1.4 kW.

Finally, there has been two recent demonstrations of a short-pulse laser system consisting of a mode-locked semiconductor-seed-source and a Yb:fibre amplifier, which is similar to the laser system described in this thesis. Adhimoolam *et al.* have reported on a 1.4 GHz actively mode-locked InGaAs-GaAs semiconductor-seed-source and a large-mode-area (LMA) Yb:fibre amplifier [22]. The oscillator is capable of generating wavelength-tunable pulses with a duration of 30 ps and an average power of 15 mW. Amplification of the pulses in the fibre at a pump power of 25 W provided up to 9 W of average output power, over a wavelength tuning range of ~1050–1085 nm. A high-power Yb:fibre-based system was also demonstrated by Dupriez *et al.* [23]. Short pulses emitted by a passively mode-locked VECSEL were amplified in multiple Yb:fibre amplifiers. The system operated at 1055 nm and contained two Yb:fibre pre-amplifiers and one LMA Yb:fibre power-amplifier. The seed pulses had a duration of 4.6 ps, repetition rate of 910 MHz, and an average power of 8 mW. After the two pre-amplifiers, 2 W of average power was generated. The final power amplifier stage was pumped with a launched power of 350 W, yielding an amplified average power of 255 W. The amplified pulses had a duration of 5.8 ps and a peak power 38 kW. Further compression of the amplified pulses resulted in a duration of 280 fs.

1.3.3 Summary

While the above discussion is far from complete, it does provide an indication of the level of performance that can be achieved using a mode-locked semiconductor oscillator and various forms of external amplification. The interested reader is referred to references [5], [24]-[26] for a more thorough account of the experimental research on the mode-locking of diode lasers. The experimental results presented in this section are summarized in Table 1-1.

Table 1-1: Performance characteristics of various mode-locked semiconductor laser systems.

Mode-Locking Method	Amplifier Type	Center Wavelength (nm)	Rep. Rate (GHz)	Pulse Duration (ps)	Average Power (mW)	Ref.
Active	-	800	3	20	-	[6]
Active	-	~800	0.25	6	-	[7]
Active	-	870	0.66	3	-	[8]
Active	-	1550	0.30	30	0.1	[9]
Passive	-	~800	0.85	5	5	[10]
Passive	-	850	0.50	1.6	1	[11]
Passive	-	1540	3.5	0.6	1	[12]
Passive	-	1565	8.6	5.5	-	[13]
Passive	-	1570	3.7	1.2	-	[14]
Passive	-	1034	10	0.5	30	[15]
Active	SOA, narrow	1300	4	12	12	[16]
Active	SOA, narrow	870	0.90	15	46	[17]
Passive	SOA, flared	940	2.5	3.7	296	[19]
Active	SOA, flared	800	0.80	8	80	[20]
Hybrid	SOA, multi	974	0.09	0.6	1000	[21]
Active	Yb:fibre	1070	1.4	30	9000	[22]
Passive	Yb:fibre, multi	1055	0.91	5.8	255 000	[23]

1.4 Project Contributors

The key findings of this thesis have been previously published in the form of four refereed journal articles and one manuscript accepted for journal publication. The majority of the presented work has been obtained directly as a result of the author's efforts. The one exception is Paper 1, for which I am a co-author. Acknowledgements specific to each publication, as well as a discussion of the contributions of co-authors, will be included prior to the presentation of each article. Work performed by the author includes laser/SOA design and fabrication (e.g. photolithography, oxide and metal deposition, AR coatings), developing control and acquisition software, configuring and conducting experiments and numerical simulations, analysis of data, and the writing of the manuscripts. However, since the work presented in this thesis is part of an on-going group research project, contributions from previous students have also had an impact on the work. The contributions from these individuals, as well as those from several research associates, are summarized below.

- Brad Robinson is responsible for growing all of the laser and SOA structures using the molecular beam epitaxy facility at McMaster University. Brad has also contributed to a number of technical discussions related to the design and fabrication of semiconductor lasers and amplifiers.
- Steve Wallace made a number of contributions during the initial development stages of the short-pulse diode laser project while completing research for his Ph.D. degree. In particular, Steve contributed to laser design, laser processing, design and characterization of anti-reflection coatings, and preliminary mode-locking at 980 nm.
- Joel Milgram was responsible for the development of the 980-nm narrow-stripe SOAs while completing research for his Master's degree. Joel also contributed to the design of anti-reflection coatings and experimental SOA techniques.
- Mike Brennan was responsible for the design and development of the broadly-tunable 980 nm mode-locked diode laser system while completing research for his Ph.D. degree. Mike is responsible for the design of the curved-waveguide structure which is used in the mode-locked oscillators of this thesis and he also collaborated on the initial development of the long-wavelength mode-locked system. He contributed to the design of

anti-reflection coatings, control and acquisition software, and numerous technical discussions.

- Andrew Logan was responsible for conducting studies on the feasibility of using mode-locked diode lasers as sources for two-photon excitation while completing research for his Master's degree. Andrew also contributed to the early development of the fibre amplifier system through his daily involvement in the group research project.
- Jonathan Waisman is responsible for developing simulation software to study the propagation of short optical pulses through doped fibres while completing research for his Master's degree. The simulation groundwork laid out by Jonathan was a key factor for future modeling work conducted by the author.
- Henry Tiedje has contributed to numerous discussions on experimental techniques and laser theory, and was particularly helpful with measurements on laser noise.
- Sarah Golin contributed to the development of the second mode-locked oscillator used in the dual-wavelength source while completing research for her undergraduate thesis project.

Chapter 2 Background

2.1 Introduction

This chapter provides an overview of the background material relevant to the development of an external-cavity mode-locked diode laser system. The first section of this chapter discusses ultrashort-pulse generation with diode lasers using the technique of mode-locking. Details associated with the design and operation of the external-cavity semiconductor oscillator are presented. Subsequent sections of this chapter focus on two amplifying schemes, namely the SOA and YDFA, which were developed to scale the power level of the mode-locked pulses. The key features of each amplifying medium will be discussed, as well as the design constraints imposed on each amplifier due to the unique properties of the mode-locked semiconductor-seed-laser.

2.2 Mode-Locked Semiconductor Lasers

2.2.1 Short-Pulse Generation with Semiconductor Lasers

There are three main techniques used to generate short pulses with diode lasers: gain-switching, Q-switching, and mode-locking. A more thorough theoretical and experimental account of each of these techniques can be found in [27]. Gain-switching involves the rapid switching of the optical gain of a semiconductor through the modulation of the drive current. A pulsed current is superimposed on a DC bias and optical pulses in the nanosecond to picosecond range [28]-[30] can be obtained by minimizing the temporal width of the electrical pulses that drive the laser. This method of pulse generation is very convenient as it does not require sophisticated laser structures or fabrication techniques. A noteworthy result for ultrashort-pulse generation using a semiconductor laser was obtained using a gain-switched laser delivering 7.5-ps-pulses which were subsequently compressed down to 22 fs [31].

Q-switching is the inverse analogue of gain-switching: instead of modulating the gain, the optical loss or Q (quality-factor) of the laser resonator is modulated. This requires the fabrication or incorporation of an intracavity element that provides variable optical absorption. Initially the cavity is forced to operate in a low Q state (high loss) while the population inversion builds in the gain medium. When the stored energy in the gain medium reaches a maximum value, the cavity Q is abruptly switched by an external signal to a high state (low loss) and the intensity in the cavity rapidly increases due to repeated stimulated emission, resulting in the depletion of the inversion and the creation of a pulse of light. The process is then repeated by switching of the cavity Q to a low state. Typical pulse durations are in the 20–40 ps range [32]-[34]. The main advantage that this technique offers is the ability to generate pulses with a peak power that is a few orders of magnitude higher than that of gain-switched or mode-locked pulses. For instance, Q-switched pulses with energies exceeding 100 pJ have been reported [33].

Each pulse generated from either gain-switching or Q-switching originates independently from the build-up of random spontaneous emission events in the gain medium. As such, there is a lack of phase correlation between neighboring pulses in the emitted pulse train, leading to an enhancement in the pulse-to-pulse timing jitter or noise of the laser. In comparison, pulses emitted by a mode-locked laser tend to exhibit lower timing jitter due to the strong coupling between spectral modes [35]. This coupling (or locking) of modes produces a pulse which circulates in the cavity. Each time the pulse is incident at the laser output coupler, a fraction of the pulse is coupled out of the cavity to form the output beam and a fraction is reflected back to undergo further amplification during another round-trip through the laser cavity. Consequently, each pulse in the output of a mode-locked laser can be considered as a modified replica of the pulse preceding it in time, with additional phase and amplitude changes from the extra round-trip propagation through the laser cavity. The circulating nature of a pulse in a mode-locked laser forces neighboring pulses to couple to one another, which limits the overall phase excursions of each pulse and reduces timing fluctuations. In addition to exhibiting lower timing jitter levels, mode-locked lasers can typically produce optical pulses which are much shorter than that produced by either gain- or Q-switched lasers. Since mode-locking of diode lasers is a key component upon which the results presented in this thesis are based, the technique will be covered in greater detail.

A basic description of mode-locking can be obtained by considering the longitudinal cavity modes in a Fabry-Perot laser. The frequency spacing between longitudinal modes, $d\omega$, is given by

$$\delta\omega = \frac{\pi c}{n_g L} \tag{2.1}$$

where c is the speed of light in vacuum and n_g is the group refractive index of the medium filling the cavity of length, L. If the gain bandwidth of the laser is broader than the mode spacing, then in principle, more than one longitudinal mode can oscillate. The electric field of the laser output consists of a sum over all frequency components corresponding to oscillating modes and is given by

$$E(t) = \sum_m A_m e^{i(\omega_o t + m\delta\omega t + \phi_m)} + c.c. \tag{2.2}$$

where A_m and ϕ_m represent the amplitude and phase of the m^{th} mode having angular frequency $\omega_m = \omega_o + m\delta\omega$. Under normal operating conditions, the relative phases between cavity modes are independent and random, which results in an output that is nearly continuous in time (cw). If, however, there exists a mechanism in the laser resonator to force neighbouring cavity modes to maintain a fixed phase relationship, then the output of the laser will consist of a periodic function in time and the process is termed mode-locking. A necessary condition for mode-locking is that an intracavity loss or gain modulator must operate at the cavity round-trip frequency ($\delta\upsilon = \delta\omega/2\pi$) in order for the oscillating modes to phase lock. The modulation results in the generation of frequency side-bands which give rise to an energy transport between neighbouring modes.

An example of the output intensity or envelope of $E^2(t)$ is plotted in Figure 2-1 using Equation (2.2) for $N = 5$ and $N = 25$ locked modes that have a constant amplitude and a linear phase relationship (constant phase offset from mode to mode). Also shown is the cw intensity for five modes with random phase. As illustrated in the figure, the output of a mode-locked laser consists of a train of short pulses with duration inversely proportional to the spectral width ($N \times \delta\omega$) and an instantaneous peak intensity that is proportional to N^2. A pulse is

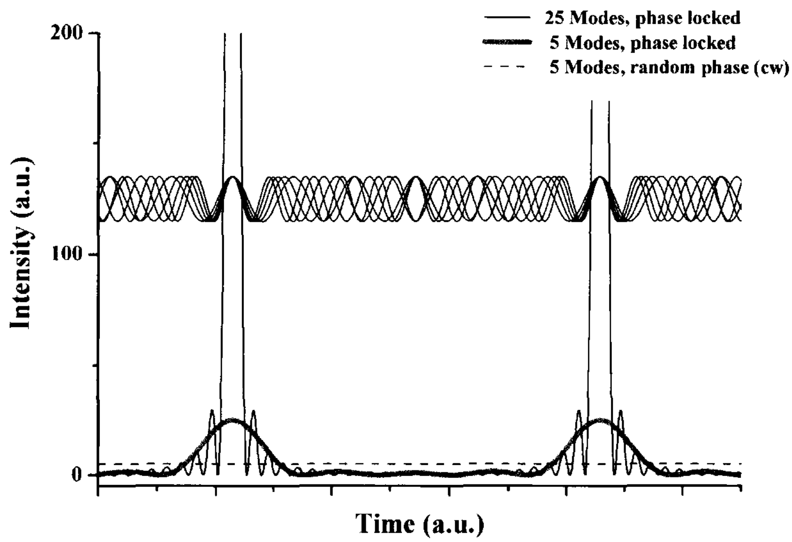

Figure 2-1: Simulation of the intensity output of a laser under cw and mode-locked conditions. The upper trace gives an example of the individual electric fields for the case of five locked modes.

generated once per round-trip due to the constructive interference of N modes with adjacent pulses separated in space by $2Ln_g$ and in time by $d\upsilon^{-1} = 2n_gL/c$.

2.2.2 Methods of Mode-Locking Semiconductor Lasers

There are three main methods to mode-lock a semiconductor laser, namely, active mode-locking, passive mode-locking, and hybrid mode-locking. Active and passive mode-locking employ different pulse-shaping mechanisms, while hybrid mode-locking is a combination of the active and passive methods. The results presented in this thesis have been obtained with passively and hybridly mode-locked lasers.

Short pulses can be generated with active mode-locking by applying an external signal to the diode which modulates the gain/loss of the laser at a frequency that corresponds to the longitudinal mode-spacing of the resonator. The modulation produces side-band signals on each longitudinal mode which overlap in frequency with adjacent longitudinal modes, forcing the phases of the modes to become locked by the external modulation. Although diode lasers can be directly modulated by driving the laser with a time-varying current, their small dimensions (e.g., $L = 500$ μm) results in very high modulation frequencies ($d\upsilon \sim 90$ GHz). As these frequencies are near the upper limit of existing radio-frequency (RF) technology, it is necessary to reduce the intermodal spacing by lengthening the cavity for active mode-locking to be practical. Typically, this is accomplished by working with extended cavity devices [36] or by operating the laser in an external cavity (discussed below in Section 2.2.6) which reduces $d\upsilon$ to a range of around 0.2 to 20 GHz. Even with reduced RF drive requirements, special considerations must be made during the design of the device and the packaging of the laser to ensure that parasitic capacitances are low in order to minimize RF coupling losses. Typical pulse durations obtained directly with actively mode-locked diode lasers are in the few picosecond to tens of picosecond range [7], [8], [18], [36], [37], although pulses as short as 580 fs have also been reported [38].

Passive mode-locking differs from active mode-locking in that no external signal is required to initiate mode-locking. A passively mode-locked laser is typically biased using DC sources and relies on the action of a suitable [39] saturable absorber to lock the cavity modes in phase. A saturable absorber exhibits a nonlinear transmission characteristic such that the absorption of the medium decreases with optical intensity, eventually reaching a state of saturation where the medium is optically transparent. An excellent description of the temporal dynamics involved in passive mode-locking can be found in [40]. The interplay between gain/absorber saturation and carrier recovery times in the gain/absorber regions gives rise to a self-stabilized circulating pulse. One of the requirements of passive mode-locking is that the saturation energy of the absorber must be lower than that of the gain medium in order to create a window of net gain for pulse amplification. Although this type of mode-locking can be attractive as it does not require expensive RF driving electronics, it does require a slightly more sophisticated laser structure or cavity design to incorporate separate regions providing gain and saturable absorption. Fortunately, with semiconductor lasers, this can be easily accomplished using standard photolithography techniques by fabricating an integrated multi-section device [24], whereby one section is reverse voltage biased to provide optical absorption and a second section is forward biased using a current source to provide optical gain. After the pulse passes through the absorber, the reverse bias quickly returns the section to an attenuating state by sweeping the photo-generated charge carriers out of the active region. Experiments have demonstrated that reverse-biased waveguide saturable absorbers can exhibit a fast recovery time, on the order of a few picoseconds [24], [41], which is essential to obtaining short picosecond pulses and high pulse repetition rates. An alternate method for achieving passive mode-locking is through the use of an external element that provides saturable absorption, such as a semiconductor saturable absorber mirror (SESAM) [42]. In this approach, a multiple quantum-well structure is either mounted on a mirror or grown onto a Bragg reflector and is used as the feedback element in the laser cavity. One of the main advantages offered by passive mode-locking over active methods is the ability to generate shorter pulses due to the enhanced pulse shaping provided by the saturable absorber. On each round-trip in the cavity, the leading edge of the pulse is attenuated, effectively shortening the pulse, and in the steady-state, this shortening is balanced by broadening mechanisms such as dispersion and gain narrowing. Sub-picosecond pulses can be generated directly with passively mode-locked diode lasers (e.g., 0.78 ps [43], 0.65 ps [44], 0.64 ps [12], and 0.39 ps [45]) and pulses on the order of a picosecond or a few picoseconds have been commonly reported [11], [13], [14], [24], [46], [47]. Another important characteristic of passive mode-locking is that the lack of an external modulating signal greatly relaxes the electrical bandwidth limitations imposed on the resultant pulse repetition rate. In general, semiconductor lasers are capable of producing higher mode-locked frequencies than any other type of laser, by virtue of their relatively small cavity length. When combined with the technique of harmonic mode-locking [48], which is a condition where multiple pulses circulate in the resonator, compound-cavity diode lasers have generated ultrahigh repetition frequencies of up to 1.5 THz [49] and 2.1 THz [50]. Such passively mode-locked lasers are interesting for high-speed optical communication systems, ultrafast data processing, and as compact sources of terahertz radiation.

Hybrid mode-locking is a combination of active and passive methods, where both a passive element and an external modulating signal are used to produce ultrashort pulses. A hybrid mode-locking scheme combines the advantageous features of both methods, such as the increased stability and lower phase noise characteristics exhibited by the actively mode-locked system [51], and the additional pulse-shortening mechanisms provided by the saturable absorber. (The noise properties of semiconductor lasers operated under various forms of mode-locking will be discussed in Section 4.6.) Either the gain or the absorber section of a multi-contact diode laser can be connected to the external modulation to induce hybrid mode-locking. Pulse durations in the sub-picosecond to short picosecond range have also been obtained using various hybrid mode-locking schemes [18], [46], [51]-[55].

2.2.3 Laser Active Region Design

As discussed previously, the motivation behind this work is the development of an ultrashort-pulse laser system based on a mode-locked semiconductor-seed-oscillator. With the recent development of cladding-pumped Yb:fibre amplifiers, novel master-oscillator power-amplifier systems can be explored in the 1 μm wavelength region. To investigate the feasibility of using a mode-locked diode oscillator as a short-pulse seed-source for a YDFA, semiconductor lasers are fabricated to operate at wavelengths that correspond to optical transitions in Yb^{3+}. Although Yb-doped fibres can deliver gain over a very broad wavelength range from 975 to ~1200 nm, they are more typically operated as amplifiers at wavelengths between 1030–1100 nm. Given this wavelength requirement, semiconductor lasers are designed using the InGaAs-GaAs material system containing an InGaAs quantum-well active region. Quantum-well diode lasers have numerous advantages over bulk semiconductor lasers, such as higher efficiency, larger differential gain, and lower threshold current [56]. In addition, the ability to vary the lasing wavelength of a quantum-well laser by modifying the composition or thickness of the well layer offers tremendous flexibility in terms of tailoring the output wavelength to a specific application. With these ideas in mind, the laser structure shown in Table 2-1 was fabricated for light emission at a target wavelength of 1065 nm. The structure is based on an optimized design developed for InGaAs quantum-well diode lasers operating near 980 nm [57].

The structure was grown latticed-matched to GaAs using gas-source molecular beam epitaxy (MBE) and consists of a 100 nm *n*-type GaAs buffer

Table 2-1: InGaAs-GaAs quantum-well laser structure.

Layer	Material	Thickness
Contact	p^+ GaAs	150 nm
Cladding	*p* InGaP	1.25 μm
Etch Stop	*p* GaAs	5 nm
Cladding	*p* InGaP	120 nm
Barrier	GaAs	110 nm
Quantum-well	InGaAs	6 nm
Barrier	GaAs	110 nm
Cladding	*n* InGaP	1.37 μm
Buffer	n^+ GaAs	100 nm
Substrate	n^+ GaAs	

layer on a n-type GaAs substrate, a 1.37 μm n-type InGaP cladding layer, a 60 Å InGaAs quantum-well surrounded by 110 nm GaAs barrier layers, a 1.37 μm p-type InGaP cladding, and a 150 nm p-type GaAs contact layer. A 50 Å GaAs etch stop layer is positioned 1.4 μm below the p-contact of the laser and assists with the fabrication of the optical ridge waveguide. The conduction band profile of the laser structure is shown in Figure 2-2. The GaAs layers in the active region of the laser serve two primary functions: (1) they form an energy barrier such that injected charge carriers are confined to the InGaAs quantum-well, and (2) they form the waveguide core, which provides transverse optical confinement between the lower-index InGaP cladding layers.

GaAs-$In_xGa_{1-x}As$-GaAs quantum-well devices are fabricated containing an indium fraction of x = 0.27, which yields a peak photoluminescence wavelength of approximately 1067 nm. As the lattice constant of GaAs (5.6533 Å) is smaller than that of $In_{0.27}Ga_{0.73}As$ ($a_{In_xGa_{1-x}As}$ = 5.6533 + 0.4051x Å) [58], epitaxial growth of $In_xGa_{1-x}As$ on GaAs results in a compressively-strained quantum-well. Excessive strain in a semiconductor can lead to the formation of defects in the crystal lattice if the thickness of the strained layer is larger than a certain critical thickness, t_c. For a quantum-well comprising $In_xGa_{1-x}As$ with GaAs barriers, the critical thickness of the strained layer is $t_c \sim 9$ nm for $x = 0.27$ [59]. This value imposes a constraint on the design of the active region as it limits the number of quantum-wells that can be incorporated into the laser structure. Diode lasers that contain a multiple quantum-well active region can achieve a higher

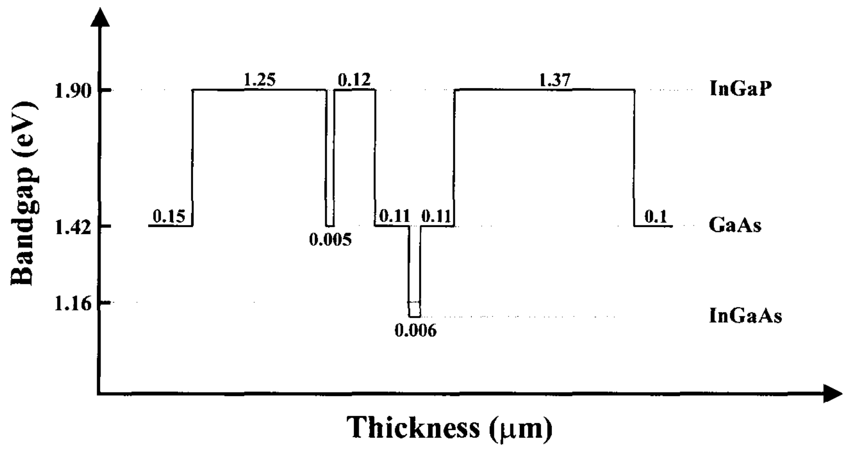

Figure 2-2: Conduction band profile of the InGaAs-GaAs quantum-well laser structure. Thickness axis not to scale.

modal gain when operated at an elevated current density than lasers that contain a single well [60]. In addition, the gain-bandwidth of the laser medium can be significantly broadened through the use of an asymmetric multiple quantum-well structure [61], [62], in which the transition energies of the wells differ due to a variation in the composition and/or thickness of the well material. Asymmetric quantum-well lasers with enhanced gain-bandwidths have demonstrated broad spectral tuning [63]. On account of the critical thickness constraint stated above for InGaAs-GaAs operating at a transition wavelength near 1065 nm, initial device designs were limited to a single quantum-well, which is undesirable from a gain-bandwidth perspective. However, after characterizing the lasers based on the design of Table 2-1, it was discovered that the devices could be mode-locked over a relatively large wavelength range from 1030 to 1090 nm. Since this tuning range was sufficient for seeding over a substantial fraction of the YFDA gain-bandwidth, further refinements to the design of active region were deemed unnecessary. Lasers containing a multiple quantum-well active region could be investigated in the future, as a means of extending the tuning range of current devices. One approach to overcome the accumulation of strain in a multiple InGaAs quantum-well laser is to use strain-compensating GaAsP barriers [64], which would introduce tensile strain into the structure, thus lowering the overall strain in the active region.

2.2.4 Laser Waveguide Structure

Laser structures are processed into edge-emitting ridge-waveguide devices using conventional photolithography and wet chemical etching. A summary of the processing steps can be found in Appendix B. A schematic of the ridge-waveguide cross-section is shown in Figure 2-3. The ridge is fabricated by etching the *p*-doped GaAs and InGaP semiconducting layers at the top of the structure down to the GaAs etch stop. This creates a ridge profile with a lateral width of 2–5 μm (lasers with different ridge widths are studied) and a transverse (growth direction) width of 1.4 μm. Further processing of the device involves the deposition of an isolation dielectric (SiO_2) and metallic contacts. A small via or opening is etched in the SiO_2 layer at the top of the ridge which ensures that current only enters the laser through the top of the ridge. Confining the current to the region under the ridge ensures that light generated in the quantum-well is guided by the ridge, which provides lateral optical confinement.

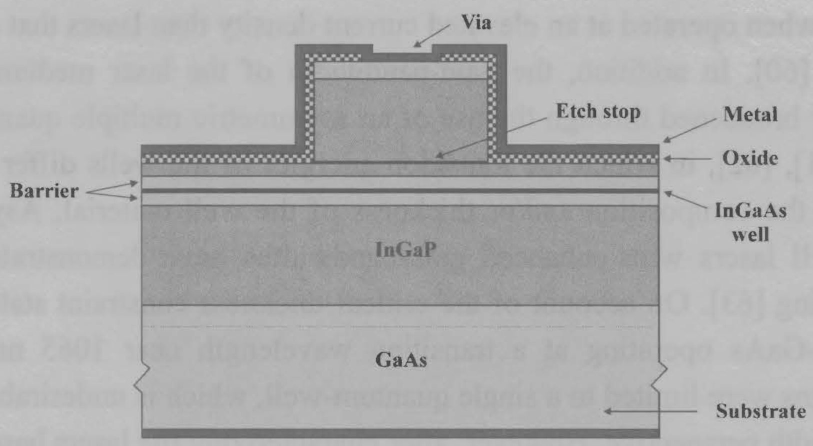

Figure 2-3: Cross-sectional view of a ridge-waveguide laser. Not drawn to scale.

2.2.5 Two-Contact Ridge-Waveguide Structure

Separate regions providing gain and saturable absorption can be monolithically integrated into a semiconductor by fabricating a multi-electrode laser structure. As described earlier, a saturable absorber is a necessary element for passive mode-locking and in the case of hybrid mode-locking, the absorber can provide enhanced pulse shaping. Two-section devices are fabricated by etching a gap through the ridge waveguide (Figure 2-4). The *p*-contact metallization is further confined to areas containing a ridge, thereby creating two contact regions. The electrical isolation between the two contacts should be

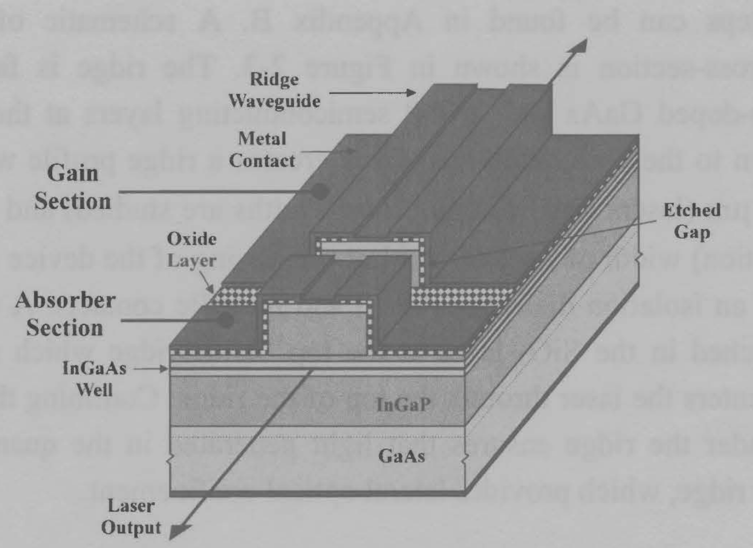

Figure 2-4: Two-contact ridge-waveguide laser structure.

sufficiently high to allow for independent biasing of the gain and absorber regions. The absorber must be biased below its transparency point whereas the gain section is biased above its transparency point. The resistance between the two contacts is affected by the length of the etched gap and also by the doping level and thickness of the InGaP cladding layer directly beneath the etch-stop. Since an excessive gap in the ridge-waveguide will introduce additional optical losses for the device, the gap length should be kept as small as possible. Fabrication issues concerning the removal of the *p*-contact metal layers in the region of the etched gap limited the gap size to a length of 10 μm, resulting in a resistance of ~10 kΩ between the two *p*-contacts.

Typical device lengths range from 500 to 1000 μm, with an absorber length of around 10 % of the total device length. The ratio of absorber-length to gain-length can have a dramatic impact on the ability to generate short pulses. An absorber that is too long will hinder mode-locking since radiation that is generated in the gain section will be significantly attenuated after propagating through the absorber. Alternatively, an absorber that is too short will provide weak pulse-shortening, limiting the minimum achievable pulse duration. Experimentally, it was found that an absorber length that constitutes around 10 % of the total device length is optimal for generating the shortest pulses.

2.2.6 External-Cavity Mode-Locking

As discussed previously, one of the reasons for operating a mode-locked diode laser in an external cavity is to decrease the longitudinal mode-spacing of the resonator, which lowers the modulation frequency required for active and hybrid mode-locking. Another reason for coupling light out of the diode chip and into an external resonator is to gain greater control and flexibility over the properties of the emitted pulse train. This can be understood by considering the basic external-cavity arrangement shown in Figure 2.2, which consists of a two-contact diode chip, two lenses, and an external feedback element. By translating the external element longitudinally, the round-trip time of the cavity changes, thus providing control over the pulse repetition rate. If the feedback element consists of a diffraction grating, then control over the operating wavelength of the laser can be achieved through a rotation of the grating, which selects the bandwidth of cavity modes for oscillation. A number of external-cavity configurations are possible, which can differ somewhat from the design of Figure 2-5, and may contain additional intracavity elements, such as etalons and optical fibres [65].

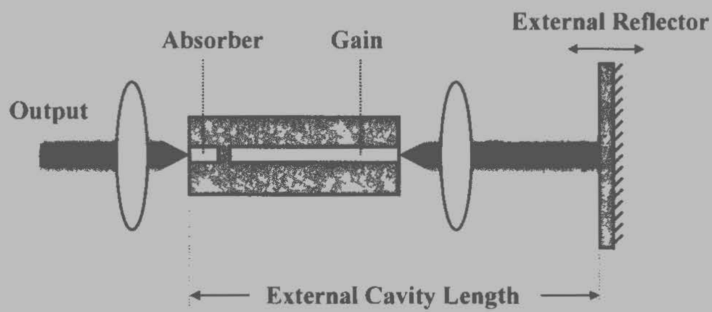

Figure 2-5: Schematic top-view of a basic external-cavity mode-locked laser.

Although mode-locking with a diode in an external resonator can offer advantages such as the ability to tune the wavelength and repetition rate of the laser, there are some performance trade-offs and difficulties that must be overcome for the technique to be successful at generating a train of ultrashort pulses free of satellite or secondary pulses. The main difficulty arises from the fact that placing a diode into an external cavity creates a composite or coupled-cavity. Reflections are possible at the external feedback element, as well as at the diode facet coupled to the external cavity. Consequently, the amplitudes of the external-cavity Fabry-Perot modes become modulated at a frequency that corresponds to the Fabry-Perot mode-spacing of the diode chip, which can affect the phase-locking of the external-cavity modes. In addition, satellite pulses, delayed in time from the main mode-locked pulse by the round-trip time of the diode chip, can be introduced into the pulse train. The generation of satellite pulses is undesirable since they may contain substantial energy that would otherwise contribute to the peak power of the primary pulse and they can degrade the temporal resolution that the laser would be capable of in a time-resolved application, such as a pump-probe experiment. A solution to this problem is to reduce the modal reflectivity of the diode chip by resorting to a slightly more sophisticated laser design that includes the deposition of an AR coating. The other main performance trade-off that can occur with mode-locking in an external-cavity is higher noise (amplitude and phase) on the output pulse train due to the increased sensitivity of the laser caused by the external-cavity elements. Noise issues will be further addressed in Section 4.6. Ultimately, the decision to resort to an external-cavity approach will be dictated by the needs of the intended application. For the work described in this thesis, the benefits associated with having greater control over the tunability of the laser outweighed the trade-offs.

Due to the large single-pass gain of a semiconductor, it has been shown that the modal power reflectivity of the diode facet should be reduced to ~10^{-4} to ensure good external-cavity mode-locking [66]. One approach for suppressing the internal Fabry-Perot modes of the diode chip is to deposit a single-layer AR coating on the facet. Details associated with the design, deposition method, and analysis of the AR thin films used in this thesis have been thoroughly documented by others [57], [67], [68]. The optimal target index and thickness for a single-layer SiO_xN_y AR film deposited on the laser structure outlined in Table 2-1 at an operating wavelength of 1070 nm are 1.880 and 155 nm, respectively [67]. Unfortunately, as shown in [67], the bandwidth over which the modal reflectivity of an ideal single-layer AR coating is 10^{-4} or better is only around 20 nm. In practice, the finite tolerances associated with chemical vapor deposition (CVD) will reduce this bandwidth due to the difficulty of precisely achieving the intended target index and thickness. A limited low-reflectivity bandwidth will have consequences for achieving a large mode-locked tuning range and making full use of the laser's gain-bandwidth.

An alternate approach to achieving low facet reflectivity over a broad spectral bandwidth consists of modifying the design of the device structure such that the laser ridge-waveguide terminates at an angle relative to the cleaved facet. This is known as an angled-facet design. With the aid of Figure 2-6, the impact of such a structure becomes clear. Light that is guided by the ridge undergoes reflection at the angled-facet and only a fraction of the reflected power couples back into the waveguide, yielding a low modal reflectivity. Also, the low-reflectivity that can be achieved is nearly independent of wavelength. Theoretical investigations of angled-facet semiconductor devices have revealed that a facet angle of 5° can reduce the modal reflectivity to 10^{-2} for a waveguide dimension of 3×0.15 μm [69], [70]. Increasing the facet angle or decreasing the mode

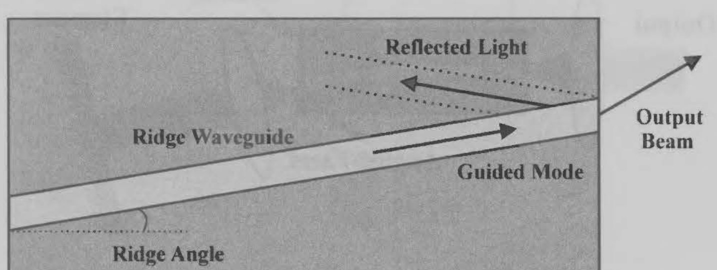

Figure 2-6: Illustration of a simple angled-facet device.

confinement in the waveguide can yield a lower modal reflectivity, however, at larger facet angles (>9°), the transmitted output beam begins to refract at a large angle relative to the facet normal, complicating the output coupling, and the far-field beam profile becomes more asymmetric [71], which can reduce the input coupling efficiency of the beam into fibres and other devices. Further reduction of the modal reflectivity can be achieved through the deposition of an AR coating on the angled-facet. It has been shown theoretically [69] and experimentally [72] that residual reflectivities on the order of 10^{-5} can be achieved with an AR-coated angled-facet device. Furthermore, the spectral bandwidth over which the reflectivity is below 10^{-4} should be sufficiently high. Indeed, good external-cavity mode-locked performance has been demonstrated over a 61 nm tuning range with 980 nm diode lasers containing AR-coated angled-facets [73]. The approach taken in this thesis has been to deposit single-layer AR coatings on angled-facets using the film properties (t = 155 nm, n = 1.880) given above for an AR coating on a standard laser where the waveguide is oriented perpendicular to the cleaved facet. Calculations have shown that the optimized index and thickness of a single-layer AR coating on an angled-facet differ by a few percent from the parameters for a normal-incidence facet [74]. A summary of the laser bar mounting procedure used for depositing the AR films is given in Appendix B.

To effectively incorporate an angled-facet into a laser structure it is necessary to modify the waveguide design of the device. A suitable design was developed in the Ph.D. work by M. Brennan for the generation of broadly-tunable ultrashort pulses at 980 nm [67]. The concept is extended to mode-locked lasers operating at 1070 nm. A schematic of the modified laser structure is shown in Figure 2-7. Conceptually, the design is not much different from that of Figure 2-5

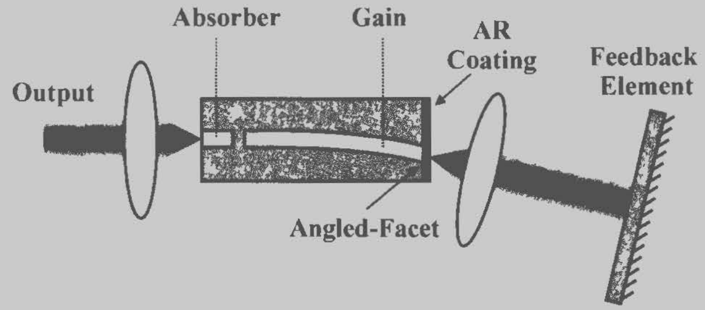

Figure 2-7: Schematic of an optimized laser design for mode-locking in a linear external cavity. The external feedback element can consist of either a mirror or a diffraction grating.

except for the curved waveguide of the gain section. The curved waveguide allows for the creation of an angled-facet at the external-cavity end of the device and a normal-incidence facet at the absorber end, which functions as the output coupler. The gain section facet is further AR coated, allowing for mode-locked operation in a compact, linear external cavity. The oscillator design of Figure 2-7 is used to obtain all of the short-pulse laser results presented in this thesis.

2.3 Optical Amplification

Conventional mode-locked semiconductor lasers operate with average output powers typically around a milliwatt. For a train of 5-ps-pulses at a repetition rate of 0.5 GHz, this translates into a pulse energy of 2 pJ and a peak power of 0.4 W. Simply increasing the drive current to the gain section will not yield a substantial increase in output power. In fact, increasing the gain section current beyond a certain value can inhibit the generation of pulses because of the delicate balance between the magnitude of gain and absorption in a mode-locked laser. In order to achieve the higher powers that are often required for many applications, it is necessary to use post-amplification methods.

When an oscillator is used in conjunction with an external amplifier for the purpose of generating high output power, the combined laser system is called a master-oscillator power-amplifier (MOPA) configuration. The advantage that a MOPA setup provides is the ability to optimize the biasing and operating parameters of the mode-locked oscillator in order to yield the shortest pulses, while allowing the external amplifier to be simultaneously driven at high levels to produce significant power gains. An optical isolator is usually placed in between the amplifier and oscillator to prevent radiation from the amplifier from coupling back into the oscillator and disrupting the mode-locking. Optical isolators with high isolation ratios are typically required for semiconductor master-oscillators due to their large single-pass gain.

In this thesis, MOPA systems based on a semiconductor optical amplifier (SOA) and a ytterbium-doped fibre amplifier (YDFA) are studied. Their theory of operation will be discussed in subsequent sections. An optical amplifier increases the power level of incident light through a stimulated emission process. The pumping mechanism that creates the necessary population inversion needed for stimulated emission can be electrical in nature in the case of an SOA, or optical in the case of the YDFA. SOAs have the advantage of being more compact, can be monolithically integrated with other photonic devices, and have the potential for lower cost. Also, SOAs have a rapid gain response, on the order of 1 ps to 1 ns, which can be advantageous for signal switching and processing applications, or disadvantageous because of cross-talk interference effects. One of the main drawbacks of an SOA is the high nonlinearity encountered at moderate power levels, which is due to the strong coupling between the gain and refractive index of a semiconductor. In contrast, doped-fibre amplifiers tend to exhibit nonlinear optical effects only at very high intensities. Fibre amplifiers are also capable of higher gain and better amplified beam quality, but require an external pump laser.

An amplifier is driven into a state of saturation when the local gain coefficient of the medium begins to decrease at any point along the amplifier. Saturation occurs due to a depletion of the population inversion caused by stimulated emission with a sufficiently large optical signal. Saturation effects can be observed at relatively low input power levels in a high-gain amplifier, or at high input power levels in the case of a low-gain system. A simple expression relating the single-pass gain of a homogenously-broadened amplifier to the input power can be obtained using a basic rate equation for the time-dependent gain [75],

$$\frac{dg}{dt} = \frac{g_o - g}{\tau_g} - \frac{gP}{E_{sat}} \tag{2.3}$$

where g is the local gain coefficient (gain per unit length), g_o is the small-signal or unsaturated gain, τ_g is the gain recovery time, P is the power of the amplified signal, and E_{sat} is the saturation energy of the amplifying medium. The above equation indicates that the gain tends to saturate in the presence of a signal and tends to recover to an equilibrium value, g_o, after the signal passes through the medium. The steady-state solution to Equation (2.3) is given by

$$g = \frac{g_o}{1 + \frac{P}{P_{sat}}} \tag{2.4}$$

where $P_{sat} = E_{sat}/\tau_g$ is the saturation power. The above equation indicates that the gain coefficient is reduced by a factor of 2 when the internal signal power is equal to the amplifier saturation power. Since g and P are both dependent on the position, z, along the amplifier, the increase in optical power of the signal (neglecting loss) in a length, dz, is

$$dP = gPdz \tag{2.5}$$

Substituting Equation (2.4) into (2.5), and integrating from $z = 0$ ($P = P_{in}$) to $z = L$ ($P = P_o$) yields

$$P_o = \frac{GP_{sat}}{G-1}\ln\left(\frac{G_o}{G}\right) \tag{2.6}$$

where $G_o = \exp(g_oL)$ is the unsaturated single-pass gain and $G = P_o/P_{in}$ is the saturated single-pass gain of the amplifier. Figure 2-8 illustrates the resulting amplifier input/output power saturation curves using Equation (2.6) for two different small-signal gain values. When the output power is equal to the amplifier saturation power, the gain is saturated and for large G_o, $G \sim G_o/e$. Alternatively, when the input power is equal to the saturation power, the gain is heavily compressed and a large fraction of the available power in the amplifier is extracted by the amplified signal. Power extraction reaches a maximum value when the amplifier is driven to transparency (G = 0 dB). An important

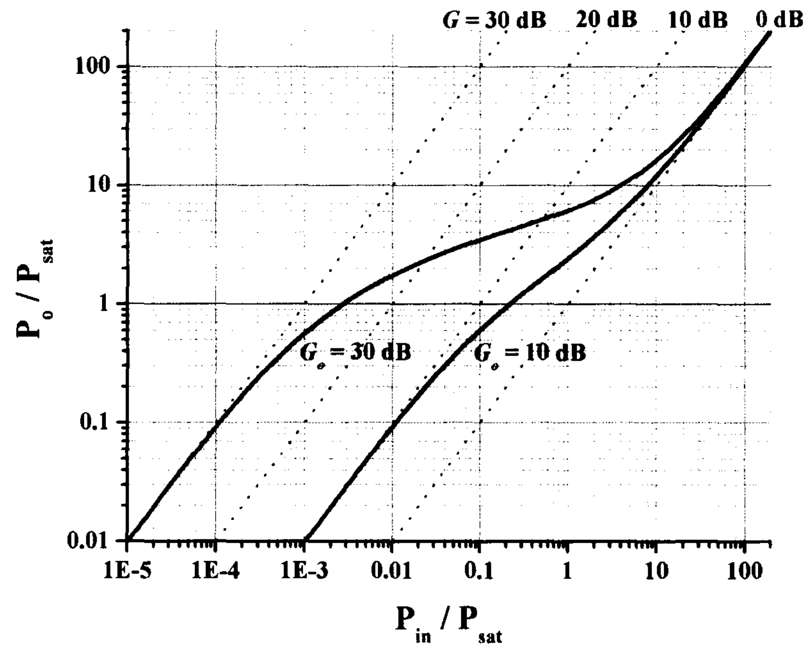

Figure 2-8: Normalized amplifier output power versus input power for small-signal gain values of G_o = 30 and G_o = 10 dB.

characterization parameter of an SOA that is typically quoted along with the saturated and small-signal gain is the output saturation power, P_{3dB}, which represents the amplified output power required to saturate the device gain from $G = G_o$ to $G = G_o/2$. For large G_o, $P_{3dB} \sim P_{sat}\ln(2)$.

2.4 Semiconductor Optical Amplifiers

2.4.1 Narrow-Stripe SOA Design

The basic operating principle of an SOA is very similar to that of a semiconductor laser without any feedback. An external current source injects charge carriers into the structure, creating a population inversion in the active layer where stimulated emission with an incoming signal causes electrons to drop in energy from the conduction band to the valence band. Figure 2-9 shows a schematic of the SOAs fabricated in this thesis. An SOA based on the design of Figure 2-9 is referred to as a narrow-stripe device because of the fact that the lateral dimension of the ridge-waveguide remains constant along the length of the amplifier and is small enough to ensure single-spatial-mode operation. Other SOA designs, such as broad-area and flared-waveguide devices, have modified waveguide geometries to enhance the performance of the amplifier.

The design of the narrow-strip amplifier is very similar to the two-contact mode-locked laser structure shown in Figure 2-4, except for the fact that only a single biasing electrode is necessary. Also, the ridge-waveguide is titled with

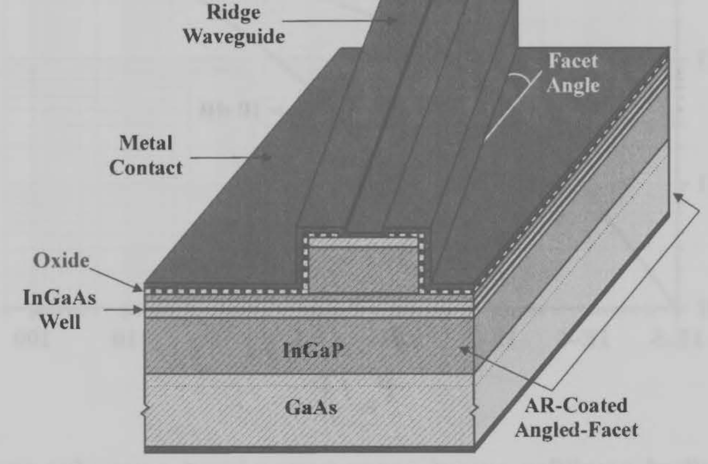

Figure 2-9: Design of a narrow-strip ridge-waveguide SOA.

respect to the facet cleavage-plane, creating angle-facets at both the input and output of the device. Facet angles of 5° and 7° are commonly used in this thesis with typical device lengths ranging from 500 to 1000 μm. Both facets are further AR-coated with a single-layer SiO_xN_y thin film using the parameters given in Section 2.2.6. Reducing the reflectivity of both facets is necessary for the SOA to behave as a traveling-wave amplifier, which implies that the amplified signal experiences negligible cavity resonance. Suppressing the cavity resonance limits the build-up of amplified spontaneous emission (ASE) inside the amplifier, produces a smooth gain spectrum with little modulation, and allows higher power to be coupled into and out of the amplifier due to the elimination of reflection losses.

Light from the mode-locked laser is coupled into the active region of the SOA where it becomes guided by the ridge and experiences amplification as a result of stimulated emission. Narrow-stripe SOAs are fabricated from the same quantum-well material structure as contained in the mode-locked lasers (Table 2-1), thus ensuring good spectral overlap of the SOA gain with the mode-locked pulses. SOAs based on quantum-well materials have advantages over bulk materials such as broader gain-bandwidths and higher saturation powers [75]. A summary of the SOA processing steps and mounting procedure for AR depositions is given in Appendix B.

2.4.2 Pulse Amplification with SOAs

When an optical pulse is injected into an SOA the amplifier gain becomes time dependent. This can be understood by considering that stimulated emission with the front of the pulse depletes the carrier density in the active region, causing the gain to saturate as the pulse propagates through the amplifier. The amplification dynamics of the SOA will depend on the energy, duration, and repetition-rate of the incident pulses, as well as on the recovery time of the gain medium. SOAs have two main recovery components: an ultrafast partial recovery time of less than 1 ps [76] and a slower component, τ_g, of around 100–500 ps [16], [77]-[79]. The former arises due to intraband carrier relaxation processes, while the latter represents the time required for full gain recovery due to the replenishing of carriers in the active region. The slow recovery component can be bias or structure dependent [16], leading to a large variation in reported values. For the amplification of pulses longer than a picosecond, the recovery of the SOA gain is dominated by the slow component. If the incident pulses are much shorter than τ_g and the period between pulses is longer than τ_g, then the gain can make a full recovery between pulses. The leading edge of each pulse is then amplified with gain coefficient $g = g_o$, while the trailing parts experience a saturated gain. The SOA experiments described in this thesis fall into such a regime of pulse amplification. Under the condition of full gain recovery between pulses, the amplifier gain saturates according to [80]

$$G_E = \frac{\ln\left[(G_o - 1)/(G_f - 1)\right]}{\ln\left[(G_o - 1)/(G_f - 1)\right] - \ln\left(G_o/G_f\right)} \tag{2.7}$$

where $G_E = E_o/E_{in}$ is the saturated single-pass pulse-energy gain which varies between G_o and 1. E_{in} and E_o are the input and output pulse energies, respectively, and G_f is the final gain or the gain experienced by the trailing edge of the pulse, which is given by

$$G_f = \frac{G_o}{G_o - (G_o - 1)\exp\left(-E_{in}/E_{sat}\right)} \tag{2.8}$$

Substitution of Equation (2.8) into (2.7) yields the quantities G_o and E_{sat} using measured values of E_{in} and G_E.

The above description of pulse-energy gain saturation excludes the effects of ASE. Modeling the saturation characteristics of the time-dependent amplifier gain including ASE is more complicated due to the fact that the build-up of both forward and backward propagating ASE signals can significantly deplete the carrier density in the interval between pulses. In the limit of a noise-less amplifier and for pulses separated by less than τ_g, low-repetition-rate pulses can extract more energy and have higher peak powers than high-repetition-rate pulses. When the pulse repetition rate becomes lower than the inverse of τ_g, the gain can make a full recovery between pulses and energy extraction can reach a maximum. For an amplifier with ASE, the performance of the amplifier becomes a strong function of the incident pulse repetition rate relative to the gain recovery time. Amplifier performance is degraded due to the fact that the build-up of ASE between pulses lowers the available gain for the pulses, and creates a cw-like background signal which lowers the amplified signal-to-noise ratio and produces low-contrast output pulses. Pulses separated in time by more than τ_g will have high levels of ASE, which can be effectively lowered by increasing the input pulse repetition rate. Thus, there exists a trade-off between high-peak-power amplified pulses and high signal-to-background ratio. Simulations have shown that to obtain high-peak-power pulses with relatively good signal-to-noise, the repetition rate of the pulses should be chosen to be on the order of the inverse of the gain recovery time of the amplifier [81].

A consequence of the rapid gain dynamics of an SOA is that the amplified pulses can become temporally distorted. Gain saturation during the transit-time of the pulse can lead to asymmetric amplified pulse shapes with short rise-times, resulting from the fact that the leading edge experiences larger gain than the trailing edge [82]. Short pulses can also be spectrally distorted when amplified in an SOA due to a self-phase modulation (SPM) process. The gain and refractive index of a semiconductor are coupled through the linewidth enhancement factor, α, which is given by [83]

$$\alpha = -\frac{4\pi}{\lambda}\frac{dn/dN}{dg/dN} \tag{2.9}$$

where dn/dN is the change in refractive index with carrier density, dg/dN is the change in gain with carrier density, and λ is the wavelength. Equation (2.9) describes the carrier-induced refractive index change resulting from changes in the gain. Therefore, temporal variations in the carrier density caused by local gain saturation can lead to variations in the refractive index as a pulse propagates

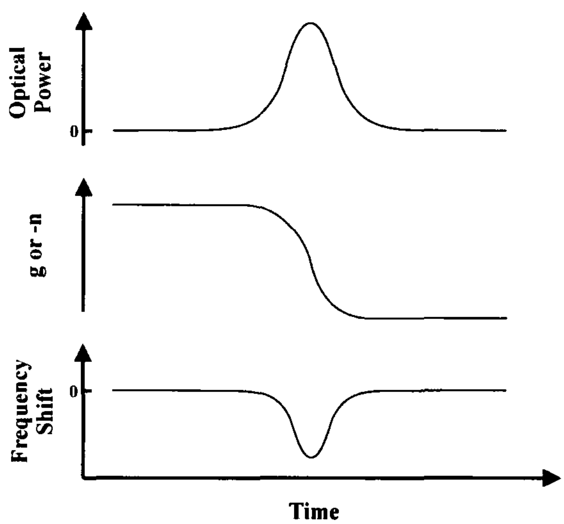

Figure 2-10: Chirp generation in an amplifier caused by gain-saturation-induced SPM. g: gain; n: refractive index.

through the amplifier. It has been shown theoretically and experimentally that this effect produces SPM, resulting in spectrally modified pulses [84]. SPM can impose a nonlinear frequency chirp on the pulse, which is a temporal variation in the optical frequency of the pulse. This effect is qualitatively illustrated in Figure 2-10 using the fact that the shift in optical frequency is proportional to the time rate of change of the refractive index. Using the simple example of Figure 2-10, distortions to the amplified pulse consist of a red-shifted spectrum that is spectrally broader as a result of the imposed frequency chirp. In general, the amount of spectral modification caused by gain-saturation-induced SPM is a complex function of the saturation characteristics of the amplifier, as well as the input pulse shape, energy, and chirp. Finally, it should be noted that minimal pulse distortion can be achieved following amplification if the amplifier is operated below saturation [85].

2.4.3 Flared-Waveguide SOAs

The saturation energy of a semiconductor amplifier is given by [86]

$$E_{sat} = \frac{h\nu A}{\Gamma\, dg/dN} \tag{2.10}$$

where h is Planck's constant, ν is the optical frequency, A is the cross-sectional area of the active region, Γ is the confinement factor, and dg/dN is the differential gain. Typical values of E_{sat} for index-guided quantum-well narrow-stripe amplifiers are around a few pJ [85], [86]. The saturation energy is an important device parameter which affects the performance of both mode-locked diode lasers and SOAs. The pulse energy that can be achieved at the output of a mode-locked laser will be on the order of the saturation energy and in the case of an SOA, the saturation energy describes the amplified pulse energy beyond which the gain is saturated and distortions to the pulse shape and spectrum are expected. Thus, by increasing the saturation energy, the pulse amplification characteristics of an SOA can be significantly improved, yielding higher-energy output pulses with less distortion.

Upon examining Equation (2.10) it is clear that a direct way of improving the saturation characteristics of a semiconductor amplifier is by scaling the size of the active area. Indeed, this can be easily accomplished by increasing the ridge width of a conventional narrow-stripe amplifier. Such devices are termed broad-area amplifiers and are capable of producing multi-watt amplified output powers for lateral waveguide dimensions of several hundred microns [87]. Broad-area amplifiers can exhibit saturation powers exceeding that of conventional narrow-stripe devices (ridge widths ~1–3 μm) by more than a factor of 100. However, there are two problems with such devices. First, the large lateral waveguide results in the excitation of higher order spatial modes in the waveguide, causing the total output power to be distributed amongst a number of modes, which is undesirable for many applications. Second, the input energy required to saturate the initial sections of the amplifier is high. Since the output average power of a mode-locked laser is typically less than one milliwatt, the input pulses would not have sufficient energy to suppress the build-up of ASE and the amplifier output would mainly consist of ASE.

A solution that overcomes the problems associated with a broad-area SOA and improves upon the saturation characteristics of a narrow-stripe amplifier is based on combining the design principles of both devices. By incorporating a narrow-stripe waveguide region at the input of the amplifier which laterally expands toward the output, an optimized design is achieved which offers single-mode amplification with high E_{sat}. These devices are termed flared-waveguide SOAs. An example of a flared-waveguide device developed in this thesis for short-pulse amplification is illustrated in Figure 2-11. The operating principle behind a flared-amplifier is that the width of the active layer is gradually increased along the longitudinal axis, causing the local saturation energy to slowly increase from input to output. This results in a low E_{sat} at the input for effective

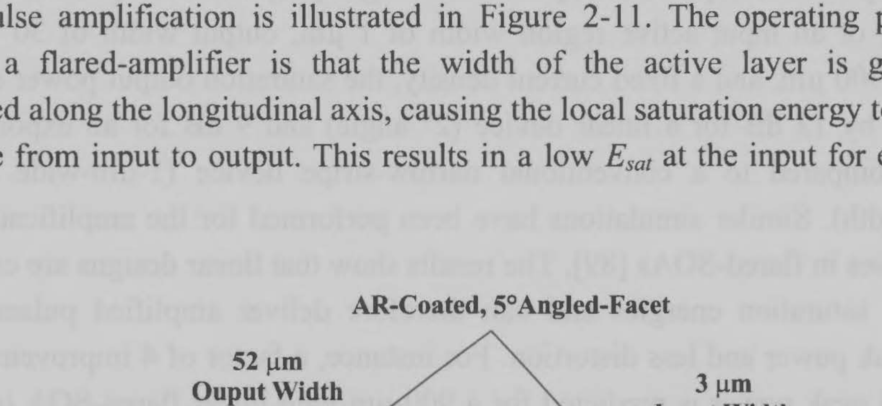

Figure 2-11: Schematic top-view of a 2° flared-waveguide SOA developed for short-pulse amplification.

amplification of the low-energy pulses from the mode-locked laser and higher values of E_{sat} near the output to increase overall energy extraction. Moreover, the flared structure allows the amplified intensity to grow slowly, resulting in a more uniform gain saturation throughout the amplifier, which leads to lower temporal and spectral pulse distortion. The purpose of the narrow-stripe region at the input is to allow the pulse energy to build to a point where it can begin to saturate the larger gain of the flared region. If the waveguide is flared at a relatively modest angle, then light that is coupled into a single spatial mode at the input will remain guided along the amplifier in a single mode, but with a broadened spatial width. Typical flared-amplifiers have lateral waveguides that expand at angles of less than 5°.

For the flared SOA shown in Figure 2-11, the difference in active area between the input and output results in a relative change in saturation energy of $E_{sat,out} \sim 17 \times E_{sat,in}$. Various flared-waveguide profiles have been proposed to improve the saturation characteristics of the amplifier, such as linear (Figure 2-11), exponential, quadratic, and Gaussian. Simulations of flared-SOAs under cw injection conditions have shown that devices with linear profiles have higher saturation powers compared to exponential designs [88]. For example, for devices consisting of an input active region width of 1 μm, output width of 30 μm, a length of 900 μm, and a fixed current density, the saturation output power can be improved by 13 dB for a linear device (2° angle) and 9 dB for an exponential device, compared to a conventional narrow-stripe device (1-μm-wide active region width). Similar simulations have been performed for the amplification of 10-ps-pulses in flared-SOAs [89]. The results show that linear designs are capable of higher saturation energies and can therefore deliver amplified pulses with higher peak power and less distortion. For instance, a factor of 4 improvement in the output peak power is predicted for a 900-μm-long linear flared-SOA (output width of 10 μm) compared to a 1-μm-wide narrow-stripe device of the same length and current density [89].

The output spatial beam profile of a flared amplifier is highly astigmatic. This is due to the fact that in the transverse direction the beam appears to emanate from a point located at the output facet, whereas in the lateral direction, the flared-waveguide causes the beam to emanate from a point located some distance behind the output facet [90]. To correct the astigmatism, a cylindrical lens is used in conjunction with a spherical lens to fully collimate the output beam (Figure 2-11). If the lateral waveguide of a flared-SOA expands at a relatively large angle, distortions can occur to the spatial profile of the amplified beam due to the excitation of higher-order modes in the flared region. For high-power amplifiers that operate at many amps of drive current, beam distortions can also be caused by carrier- and thermal-induced lensing effects [90].

Devices based on novel waveguide geometries, such as the inverse bow-tie SOA [91], have also been developed in order to further enhance the performance of a basic flared-SOA. The inverse bow-tie design consists of a standard flared-waveguide region followed by a tapered region where the width of the lateral waveguide decreases with length. The salient feature of this device is that one can achieve the high saturation powers that are characteristic of flared devices while maintaining a single spatial mode with an astigmatism that can be more easily compensated.

Further discussions of flared-waveguide and narrow-stripe SOAs can be found in [75].

2.5 Yb-Doped Fibre Amplifiers

Recently, there has been intense interest in the development of optical sources based on Yb-doped fibres. The reasons for such interest is due to the number of attractive features exhibited by Yb:fibre systems: they can deliver gain over a very broad wavelength range from approximately 975 to 1200 nm, are capable of extremely high gain, good power conversion efficiency, and excellent amplified beam quality. From the perspective of developing a short-pulse laser system operating near 1 μm, a Yb:fibre amplifier fulfills many of the requirements of a power-amplifier. Indeed, the attractive features of the Yb:fibre amplifying medium and its ability to provide gain near 1 μm were the main driving force behind the group's development of mode-locked semiconductor oscillators at 1070 nm.

2.5.1 Doped Fibre Optical Amplifiers

An optical fibre amplifier consists of an optical fibre that has been lightly doped with a rare-earth (RE) element. Doping is usually confined to the core of the fibre with concentrations ranging from hundreds to thousands of parts per million (ppm) by weight. RE dopants are incorporated into the silica matrix in the form of RE_2O_3 using a solution doping technique [92]. When introduced into silica or other glass fibres, the RE elements become triply ionized through the removal of two outer 6*s* electrons and an inner 4*f* electron. Many different RE ions, such as Nd^{3+}, Yb^{3+}, Er^{3+}, Tm^{3+}, Ho^{3+}, and Pr^{3+}, can be used to make fibre amplifiers operating at wavelengths spanning the visible to the infrared regions (~3 μm) [93]. The specific operating wavelength and gain-bandwidth of a given RE-doped fibre amplifier can depend on the intensity and wavelength of light that is used to pump the amplifier. Some examples of where gain has been achieved with specific RE ions include: Er^{3+} pumped at 980 nm or 1480 nm can yield gain between 1530–1620 nm [94]; Nd^{3+} pumped at ~800 nm can provide gain between 905–940 nm or 1060–1120 nm [95], [96]; Yb^{3+} pumped at 975 nm can provide gain between 1030–1150 nm [96], [97]; and Tm^{3+} pumped at ~800 nm can provide gain between 1730–2100 nm [96], [98].

Gain in a fibre amplifier is achieved as a result of a population inversion of the RE ions. A pump laser with an emission spectrum that corresponds to the absorption bands of the RE ions is used to optically excite the ions to a metastable energy level, which typically has a radiative lifetime on the order of milliseconds. The stored energy is then used to amplify a signal beam through stimulated emission.

Doped fibre amplifiers offer some important advantages over 'bulk' (i.e. non-waveguiding) solid-state amplifiers. Tight beam confinement in a single-mode core ensures robust single-mode operation, which is necessary for many applications. Fibres also allow for the possibility of long interaction lengths, leading to high overall gain. In addition, the large ratio of surface-area to active-volume of a fibre results in excellent heat dissipation, allowing fibre amplifiers to operate at elevated power levels with reduced thermo-optic effects. A performance trade-off associated with the tight mode confinement and long interaction length of a fibre is that intensity-dependent nonlinear optical effects are more apparent than in bulk hosts. Nonlinear effects such as SPM can distort short pulses, while inelastic scattering processes can cause significant loss of power from the amplified beam [93]. The threshold for the onset of nonlinear optical effects can be reduced, however, by scaling the size of the core to reduce the peak intensity in the fibre and by highly doping the fibre to minimize the overall length needed to achieve a specific gain [99]. Nonlinear optical effects in fibre amplifiers will be further discussed in Chapter 4.

2.5.2 Spectroscopic Properties of Yb:Fibre

Compared to other RE ions, the spectroscopy of Yb^{3+} is very simple. For all optical wavelengths, only two manifolds are relevant: an excited manifold consisting of 3 sublevels and a ground manifold consisting of 4 sublevels. The sublevels in each manifold arise due to the Stark effect [94]. Figure 2-12 shows

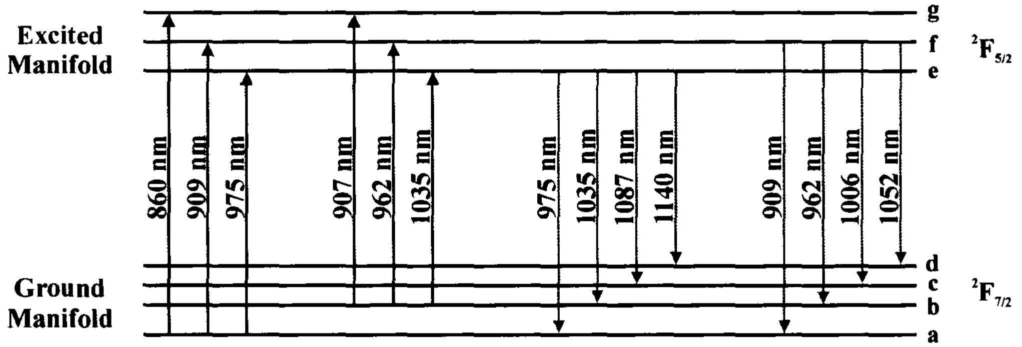

Figure 2-12: Energy level structure of Yb^{3+} consisting of two manifolds. The wavelengths of the optically important transitions are obtained from [100].

the energy level structure of Yb^{3+} in silica glass. The optically important transitions between sublevels are noted in the figure and are provided as an approximate guide. In practice, the transitions between sublevels cannot be fully resolved at room temperature due to the homogeneous and inhomogeneous broadening effects of the glass [97]. The simple energy structure of Yb eliminates several undesirable effects that serve to reduce the efficiency of the gain medium. Examples of such effects, which are typically encountered in other RE-doped fibres, include multi-phonon non-radiative decay, concentration quenching, and excited-state absorption [97]. Concentration quenching, such as that observed in Er-doped fibres, is an effect that manifests itself at high doping levels and leads to a reduction in the radiative lifetime of the metastable energy state [94]. Since this effect is absent in fibres doped with Yb, it is possible to achieve very high doping levels in the core (above 10 000 ppm), allowing for large unsaturated gains in short lengths of fibre. Another important consequence of the simple energy structure of Yb is that the quantum energy defect, or the difference between pump and signal wavelengths, is very small (as low as 5 %), which results in very little thermal energy transferred to the host. As a result, Yb:fibre systems can exhibit excellent optical-to-optical power conversion efficiencies, as high as 90 % with respect to the pump power launched into the fibre [101].

Figure 2-13 shows the effective absorption and emission cross-sections for Yb^{3+} in a germano-silicate host. The absorption and emission spectra are both dominated by a prominent peak at 975 nm resulting from transitions between the two lowest sublevels in each manifold. Pumping at 975 nm accesses the largest absorption cross-section, which is useful when the shortest fibre length possible is required. The relatively narrow linewidth of the 975 nm peak implies that the

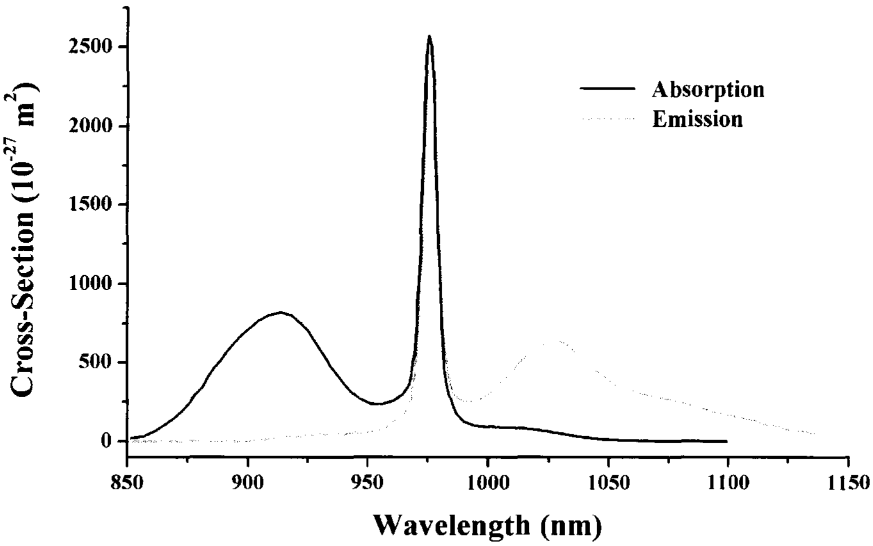

Figure 2-13: Absorption and emission cross-sections of Yb^{3+} in a germano-silicate host. Quoted values are obtained from [97].

spectral output of the pump laser should be correspondingly narrow and preferably wavelength-stabilized to ensure that pump radiation is efficiently absorbed. The second main absorption peak centered near 910 nm is typically used when gain is required at 975 nm.

The broad peak in the emission spectrum near 1030 nm corresponds to the spectral region where Yb-doped fibres are normally operated as amplifiers and lasers. The long emission tail of this peak, which extends beyond 1150 nm, results from transitions between the lowest sublevel in the excited manifold and sublevels *b*, *c*, and *d* of the ground manifold (Figure 2-12). The wide shape of the emission spectrum at long wavelengths makes Yb-doped fibres particularly suitable for amplifying short optical pulses over a broad range of wavelengths. The small tail in the absorption spectrum which extends into this region can have an effect on the performance of both fibre amplifiers and lasers. The origin of the absorption at wavelengths between 1000 to 1100 nm is due to the fact that the sublevels of the ground manifold are thermally-populated at room temperature, resulting in transitions from sublevels *c* and *b* in the ground manifold to sublevel *e* in the excited manifold. Although the magnitude of the absorption is relatively weak, the long-wavelength shoulder in the absorption spectrum can be a source of loss in unpumped or weakly pumped sections of the fibre, leading to the attenuation of the amplified signal radiation.

The properties of the Yb^{3+} absorption and emission spectra are dependent on the composition of the host glass [102]. Even within the same glass family, additional dopants present in the core can modify the characteristics of the transition cross-sections. In the case of a germano-silicate glass fibre, the cross-sections can deviate by as much as 30 % depending on the concentration of index-modifying co-dopants in the core, such as aluminum, germanium, and boron [97]. The composition of the glass host can also affect the florescence lifetime of the excited Yb^{3+} manifold. Ytterbium in pure silica has a lifetime of around 1.5 ms, whereas a standard Yb-doped germano-silicate glass fibre has a lifetime of around 0.8 ms [97].

2.5.3 Double-Clad Doped Fibres

A conventional RE-doped fibre consists of a single-mode doped core surrounded by a single silica cladding and a protective jacket layer. Pump light is coupled into the core along with the signal to be amplified. This fibre geometry works well for low to moderate amplified power levels, yielding relatively high gain in short lengths of fibre due to the high degree of spatial overlap of both the pump and signal beams with the doped core. When higher output power is required (more than ~1W), there is an increased likelihood of damage at the facet of the fibre due to the tight focus required to couple the pump light into the small core of a single-mode fibre. A solution that overcomes the power limitation of the conventional fibre geometry is the so-called double-clad fibre, whereby a doped core is surrounded by inner and outer cladding layers. The signal light to be amplified is coupled into the doped single-mode core and the pump light is launched into and guided by a multimode inner cladding. By de-coupling the pump and signal waveguides, the area of the inner cladding can be scaled in order to accommodate higher pump powers, while the signal radiation remains guided in a single spatial mode. A consequence of having separate pump and signal waveguides is that the absorption per unit length of the pump light propagating in the inner cladding is reduced by a factor approaching the ratio of the inner cladding to core areas. The reduced pump absorption of cladding-pumping compared to direct core-pumping can be compensated by using a higher doping concentration in the core, longer fibre length, and by optically pumping at a wavelength that corresponds to the peak absorption cross-section of the RE dopant. Since the inner cladding of a double-clad fibre is typically greater than 100 μm, high-power multi-spatial-mode pump lasers can be used for optical pumping, allowing the amplified signal to be significantly scaled in power. Other

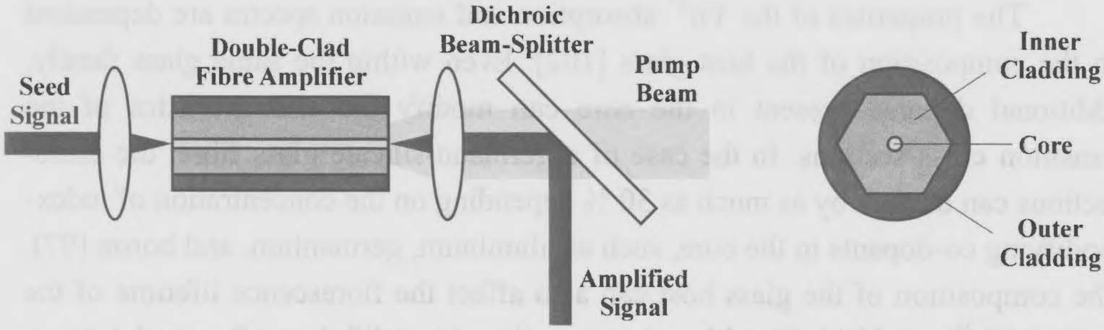

Figure 2-14: (*left*) Schematic of a double-clad fibre amplifier with a counter-directional optical pumping scheme. (*right*) Cross-sectional view of a typical double-clad fibre with a hexagonal-shaped inner cladding.

advantages of double-clad fibres include improved launch efficiency of the pump beam and reduced alignment tolerances for the pump coupling.

A schematic of a typical seeding and pumping configuration of a double-clad fibre is illustrated in Figure 2-14. When working with free-space optics, the counter-directional seeding geometry shown in the figure allows the coupling of the pump and signal beams to be independently optimized using separate lenses. A dichroic beam-splitter with wavelength-dependent transmission and reflection characteristics is used to separate the amplified signal from the pump beam. Fibre components, such as splitters and combiners, can also be used for easier and more efficient launching of the signal and pump beams into the fibre. The pump waveguide of a double-clad fibre is usually non-circular in shape, which is necessary to avoid the excitation of helical cladding modes that have poor overlap with the doped core. By resorting to a hexagonal, octagonal, or a D-shaped inner-cladding geometry, the guided modes of the pump beam are effectively scattered as they propagate along the fibre, resulting in a greater probability of overlap with the core, which increases the overall pump absorption.

Cladding-pumping is particularly advantageous with Yb-doped fibres due to the fact that the peak absorption of Yb^{3+} is at a wavelength of 975 nm. As a result of the well-established field of fibre-optic telecommunications, there is an abundance of highly efficient, powerful, and inexpensive InGaAs diode laser pump sources that operate in the vicinity of 980 nm. Therefore, the overall operating efficiency of a cladding-pumped Yb:fibre system can be quite high, due to the high intrinsic optical-to-optical conversion efficiency of the Yb^{3+} gain medium (90 %) and the high electrical-to-optical efficiency that can be achieved using a semiconductor pump laser (~50 %). System electrical-to-optical power conversion efficiencies as high as 40 % have been reported [101].

Specialized fibre structures can also be employed to further enhance the performance of a fibre amplifier. When operating at elevated power levels, nonlinear optical effects in the core of the fibre can negatively affect the performance characteristics of the amplified signal. One method of mitigating the onset of nonlinear effects is by increasing the core diameter of the fibre, which reduces the intensity of the amplified signal. Scaling of the core diameter also requires that the numerical aperture (NA) of the fibre be simultaneously reduced to preserve single-mode operation. Such large-mode-area (LMA) fibres can have core diameters of 20 μm or more and are typically used in the development of high-power Yb:fibre systems. Micro-structured or photonic crystal fibres have recently drawn considerable interest as a means of achieving the LMA fibre concept [103], [104]. The double-clad fibre geometry can also be extended to a triple-clad design [105], [106], where the third cladding layer provides an additional degree of freedom by which the NA of the core can be tailored in the design of a LMA fibre.

2.5.4 Calculation of Yb^{3+} Gain

Numerical modeling of Yb-doped fibre amplifiers can be relatively straightforward due to the simple energy level structure of Yb^{3+}. Calculations of the single-pass small-signal gain spectrum are made in order to obtain insight into the behavior of the amplifier as a function of basic operating parameters, such as the pump power and fibre length. A simple rate-equation approach is used to calculate the steady-state gain of a double-clad fibre amplifier that has properties very similar to the Yb-doped fibres used in the experiments. The simulation results presented here for a Yb-doped double-clad fibre are complementary to those obtained by other groups for a single-clad fibre [97], [100]. The modeling approach follows a similar method outlined in [97]. Some approximations are made to simplify the rate equations. The Yb-doping profile is assumed to be uniform over the area, A, of the core. Also, the signal and pump intensity profiles are assumed to be uniform over the area of the core and inner cladding, respectively. Finally, ASE and the intrinsic background loss of the fibre are neglected in the current model. A more sophisticated modeling approach which accounts for the aforementioned effects will be presented in Section 4.7.

The gain of a Yb:fibre system can be calculated using a simplified two-level model for the energy level structure, whereby N_1 and N_2 are the population densities of the excited and ground manifolds, respectively. This simplified modeling approach is appropriate for RE-doped fibres when using the effective (experimentally measured) values of the transition cross-sections, which take into account the fast thermalization rate of each manifold [94].

The spatially-dependent population and power-propagation rate equations are given by

$$\begin{aligned}\frac{dN_2}{dt} &= \frac{D\lambda_p}{hcA}\left[\sigma_a(\lambda_p)N_1 - \sigma_e(\lambda_p)N_2\right]P_p(\lambda_p) \\ &+ \frac{\lambda_s}{hcA}\left[\sigma_a(\lambda_s)N_1 - \sigma_e(\lambda_s)N_2\right]P_s(\lambda_s) \\ &- \frac{N_2}{\tau}\end{aligned} \quad \textbf{(2.11)}$$

$$N_1 = N_T - N_2 \quad \textbf{(2.12)}$$

$$\frac{dP_p(\lambda_p)}{dz} = D\left[\sigma_e(\lambda_p)N_2 - \sigma_a(\lambda_p)N_1\right]P_p(\lambda_p) \quad \textbf{(2.13)}$$

$$\frac{dP_s(\lambda_s)}{dz} = \left[\sigma_e(\lambda_s)N_2 - \sigma_a(\lambda_s)N_1\right]P_s(\lambda_s) \quad \textbf{(2.14)}$$

where N_T is ytterbium doping density, and $P_s(\lambda_s)$, $P_p(\lambda_p)$ are the signal and pump powers at wavelengths λ_s and λ_p, respectively. The effective absorption and emission cross-sections of Yb^{3+} (Figure 2-13) are given by σ_a and σ_e, respectively, and τ is the fluorescence lifetime of the excited manifold. The reduced spatial overlap of the pump beam with the doped core in a double-clad fibre is accounted for by the parameter, D, which is the ratio of the core to inner cladding areas. Equation (2.11) describes the changes to the population density of the excited manifold due to stimulated absorption and emission of both pump and signal waves, while Equations (2.13) and (2.14) describe the evolution of the pump and signal power along the longitudinal axis of the fibre, z.

Equations (2.11) to (2.14) are numerically solved under steady-state conditions using the finite difference method. The parameters used for a typical double-clad Yb-doped fibre with a 6 μm core diameter and 125 μm inner cladding diameter are τ = 0.8 ms and N_T = 8×10^{25} m^{-3}. Figure 2-15 shows the calculated single-pass small-signal gain spectra of a 1-m-long and 20-m-long fibre amplifier

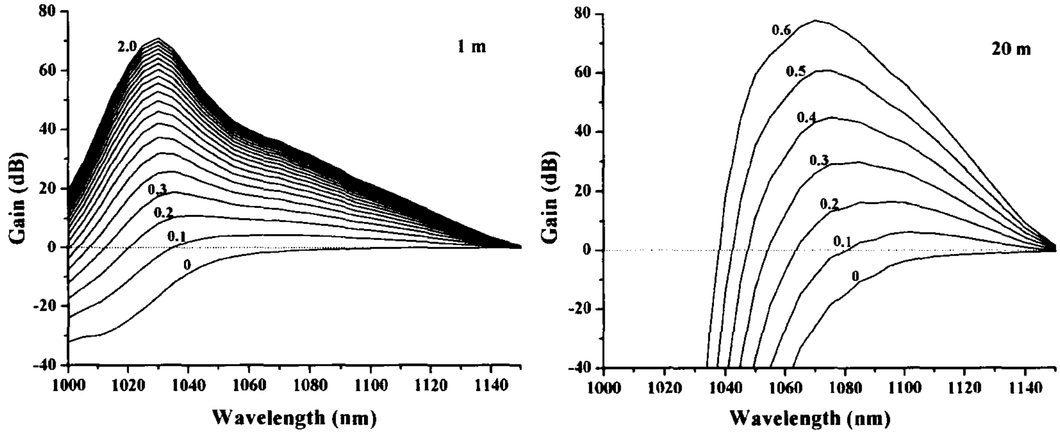

Figure 2-15: Calculated small-signal single-pass gain spectra of a Yb:fibre amplifier pumped at 975 nm with a fibre length of (*left*) 1 m and (*right*) 20 m. Curves are labeled with the launched pump power in watts and are incremented by 0.1 W. Note: the scales of both graphs are kept the same.

when pumped at the peak absorption cross-section of 975 nm. The launched pump power is incremented in intervals of 0.1 W, from 0 to 2.0 W. The scale of the gain axis is kept the same for both graphs in order to allow comparisons to be made regarding the shapes of the gain spectra. As a result, the launched pump power in the case of the 20 m amplifier has been limited to 0.6 W. Gain spectra of the 20 m amplifier for the full range of optical pumping of up to 2.0 W of power are shown in Figure 2-16. By comparing the plots in Figure 2-15, several trends can be identified regarding the performance of the Yb:fibre amplifiers. First, for a given value of the launched pump power, the peak gain is higher in the case of the longer amplifier. This simply reflects the fact that a greater amount of pump power is absorbed in the 20 m amplifier due to the longer interaction length. The small-signal absorption coefficient of the pump beam propagating in the inner cladding is $\exp[-N_T D \sigma_a(\lambda_p) z]$, which is 2.0 dB/m at 975 nm for the fibre parameters stated above. Second, the spectral gain peak and shape of the gain spectrum is dependent on the fibre length and pump power. At low pump levels, or for long fibres, the gain peak is located at long wavelengths. This behavior is a consequence of the finite tail in the absorption spectrum of Yb^{3+} (Figure 2-13), which decreases in amplitude as a function of wavelength. As a result, for long fibres where the magnitude of the pump power is weak near the end of the fibre, or for short fibres with a low launched pump power, short-wavelength signals suffer from greater reabsorption losses causing the gain to shift to longer wavelengths where the absorption cross-sections are much smaller in magnitude.

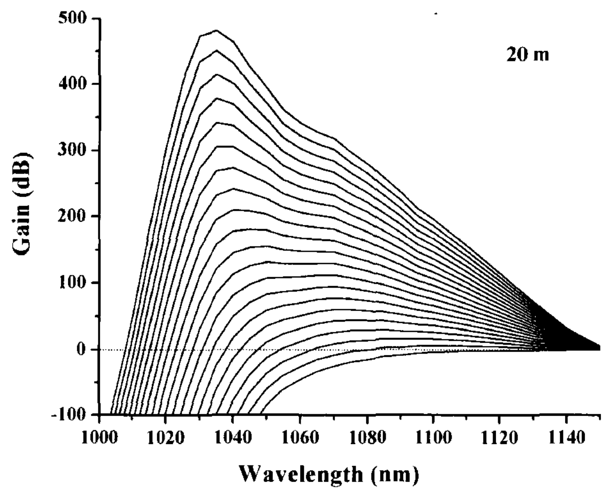

Figure 2-16: Calculated small-signal single-pass gain spectra of a 20-m-long Yb:fibre amplifier pumped at 975 nm for different values of launched pump power (in intervals of 0.1 W, from 0 to 2.0 W).

This behavior is also illustrated in Figure 2-16 for the 20 m fibre. With sufficient pumping to overcome the reabsorption losses, the peak gain is shifted to short wavelengths (~1030 nm). Thus, from the perspective of optimizing the amplification performance of a YDFA, there exists an optimal length of fibre for maximizing the gain at a specific operating wavelength for a given value of pump power.

In examining Figure 2-15 and Figure 2-16 more closely, it is evident that the magnitude of the small-signal gain is very large. In practice, it would not be possible to achieve such large values of gain due to self-saturation effects by ASE. The build-up of forward and backward propagating ASE in the fibre depletes the population density of the excited manifold, reducing the attainable small-signal gain by around a factor of 10 from the values given in Figure 2-16. In the limit of zero ASE, the maximum possible amplifier gain can be calculated based on two fundamental principles. It can be useful to calculate such a value in order to identify the upper-limit to the achievable gain. For the case of optical pumping of Yb^{3+} at 975 nm, a strong pump will invert 50 % of the Yb ions to the excited manifold since the absorption and emission cross-sections are equal at this wavelength. Under this pumping condition, assuming reabsorption losses are negligible, the small-signal gain can be described by

$$G = \exp\left(\frac{N_T}{2}\sigma_e(\lambda_s)z\right) \tag{2.15}$$

The gain expressed in the above equation cannot be increased indefinitely by increasing the fibre length or dopant concentration due to energy conservation. The maximum output power is in fact limited by the magnitude of the pump power which is expressed by the following

$$P_s^{out} \leq P_s^{in} + \frac{\lambda_p}{\lambda_s} P_p^{in} \tag{2.16}$$

where P^{out} and P^{in} correspond to output and input powers, respectively. Equation (2.16) places a constraint on the extractable output power and the power conversion efficiency of the amplifier, which has a maximum value given by the quantum defect, λ_p/λ_s. Dividing Equation (2.16) by the input power of the signal yields the gain

$$G \leq 1 + \frac{\lambda_p}{\lambda_s}\frac{P_p^{in}}{P_s^{in}} \tag{2.17}$$

Equations (2.15) and (2.17) therefore represent the two fundamental limits to the maximum fibre gain. The achievable upper-limit to the gain is given by the lowest value of either equation, which can be stated as [94]

$$G \leq \min\left\{ 1 + \frac{\lambda_p}{\lambda_s}\frac{P_p^{in}}{P_s^{in}},\ \exp\left(\frac{N_T}{2}\sigma_e(\lambda_s)z\right)\right\} \tag{2.18}$$

For amplification at 1080 nm in 1-m-long fibre pumped with 2.0 W of power at 975 nm and using the fibre parameters given earlier, Equation (2.15) yields $G \sim$ 42 dB and Equation (2.17) yields $G \sim$ 500 dB. As noted above, the actual small-signal gain will be limited by ASE, as well as by other effects, such as the intrinsic background loss of the fibre and the spatial overlap functions of the signal and pump beams with the doped core.

Chapter 3 Experimental Setup

3.1 Introduction

This chapter describes the various components that comprise the experimental setup used for the generation and amplification of short optical pulses. Details concerning the mounting procedure of the diode lasers and SOAs will be presented first, followed by discussions of the diagnostic and characterization equipment.

3.2 Device Mounting

In order to effectively operate a diode laser in an external cavity there are a number of technical issues that must be addressed. The mounting setup should provide good thermal and mechanical stability, allow electrical connections to be made to the device contacts through the use of wire-bonding or rigid metallic probes, and both laser facets should be accessible. These technical details are equally important for the mounting of SOA devices. Since most commercially available diode laser sub-mount assemblies only allow access to one laser facet, a custom design was used to mount the devices. A schematic of the mounting setup is shown in Figure 3-1. Devices in chip or bar format are bonded to a 1-mm-thick copper carrier using electrically conductive silver epoxy (H20E, Epotek). Since most of the lasers tested are less than 1 mm in length, the top of the copper carrier is beveled to prevent excess epoxy from coming in contact with the facets. Curing of the epoxy layer is achieved by baking at 80°C for 1.5 hours using a hot plate. Bonding increases the mechanical stability of the devices and decreases the thermal resistance between the diode and the copper carrier, which increases the efficiency of the lasers. Since the bonding process is permanent, the carriers are designed to be easily removed using mounting slots. The carrier is attached to a

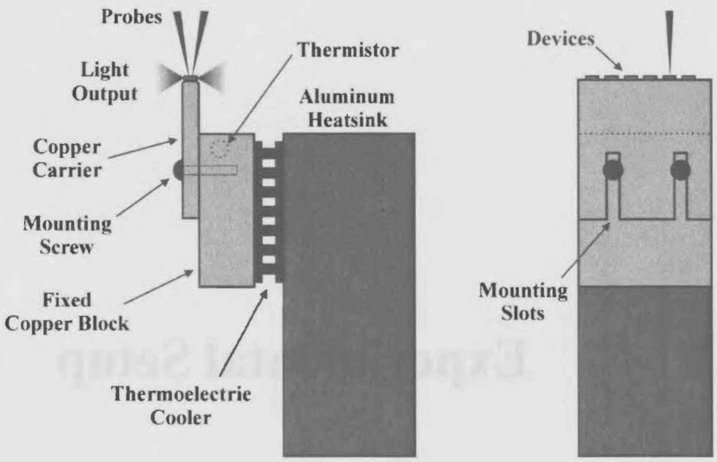

Figure 3-1: Schematic of the mounting setup used for the oscillator.

fixed copper block using stainless steel screws and thermal paste (126-2, Wakefield) is applied at the interface between the copper carrier and the fixed block to improve heat conduction. The fixed copper block is kept at a constant temperature of 20°C using a 3.2 W thermoelectric cooler (Melcor) which is attached to an aluminum heat-sink. A 10 kΩ thermistor embed in the fixed copper block is used to monitor the temperature of the mounting assembly. Electrical contact to each section of the device is made using two rigid probes mounted on 3-axis translations stages. Light from each facet is collected using a 3 mm focal length AR-coated aspheric lens (C330TME-B, Thorlabs) which is attached to a 3-axis flexure stage. A manually controlled flexure stage (MDT616, Thorlabs) is used for the output coupling lens and a precision piezo-controlled flexure stage (MDT630, Thorlabs) is used to provide control over the coupling to the external cavity. A photograph of the mounting setup for the two-contact diode laser is shown in Figure 3-2. Since both lenses must be positioned within a few millimetres of the diode, the braided metallic isolation sheath had to be removed at the end of each probe to allow both probes to fit in the space between the lenses. The removal of the braided sheath from the gain section probe will result in some RF radiation losses during hybrid mode-locking.

The mounting configuration used for the testing of SOA devices is very similar to that of the oscillator. Light is coupled into and out of the SOA using 3 mm focal length AR-coated aspheric lenses (C330TME-B, Thorlabs) attached to 3-axis flexure stages (MDT616, Thorlabs). The SOAs are bonded to a thicker copper carrier (2 mm), since they are typically longer then the devices used in the

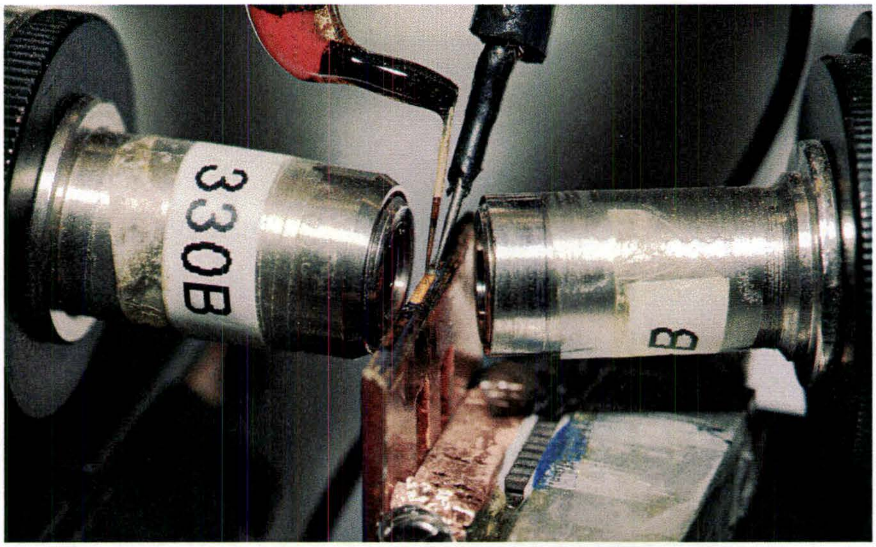

Figure 3-2: Photograph of the mounting setup of the mode-locked semiconductor oscillator.

oscillator, and require only a single probe for biasing. Also, the size of the SOA mounting assembly is much larger due to the fact that the SOAs, particularly the flared-waveguide devices, are electrically biased at much higher drive currents (up to 1 A). Improved heat dissipation is achieved by scaling the cross-sectional area of the carrier and fixed copper block, and a higher power thermoelectric cooler (18.7 W, Melcor) is used in conjunction with an aluminum heat-sink which can be convectively cooled. A photograph of the SOA mounting setup is shown in Figure 3-3.

3.3 Fast-Photodiode and Sampling Oscilloscope

A 20 GHz fibre-coupled photodetector (1414, New Focus) and a sampling oscilloscope (CSA 803, Tektronix) with a 50 GHz sampling head (SD-23, Tektronix) are used to monitor and study the time-dependent pulsing characteristics of the mode-locked oscillator. This diagnostic tool proved to be invaluable for assessing the operating regime of the mode-locked oscillator. By coupling a portion of the oscillator output beam into a fast-photodiode, the properties of mode-locked pulse train can be monitored during the course of an experiment to ensure that the pulse train remains stable in time and free of satellite pulses. Since both the oscilloscope and photodetector are electrically DC-

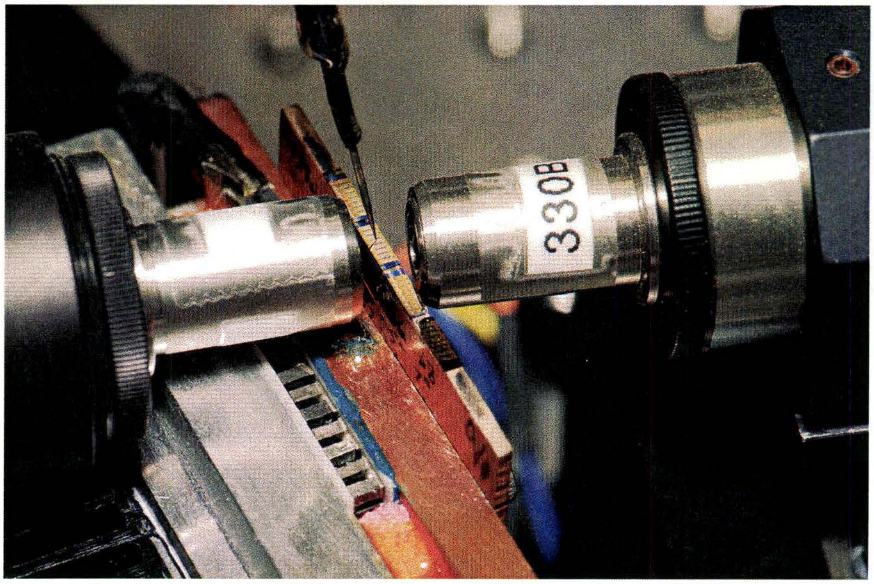

Figure 3-3: Photograph of the SOA mounting configuration.

coupled, this system can also detect the presence of a cw-like background signal on the main mode-locked signal.

The sampling oscilloscope must be triggered using an external signal that has root mean square (rms) amplitude of at least 7 mV. In the case of hybrid mode-locking, a fraction of the RF power from the output of the signal generator can be used for triggering. In the case of passive mode-locking, the trigger signal can be derived from the mode-locked pulse train. This can be accomplished by splitting the output of a photodetector into two signals such that only a small fraction of power is used as the trigger signal. However, since the use of a power splitter will increase the impulse response time of the system, a slightly more complex triggering method was chosen in order to maximize the bandwidth of the detection system. A schematic of the triggering approach is shown in Figure 3-4. The output beam from the mode-locked oscillator is split into two beam paths with 80 % of the optical power incident on the 20 GHz photodetector that is directly connected to the sampling head of the oscilloscope. The other 20 % of optical power is directed to a 3 GHz silicon photodiode (PD30, Opto-Electronics). The trigger for the oscilloscope is obtained by amplifying the output of the 3 GHz photodiode using a cascaded chain of RF amplifiers (ZX60-14012L and ZX60-4016E, Mini-Circuits) with a total gain of around 50 dB. Figure 3-4 shows the impulse response of this time-domain measurement system using a train of 1-ps-

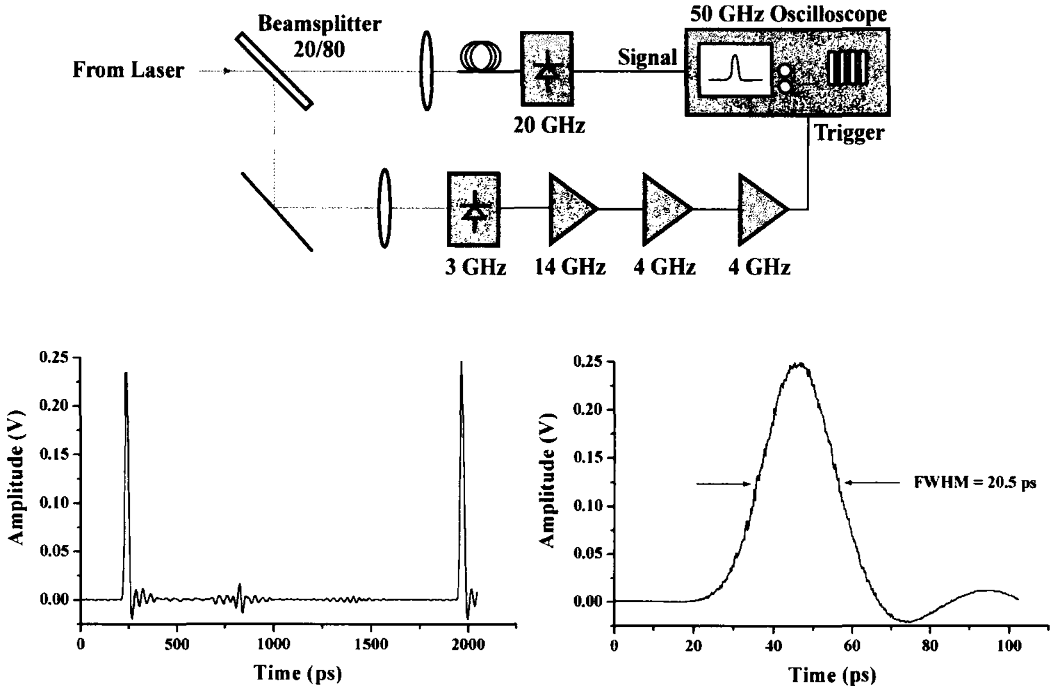

Figure 3-4: (*upper*) Time-domain measurement setup for detecting a passively mode-locked pulse train; (*lower-left*) Response of the system to a 1 ps pulse train at 577 MHz; (*lower-right*) The measured FWHM impulse response time is 20.5 ps.

pulses at a repetition rate of 577 MHz. The measured response has a full-width at half-maximum (FWHM) of 20.5 ps, which agrees reasonably well with a value of 23 ps calculated from the specified bandwidths of the photodetector and oscilloscope [107]. The small subsidiary peaks in the interval between pulses are due to residual electronic ringing of the sampling-head/oscilloscope.

As indicated by Figure 3-4, the intended use of the fast-photodiode detection system is not for making measurements of the temporal profile of the short pulses generated in this work, but rather to ensure that pulse train is stable and free of satellite pulses in the period between mode-locked pulses. This measurement configuration was also particularly useful for determining the repetition rate of oscillator when operated under conditions of harmonic mode-locking, in which the repetition rate of the laser was varied from 500 MHz to over 7 GHz. In addition, the sampling oscilloscope was an essential component in experiments involving the synchronization of two mode-locked diode lasers. Synchronization was achieved by detecting the pulses from both lasers using the oscilloscope, which then allowed the relative timing jitter between the lasers to be minimized by improving the stability of the measured traces. Synchronization details will be elaborated on in Section 4.7.

3.4 Auto-Correlation and Cross-Correlation

Intensity auto-correlation and cross-correlation are two diagnostic techniques that are used in this thesis to characterize ultrashort pulses. Auto-correlation is a widely used technique for determining the duration of an ultrashort laser pulse, while cross-correlation can yield information about the temporal profile of a pulse, as well as an estimate of the relative timing jitter between synchronized lasers.

3.4.1 Auto-Correlation

The limited response time of current semiconductor-based photodetectors prevents the direct measurement of ultrashort optical pulses. To determine the duration of a pulse in the few ps to sub-ps regime, an indirect method based on auto-correlation can be used. A good overview of auto-correlation techniques can be found in a number of textbooks [108], [109]. A standard auto-correlator consists of a beam-splitter which separates an input pulse into two replicas. After propagating along different paths, the two pulses are recombined. By intentionally varying the path length of one of the pulses with respect to the other, the two pulses can be swept through each other, providing a mechanism to infer the pulse width.

A schematic of the auto-correlator constructed in this work is shown in Figure 3-5. The auto-correlator is based on a Michelson interferometer and is designed to measure the second-order interferometric auto-correlation, as well as the background-free (noncollinear) intensity auto-correlation. A 3-mm-thick 50/50 beam-splitter (20RQ00UB.2, Newport) with an AR coating applied to one surface separates the input beam into two replicas. In the case of the interferometric auto-correlation, the two pulses are retro-reflected and then recombined into a single collinear beam, as indicated in Figure 3-5(a). In the case of the background-free measurement, retro-reflector #1 is translated laterally such that the beam from one arm is displaced relative to the other (Figure 3-5(b)). Retro-reflector #2 is attached to a translation stage containing a motorized micrometer (Encoder Mike 18254, Oriel), which allows the path-length of the arm to be varied using a computer. The micrometer has a maximum travel of 25 mm and a resolution of 0.1 μm. The recombined pulses are focused into a 1-mm-thick

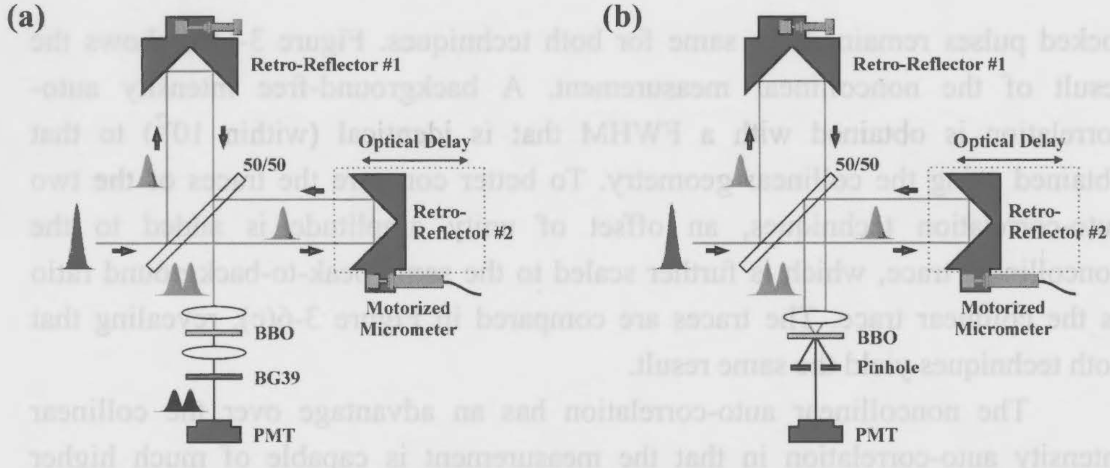

Figure 3-5: Schematic of an (a) interferometric auto-correlator with collinear pulses and (b) intensity auto-correlator with noncollinear pulses.

beta barium borate (BBO) nonlinear crystal and a photomultiplier tube (PMT) (1P28, Hamamatsu) is used in combination with a lock-in amplifier (SR510, Stanford) for detection.

Figure 3-6(a) shows a typical auto-correlation trace of a 3 ps pulse using the collinear configuration of Figure 3-5(a). The integration time of the lock-in amplifier is such that only the slowly varying envelope of the interferometric correlation function is recorded, effectively reducing the measurement to an intensity auto-correlation with background. Auto-correlation measurements are also made using the noncollinear configuration of Figure 3-5(b), in order to compare the results of the two auto-correlation techniques. Measurements are made within minutes of each other to ensure that the properties of the mode-

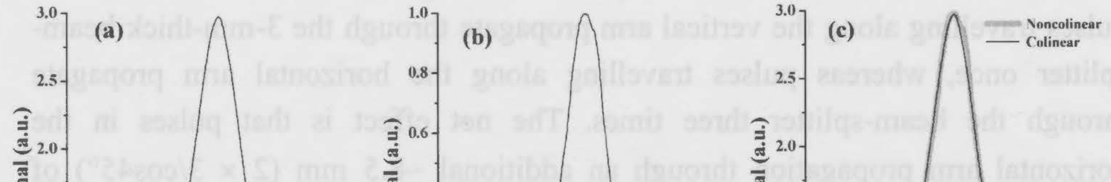

Figure 3-6: Intensity auto-correlation traces of a 3 ps pulse using (a) collinear and (b) noncollinear geometries. The two auto-correlation techniques are compared in (c).

locked pulses remained the same for both techniques. Figure 3-6(b) shows the result of the noncollinear measurement. A background-free intensity auto-correlation is obtained with a FWHM that is identical (within 10^{-2}) to that obtained using the collinear geometry. To better compare the traces of the two auto-correlation techniques, an offset of unity amplitude is added to the noncollinear trace, which is further scaled to the same peak-to-background ratio as the collinear trace. The traces are compared in Figure 3-6(c), revealing that both techniques yield the same result.

The noncollinear auto-correlation has an advantage over the collinear intensity auto-correlation in that the measurement is capable of much higher dynamic range [110]. The peak-to-background ratio of a collinear intensity auto-correlation is necessarily limited to a maximum value of 3 [111], whereas the noncollinear intensity autocorrelation can have a much higher ratio due to the absence of a background signal, yielding a more sensitive measure of the wings in the auto-correlation trace. In spite of the improved dynamic range of the noncollinear setup, in practice, intensity auto-correlations are made using the collinear geometry since it is far easier to align when working with relatively low-average-power pulses, such as those generated from a mode-locked semiconductor laser. The intricacy involved with the alignment of the noncollinear configuration stems from the fact that a signal is generated only when pulses overlap in both space and time in the nonlinear crystal, which can be a difficult condition to detect when working with relatively weak pulses.

From the definition of auto-correlation, the pulses in each arm of the interferometer should be identical in amplitude and phase. When the pulses are not identical, the measurement may be referred to as an unbalanced auto-correlation or a cross-correlation. Upon examining Figure 3-5, it is clear that pulses travelling along the vertical arm propagate through the 3-mm-thick beam-splitter once, whereas pulses travelling along the horizontal arm propagate through the beam-splitter three times. The net effect is that pulses in the horizontal arm propagation through an additional ~8.5 mm ($2 \times 3/\cos 45°$) of glass, or a net optical path length of ~12 mm. Pulses in the horizontal arm will differ from those in the vertical arm due to the dispersion of the glass, which causes additional pulse stretching and frequency chirping. To compensate for this effect, a piece of glass identical in thickness and composition to that of the beam-splitter can be placed in the vertical arm, eliminating the unbalance of the interferometer. To test whether the unbalanced auto-correlator of Figure 3-5 had a significant effect on the measurement of the pulses generated in this thesis, auto-

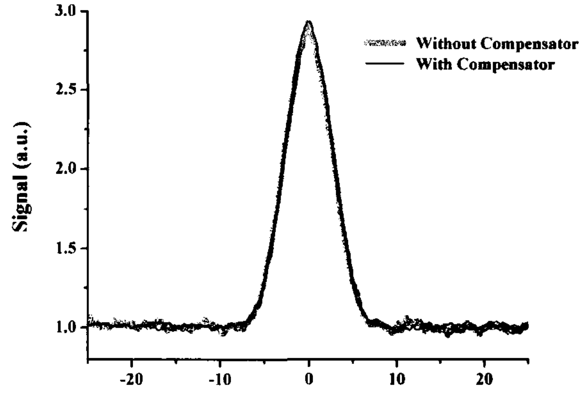

Figure 3-7: The effect of a compensating plate on the measured intensity auto-correlation of a 3.8 ps pulse. The unbalanced auto-correlator of Figure 3-5 (without compensator) is balanced by placing a 3 mm glass plate in the vertical arm of interferometer (with compensator).

correlations were conducted with and without a compensation plate. The results are shown in Figure 3-7 for a 3.8 ps pulse. Both auto-correlation traces are similar, indicating that the auto-correlator of Figure 3-5 is suitable for the measurement of the picosecond pulses. The lack of a measurable difference is not surprising since the additional 12 mm of glass will stretch a bandwidth-limited 1 ps Gaussian pulse by about 10^{-6} ps.

To determine when the compensation plate would be required, numerical simulations of the second-order interferometric auto-correlation were conducted using the formalism presented in [108]. Bandwidth-limited Gaussian-shaped pulses are assumed and the changes to the amplitude and phase of the electric field of the pulse due to the second-order dispersion of the glass are calculated using the equations given in [112]. The simulations revealed that a compensation plate is likely necessary when the level of unbalance is such that the pulses of each arm differ by more than a few percent in duration. Some of the simulation results are shown in Figure 3-8 for 100 fs and 30 fs pulses. The results are computed for an auto-correlator with an unbalance of 12 mm (optical path length) and correspond to the field-averaged interferometric (intensity) auto-correlation. The lack of a compensation plate becomes more prominent for shorter pulses, resulting in a reduction in the ratio and FWHM of the auto-correlation trace. Therefore, for sub-100-fs pulses, an unbalanced auto-correlator of the design used in this thesis could lead to an inaccurate estimate of the pulse duration.

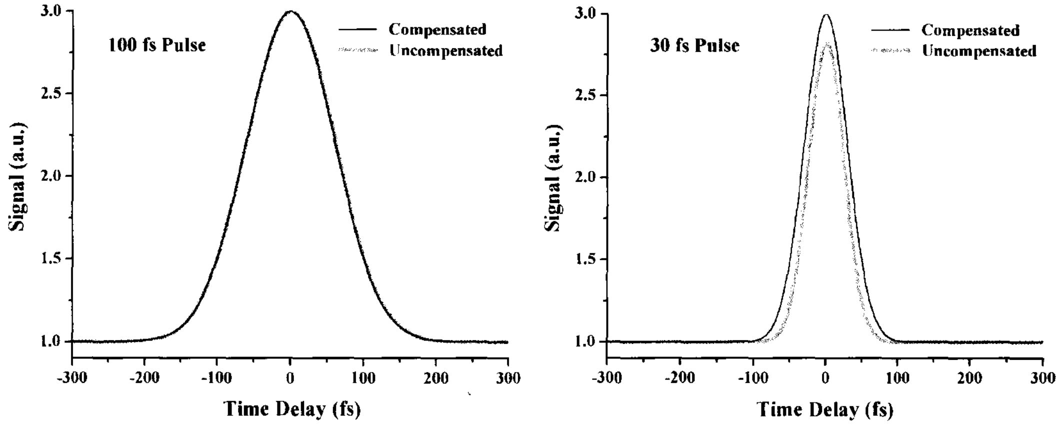

Figure 3-8: Simulated intensity auto-correlations showing the effect of a compensated interferometer for (*left*) 100 fs and (*right*) 30 fs bandwidth-limited Gaussian-shaped pulses.

The main limitation of the intensity auto-correlation technique is that it cannot provide a measure of the shape or phase of the optical pulse. By definition, the second-order auto-correlation yields a symmetric result. It has been shown that many different pulse intensity profiles can produce nearly the same intensity auto-correlation [109]. To obtain a measure of the pulse intensity profile, a more sophisticated spectrally-resolved auto-correlation technique can be adopted, such as the frequency-resolved optical gating approach [109]. The intensity profile of an ultrashort laser pulse can also be obtained using the optical cross-correlation measurement discussed below. For the measurements described in this thesis, a basic intensity auto-correlator is utilized since it is easily implemented and can provide a sufficient level of information on the mode-locked pulses, including a reasonable estimate of the duration of the generated and amplified pulses.

To obtain an estimate of the pulse duration from an intensity auto-correlation measurement, the auto-correlation data must be de-convolved by assuming an intensity profile for the pulse. For the results presented in this thesis, a sech^2 intensity profile is typically assumed since it produces a better fit to the auto-correlation data than other pulse shapes. However, it should be noted that the true intensity profile of a pulse generated by a mode-locked semiconductor laser is expected to exhibit some degree of temporal asymmetry [67]. For the laser synchronization experiments described in Paper 5 of Section 4.7, the auto-correlation traces were de-convolved by assuming a Gaussian pulse shape, which allowed the interlaser timing jitter to be easily calculated using a Gaussian distribution for the probability function of the relative timing jitter.

3.4.2 Cross-Correlation

The intensity cross-correlation of two pulses can be defined as [108]

$$A_c(\tau) = \int_{-\infty}^{\infty} I_s(t) I_r(t-\tau) dt \tag{3.1}$$

where $I_s(t)$ is the temporal intensity profile of a signal pulse, $I_r(t)$ is the temporal intensity profile of a reference pulse, and τ is the temporal delay between the two pulses. The measured signal, $A_c(\tau)$, differs from zero only when the two pulses overlap in time. Therefore, the reference pulse can be viewed as a measurement window which is shifted in time in order to sample $I_s(t)$. If $I_s(t) = I_r(t) = I(t)$, then Equation (3.1) simply reduces to an auto-correlation. If, however, the two pulses are different and the duration of the reference pulse is considerably shorter than that of the signal pulse, cross-correlating the two pulses can yield information about the temporal shape of the signal pulse. The ideal limit is achieved when $I_r(t)$ is a delta function, which reduces the measured correlation signal $A_c(\tau)$ to $I_s(t)$.

In this thesis, cross-correlation is used to obtain an estimate of the relative timing jitter between two synchronized lasers. In this case, $I_s(t)$ represents a pulse from one laser and $I_r(t)$ represents a pulse from the second laser. A variable delay present in the beam path of one laser allows the two pulses to be swept through each other as a function of time. Since the lasers are not perfectly synchronized, noise will cause each pulse to jitter in time about its mean position, changing the relative delay. Therefore, in the presence of timing noise, τ will effectively vary according to a statistical probability distribution and will lead to a broadening of $A_c(\tau)$. In the limit of low jitter, $A_c(\tau)$ is a standard cross-correlation, yielding information about the shape and width of each pulse. However, if the relative timing jitter is large enough such that the width of the jitter distribution is greater than the width of each laser pulse, then the cross-correlation signal begins to represent a measure of the temporal distribution of the relative timing jitter.

Intensity cross-correlation measurements are made by focusing pulses from both lasers into a 2-mm-thick BBO nonlinear crystal (Figure 3-9). A PMT (R6358, Hamamatsu) is used in combination with a lock-in amplifier (SR510, Stanford) to detect the sum-frequency cross-correlation signal generated by the BBO crystal.

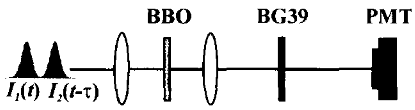

Figure 3-9: Configuration used for measuring the intensity cross-correlation of two pulses.

3.5 Pulse Compressor

A single-pass modified grating-pair pulse compressor [113] is used to reduce the temporal duration of chirped pulses. Chirped pulses can be obtained directly from the output of a mode-locked semiconductor laser or bandwidth-limited pulses can become chirped after propagating through a dispersive medium, such as an optical fibre. Pulse compression involves the canceling of the initial chirp of a pulse by sending it through a dispersive medium that exhibits a dispersion-induced chirp of the opposite sign. A schematic of the compressor is illustrated in Figure 3-10. Grating compressors primarily compensate for a linear frequency chirp (instantaneous carrier frequency increases linearly across the pulse in time). Light that is incident on the first grating is angularly dispersed, causing each frequency component to travel a slightly different path length. If the sign of the compressor dispersion is properly chosen, frequency components at the trailing edge of the pulse will travel a shorter path length, while frequency components at the front of the pulse will travel a greater path length, effectively narrowing the overall duration of the pulse.

The compressor consists of two 1800 lines/mm diffraction gratings and two lenses configured in a telescoped arrangement. The telescope is mounting on

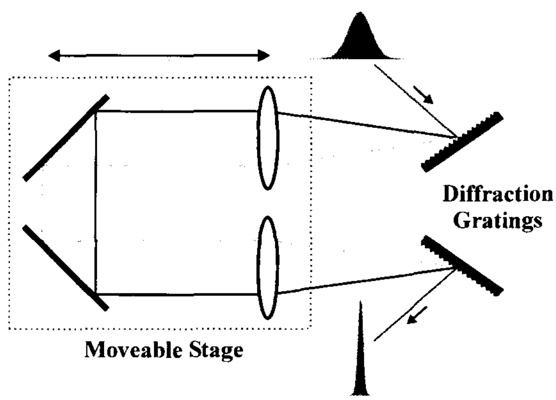

Figure 3-10: Schematic of the modified grating compressor used for pulse compression.

a moveable stage which permits the dispersion of the compressor to be adjusted. The transmission efficiency of the entire system is around 50 % due to the losses of the diffraction gratings.

3.6 Subtraction of ASE from Amplified Power Measurements

The optical output of an amplifier is composed of the amplified signal and ASE. In order to obtain a meaningful measure of the amplified signal power and therefore, the gain of the amplifier, the ASE power should be subtracted from the total power measurement. Although in practice the spectral amplitude of the ASE may be rather small, the broadband nature of the signal can result in a significant amount of power integrated over the entire spectrum of the ASE. For example, the FWHM bandwidth of a short picosecond pulse may only be 0.5 to 5 nm, whereas the FWHM of the ASE spectrum can be as large as 50 nm depending on the type of gain medium and level of pumping of the amplifier. ASE levels are expected to be the highest when the amplifier is operated at elevated pumping levels and the injected seed power is well below the saturation power of the amplifier.

ASE power is removed from the total amplified power using two methods. In the first approach, the total output power of the amplifier is measured using a thermal power meter which has a spectrally-flat responsivity over the bandwidth of the power measurement. The output of the amplifier is then coupled into an optical spectrum analyzer (OSA) to record the spectrum of the amplified signal and the ASE. By numerically integrating the measured spectrum, the percentage contribution of the ASE to the total power can be calculated.

The second approach involves using a monochromator to filter the broadband ASE from the amplified signal. The monochromator is configured to act as a band-pass filter, transmitting only a bandwidth of wavelengths that correspond to the spectrum of the amplified pulse. This is achieved using the following method. First, pulses from the mode-locked oscillator are coupled into the monochromator to obtain a measure of the system response of the monochromator at the wavelength of the pulses. The input slit of the monochromator is fully opened and the output slits are opened just enough to allow the mode-locked signal to pass through with minimal attenuation (relative signal change of less than $\sim 10^{-3}$). A wide-area photodiode and lock-in amplifier are used for detection. By recording the power of the oscillator beam prior to entering the monochromator and using the measured signal from the lock-in amplifier, the transmission efficiency of the system can be calibrated. Pulses from the oscillator are then coupled into the SOA and the amplified beam is sent into the monochromator along the same beam path as the oscillator. Using the calibration value, the amplified power within the bandwidth of the mode-locked signal can be calculated. There is still ASE within the finite bandwidth of the pulses (~0.5–5 nm), which can be accounted for to a degree. By blocking the optical input to the amplifier, the ASE at its highest possible unquenched value is recorded within the signal bandwidth. The power of the unquenched ASE can then be subtracted from the amplified power to obtain a worst-case estimate of the amplified signal power. A more accurate measure is obtained by taking into account the quenching of the ASE that occurs when the gain of the amplifier saturates due to the injection of a signal. This value is obtained by tuning the wavelength of the monochromator a few nanometers off the center of the signal (keeping the transmission bandwidth constant) in order to sample only the ASE. By blocking and unblocking the input to the amplifier, the relative quenching of the ASE can be obtained for a given set of operating parameters.

Both measurement approaches can provide a good estimate of the amplified signal power at the output of an optical amplifier. However, in practice, the first measurement approach is far more appealing due to the faster speed and convenience of the OSA. The uncertainty in the estimate of the amplified signal power using both techniques is expected to be less than 2 %.

An example of ASE quenching is illustrated in Figure 3-11 for a flared-SOA amplifying a cw signal at a wavelength of 1075 nm with a linewidth of less

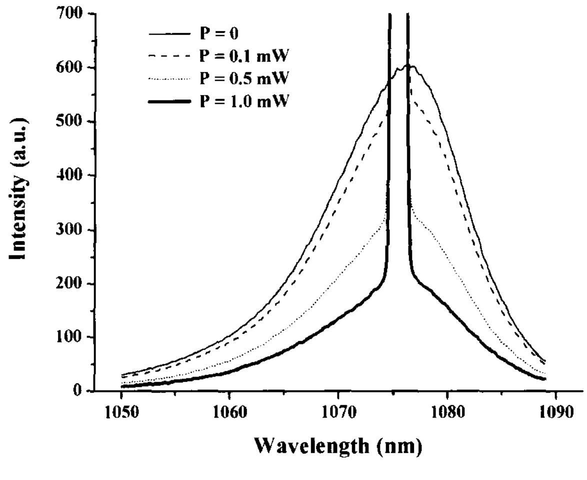

Figure 3-11: ASE quenching of a flared-SOA under cw injection conditions. The signal input power to the SOA is varied.

than 0.1 nm. The SOA is biased with a fixed current of 280 mA and the input power to the amplifier is varied. The peak of the amplified signal is truncated since the scale of the graph is chosen to emphasize the broadband ASE (the signal amplitude is $>10^4$). Near the emission peak of the ASE, the relative quenching can be as high as 70 % for an input power of 1 mW.

3.7 Experimental Configuration

Figure 3-12 shows a schematic of the experimental setup consisting of the mode-locked semiconductor oscillator, SOA, YDFA, and the diagnostic equipment. Most of the mirrors are mounted on kinematic base plates or connected to kinematic flip-mounts which allow the mirrors to be easily re-positioned in and out of the beam path giving both the laser beam and the amplified beam access to the diagnostic equipment without having to realign or alter the setup.

The oscillator is passively mode-locked by biasing the gain section with a DC current source (LDC-3724, ILX) and the absorber section with a DC voltage source (LV-2400, Keithley). The operating temperature of the laser is also maintained using the current source which has built-in temperature control capabilities. In the case of hybrid mode-locking, the RF sinusoid is generated by a signal generator (8648B, HP), amplified by a power amplifier (ZHL-2, Mini-Circuits) with a gain of 17 dB, and connected to the gain section of the oscillator using a bias-tee (ZFBT-66, Mini-Circuits). An RF power of up to 1 W is possible at the output of the RF amplifier. The feedback element in the external cavity can consist of either a diffraction grating or a mirror. Most of the mode-locking experiments were conducted using a 600 lines/mm grating, while some of the cw experiments required a 1800 lines/mm grating. In experiments involving the synchronization of two mode-locked diode lasers, the biasing for the second oscillator was provided by an additional current source (3900 with module 39427, ILX) and voltage source (238, Keithley). The ILX 3900 is a modular multi-channel laser diode controller which can independently control four different devices using separate biasing modules. The probing setup and external-cavity of the diode laser are housed in an acrylic box to minimize the accumulation of dust on the optics and to minimize air currents from perturbing the mode-locking.

The output of the oscillator is directed through a wavelength-tunable optical isolator (715 with option 730, Conoptics) containing an internal half-wave

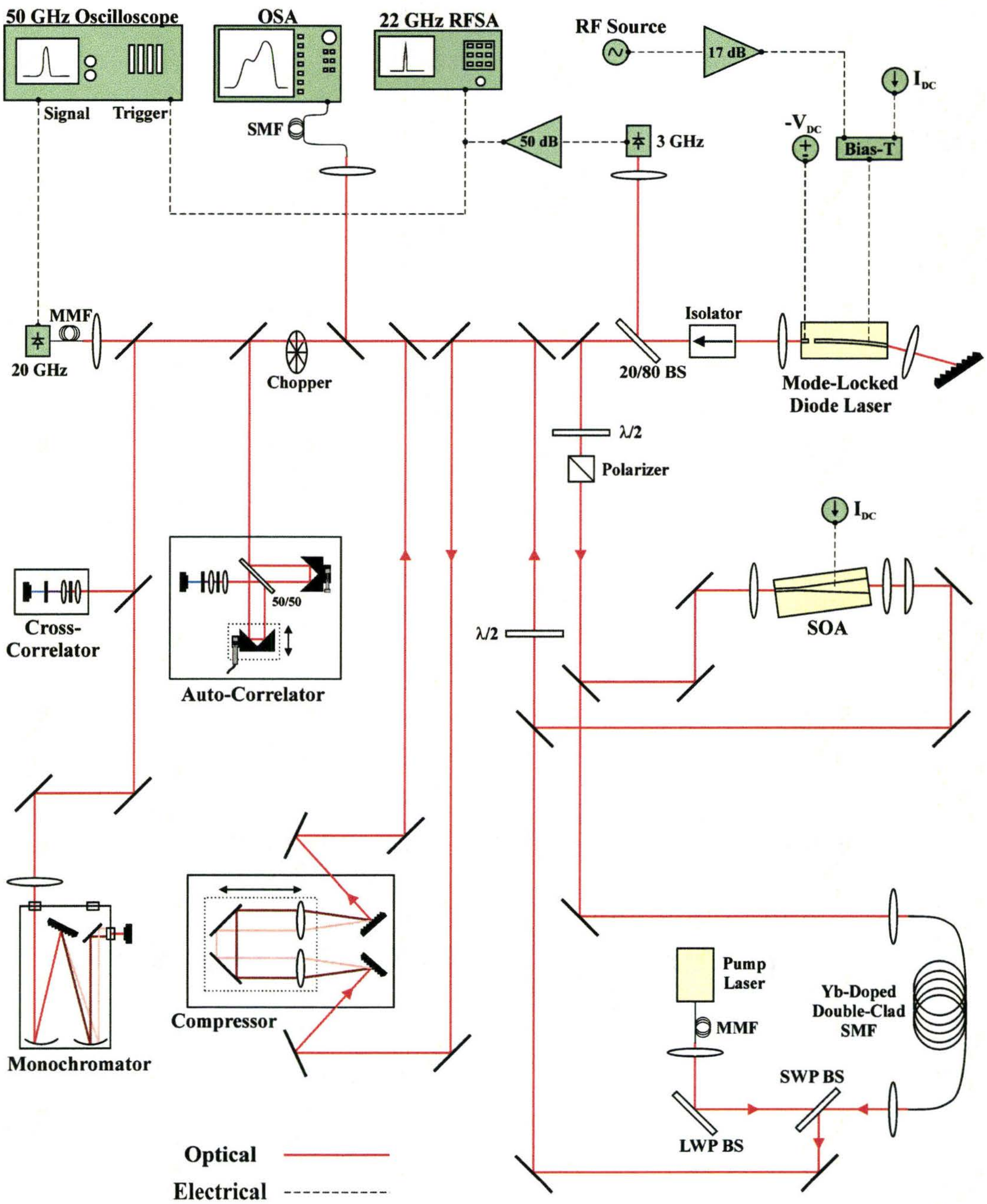

Figure 3-12: Schematic of the experimental setup consisting of the mode-locked semiconductor oscillator, SOA, YDFA, and diagnostic equipment. SMF: single-mode fibre; MMF: multi-mode fibre; BS: beam-splitter; SWP: short-wave pass; LWP: long-wave pass.

plate. A 20/80 beam-splitter reflects 20 % of the optical power to a 3 GHz photodiode for triggering purposes and the remaining power of the beam is directed to the optical amplifiers or to the diagnostic equipment. In most of the experiments, the 20/80 beam-splitter is left permanently in the beam path of the oscillator so that the properties of the mode-locked pulse train can be monitored during the course of an experiment. However, in situations where the full output power of the oscillator is required, the beam-splitter is removed.

A half-wave plate and polarizer are used to attenuate and control the input power to the optical amplifiers. The seed pulses can either be directed to the SOA or the YDFA for amplification. The SOA is biased using the ILX 3900 controller using separate modules to source current (39800) and control temperature (39427). The 39800 module is capable of supplying up to 8 A of current and is suitable for driving the flared-waveguide SOAs. A 9 cm plano-convex cylindrical lens is used at the output of the SOA to laterally collimate the beam.

The YDFA is optically pumped using a ~975 nm diode laser (LU0975M040, Lumics) which can deliver a maximum power of 4 W at the output of a 125 μm fibre pigtail. A diode laser controller (6000 with module 6560A, Newport) is used to adjust the drive current and temperature of the pump laser. The Yb-doped fibres studied in the experiments are all single-mode (core diameter ~6 μm) and are pumped counter-directionally to the propagation of the seed pulses. Coupling of the seed pulses into the doped core of the fibre is achieved using an 11 mm focal length AR-coated aspheric lens (C220TME-C, Thorlabs) and a 3-axis flexure stage (MDT616, Thorlabs). Pump light is launched into the inner cladding (diameter of ~125 μm) of the fibre using a 10× microscope objective and a 3-axis fibre coupling stage (F-916T with option F-91TS, Newport). A short-wave-pass dichroic beam-splitter (CVI) separates the amplified beam from the pump beam. The amplified beam from either the SOA or YDFA is directed back to the diagnostic equipment through a half-wave plate which orients the polarization of the beam to match that required by the auto-correlator (vertical).

Diagnostic equipment such as the sampling oscilloscope, auto-correlator, and cross-correlator have been discussed above. A small fraction of RF power is coupled from the amplified output of the 3 GHz photodiode into a 22 GHz RF spectrum analyzer (RFSA) (85938, HP) to monitor the phase noise characteristics of the mode-locked pulse train. A 1.5 GHz RFSA (E4411B, Agilent) is also used at various times for monitoring phase noise. Optical spectra are either measured using an OSA (AQ6315E, Ando) with a resolution of 0.05 nm or a monochromator (HRS-2, Jobin Yvon). The signals from the monochromator, auto-correlator, and cross-correlator are measured using lock-in detection (SR510, Stanford) and recorded using a data acquisition computer.

Power measurements are made using three different photodetectors: one semiconductor-based (PD-300-3W, Ophir) and two thermal heads (3A, 10A, Ophir). The semiconductor head comes with a detachable filter which increases the measurable power limit from 300 mW to 3 W. The 3A and 10A thermal heads are limited to 3 W and 10 W, respectively. Power measurements of the oscillator beam are typically made using the semiconductor head without the filter, while amplified power measurements are made using either the semiconductor head (with filter) or the 3A thermal head. The 10A head is used to measure the output power of the pump laser. The specified accuracy of the semiconductor head is ±5 % (without filter) and ±7 % (with filter), and the quoted accuracies of both thermal heads are ±3 %. The uncertainty in the accuracy of a power measurement is typically the largest source of error in an experiment. Since the semiconductor head is used routinely, power measurements have uncertainties of ±5 % for low-power signals and ±7 % for high-power signals, resulting in an uncertainty in the single-pass power gain of ±10 % and ±12 % for an SOA and YDFA, respectively.

Chapter 4 Experimental Results

4.1 Introduction

This chapter presents the experimental results on the development of an ultrashort-pulse laser system based on a mode-locked semiconductor oscillator operating near 1 μm. Experimental results include ultrashort-pulse generation using mode-locked diode lasers, pulse amplification using SOAs and YDFAs, and characterization of mode-locked laser noise. Near the end of this chapter, results are presented on the development a novel dual-wavelength short-pulse source based on the synchronization of two mode-locked semiconductor oscillators. Most of the results are presented in the form of four published journal articles and one manuscript accepted for journal publication (permission for the reproduction of published work is given in Appendix C). Reprints of each article are preceded by a short description of the work, as well as a discussion of the contributions of co-authors. For each article, my supervisor Prof. Harold Haugen was instrumental in the preparation of the final manuscript and provided invaluable support on the discussion and interpretation of results, including critical review. Additional discussions, experimental measurements, and comparisons to experimental results reported in the literature are provided following each contribution.

4.2 Pulse Generation with Mode-Locked Diode Lasers

This section highlights some key results on the generation of short pulses using passively mode-locked diode lasers. Since both the gain section current and absorber section voltage influence the dynamics of mode-locking, it is important to investigate and understand the optimal driving conditions for the laser. Systematic measurements of the average power, pulse duration, pulse bandwidth, and time-bandwidth product are presented for a mode-locked laser operating at a wavelength of 1075 nm and a pulse repetition rate of 577 MHz. The device used in the oscillator has a ridge width of 2.4 μm and an overall length of 640 μm. The lengths of the gain and absorber sections are 640 μm and 80 μm, respectively.

Figure 4-1 shows the variation in the pulse duration of the mode-locked laser as a function of the absorber voltage and gain current. The figure is subdivided into three regimes of operation: 1) no mode-locking, 2) stable mode-locking at the fundamental repetition rate of the cavity, and 3) unstable mode-locking and stable mode-locking at harmonic repetition rates. For gain currents less than 22 mA or for absorber voltages more positive than -0.9 V, it is not possible to generate short pulses with this device. Stable mode-locking at the fundamental repetition rate of the cavity (577 MHz) occurs for gain currents between 22–34 mA with absorber voltages in the range of -0.9 to -2.1 V. Mode-locking is defined to be stable when the generated pulses produce stable traces as measured by the sampling oscilloscope and RFSA, and when the peak-to-background ratio of the intensity auto-correlation approaches 3:1. Unstable mode-locking includes pulse trains that fluctuate in time (frequency) or intensity, contain satellite or secondary pulses, or yield auto-correlation traces with substructure or reduced peak-to-background ratios. This regime of operation tends

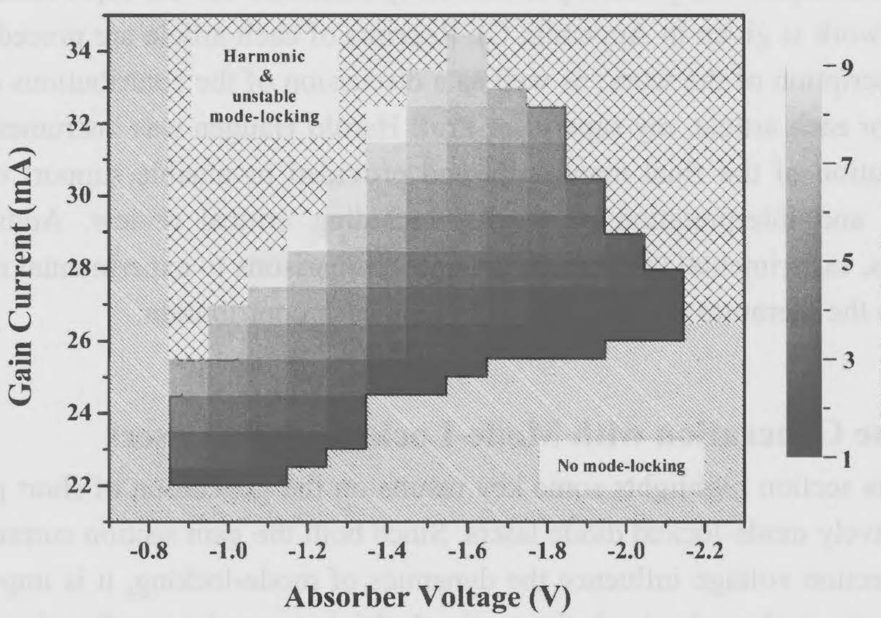

Figure 4-1: Dependence of pulse duration on absorber voltage and gain current for mode-locking at 577 MHz. Three regimes of operation are indicated in the figure. The grey-scale at the right gives the magnitude of the pulse duration under conditions of stable mode-locking.

to occur at elevated gain currents with large reverse voltages on the absorber. Harmonic mode-locking is also possible at elevated drive currents and represents a stable form of mode-locking whereby multiple, equally-spaced pulses circulate in the cavity. Harmonic mode-locking results will be presented in Section 4.5.

As illustrated in Figure 4-1, the minimum achievable pulse duration under conditions of passive mode-locking is affected by the driving conditions. Measurements are made in increments of 0.1 V and 1 mA, resulting in a discretized three-dimensional plot of the pulse duration. As indicated by the grey-scale shading, the shortest pulses are obtained for low gain currents or low absorber voltages. For a fixed gain current (absorber voltage), pulse duration decreases as the absorber voltage (gain current) is decreased. These trends are illustrated more clearly in Figure 4-2 and Figure 4-3, which also show the dependence of the average power, pulse bandwidth, and time-bandwidth on the biasing parameters. For a fixed absorber bias (Figure 4-2), a reduction in the gain section current produces pulses that are shorter and closer to the transform-limit, but with lower average power. Similarly, decreasing the absorber voltage at a fixed gain current (Figure 4-3) results in the generation of shorter pulses with a lower time-bandwidth product and a lower average power. Therefore, there exists a trade-off between minimizing the pulse duration and maximizing the average power, which cannot be overcome by varying either the absorber or gain section bias.

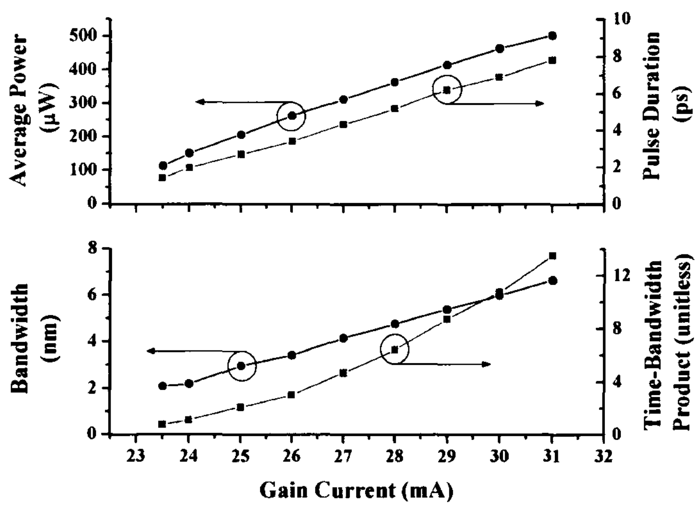

Figure 4-2: Variation of average power, pulse duration, pulse bandwidth, and time-bandwidth product for mode-locking at a fixed absorber voltage of -1.5 V.

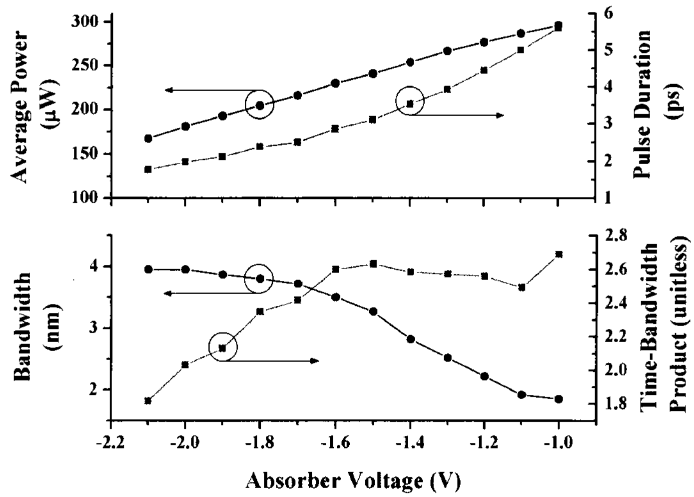

Figure 4-3: Variation of average power, pulse duration, pulse bandwidth, and time-bandwidth product for mode-locking at a fixed gain current of 25.5 mA.

The current- and voltage-dependent trends exhibited in Figure 4-1 to Figure 4-3 are typical of passively mode-locked semiconductor lasers. Increasing the current to the gain section of the laser increases the energy per pulse and decreases the recovery time of the gain medium. Pulses with higher energy lead to increased gain saturation and therefore, more SPM, resulting in spectrally broader pulses. Pulses with larger spectral content are more susceptible to temporal spreading after propagating through the gain region due to the finite frequency response of the amplifier [24], [114]. The increase in the pulse duration with drive current also occurs due to the fact that the recovery time of the gain medium varies inversely with current. As the gain recovery time decreases, the temporal window of net gain broadens during passive mode-locking, yielding a longer pulse. With respect to the absorber characteristics, increasing the magnitude of the reverse bias decreases the recovery time of the absorber [41], [115]. A shorter absorber recovery time will narrow the window of net gain, which reduces the duration of the generated pulse.

Although the results presented above are characteristic of a specific device, similar mode-locking trends were observed for other devices, including devices with different absorber and gain section lengths. The potential usefulness of the data is that in addition to determining the biasing limits of the oscillator, the data can be used as an operating map, enabling the generation of pulses optimized for a specific characteristic (e.g., short pulse duration, high average power, low chirp, etc.).

4.3 SOA Results

4.3.1 Paper 1: Narrow-Stripe Amplification of 1070 nm Mode-Locked Semiconductor Lasers

This paper presents results on the design, fabrication, and characterization of the 1070 nm mode-locked diode lasers and narrow-stripe SOAs. Details are provided on the growth of the active region, fabrication of the ridge-waveguide devices, and preliminary mode-locking and amplification results. The paper represents the first reported results of both ultrashort-pulse generation and amplification by electrically-pumped long-wavelength InGaAs-GaAs devices.

The primary author, M. Brennan, was responsible for the preparation of the majority of the manuscript. M. Brennan and I worked together on the design of the active region and the fabrication of the devices. M. Brennan was responsible for characterizing the lasers, while I was responsible for the SOA measurements. The laser and SOA structures were grown by B. Robinson, who also contributed to the manuscript by writing the section on the MBE growth of the structures.

1798 IEEE PHOTONICS TECHNOLOGY LETTERS, VOL. 16, NO. 8, AUGUST 2004

Ultrashort Optical Pulse Generation With a Mode-Locked Long-Wavelength (1075–1085 nm) InGaAs–GaAs Semiconductor Laser

Michael J. Brennan, *Student Member, IEEE*, Andrew J. Budz, Brad J. Robinson, Peter Mascher, and Harold K. Haugen

***Abstract*—Optical pulses are generated by passive and hybrid mode-locking of a long wavelength (1075–1085 nm) InGaAs–GaAs ridge waveguide laser grown by gas source molecular beam epitaxy. The devices are fabricated with two sections, one of which contains a bend in the waveguide for coupling to an external linear cavity. Pulses 2–5 ps in duration have been generated with average powers ranging from 750 μW to 1.8 mW. Pulse compression yields durations as short as 570 fs. Post amplification with a narrow stripe InGaAs–GaAs semiconductor optical amplifier increases the average output power up to 13 mW.**

***Index Terms*—Optical pulse compression, optical pulse generation, semiconductor lasers, semiconductor optical amplifiers (SOAs).**

I. Introduction

THERE HAS been considerable interest over the last decade in the development of InGaAs–GaAs semiconductor lasers with an emission wavelength beyond 1000 nm [1]–[9]. Long wavelength operation is typically achieved by growing a single InGaAs quantum well with large indium content, incorporating strain compensating GaAsP barriers, or by growing on misoriented GaAs substrates. Most of the reported work to date deals with the continuous-wave operation of the lasers. An ultrashort pulse semiconductor laser operating within the wavelength range of 1000–1200 nm would be attractive for two-photon excitation, instrumental applications, and could be an attractive seed source for post amplification in an ytterbium-doped fiber. While direct short pulse generation from an ytterbium-doped fiber has been recently demonstrated [10], [11], rather complex cavities are required to manage the dispersion in the system. Using a short pulse semiconductor laser as a seed source would allow for a simple cavity design and the ability to achieve high, and variable, repetition rates. Garnache *et al.* have reported short pulse generation from an optically pumped passively mode-locked vertical-cavity surface-emitting laser operating at 1040 nm [12], however, to the best of the authors' knowledge, there are no reports on mode-locking of electrically pumped edge-emitting long wavelength InGaAs–GaAs lasers. In this letter, we report on our first results on the fabrication, short pulse generation, and pulse amplification of ridge-waveguide lasers and semiconductor optical amplifiers (SOAs) operating at a wavelength between 1075 and 1085 nm.

TABLE I
LONG WAVELENGTH InGaAs–GaAs LASER STRUCTURE

Layer	Material	Thickness	Doping
Contact	p+ GaAs	0.15 μm	> 1 x 10^{19}/cm^3
Cladding	p InGaP	0.95 μm	1 x 10^{18}/cm^3
Cladding	p InGaP	0.35 μm	8 x 10^{17}/cm^3
Etch stop	p GaAs	5 nm	5 x 10^{17}/cm^3
Cladding	p InGaP	0.12 μm	3 x 10^{17}/cm^3
Barrier	GaAs	110 nm	-
Quantum Well	InGaAs	6 nm	-
Barrier	GaAs	110 nm	-
Cladding	n InGaP	1.37 μm	1 x 10^{18}/cm^3
Buffer	n+ GaAs	0.1 μm	> 1 x 10^{18}/cm^3
Substrate	n+ GaAs	0.1 μm	> 1 x 10^{18}/cm^3

II. Laser Structure and Waveguide Geometry

The material structure used for both the oscillator and the SOA is shown in Table I. The structure was grown by gas-source molecular beam epitaxy (GS-MBE) in which the group V species, As_2 and P_2, are derived from cracking AsH_3 and PH_3 over a Ta filament at 1000 °C, while the group III species are derived from elemental Ga and In evaporated from conventional effusion cells. The p-type and n-type dopants, also obtained from conventional effusion cells, are Be and Si, respectively. Prior to growing the final device structure, calibration runs were performed to evaluate the growth conditions for the GaAs–InGaAs–GaAs quantum well and to achieve a room-temperature photoluminescence (PL) wavelength for the quantum well of approximately 1065 nm. The PL wavelength of 1065 nm was obtained for an In fraction of about 0.27. In this GS-MBE machine, the optimized substrate growth temperature (based on PL intensity and linewidth) for a 980-nm quantum well is 515 °C. However, for higher In content required for PL emission at 1065 nm, a temperature of 515 °C results in a broadened PL linewidth (about 100 nm) and relatively low intensity. Lowering the temperature to 480 °C increased the PL intensity by a factor of four and reduced the linewidth to 37 nm. The mechanism responsible

Manuscript received April 13, 2004; revised May 6, 2004. This work was supported in part by the Canadian Institute for Photonics Innovations, in part by the Networks of Centres of Excellence, and in part by the Natural Sciences and Engineering Research Council of Canada.

M. J. Brennan, A. J. Budz, and P. Mascher are with the Department of Engineering Physics, McMaster University, Hamilton, ON L8S 4L7, Canada (e-mail: brennamj@mcmaster.ca).

H. K. Haugen is with with the Department of Engineering Physics, McMaster University, Hamilton, ON L8S 4L7, Canada, and also with the Department of Physics and Astronomy, McMaster University, Hamilton, ON L8S 4L7, Canada.

B. J. Robinson is with the Centre for Electrophotonic Materials and Devices, McMaster University, Hamilton, ON L8S 4L7, Canada.

Digital Object Identifier 10.1109/LPT.2004.831320

1041-1135/04$20.00 © 2004 IEEE

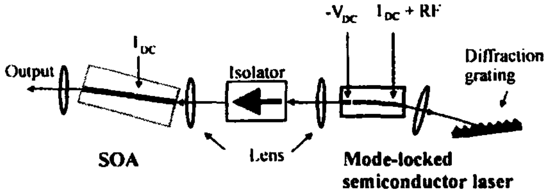

Fig. 1. Experimental setup for short pulse generation and amplification. Note that in some of the external cavities used, a mirror was used in place of the diffraction grating.

for PL degradation at the higher growth temperature is expected to be In segregation in both the growth and lateral directions. The segregation is driven by the strain arising from the lattice mismatch between the InAs and GaAs constituents of the InGaAs alloy. Lowering the growth temperature reduces the In adatom surface mobility which in turn suppresses the segregation process. Consequently, the active region of the device structure was grown with the lower substrate temperature of 480 °C.

Ridge-waveguide devices with ridge widths measuring approximately 3 μm are fabricated from the material using conventional photolithography processes and wet chemical etching. The bottom contact consists of a Ni–Ge–Au alloy and Ti–Pt–Au is used for the top contact. All of the devices are cleaved and bonded n-side down to a copper heat sink using silver epoxy.

The threshold current of a 300-μm-long as-cleaved device operating at 20 °C was 9 mA. The laser had a differential quantum efficiency of 0.62 W/A, which was found to be typical for this device length. At a drive current of 30 mA, the laser oscillates at a wavelength of 1081 nm. A maximum output power of 10 mW is achievable at a drive current of 65 mA. Beyond 65 mA, the performance of this short device degrades permanently. The output mode profile consists of a single mode in the lateral direction while the transverse direction contains substructure. It is believed that modifications to the waveguide design would improve the spatial output profile in the transverse direction.

The devices used for short pulse generation consist of geometry similar to that reported in [13]. A two-section device is fabricated by etching through the ridge during the device processing stage. The gain section of the device contains a bend such that the ridge terminates at an angle of 7° relative to one of the facets. The device measures 900 μm in length. The absorber section is 90 μm long and is separated from the gain section by a 10-μm gap. The 800-μm-long gain section consists of a 700-μm-long bend with a radius of curvature of 5700 μm and a 100-μm-long straight section. A SiO_xN_y antireflection (AR) coating is deposited on the angled facet by plasma-enhanced chemical vapor deposition.

The SOAs used in the experiment are narrow-stripe ridge-waveguide devices measuring 800 μm in length. The waveguide terminates at an angle of 7° relative to the facet normal at both ends of the device. AR coatings are deposited on both facets.

III. Experimental Setup and Results

The experimental setup is shown in Fig. 1. The master oscillator is mounted in a linear external cavity with the feedback element consisting of either a diffraction grating or a mirror. The

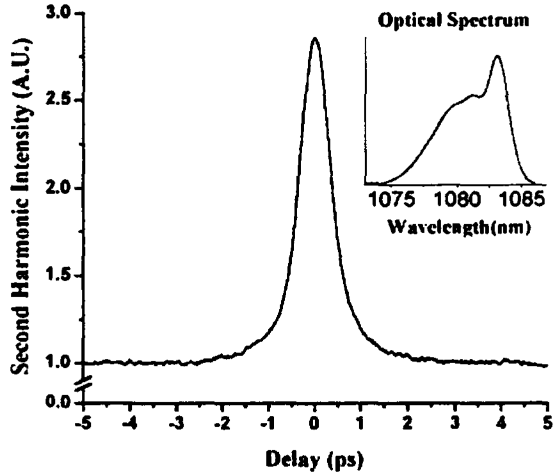

Fig. 2. Autocorrelation trace of a pulse following compression. Assuming a Gaussian pulse shape, the pulse duration measured 570 fs. The optical spectrum of the pulse train is shown in the inset.

external cavity allows for control over the wavelength of operation and the pulse repetition rate of the oscillator. The gain section of the oscillator is connected to a dc bias and a radio-frequency (RF) source via a bias-T. The RF signal is generated by an HP 8648B signal generator and amplified by a Mini-Circuits ZHL-2-S microwave amplifier. The total RF power can be as high as 1 W measured at the output of the amplifier. A reverse dc bias is applied to the absorber section of the device. Pulses are generated by either passive mode-locking, in which case there is no RF applied, or hybrid mode-locking. In order to increase the power of the pulse train, an SOA is used for post amplification. Pulse durations are measured with a collinear second order intensity autocorrelator employing a 2-mm-thick beta-barium-borate crystal and spectra are measured using a monochromator.

Pulses generated by the oscillator under passive mode-locking and hybrid mode-locking are typically 2–5 ps long. The duration is determined by measuring the full-width at half-maximum of the autocorrelation trace with an assumed Gaussian pulse shape. The length of the external cavity used corresponds to a repetition rate of approximately 850 MHz. Average powers at the output of the oscillator vary from as low as 750 μW to as high as 1.8 mW. Under the experimental conditions tested, there was no discernable difference in minimum pulse duration achievable under passive mode-locking as compared with hybrid mode-locking. However, hybrid mode-locking has the advantage of increased stability and a larger parameter range over which the oscillator will remain mode-locked. This allows the operating parameters to be modified to optimize the output power, and as such, hybrid mode-locking of this oscillator tends to yield higher average output powers as compared with passive mode-locking of the oscillator.

An external modified grating pair compressor consisting of two 1800-lines/mm diffraction gratings is used to compress the pulses generated by the oscillator. Pulse durations as short as 570 fs are obtained following compression. The autocorrelation trace of a 570-fs pulse train is shown in Fig. 2. The uncompressed pulse measures 4.2 ps in duration, and is obtained via

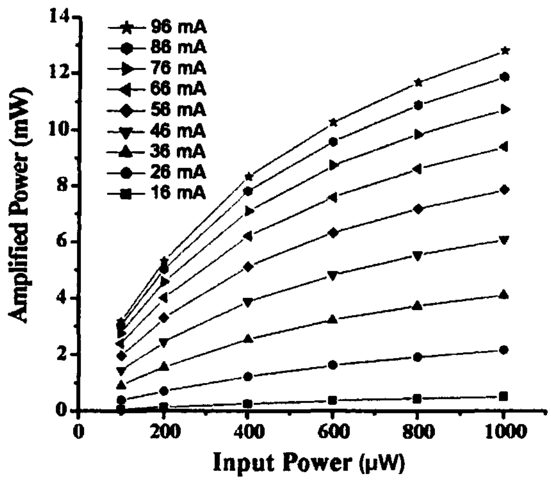

Fig. 3. Average output power following amplification of 3-ps pulses operating at a repetition rate of 850 MHz, tuned to the gain peak of the SOA (1077 nm). The SOA drive current is varied from 16 to 96 mA. Amplified spontaneous emission has been subtracted from the measurements by filtering the signal with a monochromator.

hybrid mode-locking at a repetition rate of 873 MHz with an RF power of 11 dBm. The absorber section is biased with −1.4 V and the gain section is driven with 56 mA. A mirror is used as the feedback element in the external cavity. The average power is reduced from 1.8 mW to approximately 900 μW following compression due to the losses of the diffraction gratings.

Average powers as high as 13 mW are obtained by post amplification with an SOA. This output power is obtained by amplifying an 850-MHz 3-ps pulse train with an average power of 1 mW with a central wavelength of 1077 nm. Note that 1077 nm corresponds to the gain peak of the SOA. The drive current on the SOA measures 96 mA. The output power of the amplifier versus input power for different injection currents into the SOA is shown in Fig. 3. At the highest current tested, the gain of the SOA for low input levels is 15 dB, while increased saturation reduces the gain to 11 dB for larger input powers. It should be noted that the gain values quoted are the system gain of the SOA and do not take into account the substantial coupling losses at the input of the SOA. Under the conditions tested, there was minimal distortion to the pulsewidth and pulse spectrum following amplification.

IV. Summary

We have demonstrated for the first time ultrashort pulse generation and pulse amplification by electrically pumped long wavelength (1075–1085 nm) InGaAs–GaAs devices. Pulse compression yields durations as short as 570 fs while post amplification with an SOA yields average powers as high as 13 mW. Work is currently underway to further increase the amplifier output power by using a flared geometry SOA. Future work could explore the possibility of asymmetric quantum-well structures [13] yielding broader tuning ranges relevant to biophotonics studies. Overall, this system appears to be attractive for a range of applications and as a seed source for short pulse amplification in ytterbium-doped fiber power amplifiers.

Acknowledgment

The authors would like to thank S. McFaul for her help with device processing and device testing and S. G. Wallace for past contributions to the project.

References

[1] R. G. Waters, P. K. York, K. J. Beernink, and J. J. Coleman, "Viable strained-layer laser at λ = 1100 nm," *J. Appl. Phys.*, vol. 67, pp. 1132–1134, Jan. 1990.

[2] A. Ishihara and H. Watanabe, "Long-wavelength (1072 nm) strained InGaAs quantum-well lasers grown on 1.0° misoriented (111)B GaAs," *Jpn. J. Appl. Phys.*, vol. 33, pp. 1361–1362, Mar. 1994.

[3] N. K. Dutta, W. S. Hobson, D. Vakhshoori, H. Han, P. N. Freeman, J. F. de Jong, and J. Lopata, "Strain compensated InGaAs-GaAsP-InGaP laser," *IEEE Photon. Technol. Lett.*, vol. 8, pp. 852–854, July 1996.

[4] D. Schlenker, T. Miyamoto, Z. Chen, F. Koyama, and K. Iga, "1.17 μm highly strained GaInAs-GaAs quantum-well laser," *IEEE Photon. Technol. Lett.*, vol. 11, pp. 946–948, Aug. 1999.

[5] H. Asano, M. Wada, T. Fukunaga, and T. Hayakawa, "Temperature-insensitive operation of real index guided 1.06 μm InGaAs/GaAsP strain-compensated single-quantum-well laser diodes," *Appl. Phys. Lett.*, vol. 74, pp. 3090–3092, May 1999.

[6] F. Bugge, G. Erbert, J. Fricke, S. Gramlich, R. Staske, H. Wenzel, and U. Zeimer, "12 W continuous-wave diode lasers at 1120 nm with InGaAs quantum wells," *Appl. Phys. Lett.*, vol. 79, pp. 1965–1967, Sept. 2001.

[7] T. Piwoński, P. Sajewicz, J. M. Kubica, M. Zbroszczyk, K. Regiński, B. Mroziewicz, and M. Bugajski, "Long-wavelength strained-layer InGaAs/GaAs quantum-well lasers grown by molecular beam epitaxy," *Microwave Opt. Technol. Lett.*, vol. 29, pp. 75–77, Apr. 2001.

[8] N. Tansu and L. J. Mawst, "High-performance strain-compensated InGaAs-GaAsP-GaAs (l = 1.17 μm) quantum-well diode lasers," *IEEE Photon. Technol. Lett.*, vol. 13, pp. 179–181, Mar. 2001.

[9] L. W. Sung and H. H. Lin, "Highly strained 1.24 μm InGaAs/GaAs quantum-well lasers," *Appl. Phys. Lett.*, vol. 83, pp. 1107–1109, Aug. 2003.

[10] B. Ortac, A. Hideur, T. Chartier, M. Brunel, C. Ozkul, and F. Sanchez, "90-fs stretched-pulse ytterbium-doped double-clad fiber laser," *Opt. Lett.*, vol. 28, pp. 1305–1307, Aug. 2003.

[11] O. G. Okhotnikov, L. Gomes, N. Xiang, T. Jouhti, and A. B. Grudinin, "Mode-locked ytterbium fiber laser tunable in the 980–1070 nm spectral range," *Opt. Lett.*, vol. 28, pp. 1522–1524, Sept. 2003.

[12] A. Garnache, S. Hoogland, A. C. Tropper, I. Sagnes, G. Saint-Girons, and J. S. Roberts, "Sub-500-fs soliton-like pulse in a passively mode-locked broadband surface-emitting laser with 100 mW average power," *Appl. Phys. Lett.*, vol. 80, pp. 3892–3894, May 2002.

[13] M. J. Brennan, J. N. Milgram, P. Mascher, and H. K. Haugen, "Wavelength tunable ultrashort pulse generation from a passively mode-locked asymmetric-quantum-well semiconductor laser," *Appl. Phys. Lett.*, vol. 81, pp. 2502–2504, Sept. 2002.

As the above letter was only an initial report on the design and characterization of ultrashort-pulse generation and amplification using long-wavelength InGaAs-GaAs devices, additional narrow-stripe SOA results are included below. Figure 4-4 shows the measured gain profile of the amplifier. Measurements are made with the oscillator operating in a cw mode using the 1800 lines/mm diffraction grating in the external cavity, which creates a narrow emission linewidth of less than 0.1 nm. The input power to the amplifier is 1 mW and the gain is measured for several different drive currents. The measured gain values represent the system gain of the SOA and do not take into account the efficiency with which light is coupled into the active region of the SOA. Although the amplification of a cw signal is less relevant to this thesis than the amplification of pulsed light, the measurement is nevertheless useful for characterizing the gain spectrum of the amplifier. The 3 dB gain bandwidth is estimated to be greater than 50 nm at the highest bias current.

The measured auto-correlation traces and spectra of the seed and amplified pulses for the SOA experiments described in Paper 1 are presented in Figure 4-5. The pulse duration remains unchanged following amplification (3 ps) and only minimal spectral distortion is obtained for the operating conditions tested. The noise ratio of the amplified output beam, defined as the ratio of the ASE power to the combined amplified signal plus ASE power, is less than 1 %. Although the amplified average signal power is relatively low (13 mW), the spectral purity of

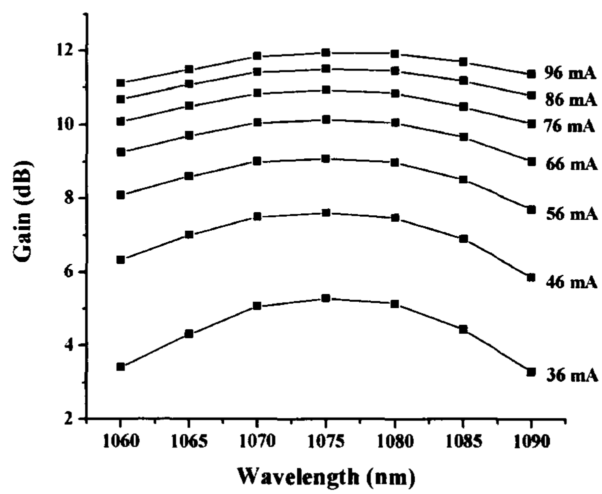

Figure 4-4: Measured gain spectrum of an 800-μm-long narrow-stripe SOA for different bias currents. The cw input power is 1 mW.

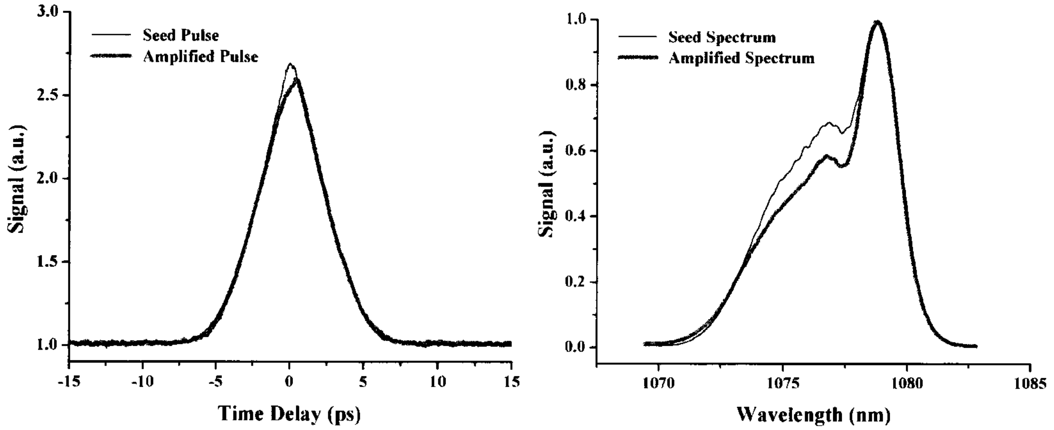

Figure 4-5: (*left*) Auto-correlation traces and (*right*) spectra of the seed and amplified pulses used in the narrow-stripe SOA experiments of Paper 1.

the amplified signal is very good and excellent performance would be obtained by injecting the amplified pulses into a second stage of amplification (power-amplifier). Therefore, the narrow-stripe SOAs fabricated for this thesis can be regarded as good-performance low-power pre-amplifiers.

An estimate of the small-signal gain and saturation energy of the 800-μm-long narrow-stripe SOA can be obtained by applying Equation (2.7) to the data presented in Fig. 3 of Paper 1. For these calculations, the coupling efficiency at the input (18 %) and the capture efficiency at the output (80 %) of the SOA are taken into account in order to determine the internal parameters of the SOA chip. Figure 4-6 shows the measured gain of the SOA as a function of the average output power, as well as the results of the nonlinear curve fitting using Equation (2.7). Accurate low-power measurements were not made in the linear (unsaturated) gain regime of the SOA since the amplifier output would be composed of mainly ASE at low input powers and the uncertainty in the measurement of the amplified signal power would be large. Therefore, the small-signal gain and saturation energy of the SOA can only be estimated based on the nonlinear curve fits to the measured data. At the highest current tested, the small-signal gain and saturation energy are ~25 dB and ~10 pJ, respectively.

The performance of the 1070 nm narrow-stripe SOAs are on par with other narrow-stripe amplifiers, though it is difficult to make a fair comparison for several reasons. First, there are no reported results of short-pulse amplification using long-wavelength InGaAs-GaAs devices. Second, when comparing the performance of the 1070 nm InGaAs devices to other SOAs operating at different

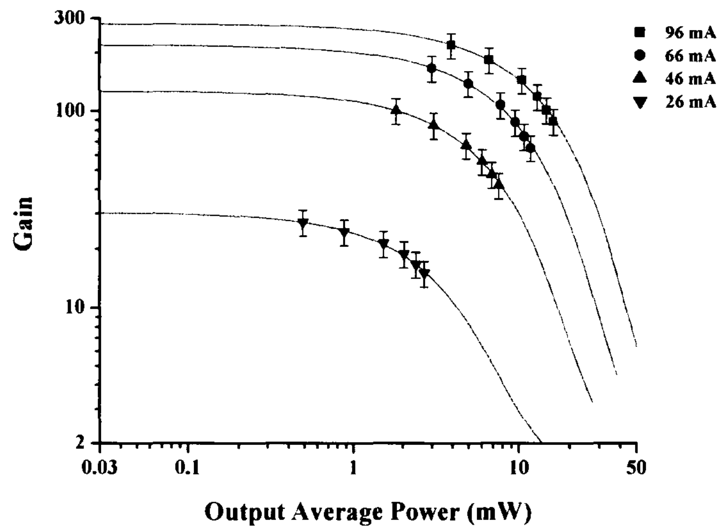

Figure 4-6: Gain versus output average power for the narrow-stripe experiments described in Paper 1. The SOA is amplifying an 840 MHz train of 3 ps pulses at 1077 nm. The saturation curves are fitted to the measured data using Equation (2.7).

wavelengths and based on different materials, the active regions are usually quite dissimilar. For example, most of the reported narrow-stripe SOAs are either based on bulk active layers or multiple quantum-well active regions, whereas the current devices contain only a single quantum-well. Finally, the relevant design and operating parameters (e.g., active region volume, bias current, pulse duration, pulse repetition rate, coupling losses, how ASE is accounted for) are not the same and are not always quoted in the literature. In spite of the above issues, some performance benchmarks of 980 nm SOAs will be given, followed by relevant results from the literature, in an attempt to put the results obtained from the 1070 nm narrow-stripe SOAs into context.

Measurements have been made on the amplification characteristics of 980 nm narrow-stripe SOAs containing two compositionally asymmetric quantum-wells. The SOA is 550-μm-long with a 4 μm ridge width and the transition wavelengths of the two wells are 965 and 995 nm. At a bias current of 80 mA and an input average power of 1 mW, approximately 14 mW of amplified signal is obtained. The input pulses have a duration of 2.7 ps, center wavelength of 975 nm, and repetition rate of 687 MHz. The estimated small-signal system gain (does not include coupling losses) is 20 dB and the saturation energy is 5 pJ. Additional measurements have been made in our research group on the amplification of short pulses using 980 nm narrow-stripe SOAs containing two symmetric quantum-wells [116]. For an 870-μm-long SOA biased at a current of 130 mA, 15 mW of amplified power is obtained for a 550 μW input signal consisting of 3.5-ps-pulses at a repetition rate of 750 MHz and a center wavelength of 985 nm.

Delfyett *et al.* have characterized a 250-μm-long bulk active layer AlGaAs narrow-stripe SOA operating at a wavelength of 870 nm [18]. For an amplifier bias current of 225 mA and an injected power of 480 μW, the average power following amplification is 14 mW. The input pulses are 15 ps in duration and have a repetition rate of 960 MHz. Amplified pulses are reported to be free of temporal and spectral distortions. Saitoh *et al.* have obtained a small-signal gain of 24.5 dB and a saturation energy of 3.5 pJ for a 250-μm-long bulk active layer 1.3 μm InGaAsP SOA [117]. The SOA is biased at 70 mA of current and is characterized using 100 MHz pulses that range in duration from 0.49 to 21 ps. The saturation characteristics of the SOA are shown to be independent of the pulse duration for conditions tested. Finally, Eisenstein *et al.* have reported on the amplification of 10 ps pulses at a repetition rate of 76 MHz using a 1.5 μm multiple quantum-well InGaAsP SOA [78]. For a device length of 250 μm, the small-signal gain is 15 dB and the saturation energy is 4 pJ at a bias current of 150 mA.

4.3.2 Paper 2: Flared-Waveguide Amplification of 1070 nm Mode-Locked Semiconductor Lasers

As the output power of a narrow-stripe SOA is somewhat limited, flared-waveguide devices were investigated as a means of scaling the power level of the ultrashort-pulse laser system. A flared-waveguide SOA could be used as a pre-amplifier for a much higher gain Yb-doped power-amplifier. This paper presents results on the design and characterization of a MOPA system consisting of a flared-waveguide SOA. I was responsible for the writing of the manuscript, fabrication of the devices, experimental measurements, and analysis. I would like to acknowledge B. Robinson for the growth of the SOA structure using the MBE facility at McMaster University.

3766 JOURNAL OF LIGHTWAVE TECHNOLOGY, VOL. 25, NO. 12, DECEMBER 2007

Ultrashort Pulse Amplification at 1080 nm With a Long-Wavelength InGaAs–GaAs Flared Amplifier

A. J. Budz, *Student Member, IEEE*, and H. K. Haugen

***Abstract*—Pulses of 5 ps in duration have been amplified using a long-wavelength InGaAs–GaAs semiconductor optical amplifier containing a flared waveguide. The amplifier is seeded using short pulses emitted by a passively mode-locked semiconductor laser. Average output powers of 50 mW have been obtained at a center wavelength of 1080 nm for a drive current of 290 mA. Pulse compression yields durations as short as 520 fs and peak powers as high as 40 W. Perspectives for combining the semiconductor master oscillator power amplifier with Yb fiber amplifiers in a hybrid configuration are also briefly discussed.**

***Index Terms*—Optical pulse amplifiers, semiconductor lasers, semiconductor optical amplifiers (SOAs).**

I. Introduction

COMPACT sources of ultrashort optical pulses with emission wavelengths in the near infrared ($\sim$1 μm) are attractive for a number of applications. Mode-locked semiconductor lasers have drawn considerable attention as inexpensive and reliable sources of short pulses. Long-wavelength semiconductor lasers operating at wavelengths above 1000 nm can be developed using the InGaAs–GaAs material system through the growth of strained InGaAs quantum wells that contain a relatively large concentration of indium [1], [2]. Recently, we have reported the first results on the mode locking of electrically pumped long-wavelength InGaAs–GaAs lasers, where we obtained 2-ps pulses at a center wavelength of 1080 nm [3]. Although ytterbium-doped fibers are capable of directly generating short pulses in the 1030- to 1100-nm range [4], semiconductor oscillators can offer attractive features such as lower complexity, simple cavity design, and the ability to readily achieve high and variable pulse repetition rates. When combined with a semiconductor optical amplifier (SOA) in a master oscillator power amplifier (MOPA) scheme, an all-semiconductor MOPA offers an attractive alternative for generating high power from an inexpensive and compact package. The monolithic integration of a pulsed semiconductor MOPA is still currently limited by the requirement for an integrated optical isolator, with the current technology offering insufficient isolation for mode-locked master oscillators (see, for example, [5]).

Manuscript received April 18, 2007; revised July 19, 2007. This work was supported in part by the Canadian Institute for Photonics Innovations, within the Networks of Centres of Excellence, and by the Natural Sciences and Engineering Research Council of Canada.

A. J. Budz is with the Department of Engineering Physics, McMaster University, Hamilton, ON L8S 4L7, Canada (e-mail: budzaj@mcmaster.ca).

H. K. Haugen is with the Department of Engineering Physics and Department of Physics and Astronomy, McMaster University, Hamilton, ON L8S 4L7, Canada.

Digital Object Identifier 10.1109/JLT.2007.909356

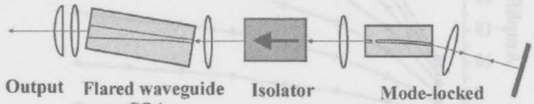

Fig. 1. Schematic of the mode-locked oscillator and flared amplifier. A mirror is used as the feedback element in the external cavity of the laser.

Novel SOA waveguide geometries such as flared [6] and inverse bow tie [7] have typically been used in high-power semiconductor systems. Although amplification has been demonstrated using GaAs-based flared-waveguide SOAs in the 780- to 980-nm range [8]–[10], we are not aware of pulse amplification using long-wavelength InGaAs–GaAs devices other than the preliminary results reported by our group [3], [11]. In this paper, we report on the picosecond-pulse amplification in a long-wavelength InGaAs–GaAs quantum-well flared-waveguide SOA, including details on the spectral, temporal, and spatial output characteristics, as well as the signal to amplified spontaneous emission (ASE) levels.

II. Device Structure and Experimental Setup

The material structure of the SOA is identical to the mode-locked semiconductor oscillator that has been previously described [3]. The epitaxial structures are grown lattice matched to GaAs using the gas-source molecular beam epitaxy facility at McMaster University. The design of the active region consists of a single 6-nm-thick compressively strained InGaAs quantum well surrounded by 110-nm GaAs barriers and an InGaP cladding. With an indium mole fraction of approximately 0.27, the quantum well layer is below the critical layer thickness [12]. Ridge waveguide devices are fabricated from the material using wet chemical etching and conventional photolithography.

The oscillator and the flared SOA are configured as a MOPA with an optical isolator that prevents the feedback of ASE into the oscillator (Fig. 1). The waveguide geometry of the SOA consists of a 310-μm-long narrow stripe section followed by a 2° linear flared section. The input ridge width is 3 μm, and the overall length of the amplifier is 1700 μm. Since the average power of the oscillator is relatively low, we use a fairly modest flare angle to limit the input power required to saturate the amplifier gain. Both amplifier facets are angled at 5° relative to the center axis of the waveguide and are antireflection (AR) coated with a single-layer SiO_xN_y thin film. Light is coupled into and out of the amplifier using either 3.1- or 4.5-mm focal-length AR-coated aspheric lenses. A cylindrical lens with a focal length of 9 cm is also used at the output of the flared SOA to collimate the amplified beam. The cylindrical

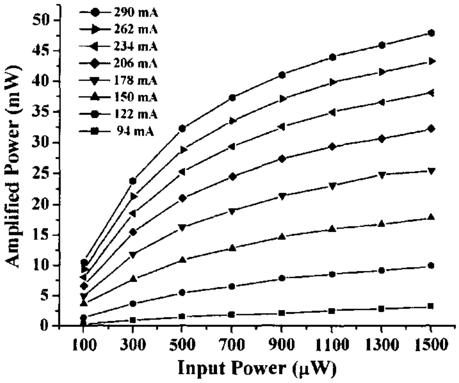

Fig. 2. Average output power following the amplification of 5-ps pulses operating at a repetition rate of 840 MHz. The input power is measured prior to coupling into the SOA (coupling efficiency is ~20%).

lens compensates for the output astigmatism that is introduced inside the amplifier as the optical mode laterally expands along the length of the device. The amplifier is thermally bonded to a length-matched copper heat sink using conductive silver epoxy, and the stage temperature is maintained at 20 °C.

Short pulses are generated by passively mode-locking an external-cavity semiconductor-based oscillator. The semiconductor chip contains integrated gain and saturable absorber sections, as well as a curved ridge waveguide that permits operation in a linear external cavity. Details regarding the design and operation of the oscillator can be found in [3]. Passive mode locking occurs over a broad bias parameter range with typical gain section currents of 20–50 mA and saturable absorber reverse voltages of −0.8 to −2.2 V. Pulse durations vary between 2 and 5 ps with repetition rates ranging from 0.8 to 6 GHz, and the average output powers are less than 2 mW.

Amplified power measurements are calculated by passing the amplified pulse train through a filtering monochromator to remove the broadband ASE from the mode-locked signal. Pulse durations are measured using a collinear intensity autocorrelator that contains a beta-barium-borate crystal, and the spectra are measured using a spectrometer with a resolution of 0.1 nm. The quoted pulsewidths are calculated by deconvolving the autocorrelation width using a hyperbolic-secant-squared pulse shape.

III. Results and Discussion

The saturation behavior of the SOA is characterized by operating the mode-locked oscillator close to the amplifier gain peak of 1077 nm. The seed pulses have a duration of 5 ps, center wavelength of 1080 nm, and repetition rate of 840 MHz. Fig. 2 shows the output power of the flared amplifier as a function of incident power for several drive currents. At a maximum current of 290 mA, approximately 50 mW of the amplified signal is obtained. At the highest current tested, the gain of the SOA chip for low input levels is 29 dB, whereas an increased saturation reduces the chip gain to 22 dB for an input power of 1.5 mW. The output saturation energy of the flared SOA is inferred from the gain measurements and has a value of 24 pJ. The characterization of the amplifier gain bandwidth is performed under continuous-wave (cw) injection conditions. The oscillator is operated in cw mode with a narrow emission linewidth of less than 0.1 nm. The measured 3-dB gain bandwidth is 28 nm for an incident power of 1 mW.

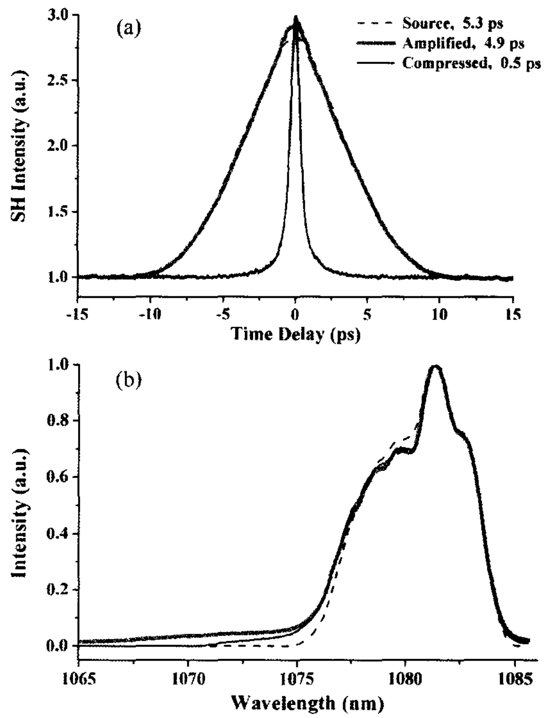

Fig. 3. (a) Second harmonic (SH) autocorrelation traces of the pulse train following amplification and compression. (b) Corresponding normalized optical spectra.

Fig. 3 illustrates the changes that occur to the pulse duration and spectrum following amplification. The pulse duration is slightly decreased, and only minor distortions are introduced to the optical spectrum as a result of amplification. The cause of pulse distortion in an SOA is due to gain saturation with the degree of distortion dependent on the level of saturation. Moreover, injecting chirped pulses into an SOA can affect the amount of spectral modification occurring during amplification, depending on the functional form of the initial chirp. As the seed pulses from the oscillator are quite low in energy relative to the amplifier saturation energy (~0.02), and the pulses are highly chirped, significant modifications to the pulse are not necessarily expected during amplification [13], given that there are uncertainties in the exact nonlinearity of the chirp and the temporal profile of the pulse. However, the presence of a cw component or satellite pulses with the main mode-locked signal could also lead to a lower degree of pulse modification than expected through amplification. Additional measurements are performed with a 50-GHz sampling oscilloscope and a 20-GHz photodiode, which provide a 20-ps impulse response time. They confirm that the seed pulses from the oscillator are stable in time with no observable cw component, as determined with a

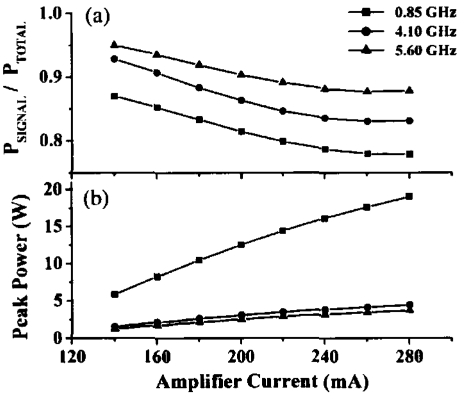

Fig. 4. (a) Relative signal level and (b) pulse peak power emitted by the diode MOPA as a function of the flared amplifier current for various pulse repetition rates. Note that $P_{\rm signal}$ is the amplified signal with ASE filtering, and $P_{\rm total}$ is the combined signal plus ASE power.

detection sensitivity of 10 μW of the optical power. In addition, the combination of the 20-GHz photodiode setup and the long-baseline scans of the autocorrelator over a time frame of 100 ps reveal no satellite pulses from the oscillator.

A modified grating pair compressor consisting of two 1800-lines/mm diffraction gratings is used to compress the amplified pulses. Pulse durations as short as 520 fs are obtained with compression. Due primarily to the losses of the diffraction gratings, the average power at the output of the compressor is reduced to 20 mW, which provides a peak power of over 40 W. A further benefit of compression is that it acts to spatially filter out the majority of the ASE from the amplified signal, which is evident in the compressed pulse trace in Fig. 3(b). The pulse spectral bandwidth after compression is 5.8 nm, which results in a time–bandwidth product of 0.77. The resulting pulses are a factor of 2.5 above their Fourier transform limit, which indicates the need for higher order dispersion compensation.

To examine the influence of ASE on amplifier performance and to determine the feasibility of the MOPA for nonlinear optical experiments, the amplified average signal level on a normalized scale and the pulse peak power are measured for various pulse repetition rates. The oscillator is tuned to the fundamental frequency of 850 MHz and to two harmonics, i.e., 4.1 and 5.6 GHz. Access to higher repetition rates is accomplished by operating the oscillator at the harmonics of the cavity round-trip frequency. Harmonic mode locking [14] is achieved by tuning the position of the external cavity mirror and by adjusting the bias parameters of the oscillator until the appropriate signal appears on a radio frequency spectrum analyzer. Fig. 4 shows the amplified relative signal level and pulse peak power (without post compression) as a function of the flared amplifier drive current for the three repetition rates. The average input power is kept constant at 1 mW for each trace. Fig. 4(a) illustrates the influence of ASE on the performance of the amplifier. The ASE buildup in an SOA is a competing process to the amplification of the mode-locked signal that limits both the gain and the output power. The growth of spontaneous emission between the optical pulses is a consequence of the finite gain recovery time of the semiconductor amplifier and is affected by the repetition rate of the injected pulses [15]. At the highest drive current, the amplified relative signal level increases from 77% to 88% as the repetition rate is increased from 0.85 to 5.60 GHz. Fig. 4(b) shows that the optimal MOPA peak power of 19 W is obtained at a repetition rate of 0.85 GHz.

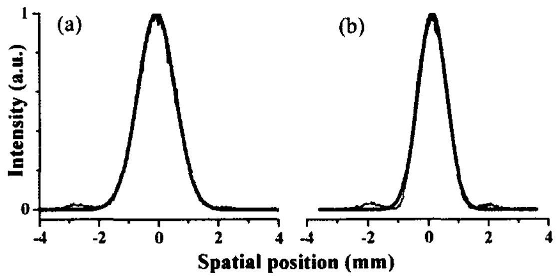

Fig. 5. (a) Lateral and (b) transverse sliced spatial profiles of the amplified beam using a 3.1-mm focal length collimating lens. Thick curves are Gaussian fits to the data.

The collimated spatial profile of the flared SOA at maximum output power is approximately Gaussian, as shown in Fig. 5. The subsidiary peaks in the profiles are the result of residual diffraction created by the coupling optics. We originally used a 4.5-mm collimating lens (for results shown in Figs. 2–4) at the SOA output, which resulted in an enhanced diffraction substructure in the transverse mode. Optimizing the output coupling by switching to a shorter focal length lens (3.1 mm) significantly reduced the effects of diffraction and further increased the amplified output power by about 7%.

The maximum drive current for this flared amplifier is limited to 290 mA. Much above this value, the device permanently degrades. When operated below the maximum drive current, we did not observe any decline in device performance during the course of the characterization experiments. The cause of the premature failure at high drive currents is believed to be associated with the fabrication of the oxide window on top of the ridge waveguide, which can be remedied by optimizing the processing parameters and particularly by optimizing mask designs in the future. Considering the restriction in current, the amplifier described here exhibits similar performance as the other flared amplifiers operating in other wavelength regimes at the same carrier density and input power [8], [9]. With an optimized device structure, we would expect to be able to scale the performance of the current flared amplifiers to several hundreds of milliwatts of average output power, which has been achieved with AlGaAs–InGaAs–GaAs devices operating at 940 nm [8].

In addition to stand-alone applications, semiconductor sources can be combined with the doped fiber technology in hybrid systems. We have recently demonstrated a passively mode-locked semiconductor laser as a seed source for a ytterbium-doped fiber amplifier (YDFA) [16]. The power launched into the Yb fiber ranged from 70 to 320 μW, and a maximum average output power of 0.8 W was achieved.[1] In

[1] Without beam-shaping optics, our measured coupling efficiencies for the oscillator and SOA output beams into the core of a single mode fiber (core diameter of 6 μm) are 40%–45% and 35%–40%, respectively.

other works, Dupriez *et al.* reported utilizing a gain-switched laser diode to seed a 20-ps high-average-power ytterbium fiber source at 1060 nm [17], and Adhimoolam *et al.* used an actively mode-locked diode laser in combination with a single YDFA [18]. Provided that the ASE levels can be adequately controlled, a semiconductor MOPA could be considered as a potential seed source for a YDFA of substantially higher gain than reported in [16]. Due to the relatively low average power of picosecond-pulsed semiconductor master oscillators, a flared preamplifier could provide the necessary power required to saturate the gain of a high-power YDFA. Such a hybrid configuration would be complementary to using fiber-based preamplification stages without the added dispersion. In the case of the MOPA, the level of ASE could be minimized, especially for higher repetition rates (Fig. 4). The approaches to achieve minimal ASE include increasing the oscillator output power and insertion of a bandpass filter, as well as by using pulse compression either before or after the final fiber amplification [10]. In addition, alternative waveguide designs of the SOA could be adopted to decrease the spontaneous emission background [19]. For example, the use of an exponential waveguide flare instead of a linear one or developing a monolithic two-section amplifier consisting of a narrow stripe and a flared section, each of which is independently biased, could be explored in the future work.

IV. Conclusion

We have reported short pulse amplification by a long-wavelength InGaAs–GaAs flared SOA. Future modifications to the waveguide geometry and fabrication procedure should improve the device maximum drive current, which would allow for much higher output powers. In addition, follow-up work on modeling the temporal, spectral, and gain saturation characteristics of the SOA output would be very useful for predicting and optimizing the performance. In conclusion, the all-semiconductor MOPA based on the InGaAs–GaAs material system is a promising source for applications requiring moderate average powers, such as various bio-diagnostics, including two-photon excitation methods. Furthermore, such a system might be used to seed higher-gain ytterbium-doped power amplifiers, which opens a wider range of possibilities, including efficient nonlinear optical conversion devices and material microprocessing applications.

Acknowledgment

The authors would like to thank M. J. Brennan and J. N. Milgram for the technical assistance and helpful comments during the early stages of SOA development.

References

[1] F. Bugge *et al.*, "Effect of growth conditions and strain compensation on indium incorporation for diode lasers emitting above 1050 nm," *J. Cryst. Growth*, vol. 221, no. 1–4, pp. 496–502, Dec. 2000.

[2] T. Piwoński *et al.*, "Long-wavelength strained-layer InGaAs/GaAs quantum-well lasers grown by molecular beam epitaxy," *Microw. Opt. Technol. Lett.*, vol. 29, no. 2, pp. 75–77, Apr. 2001.

[3] M. J. Brennan, A. J. Budz, B. J. Robinson, P. Mascher, and H. K. Haugen, "Ultrashort optical pulse generation with a mode-locked long-wavelength (1075–1085 nm) InGaAs–GaAs semiconductor laser," *IEEE Photon. Technol. Lett.*, vol. 16, no. 8, pp. 1798–1800, Aug. 2004.

[4] H. Lim, F. Ö. Ilday, and F. W. Wise, "Generation of 2-nJ pulses from a femtosecond ytterbium fiber laser," *Opt. Lett.*, vol. 28, no. 8, pp. 660–662, Apr. 2003.

[5] J. S. Yang *et al.*, "An integrated optical waveguide isolator based on multimode interference by wafer direct bonding," *IEEE Trans. Magn.*, vol. 41, no. 10, pp. 3520–3522, Oct. 2005.

[6] G. Bendelli, K. Komori, and S. Arai, "Gain saturation and propagation characteristics of index-guided tapered-waveguide traveling-wave semiconductor laser amplifiers (TTW-SLA's)," *IEEE J. Quantum Electron.*, vol. 28, no. 2, pp. 447–458, Feb. 1992.

[7] S. Gee, G. Alphonse, J. Connolly, and P. J. Delfyett, "High-power mode-locked external cavity semiconductor laser using inverse bow-tie semiconductor optical amplifiers," *IEEE J. Sel. Topics Quantum Electron.*, vol. 4, no. 2, pp. 209–215, Mar./Apr. 1998.

[8] A. Mar, R. Helkey, J. Bowers, D. Mehuys, and D. Welch, "Mode-locked operation of a master oscillator power amplifier," *IEEE Photon. Technol. Lett.*, vol. 6, no. 9, pp. 1067–1069, Sep. 1994.

[9] S. O'Brien, R. S. Geels, W. E. Plano, and R. J. Lang, "1.26 W CW diffraction-limited InGaAsP flared amplifier at 780 nm," *Electron. Lett.*, vol. 33, no. 4, pp. 328–330, Feb. 1997.

[10] K. Kim, S. Lee, and P. J. Delfyett, "1.4 kW high peak power generation from an all semiconductor mode-locked master oscillator power amplifier system based on eXtreme chirped pulse amplification (X-CPA)," *Opt. Express*, vol. 13, no. 12, pp. 4600–4606, Jun. 2005.

[11] A. J. Budz, M. J. Brennan, and H. K. Haugen, "Generation and amplification of ultra-short optical pulses from a mode-locked long-wavelength (1075 nm–1085 nm) InGaAs/GaAs quantum well laser," presented at the Conf. Lasers Electro-Optics, San Francisco, CA, 2004, Paper CTuP6.

[12] T. G. Andersson, Z. G. Chen, V. D. Kulakovskii, A. Uddin, and J. T. Vallin, "Variation of the critical layer thickness with In content in strained $In_xGa_{1-x}As$-GaAs quantum wells grown by molecular beam epitaxy," *Appl. Phys. Lett.*, vol. 51, no. 10, pp. 752–754, Sep. 1987.

[13] G. P. Agrawal and N. A. Olsson, "Self-phase modulation and spectral broadening of optical pulses in semiconductor laser amplifiers," *IEEE J. Quantum Electron.*, vol. 25, no. 11, pp. 2297–2306, Nov. 1989.

[14] S. Sanders, A. Yariv, J. Paslaski, J. E. Ungar, and H. A. Zarem, "Passive mode locking of a two-section multiple quantum well laser at harmonics of the cavity round-trip frequency," *Appl. Phys. Lett.*, vol. 58, no. 7, pp. 681–683, Feb. 1991.

[15] C. Lee and P. J. Delfyett, "Limits on amplification of picosecond pulses by using semiconductor laser traveling-wave amplifiers," *IEEE J. Quantum Electron.*, vol. 27, no. 5, pp. 1110–1114, May 1991.

[16] A. J. Budz, A. S. Logan, D. Strickland, and H. K. Haugen, "Ultrashort pulses from a mode-locked diode-oscillator Yb-fiber-amplifier system," *IEEE Photon. Technol. Lett.*, vol. 19, no. 2, pp. 94–96, Jan. 2007.

[17] P. Dupriez *et al.*, "High average power, high repetition rate, picosecond pulsed fiber master oscillator power amplifier source seeded by a gain-switched laser diode at 1060 nm," *IEEE Photon. Technol. Lett.*, vol. 18, no. 9, pp. 1013–1015, May 2006.

[18] B. Adhimoolam, M. G. Hekelaar, P. Gross, I. D. Lindsay, and K.-J. Boller, "Wavelength-tunable short-pulse diode-laser fiber-amplifier system around 1.06 μm," *IEEE Photon. Technol. Lett.*, vol. 18, no. 7, pp. 838–840, Apr. 2006.

[19] H. Ghafouri-Shiraz, P. W. Tan, and T. Aruga, "Picosecond pulse amplification in tapered-waveguide laser-diode amplifiers," *IEEE J. Sel. Topics Quantum Electron.*, vol. 3, no. 2, pp. 210–217, Apr. 1997.

A. J. Budz (S'05) received the B.Eng. degree in engineering physics from McMaster University, Hamilton, ON, Canada, where he is currently working toward the Ph.D. degree.

His research interests include the development of short-pulse laser systems based on mode-locked semiconductor diode lasers.

H. K. Haugen, photograph and biography not available at the time of publication.

As indicated in the paper, distortions to the pulse following amplification are minor. Additional spectral measurements are shown in Figure 4-7 for identical operating conditions as that described in the paper except that the input pulses have a lower duration of 2.5 ps and a broader spectral bandwidth. The measurements show the effect of the input power and bias current on the spectral distortion of the pulse. Again, a minimal amount of distortion is observed for the conditions tested. The lack of significant spectral modification to the amplified pulse can be explained by considering the degree of saturation of the amplifier and the amount of chirp on the seed pulses. As noted in the paper, the small-signal gain is 29 dB and the input pulse energy relative to the saturation energy of the amplifier is 0.015. Simulations by Olsson and Agrawal have shown that for an amplifier with a small-signal gain of 30 dB and an input pulse energy relative to the saturation energy of 0.03, a spectral shift of 0.3 nm is expected due to SPM induced by gain saturation [82]. The 0.3 nm red-shift in the spectrum of the amplified pulse is based on the assumption of bandwidth-limited Gaussian-shaped pulses. Further simulations by Agrawal *et al.* have shown that the temporal shape of the seed pulse and the presence of an initial chirp can influence the amount of spectral modification following amplification [84]. By considering only the level of saturation of the flared-SOA, a spectral shift on the order of a few angstroms might be expected. However, the analysis of the problem is complicated by the fact that the seed pulses are highly chirped (factor of ~20 above transform limit for the experiments of Paper 2) and the spectrum of the amplified pulse is mainly

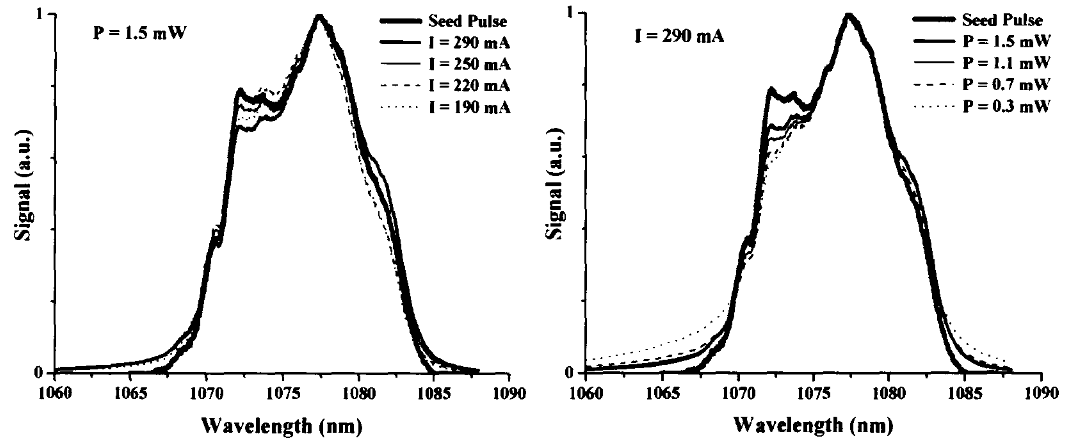

Figure 4-7: Spectral distortion of amplified pulses for the SOA operating under (*left*) constant input power and (*right*) constant drive current.

determined by the interaction of the SPM-induced chirp with the initial chirp of the seed pulse. The fact that the functional form of the chirp and the temporal shape of the pulses emitted by the mode-locked oscillator are unknown limits the ability to accurately model such distortion effects with the current SOA devices. When only the saturation state of the amplifier is considered, the spectra of the amplified pulses are consistent with theoretical models. Indeed, accurate modeling of the SOA and measurement of both the chirp and temporal profile of the seed pulses represent areas of potential future work.

The amplification experiments were conducted using two different aspheric lenses to collimate the output beam of the amplifier: a 3.1 mm and a 4.5 mm focal length lens. Originally the 4.5 mm lens was used for collimation but was found to distort the beam in the transverse (vertical) direction. Since edge-emitting semiconductor devices typically have highly divergent beams in the transverse direction due to the thin active layer, the collimating lens can act as a limiting aperture in the system by truncating the transverse component of the beam. When a lens truncates a large fraction of the beam, side lobes caused by diffraction can appear on either side of the main emission lobe and can contain a significant fraction of the total power. During the course of the SOA experiments this problem was rectified by utilizing a shorter focal length lens for the output coupling, which minimized the effects of diffraction. In switching from the 4.5 mm (NA = 0.55) to the 3.1 mm (NA = 0.68) lens, the output power increased by about 7 %, indicating that the level of beam truncation with the original setup was fairly minor. The spatial beam profile of the flared-SOA with the optimized output coupling is displayed in Figure 4-8. Almost all of the output power is contained within a single elliptically-shaped mode that can be well approximated by Gaussian distributions in both the transverse and lateral directions.

Compared to the narrow-stripe SOAs, the flared-waveguide devices deliver improved performance in many areas. The small-signal gain and amplified output power are both higher by a factor of 3 and the saturation energy is higher by about a factor of 2.5. However, these values are obtained with each SOA biased at its maximum possible drive current. Since the flared-SOA was operated at a current density that was ~7 times lower than that of the narrow-stripe SOA, the relative performance of the flared amplifier is actually much higher. In order to compare the two amplifiers at the same current density, the flared amplifier biased at 290 mA should be compared with the narrow-stripe SOA biased at only 14 mA. Under these conditions, the saturation energy, small-signal gain, and amplified output power of the flared-SOA are higher by a factor of 25, 50, and 80,

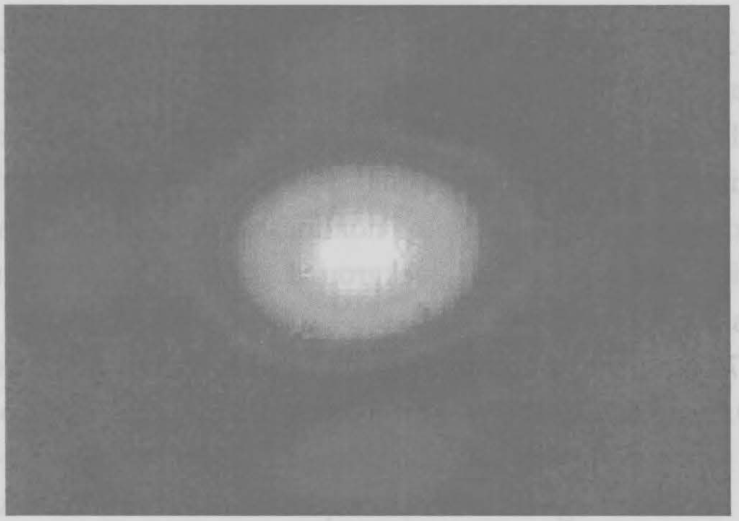

Figure 4-8: Collimated spatial beam profile of the flared-waveguide SOA at maximum output power and measured at a distance of 2.5 m from the output facet of the amplifier. An aspheric lens with a focal length of 3.1 mm is used in combination with a 9 cm focal length plano-convex cylindrical lens to collimate the beam.

respectively. The main drawback of the flared amplifier is that it generates more ASE than the narrow-stripe amplifier, leading to a higher overall noise ratio (~20 % versus <1 %, respectively). Thus, from the perspective of functioning as a pre-amplifier, the flared-SOAs are less attractive in terms of noise performance. Nevertheless, there a number of approaches to reduce the ASE as discussed near the end of Section III of Paper 2. In addition to the approaches described in the paper, a method that could be particularly effective at minimizing the ASE is pulsing the electrical bias to the SOA. By synchronizing the electrical pulses to the injected optical pulses, the gain of the SOA can be restricted to the period when a pulse propagates through the amplifier, reducing the build-up of ASE in the interval between pulses. A pulsed bias approach could be implemented by driving the SOA and mode-locked oscillator from the same RF source. After being amplified, the RF signal could be used in conjunction with a comb generator to bias the SOA. The effectiveness of a pulsed bias approach would depend on the quality of the impedance match at the diode contacts, making it more suitable for lower pulse repetition rates. It is expected that through a combination of spectral filtering (pulse compression), pulsed electrical bias, and a modified waveguide geometry for the SOA, the background ASE could be reduced well below the level of ASE that has been obtained with current devices. Spectral filtering through pulse compression can decrease the ASE level by about a factor of 2–3 (Fig. 3, Paper 2), depending on the operating parameters. By combining spectral filtering with other techniques that minimize ASE, it is expected that the fraction of ASE in the output beam could be reduced below the 5 % level. Ultimately, the tolerable signal-to-noise level will be dictated by the intended application and in the case of nonlinear frequency conversion or two-photon excitation, the presence of background ASE on the main mode-locked signal becomes less relevant.

The 1070 nm flared amplifiers exhibit similar performance as other flared-waveguide SOAs operating at the same current density and input power. Since there are no reported results of pulse amplification using long-wavelength InGaAs-GaAs flared-waveguide SOAs, comparisons must be made with devices based on different materials systems and operating at different wavelengths. As discussed previously, comparing the current devices to those reported in the literature is somewhat misleading due to the different active region designs and operating parameters that are possible. In addition, the comparison of flared-SOAs is further complicated by the fact that the shape and angle of the lateral flared-waveguide can have a significant impact on the overall saturation characteristics of the amplifier, as discussed in Chapter 2. Therefore, comparisons will be restricted to devices which have waveguide geometries that are similar to the 1070 nm amplifiers.

Mar *et al.* have reported on the development of a short-pulse MOPA system operating at 940 nm using a flared-SOA with a triple quantum-well active region [19]. The lateral waveguide expands from 4 μm at the input to 130 μm at the output, but the overall length of the amplifier is not quoted. If the same SOA structure can be assumed as that used by the research group in [118], then the length of the amplifier is 2.5 mm and the flared full-angle is 2.9°. The seed pulses have a duration of 4 ps, repetition rate of 2.5 GHz, and center wavelength of 940 nm. At a bias current of 2 A, an amplified average signal power of ~85 mW is obtained for an input average power of 1 mW. The noise ratio or the fraction of ASE power to the total output power is ~0.4. The system gain at low input powers is 19 dB. The amplifier is biased with a current density (A/m^2) that is a factor of 2 larger than the current density of the 1070 nm flared-SOAs.

Xiong *et al.* have characterized a commercial flared-waveguide SOA operating at 800 nm using 8-ps-pulses at a repetition rate of 843 MHz [20]. The material structure and active region of the amplifier are not specified. The SOA has a length of 2.75 mm, input width of 3 μm, output width of 190 μm, and a flared full-angle of 2°. For an input average power of 0.75 mW, the amplified average power is 80 mW at a drive current of 1.75 A. The amplified pulses are reported to be free of spectral distortions. ASE constitutes 3 % of the total amplifier output, which is much better than the noise ratio of the 1070 nm flared-SOAs. The above values are obtained with a bias current density that is very similar to the current density of the 1070 nm amplifiers.

Gee *et al.* have reported on the performance of a double quantum-well inverse bow-tie SOA [91], which is somewhat different than a standard flared-waveguide amplifier. The waveguide laterally expands from an input width of 5 μm to a width of 54 μm over a length of 590 μm (full-angle of 4.8°) and then laterally contracts back to an output width of 20 μm over a length of 410 μm. The overall length is 1 mm. The amplifier is biased at a current of 1 A and is seeded with pulses that have a duration of 9 ps, repetition rate of 1 GHz, and wavelength of 850 nm. An amplified average power of 400 mW is obtained for an input average power of 17 mW, which is much larger than the input power used to characterize the 1070 nm SOAs. The current density of the inverse bow-tie SOA is also larger by approximately a factor of 4. Noise ratios of 10 % are obtained for the output beam.

4.4 YDFA Results

4.4.1 Paper 3: Development of a Short-Pulse Hybrid MOPA Source at 1070 nm

This paper reports on the development of an ultrashort-pulse source based on a Yb-doped fibre amplifier and a passively mode-locked semiconductor oscillator. There has been recent intense interest in the development of optical sources utilizating a Yb-doped fibre as the amplifying medium. The majority of the reported results focus on a solid-state laser as the seed-source. This paper was one of the first reports on the development of a Yb:fibre system based on a short-picosecond-pulse mode-locked semiconductor-seed-oscillator. Details on the design and characterization of the system are presented.

The paper represents a collaborative effort between the University of Waterloo and McMaster University. D. Strickland of the University of Waterloo provided the Yb-doped fibre and the hardware for the fibre amplifier. A. Logan helped with configuring the experimental setup and assisted with the measurements. I was responsible for the experimental measurements, analysis, and the writing of the manuscript.

94 IEEE PHOTONICS TECHNOLOGY LETTERS, VOL. 19, NO. 2, JANUARY 15, 2007

Ultrashort Pulses From a Mode-Locked Diode-Oscillator Yb-Fiber-Amplifier System

A. J. Budz, *Student Member, IEEE*, A. S. Logan, D. Strickland, and H. K. Haugen

***Abstract*—Ultrashort optical pulses are generated using a hybrid master oscillator power amplifier source. Pulses 2.2 ps in duration generated by a two-contact, bent-waveguide passively mode-locked semiconductor laser are amplified in a ytterbium-doped fiber amplifier to an average power of 0.8 W. External pulse compression yields durations as low as 765 fs with peak powers as high as 0.9 kW. Amplification of the harmonically mode-locked diode output has also been demonstrated at the eighth harmonic.**

***Index Terms*—Mode-locked lasers, semiconductor lasers, ytterbium-doped fiber amplifiers (YDFAs).**

I. Introduction

MODE-LOCKING of semiconductor lasers provides a practical and efficient means of generating ultrashort optical pulses [1]. Typically, light generated by a mode-locked diode laser is sent through an external semiconductor optical amplifier in order to boost the average power to a suitable level [2]. With the recent development of cladding-pumped ytterbium-doped fiber amplifiers (YDFAs), novel hybrid master oscillator power amplifier (MOPA) systems can be explored in the 0.97–1.1-μm wavelength range. YDFAs have been used to amplify the output of short pulse solid-state lasers, providing high efficiency and excellent beam quality [3]. Pulsed semiconductor lasers have also been investigated as potential seed sources for YDFAs. Reported results include an injection-seeded gain-switched source producing 20-ps pulses [4] and an actively mode-locked 30-ps laser [5]. Amplification of a passively mode-locked vertical-external-cavity surface-emitting laser in a multistage YDFA system has also just been reported [6], including results obtained in the parabolic pulse regime. The technique of mode-locking typically generates optical pulses of shorter duration with less temporal jitter than that obtained with either gain- or q-switching [1]. Moreover, passive mode-locking has several important advantages when compared to active mode-locking such as simpler driving electronics and the potential to generate shorter output pulses due to the enhanced pulse shaping provided by a saturable absorber. In this letter, we report on a YDFA-based ultrashort pulse source consisting of a passively mode-locked two-contact diode oscillator. While complementary to fiber-oscillator-based systems, a short pulse semiconductor seed source offers a number of attractive features such as a simple cavity design, low cost, and ability to readily generate high, and variable, pulse repetition rates.

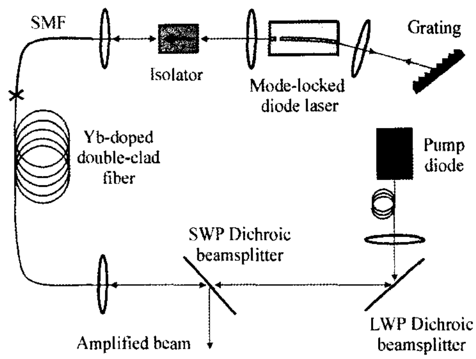

Fig. 1. Schematic of the hybrid MOPA. Short pulses emitted by a passively mode-locked external cavity semiconductor laser are amplified in 18 m of Yb-doped fiber. A 2-m-long section of SMF is spliced to the Yb-fiber. SWP: short-wave pass; LWP: long-wave pass.

II. Experimental Setup

Short optical pulses are generated and amplified using the hybrid MOPA configuration shown in Fig. 1 [7]. The semiconductor oscillator contains a bent waveguide with integrated gain and saturable absorber sections and is mounted in a linear external cavity. The active region of the oscillator consists of a single compressively strained InGaAs quantum-well (QW) and GaAs barriers. An In mole fraction of around 0.27 is sufficient to create energy transitions in the InGaAs QW that overlap with the gain spectrum of Yb^{3+}. Details regarding the growth and design of the oscillator have previously been reported [8]. When passively mode-locked, the oscillator generates pulses 2–8 ps in duration, centered at approximately 1075 nm with average output powers less than 2 mW. The feedback element in the external cavity consists of a 600-lines/mm diffraction grating which provides control over the wavelength and bandwidth of the optical pulse train, as well as the pulse repetition rate. Mode-locking can be achieved at the fundamental and also at harmonics of

Manuscript received August 24, 2006; revised November 11, 2006. This work was supported in part by the Canadian Institute for Photonics Innovations, within the Networks of Centres of Excellence, and in part by the Natural Sciences and Engineering Research Council of Canada.

A. J. Budz is with the Department of Engineering Physics, McMaster University, Hamilton ON L8S 4L7, Canada (e-mail: budzaj@mcmaster.ca).

A. S. Logan was with the Department of Engineering Physics, McMaster University, Hamilton, ON L8S 4L7, Canada. He is now with the Department of Systems Design Engineering, University of Waterloo, Waterloo, ON N2L 3G1, Canada.

D. Strickland is with the Department of Physics and Astronomy, University of Waterloo, Waterloo ON N2L 3G1, Canada.

H. K. Haugen is with the Department of Engineering Physics, McMaster University, Hamilton ON L8S 4L7, Canada, and also with the Department of Physics and Astronomy, McMaster University, Hamilton ON L8S 4M1, Canada.

Digital Object Identifier 10.1109/LPT.2006.889039

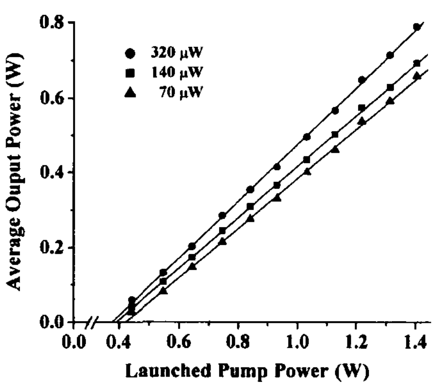

Fig. 2. Average output power of the fiber amplifier as a function of launched pump power. The seed average power is varied for each curve and represents the power that is coupled into the doped core of the fiber.

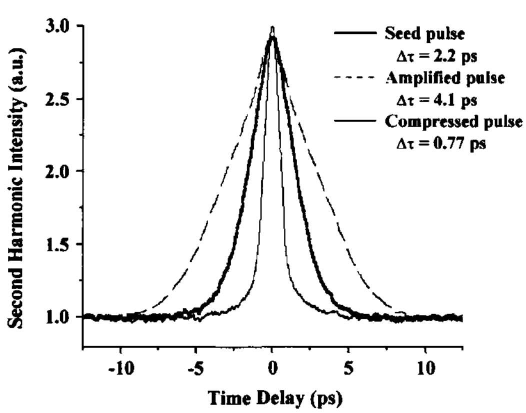

Fig. 3. Second-order intensity autocorrelation traces following amplification and pulse compression at a launched pump power of 1.4 W. The pulsewidths have been deconvolved assuming a hyperbolic-secant-squared pulse shape.

the cavity round-trip frequency, giving access to repetition rates between 570 MHz and 5 GHz. Harmonic mode-locking can be initiated by adjusting the bias parameters of the semiconductor oscillator [9]. The pulsing characteristics of the diode laser are monitored using a 22-GHz RF spectrum analyzer, and in selected experiments a 50-GHz communication signal analyzer, by coupling a portion of the output beam into a 20-GHz photodiode.

Pulses emitted by the diode laser are injected into a power amplifier stage consisting of 18 m of commercial Yb-doped double-clad fiber. The core of the fiber has a mode-field diameter of 6.5 μm, numerical aperture (NA) of 0.12, and a doping concentration of approximately 1.6% by weight. The inner cladding has a diameter of 130 μm and an NA of 0.46. A 2-m-long section of single-mode fiber (SMF) is fusion spliced to the Yb-fiber to simplify coupling of the seed pulses into the active core. Power loss at the splice is estimated to be 0.2 dB. Both ends of the fiber amplifier are angle cleaved at 8° to prevent feedback of the signal in the core. The YDFA is pumped counterdirectionally using a fiber-coupled pump diode operating at a wavelength of 971 nm. A 10× microscope objective is used to couple light from the pump diode into the inner cladding of the YDFA with an efficiency of about 70%. Dichroic beamsplitters are used to separate the pump and amplified seed signals and to prevent residual amplified signal from coupling into the pump laser. An optical isolator prevents amplified spontaneous emission (ASE) from being injected into the diode laser cavity and disrupting the mode-locking.

III. Results and Discussion

The amplification characteristics of the YDFA as a function of pump power are shown in Fig. 2. The seed pulses have a duration of 2.2 ps, center wavelength of 1075 nm, and repetition rate of 570 MHz. At a maximum launched pump power of 1.4 W, approximately 0.8 W of amplified signal is obtained. The slope efficiency with respect to launched pump power is 76% when the fiber is seeded with an average power of 320 μW, which is the highest power that could be coupled into the doped core of the Yb-fiber. Pulses emitted directly by the diode oscillator are reduced in power due to the insertion loss of the isolator (0.7 dB) and by the coupling efficiency into the SMF (40%). When the input average power is reduced to 70 μW, an output power of over 0.65 W is still obtained, indicating that this system provides good performance for low average power oscillators. The 18-m-length of fiber provides nearly complete pump absorption with less than 5% of the launched power remaining at the output. By changing the center wavelength of the pump diode from 971 to 975 nm, it should be possible to obtain complete pump absorption in shorter lengths of fiber due to the larger absorption cross section of Yb^{3+} at 975 nm [10]. The output power that could be extracted from this hybrid MOPA is currently limited by the available pump power.

Owing to the fiber dispersion at 1075 nm, the amplified pulses broaden in time from 2.2 to 4.1 ps. Fig. 3 shows intensity autocorrelation traces after amplification and subsequent compression. Pulse durations correspond to the full-width at half-maximum of the autocorrelation trace with an assumed hyperbolic-secant-squared pulse shape. However, mode-locked diode oscillators are expected to produce pulses with some degree of temporal asymmetry, which was evident in our earlier cross-correlation studies [11], but would not appear in an autocorrelation trace. The corresponding optical spectra following pulse amplification are shown in Fig. 4. The pulses undergo minimal spectral distortion after amplification with negligible self-phase modulation (SPM). The lack of significant SPM is primarily due to the fact that the signal build-up occurs mainly near the end of the fiber. However, we observed SPM by launching the fiber-amplified pulses into a section of passive SMF. The measured linewidth at the output of the fiber was in reasonable agreement with a theoretical model, given the uncertainty of the details in the pulse chirp and the temporal pulse profile [12]. The amplified spectrum shows good spectral purity with no significant build-up of ASE, indicating that the mode-locked signal sufficiently saturates the gain of the fiber. In the absence of an injected seed beam, the ASE has a center wavelength of 1070 nm and a bandwidth of 22 nm. At the

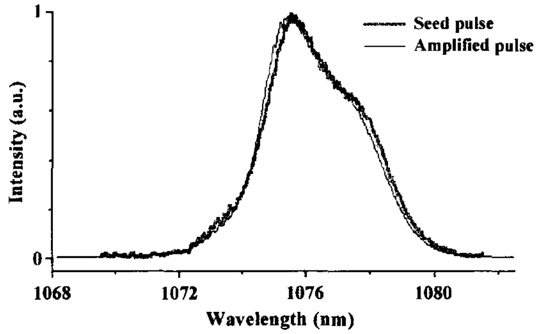

Fig. 4. Normalized optical spectra of the pulse train after amplification in the fiber at maximum pump power.

highest output power, the ASE background level is approximately 30 dB below the peak of the amplified signal emission.

The hybrid MOPA generates pulses with a time-bandwidth product (TBP) that is in excess of the transform limit. Passively mode-locked diode lasers emit predominately blue-chirped pulses due to differences in the linewidth enhancement factor in the gain and saturable absorber sections of the laser [13]. After propagating through the YDFA, the pulses become further chirped due to the normal dispersion of the fiber. External pulse compression with a 1800-lines/mm grating compressor yields pulses as short as 765 fs with peak powers as high as 0.9 kW (compressor efficiency ~50%). The pulse spectral bandwidth after compression is 3.5 nm, resulting in a TBP of 0.7. Uncompensated nonlinear chirp remains on the compressed pulses which are a factor of 2.2 above the transform limit.

The repetition rate dependence of the hybrid MOPA is also studied. The diode oscillator can be harmonically mode-locked at up to the eighth harmonic (4.6 GHz) by simply adjusting the bias parameters of the gain and absorber sections. When the fiber amplifier is seeded with 7-ps pulses at 4.6 GHz and an average power of 1.2 mW, an output power of over 1.1 W is obtained (limited by pump power), with an overall slope efficiency of 83%. Tuning of the MOPA pulse repetition rate without having to adjust the oscillator cavity length allows convenient control over the pulse peak power while maintaining optimal system performance.

IV. Conclusion

The ultrashort hybrid MOPA source presented here represents a promising approach to obtaining short pulses and moderate average powers as the attractive features of a diode oscillator and a single YDFA can be combined into a robust, compact source. Electrically driven low-power diode lasers can be readily mode-locked delivering short pulses at variable repetition rates while the YDFA provides high gain and excellent beam quality. We obtain good overall performance using a rather simple oscillator incorporating a two-section edge-emitting semiconductor seed laser. Future work will focus on increasing output power and controlling the pulse chirp in order to produce shorter pulses that are closer to the transform limit. We feel this type of hybrid source offers a complimentary approach to generating short pulses and could prove of interest for a number of applications requiring moderate intensities.

Acknowledgment

The authors would like to thank P. Carr and C. Ferrie for technical help.

References

[1] P. Vasil'ev, *Ultrafast Diode Laser*. Boston, MA: Artech House, 1995, pp. 53–144.
[2] K. Kim, S. Lee, and P. J. Delfyett, "1.4 kW high peak power generation from an all semiconductor mode-locked master oscillator power amplifier system based on extreme chirped pulse amplification (X-CPA)," *Opt. Express*, vol. 13, pp. 4600–4606, Jun. 2005.
[3] J. Limpert *et al.*, "High-average-power femtosecond fiber chirped-pulse amplification system," *Opt. Lett.*, vol. 28, pp. 1984–1986, Oct. 2003.
[4] A. Piper *et al.*, "11.1 W average power, 20 ps pulses at 1 GHz repetition rate from a fiber-amplified gain-switched 1.06 μm Fabry-Perot laser diode," presented at the Conf. Lasers Electro-Optics, Baltimore, MD, May 22–27, 2005, Paper CTuCC3.
[5] B. Adhimoolam, M. G. Hekelaar, P. Gross, I. D. Lindsay, and K.-J. Boller, "Wavelength-tunable short-pulse diode-laser fiber-amplifier system around 1.06 μm," *IEEE Photon. Technol. Lett.*, vol. 18, no. 7, pp. 838–840, Apr. 1, 2006.
[6] P. Dupriez *et al.*, "High-power, high repetition rate picosecond and femtosecond sources based on Yb-doped fiber amplification of VECSELs," *Opt. Express*, vol. 14, pp. 9611–9616, Nov. 2006.
[7] A. J. Budz, A. S. Logan, D. T. Strickland, and H. K. Haugen, "Ultrashort pulse generation at 1075 nm with a mode-locked semiconductor laser and a ytterbium-doped fiber amplifier," presented at the Conf. Lasers and Electro-Optics, Long Beach, CA, May 21–27, 2006, Paper JWB40.
[8] M. J. Brennan, A. J. Budz, B. J. Robinson, P. Mascher, and H. K. Haugen, "Ultrashort optical pulse generation with a mode-locked long-wavelength (1075–1085 nm) InGaAs-GaAs semiconductor laser," *IEEE Photon. Technol. Lett.*, vol. 16, no. 8, pp. 1798–1800, Aug. 2004.
[9] S. Sanders, A. Yariv, J. Paslaski, J. E. Ungar, and H. A. Zarem, "Passive mode locking of a two-section multiple quantum well laser at harmonics of the cavity round-trip frequency," *Appl. Phys. Lett.*, vol. 58, pp. 681–683, Feb. 1991.
[10] R. Paschotta, J. Nilsson, A. C. Tropper, and D. C. Hanna, "Ytterbium-doped fiber amplifiers," *IEEE J. Quantum Electron.*, vol. 33, no. 7, pp. 1049–1056, Jul. 1997.
[11] M. J. Brennan, H. F. Tiedje, and H. K. Haugen, "Passively modelocked semiconductor laser synchronisation and pulse cross-correlation with ti:sapphire laser," *Electron. Lett.*, vol. 38, no. 14, pp. 713–714, Jul. 2002.
[12] G. P. Agrawal, *Nonlinear Fiber Optics*, 2nd ed. San Diego, CA: Academic, 1995, pp. 89–132.
[13] M. Schell, J. Yu, M. Tsuchiya, and T. Kamiya, "Chirp of passively and actively mode-locked semiconductor lasers," *Appl. Phys. Lett.*, vol. 67, no. 13, pp. 1797–1799, Sep. 1995.

As discussed in the paper, a minimal amount of spectral distortion is obtained following amplification, indicating that SPM in the fibre amplifier is relatively weak. Given the magnitude of the pulse peak power at the output of the fibre amplifier, some level of SPM might be expected. The presence of a cw component or a satellite pulse with the main mode-locked signal could lead to a lower degree of spectral modification than expected following amplification. However, within the detection limits of the diagnostic equipment, no satellite pulses or cw component were observed. The measurement system comprised of the sampling oscilloscope and fast photodiode has a sensitivity of ~10 μW of optical power and is capable of detecting satellite pulses in the range of 40–2000 ps after the main mode-locked pulse. In addition, the auto-correlator can be scanned over a time frame of 100 ps and can therefore detect satellite pulses up to 50 ps after the mode-locked pulse.

To gain insight into the effects of SPM with the mode-locked pulses, numerical simulations were conducted. It was not possible to directly model the effects of SPM in the fibre amplifier since the spatial variation of the amplified signal along the fibre was not known. Therefore, additional measurements were conducted to investigate the ability of the fibre amplified pulses to generate SPM in a passive fibre. The measurements were compared with numerical simulations to verify that the level of broadening due to SPM was consistent with theory based on the measured intensity of the pulse. Modeling the effects of SPM in a passive fibre is far easier since the intensity of the signal remains constant with propagation distance.

The results of the experimental measurements are shown in Figure 4-9. Again, a minimal amount of spectral modification is observed following amplification. However, after propagating through 7.5 m of single-mode fibre (SMF), the spectrum of the pulse is significantly modified and has developed features that are characteristic of SPM. To determine if the observed level of spectral broadening in the SMF was consistent with the measured intensity of the pulse, numerical simulations were conducted.

SPM is a nonlinear optical effect that arises when the intensity of the pulse is sufficient to modify the refractive index of the host medium through the Kerr effect. The intensity-dependence of the refractive index leads to a temporal variation in the phase of the pulse, resulting in spectral broadening [119]. The maximum phase shift of the pulse due to SPM in a lossless fibre is given by [119]

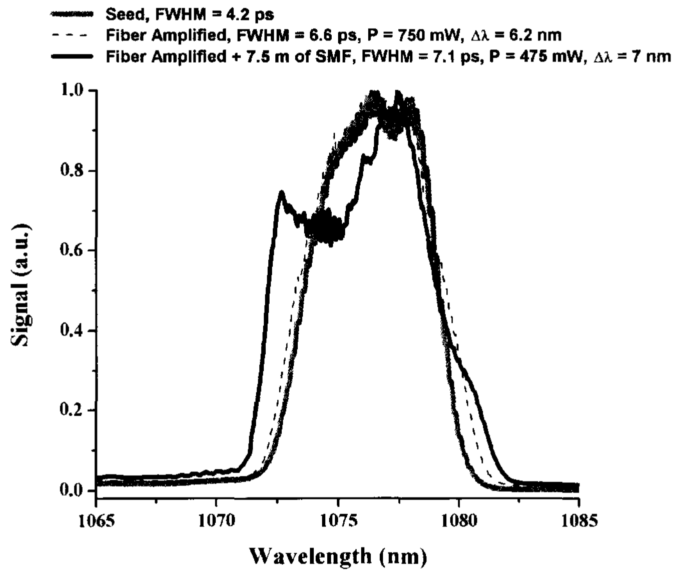

Figure 4-9: Pulses at a repetition rate of 570 MHz are amplified in the YDFA and then launched into a 7.5-m-long section of SMF to characterize the effects of SPM.

$$\varphi_{\max} = \gamma P_o L \tag{4.1}$$

where P_o is the peak power and L is the propagation distance along the fibre. The nonlinear coefficient, γ, is given by [119]

$$\gamma = \frac{n_2 \omega_o}{c A_{eff}} \tag{4.2}$$

where n_2 is the nonlinear refractive index coefficient, ω_o is the center frequency of the optical field, c is the speed of light, and A_{eff} is the effective mode-field area of the fibre core. A value of $\varphi_{max} < 1$ represents the linear propagation regime, while spectral broadening is expected for $\varphi_{max} > 1$. For the SMF used above, $\gamma = 0.006$ $W^{-1}m^{-1}$ using $n_2 = 2.2\times10^{-20}$ m^2/W [119]. The instantaneous pulse peak power at the input of the SMF is ~120 W, which yields $\varphi_{max} = 5.4$ for a length of 7.5 m. Therefore, spectral broadening of the pulses due to SPM should be observed in the SMF, which is consistent with the measured spectra of Figure 4-9.

The electric field of a Gaussian-shaped pulse can be described by

$$E = \frac{1}{2}\left\{ Ae^{-t^2/2T_o^2} e^{i(kz-\omega_o t+\varphi_c)} + c.c.\right\} \qquad \textbf{(4.3)}$$

where A is the scalar amplitude of the field, $T_o \sim T_f/1.665$, T_f is the FWHM of the intensity profile of the pulse, and φ_c is a time-dependent phase function representing the initial chirp of the pulse. After propagating through a lossless fibre of length L and assuming that the effects of dispersion can be neglected, the pulse acquires a nonlinear phase shift of [119]

$$\varphi_{NL} = k_o L n_2 I \qquad \textbf{(4.4)}$$

where the intensity is $I = \frac{1}{2} nc\varepsilon_o E^*E$. At the center of the pulse ($t = 0$), the peak intensity is given by the pulse peak power divided by the effective area, P_o/A_{eff}. Using the fact that the amplitude normalization of the field is given by $A^2 = 2P_o/A_{eff}nc\varepsilon_o$, substitution of the intensity into Equation (4.4) yields a reduced equation for the nonlinear phase shift due to SPM:

$$\varphi_{NL} = \varphi_{\max} e^{-t^2/T_o^2} \qquad \textbf{(4.5)}$$

Finally, the frequency spectrum of the pulse after SPM can be calculated by taking the Fourier transform of the complex pulse amplitude, which is given by

$$Ae^{-t^2/2T_o^2} e^{i(\varphi_{NL}+\varphi_c-\omega_o t)} \qquad \textbf{(4.6)}$$

The spectrum of the input pulse is obtained by taking the Fourier transform of Equation (4.6) without the nonlinear phase term. The inclusion of φ_c in Equation (4.6) is necessary to account for the fact that the pulses emitted by the mode-locked semiconductor laser are typically chirped. The functional form of φ_c used in the simulations is

$$\varphi_c = \frac{Bt^2}{2T_o^2} + \frac{Ct^3}{2T_o^3} + De^{-t^2/T_o^2} \qquad \textbf{(4.7)}$$

where, in general, the magnitude of the coefficients, B, C, and D, are somewhat arbitrary, since the true functional form of the pulse chirp is unknown. However, based on pulse compression measurements, the chirp of the pulse emitted by the oscillator is predominantly linear and positive, which is typical for a passively mode-locked diode laser [120]. Using this fact, the coefficients of Equation (4.7) are tailored to give the input pulses a predominately linear chirp with a spectral bandwidth that is equivalent to the bandwidth of the fibre amplified pulses used in the experiment of Figure 4-9.

The simulation results are shown in Figure 4-10 and Figure 4-11. The input pulse has a Gaussian intensity profile with a duration of 7 ps. The pulse temporal shape is slightly asymmetric to reflect the fact that pulses emitted by a mode-locked diode laser typically have a sharper leading edge [121]. Figure 4-10 shows the simulations results for the case where the input pulse to the SMF has a completely linear chirp. The coefficient for linear chirp, B, is adjusted to give the input pulse a spectral bandwidth of 6.2 nm to match the bandwidth of the input pulses used in the experiment (Figure 4-9). After propagating through 7.5 m of SMF, the pulse acquires a nonlinear frequency chirp due to SPM. The simulated spectrum of the output pulse is broadened to 9 nm, which is larger than the measured value of 7 nm. In addition, the simulated shape of the spectrum is qualitatively different than that of the measured spectrum. Figure 4-11 shows the simulation results for the case where the input pulse has linear, as well as higher-order chirp, which is more characteristic of the chirped pulses emitted by the mode-locked semiconductor oscillator. The coefficients, B, C, and D, are arbitrarily adjusted to give a predominately linear chirp on the input pulse such that the spectral bandwidth is 6.2 nm. After undergoing SPM, the simulated spectrum has a width of 7.2 nm, which is in better agreement with the measured width of 7 nm. Also, the shape of the spectrum has features that are qualitatively similar to that of the measured spectrum (Figure 4-9).

The simulations reveal that the initial chirp of the pulse has an effect on the SPM-broadened spectrum of the pulse and that higher-order chirp should be included in the modeling to determine the overall effect of SPM. Based on the simulation results, the measured linewidth of the spectrally-broadened pulses at the output of the SMF is in reasonable agreement with a model for SPM, given the uncertainties in the shape of the pulse and nonlinearity of the chirp.

The hybrid MOPA source reported in Paper 3 delivers ultrashort pulses with properties that are superior to that of the SOA-based sources described earlier. The system can deliver sub-picosecond pulses with peak powers on the order of 1 kW. The long interaction length of the fibre allows for high gain (saturated value of 34 dB) and the beam quality of the amplified signal is

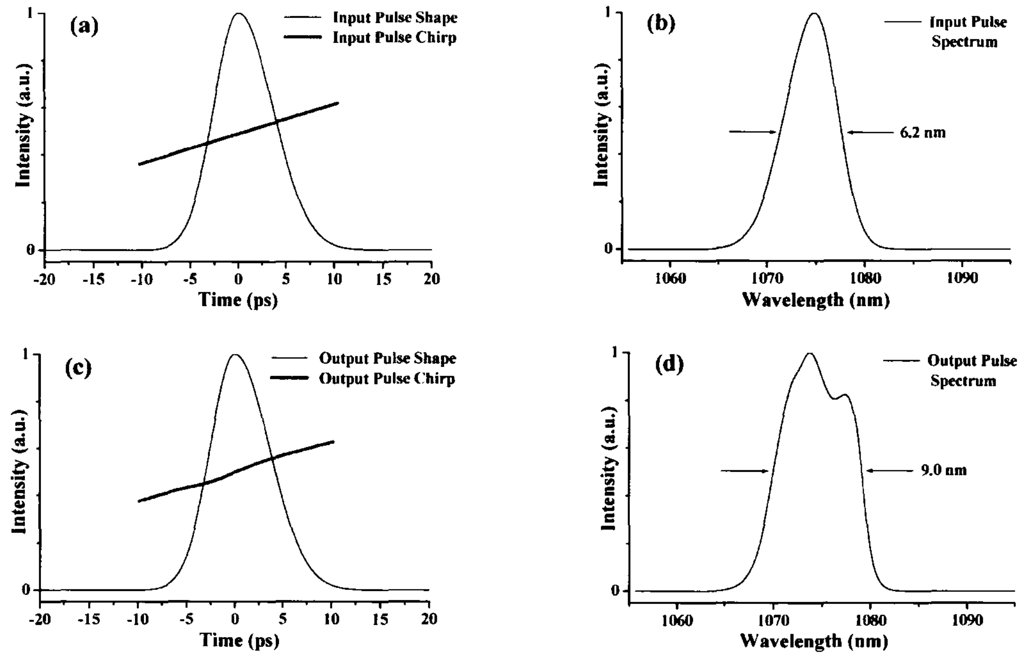

Figure 4-10: Simulations of SPM in a 7.5-m-long SMF for a linearly chirped input pulse: (a) input pulse shape, (b) input pulse spectrum, (c) output pulse shape, and (d) output pulse spectrum.

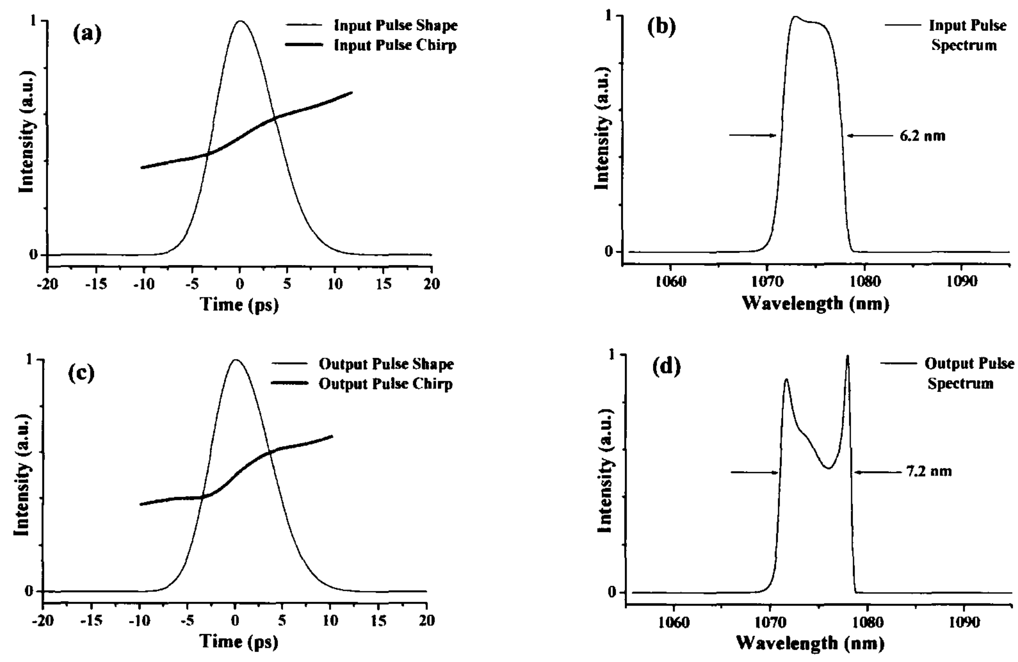

Figure 4-11: Simulations of SPM in a 7.5-m-long SMF for a nonlinearly chirped input pulse: (a) input pulse shape, (b) input pulse spectrum, (c) output pulse shape, and (d) output pulse spectrum.

excellent due to the single-mode nature of the fibre amplifier. Background ASE levels are around a few percent or less of the total amplifier output. When combined with pulse compression, this system should be a viable alternative for nonlinear optical applications such as two-photon microscopy [122]. If higher average powers are required, the output power of the system can be easily scaled by utilizing a stronger pump source.

The hybrid MOPA system described above is complimentary to the high-power Yb:fibre-based system reported by Dupriez *et al.* [23], in which short pulses emitted by a passively mode-locked vertical-external-cavity surface-emitting semiconductor laser (VECSEL) are amplified in multiple Yb:fibre amplifiers. The VECSEL offers advantages over edge-emitting semiconductor lasers such as improved beam quality and higher output power. However, one disadvantage of the VECSEL is that it requires optical pumping and an external saturable absorber, resulting in a fairly complex cavity design. The system developed by Dupriez *et al.* operates at 1055 nm and contains two Yb:fibre pre-amplifiers and one large-mode-area Yb:fibre power-amplifier. The seed pulses have a duration of 4.6 ps, repetition rate of 910 MHz, and an average power of 8 mW. After the two pre-amplifiers, 2 W of average power is generated. The final power amplifier stage is pumped with a launched power of 350 W, yielding an amplified average power of 255 W. The amplified pulses have a duration of 5.8 ps and a peak power of 38 kW. Compression of the amplified pulses results in a duration of 280 fs. While this system is more complicated than the hybrid MOPA described in Paper 3, it does give an indication of the performance and level of average power that can be generated using a mode-locked semiconductor-seed-source and a cascaded chain of Yb:fibre amplifiers.

4.5 Harmonic Mode-Locking

4.5.1 Paper 4: Wavelength and Repetition-Rate Tuning Characteristics of 1070 nm Mode-Locked Semiconductor Oscillators

Paper 1 was a report on the design, fabrication, and characterization of the long-wavelength InGaAs-GaAs 1070 nm diode lasers, including preliminary results on short-pulse generation and amplification. Paper 4 presents more detailed measurements of the wavelength and repetition-rate tuning characteristics of the 1070 nm lasers when operated under conditions of passive mode-locking. In particular, the lasers are found to exhibit a harmonic mode-locking behavior, whereby the pulse repetition rate of the laser can be easily varied through adjustment of the drive current to the gain section of the laser. The amplification characteristics of the fundamental and eighth-harmonic mode-locked pulse trains are also compared using a single-mode YDFA. The Yb:fibre amplifier reported on in this paper was developed by our research group and is different from the fibre amplifier used in the experiments of Paper 3. I was responsible for constructing and characterizing the Yb:fibre amplifier, experimental measurements, data analysis, and the writing of the manuscript.

1412 IEEE PHOTONICS TECHNOLOGY LETTERS, VOL. 19, NO. 19, OCTOBER 1, 2007

Wavelength and Repetition-Rate Tunable Mode-Locked Semiconductor-Seed-Source for Yb-Fiber-Amplifier Systems

A. J. Budz, *Student Member, IEEE*, and H. K. Haugen

***Abstract*—We present a wavelength and repetition-rate tunable passively mode-locked semiconductor-seed-source for ytterbium-doped fiber amplifiers (YDFAs). Ultrashort pulses 2–6 ps in duration are generated over a broad tuning range of 1030–1090 nm, while passive harmonic mode-locking permits pulse repetition rates to vary from 500 MHz to over 5 GHz. We compare the amplification characteristics under fundamental and eighth harmonic mode-locking using a single-mode YDFA.**

***Index Terms*—Mode-locked lasers, semiconductor lasers, ytterbium-doped fiber amplifiers (YDFAs).**

I. Introduction

THERE has been recent interest in the development of ytterbium (Yb)-doped fiber master oscillator power amplifier (MOPA) systems which utilize a short pulse semiconductor laser as the seed source [1], [2]. Semiconductor lasers that are mode-locked (ML) are well suited to seed fiber-MOPAs since they are capable of directly generating short picosecond (ps) and sub-ps pulses at up to gigahertz repetition rates while maintaining low timing jitter. Additionally, ML diode sources offer good flexibility of pulse parameters such as the duration, repetition rate, and wavelength. Despite the advantages offered by an ML diode oscillator, there has been little reported on the development of such a source for the specific purpose of seeding Yb-doped fiber amplifiers (YDFAs). Reported results include an actively ML 30-ps diode laser [2], a sub-ps passively ML vertical-external-cavity surface-emitting laser [3], and our recent report on a 2-ps passively ML two-section edge-emitting laser [4]. In this letter, we report detailed measurements on the wavelength and repetition rate tuning characteristics of our two-contact passively ML diode laser. Short ps pulses are generated over a broad tuning range of 1030–1090 nm, which is somewhat larger than the 45-nm amplified-width obtained via active mode-locking [2]. In addition, by passively mode-locking at multiple harmonics of the cavity round-trip frequency, we are able to vary the pulse repetition rate from 500 MHz to over 5 GHz. The performance limitations of the oscillator are determined over a wide range of parameters and we demonstrate that a relatively simple ML diode laser design can offer great versatility with respect to the seeding of YDFAs.

Manuscript received March 21, 2007; revised May 23, 2007. This work was supported in part by the Canadian Institute for Photonics Innovations, within the Networks of Centres of Excellence, and in part by the Natural Sciences and Engineering Research Council of Canada.

A. J. Budz is with the Department of Engineering Physics, McMaster University, Hamilton, ON L8S 4L8, Canada (e-mail: budzaj@mcmaster.ca).

H. K. Haugen is with the Department of Engineering Physics and the Department of Physics and Astronomy, McMaster University, Hamilton, ON L8S 4L8, Canada (e-mail: haugenh@mcmaster.ca).

Digital Object Identifier 10.1109/LPT.2007.902942

II. Experimental Setup

Short pulses are generated by the external-cavity mode-locking of a single InGaAs quantum-well (QW) laser containing integrated gain and saturable absorber sections [5] (see [4] for a schematic of a typical experimental setup). A 600-lines/mm diffraction grating provides external cavity feedback and controls the operating wavelength. The laser contains a curved ridge-waveguide that terminates at a 7° angle relative to the external cavity facet, which, in conjunction with a single-layer SiO_xN_y antireflection (AR) coating, prevents lasing from occurring in the diode chip.

The pulsing characteristics of the laser are monitored using a 50-GHz oscilloscope and a 22-GHz RF spectrum analyzer by coupling a portion of the beam into a 20-GHz photodetector. The trigger for the oscilloscope is derived by amplifying the output of a 3-GHz photodiode. The time-domain measurement has a total impulse response time of 20 ps. Pulse durations are determined using a collinear intensity autocorrelator (assuming a sech^2 pulse shape) and optical spectra are measured using an optical spectrum analyzer with a 0.05-nm resolution.

III. Results and Discussion

Passive mode-locking at the fundamental repetition rate of the external cavity (577 MHz) occurs over a broad bias parameter range with typical gain section currents of 20 to 40 mA and saturable absorber reverse voltages of −0.8 to −2.2 V. Pulse durations vary from as low as 1 ps to as high as 9 ps depending on the laser bias parameters, with shorter pulses typically obtained at lower gain currents and larger absorber reverse voltages. The autocorrelation trace, optical spectrum, oscilloscope trace, and photodiode RF spectrum for a typical 2-ps, 300-μW average power pulse train are shown in Fig. 1.

Mode-locking can also be achieved at harmonics of the cavity round-trip frequency by simply adjusting the gain current with the absorber bias fixed. Changes to the length of the external cavity are not necessary. Harmonic mode-locking is a condition in which multiple, equally spaced pulses circulate in the cavity, leading to a multiplication of the pulse repetition rate [6]. Fig. 2 depicts the change in mode-locking repetition rate as a function of gain current with the absorber bias fixed at −1.0 V. First-harmonic or fundamental mode-locking occurs

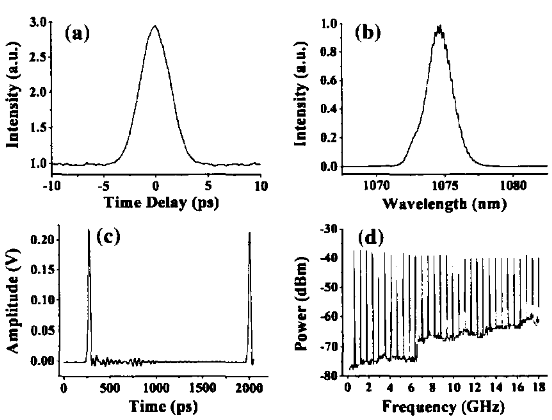

Fig. 1. Typical characteristics of a 2-ps, 577-MHz ML pulse train: (a) autocorrelation trace, (b) optical spectrum, (c) oscilloscope trace, and (d) photodiode RF spectrum. The small subsidiary peaks in (c) are electronic ringing.

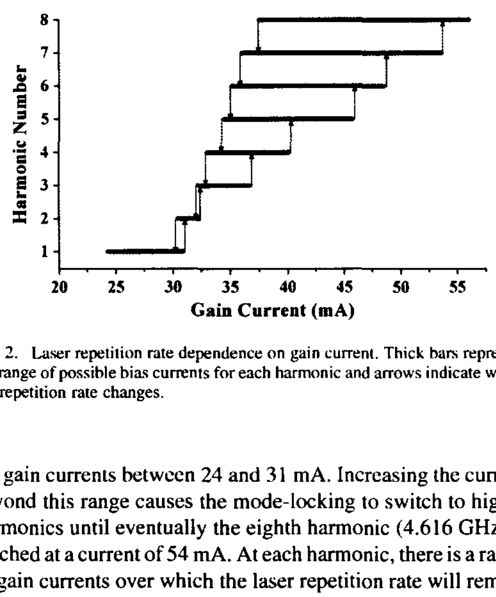

Fig. 2. Laser repetition rate dependence on gain current. Thick bars represent the range of possible bias currents for each harmonic and arrows indicate where the repetition rate changes.

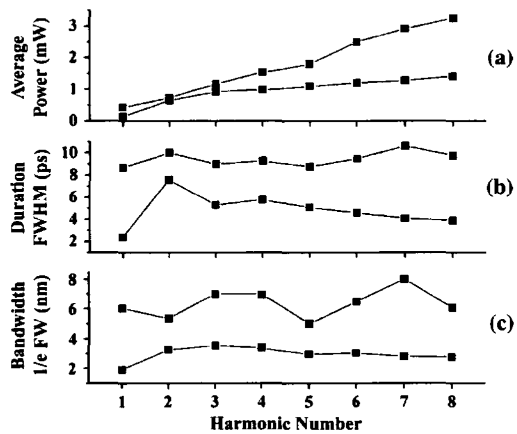

Fig. 3. Pulse parameters versus harmonic mode-locking number: (a) average power, (b) duration, and (c) bandwidth. In each plot, the two curves represent the upper (maximum gain current) and lower (minimum gain current) limits of values attainable at each harmonic.

for gain currents between 24 and 31 mA. Increasing the current beyond this range causes the mode-locking to switch to higher harmonics until eventually the eighth harmonic (4.616 GHz) is reached at a current of 54 mA. At each harmonic, there is a range of gain currents over which the laser repetition rate will remain locked. Reducing the current below the range causes the laser to drop down to the next lowest harmonic. The stability of each harmonic was confirmed by monitoring the pulse train in both the time and frequency domain with the 50-GHz oscilloscope and 22-GHz RF spectrum analyzer. By carefully aligning the external cavity prior to initiating mode-locking, the supermode noise spurs [7] could be suppressed by more than 40 dB for all eight harmonics. Mode-locking could be obtained at up to the 13th harmonic (7.5 GHz) at a drive current of 65 mA and a corresponding supermode suppression ratio of 30 dB. However, we could not observe the pulsing characteristics in the time domain beyond the eighth harmonic due to bandwidth limitations of the RF signal required to trigger the fast oscilloscope. Harmonic mode-locking could also be obtained at other absorber voltages but the switching behavior depicted in Fig. 2 was found to be optimal for biases around -1.0 V.

The variation of average power, pulse duration, and spectral bandwidth as a function of harmonic number are shown in Fig. 3. We use the $1/e$ full-width as a measure of the pulse bandwidth to account for presence of broader shoulders on some of the harmonic pulses and the fact that the shape of the spectrum changes with current. Each plot in Fig. 3 shows two curves which represent the maximum and minimum values attainable for each pulse parameter at a given harmonic and correspond directly to the maximum and minimum gain currents at a given harmonic. Fine tuning of the pulse parameters at each harmonic can be made in between the upper and lower curves through adjustment of the gain section current. For example, the pulse duration of the first harmonic pulse train varies between 2.4 ps at 24 mA of gain current and gradually increases with gain current until a final duration of 8.7 ps is obtained at 31 mA. Some general trends evident in Fig. 3 are that, at each harmonic, an increase in the gain current results in higher average power with longer pulses and more bandwidth. This behavior is typical of passively ML diode lasers where an increase in the active region carrier density increases the energy per pulse and the amount of self-phase modulation, leading to spectrally broader pulses. Pulses with larger spectral content are more susceptible to temporal spreading after propagating through the gain region due to the magnitude and phase response of the amplifier section [8]. Operating at the lowest gain current at each harmonic will provide the shortest pulses that are closest to the transform limit. However, this also results in pulses with lower average power, which may not be optimal when seeding a high-power YDFA where saturation of the amplifier gain is crucial.

The harmonic mode-locking behavior shown in Fig. 2 is a consequence of the interplay between the recovery time of the gain medium and the amount of unsaturated gain in the cavity [9]. Although the results shown above are obtained for an operating wavelength of 1075 nm, mode-locking at several different harmonic numbers could also be obtained at other wavelengths within the tuning range of the oscillator. Operation at the higher

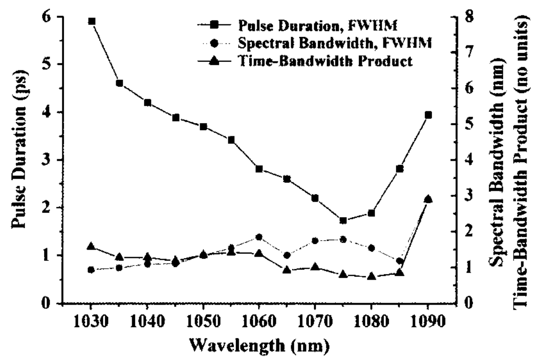

Fig. 4. Mode-locked pulse duration, spectral bandwidth, and time-bandwidth product versus wavelength at a pulse repetition rate of 577 MHz.

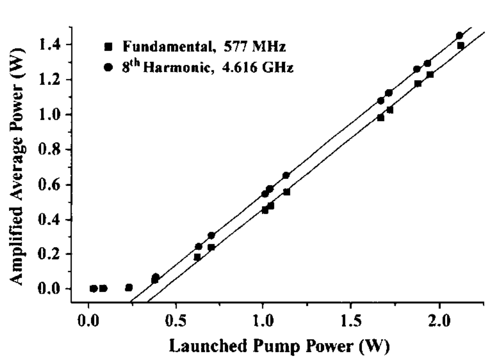

Fig. 5. Amplification characteristics of the fundamental and eighth-harmonic pulse trains at 1075 nm when coupled into a single-mode YDFA.

harmonics, however, was only possible near the gain peak of the laser (1077 nm), where the unsaturated gain of the laser can be increased to its largest value.

The wavelength-tuning characteristics of the ML oscillator when operated at the fundamental repetition rate are shown in Fig. 4. Pulses 2–6 ps in duration are obtained over a 60-nm tuning range, with time-bandwidth products as low as 0.7, and average powers around 300 μW. Since these pulses are chirped, pulse compression could be employed for further reductions in pulsewidth. The tuning results are obtained by adjusting the bias of both the absorber and the gain section in order to yield the shortest pulse duration at each wavelength. Pulses with higher average power (up to 1 mW) and longer duration (up to 10 ps) could also be generated at each wavelength by increasing the current through the gain section. At wavelengths longer than 1090 nm, small satellite pulses delayed by the round-trip time of the diode chip were visible in the autocorrelation traces, indicating the limitations of the single-layer AR coating. Tuning the wavelength below 1030 nm resulted in pulses that were unstable and had increased timing jitter which was evident by the broadening of 577-MHz RF spectral linewidth from 900 Hz (instrument limited) to greater than 15 kHz. Although the active region of these lasers contains only a single QW, the operating wavelength can still be varied by as much as 60 nm, enabling one to seed over a substantial fraction of the YDFA gain bandwidth.

Lastly, we compare the amplification of 6-ps pulses from the fundamental and eighth harmonic in a 15-m-long, 6-μm-core-diameter YDFA pumped counter-directionally at 975 nm (Fig. 5) .[1] The coupled seed average powers for the 577-MHz and 4.616-GHz signals are 0.2 and 1.3 mW, respectively. The slope efficiency of both curves is around 81% and amplified spontaneous emission background levels correspond to 3% (577 MHz) and below 1% (4.616 GHz) of the signal power. Although the amplified average power for both signals is similar, the peak power of the 4.616-GHz pulses is almost an order of magnitude lower.

IV. Conclusion

We have presented an ML diode laser that offers broad repetition-rate and wavelength tunability centered at 1060 nm. External-cavity mode-locking provides a low-complexity solution toward obtaining ultrashort pulses while still maintaining good flexibility of output pulse parameters such as duration, wavelength, average power, and bandwidth. Further work will focus on studying the timing stability and noise properties of the harmonic mode-locking. Overall, these lasers appear very promising as versatile seed-sources for high-gain YDFAs.

Acknowledgment

The authors wish to thank CorActive for providing the Yb-doped fiber used in the YDFA and M. J. Brennan for contributions made during the early stages of the fiber project.

References

[1] P. Dupriez, A. Piper, A. Malinowski, J. K. Sahu, M. Ibsen, B. C. Thomsen, Y. Jeong, L. M. B. Hickey, M. N. Zervas, J. Nilsson, and D. J. Richardson, "High average power, high repetition rate, picosecond pulsed fiber master oscillator power amplifier source seeded by a gain-switched laser diode at 1060 nm," *IEEE Photon. Technol. Lett.*, vol. 18, no. 9, pp. 1013–1015, May 1, 2006.

[2] B. Adhimoolam, M. G. Hekelaar, P. Gross, I. D. Lindsay, and K.-J. Boller, "Wavelength-tunable short-pulse diode-laser fiber-amplifier system around 1.06 μm," *IEEE Photon. Technol. Lett.*, vol. 18, no. 7, pp. 838–840, Apr. 1, 2006.

[3] P. Dupriez *et al.*, "High-power, high repetition rate picosecond and femtosecond sources based on Yb-doped fiber amplification of VECSELs," *Opt. Express*, vol. 14, pp. 9611–9616, Oct. 2006.

[4] A. J. Budz, A. S. Logan, D. Strickland, and H. K. Haugen, "Ultrashort pulses from a mode locked diode-oscillator Yb-fiber-amplifier system," *IEEE Photon. Technol. Lett.*, vol. 19, no. 2, pp. 94–96, Jan. 15, 2007.

[5] M. J. Brennan, A. J. Budz, B. J. Robinson, P. Mascher, and H. K. Haugen, "Ultrashort optical pulse generation with a mode-locked long-wavelength (1075–1085 nm) InGaAs–GaAs semiconductor laser," *IEEE Photon. Technol. Lett.*, vol. 16, no. 8, pp. 1798–1800, Aug. 2004.

[6] A. Siegman, *Lasers*. Mill Valley, CA: Univ. Science Books, 1986.

[7] F. Rana *et al.*, "Characterization of the noise and correlations in harmonically mode-locked lasers," *J. Opt. Soc. Amer. B*, vol. 19, pp. 2609–2621, Nov. 2002.

[8] D. J. Derickson, R. J. Helkey, A. Mar, J. R. Karin, J. G. Wasserbauer, and J. E. Bowers, "Short pulse generation using multisegment mode-locked semiconductor lasers," *IEEE J. Quantum Electron.*, vol. 28, no. 10, pp. 2186–2202, Oct. 1992.

[9] S. Sanders, A. Yariv, J. Paslaski, J. E. Ungar, and H. A. Zarem, "Passive mode locking of a two-section multiple quantum well laser at harmonics of the cavity round-trip frequency," *Appl. Phys. Lett.*, vol. 58, pp. 681–683, Feb. 1991.

[1]The experimental setup is similar to that shown in [4] except that light from the oscillator is coupled directly into the Yb-doped fiber.

Figure 4-12 shows the oscilloscope traces for the $N = 1$ to $N = 6$ harmonically mode-locked pulse trains, where N is the harmonic number or the number of pulses circulating in the cavity. In an N^{th} harmonically mode-locked laser, longitudinal modes separated in frequency by Nf_c are locked in phase, where f_c is the cavity mode spacing. Harmonic mode-locking can be achieved via active mode-locking by modulating the laser at a harmonic of the cavity mode spacing or via passive mode-locking by operating at elevated pumping levels. Harmonic mode-locking has been demonstrated using semiconductor lasers [123], fibre lasers [124], and bulk solid-state lasers, such as Ti:sapphire [125]. The technique is useful for achieving high-frequency mode-locking of lasers that require a longer cavity length in order to accommodate intracavity elements for bandwidth limiting and dispersion compensation. Semiconductor lasers are generally capable of producing higher mode-locked frequencies than any other type of laser, by virtue of their relatively small cavity length, and when combined with the technique of harmonic mode-locking, diode lasers can generate pulses at ultrahigh repetition frequencies (e.g., 1.5 THz [49], 2.1 THz [50]). Such high repetition rate sources are interesting for high-speed optical communication systems, ultrafast data processing, and terahertz generation.

The ability to vary the repetition frequency of a passive harmonically

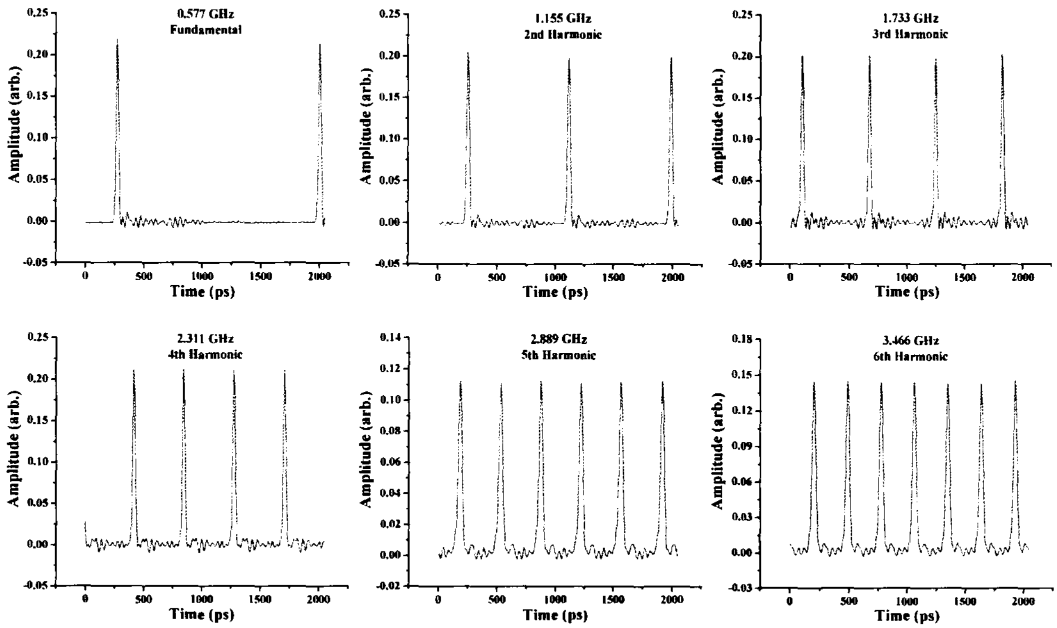

Figure 4-12: Oscilloscope traces of mode-locking at the first through sixth harmonics.

mode-locked diode laser through the adjustment of the gain current is a consequence of the interplay between the recovery time of the gain medium and the amount of unsaturated gain in the cavity [123]. As the gain current is increased, the unsaturated gain in the cavity builds, allowing for the existence of multiple pulses. This method of tuning the pulse repetition rate of the laser is very convenient as it does not require any modification to the length of the cavity or re-alignment of the external-cavity coupling. Harmonic mode-locking was observed with the majority of the devices tested and as discussed in Paper 3, operation at the higher harmonics was typically achieved near the gain peak of the laser for an optimal set of bias conditions.

The 1070 nm oscillators offer similar mode-locked performance as other diode lasers operating at different wavelengths. Mode-locked laser properties, such as pulse duration, pulse energy, and wavelength tuning range, are on par with other mode-locked diode lasers. However, the 1070 nm lasers have demonstrated the ability to produce sub-10-ps pulses over both a broad wavelength and repetition-rate tuning range, which is a characteristic that is typically not reported on in the literature. The passively mode-locked wavelength tuning range of 60 nm is good considering that the active region of the laser contains only a single quantum-well. Recall from Chapter 2 that semiconductor lasers containing asymmetric quantum-well active regions having broadened gain-bandwidths are typically used to achieve a large wavelength tuning range. Another factor that can limit the tuning range of a mode-locked laser is the residual reflectivity of the semiconductor facet that couples light to the external cavity, which depends on the quality of the AR coating. The performance characteristics of several wavelength-tunable mode-locked diode lasers will be highlighted below.

Brennan *et al.* have reported on the performance of a passively mode-locked diode laser operating near 980 nm [73]. The laser is based on a two-contact design containing a curved ridge waveguide and the active region consists of two asymmetric quantum-wells. Pulses of 2 to 4 ps in duration are generated over a 61 nm tuning range, centered at 985 nm. Average powers of 500 μW are obtained for a pulse repetition rate of 700 MHz.

A 26 nm tuning range has been reported by Schrans *et al.* for a passively mode-locked two-section laser operating near 840 nm [126]. The laser contains four quantum-wells and uses a 600 lines/mm diffraction grating for feedback. Pulses with a duration of 4 ps and a repetition rate of 550 MHz are generated.

Adhimoolam *et al.* have reported on a 1.4 GHz actively mode-locked InGaAs-GaAs semiconductor-seed-source for a Yb:fibre amplifier [22]. Pulse durations of 28–44 ps are obtained over a 45 nm wavelength range, from 1040 to 1085 nm, with average powers of 15 mW.

One of the largest reported mode-locked tuning ranges was obtained at the telecommunications wavelength of 1550 nm [9]. Pulse widths on the order of 30 ps were obtained over a 115 nm span (1448 to 1563 nm) with typical average output powers of 100 μW. The multiple quantum-well laser was actively mode-locked at 300 MHz using 150 ps electrical pulses from a comb generator.

4.6 Noise Characteristics of Mode-Locked Diode Lasers

The output of an ideal mode-locked laser consists of a train of pulses that are perfect periodic replicas of each other. In practice, the output of any mode-locked laser will exhibit random fluctuations in the properties of the emitted pulses. Such random fluctuations represent a form of noise, leading to pulse-to-pulse variations in the shape, duration, energy, period, or optical frequency of the mode-locked pulses. The measurement and stabilization of mode-locked laser noise is currently an area of active and intense research, providing important information on the dynamic operating characteristics and behavior of the laser. The present discussion of mode-locked laser noise will be limited to amplitude and phase noise, since they are typically dominant over other sources of noise. Figure 4-13 shows a conceptual diagram of a pulse train exhibiting amplitude and phase noise. Amplitude jitter is the variation in the energy per pulse, while phase or timing jitter is the variation in the repetition period of the laser. The following

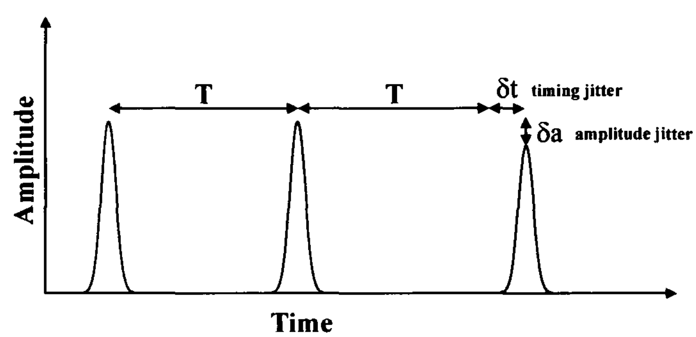

Figure 4-13: Pulse train of repetition period, T, exhibiting timing noise, δt, and amplitude noise, δa.

section will present measurements on the noise characteristics of two hybridly mode-locked diode lasers: one operating at a wavelength of 1040 nm and the second operating at 1080 nm. The noise characteristics of each laser were measured prior to synchronizing the two lasers, which will be discussed in the next section, in order to determine the dominant source of noise of each laser and to quantify the absolute magnitude of the noise.

The approach used to measure the amplitude and phase jitter is based on the frequency-domain technique described by von der Linde [127]. The measurement approach relies on recording the power spectrum of the laser intensity using a high-speed photodiode and an RF spectrum analyzer. The frequency spectrum of a mode-locked pulse train consists of a series of delta-function-like components located at the harmonics of the pulse repetition frequency. Noise on the optical pulses arising from both amplitude and phase jitter produce broad side-bands on each discrete spectral harmonic. Von der Linde has shown that phase noise can be distinguished from amplitude noise by noting that the spectral density of phase noise increases as the square of the harmonic number, whereas the spectral density of amplitude noise is independent of the harmonic number. Therefore, at sufficiently high harmonic numbers, the noise side-bands are dominated by phase noise.

The experimental setup is shown in Figure 4-14. The optical pulses are detected and amplified using a 20 GHz photodiode (1414, New Focus) and two low-noise broadband RF amplifiers (ZX60-6013E-S+, Mini-Circuits), each having a gain of around 16 dB at 0.5 GHz. A 26.5 GHz RF spectrum analyzer (E4440A, Agilent) with a resolution bandwidth of 1 Hz is used to measure and record the power spectrum of each laser. Using the above experimental setup, a measure of the absolute noise of the laser is obtained, comprising the noise from all possible sources. For the case of an external-cavity hybridly mode-locked semiconductor laser, there are many sources that contribute to the absolute noise. Included amongst these are DC current and voltage sources, the RF modulation

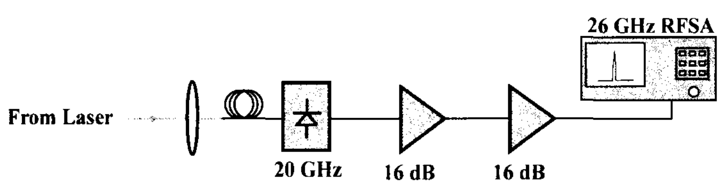

Figure 4-14: Experimental configuration used to measure the noise of a mode-locked laser.

source, thermal drift of the optical components in the external cavity, vibration of the optical components in the external cavity, air temperature and density fluctuations, and spontaneous emission. In the literature, laser noise is classified as absolute, which comprises noise from all the sources as described above, or the noise can be classified as residual, which represents the noise of the laser independent of the noise from the RF source. A measure of the residual phase noise can be obtained using a homodyne detection technique in which the output of the high-speed photodiode is mixed exactly in quadrature (90° out of phase) with a signal from the RF synthesizer [128].

The basic measurement of laser noise is obtained by converting the measured power spectra to a single-side-band (SSB) noise spectral density, from which the amplitude and phase noise content can be extracted. The noise power spectral density is normalized to the power of the carrier or the harmonic component at which the noise side-bands are measured. The normalized SSB noise spectral density, $L(f)$, is the ratio of the measured noise power in a 1 Hz integration bandwidth, $P_n(f)$, to the total carrier power, P_c, at an offset frequency, f, away from the carrier frequency [51]:

$$L(f) = \frac{P_n(f)}{P_c} \tag{4.8}$$

Noise spectral densities of mode-locked lasers are typically specified in logarithmic units of dBc/Hz (dB below the carrier, in a 1 Hz bandwidth). By converting the noise power spectral density to a normalized noise spectral density, a measure of the laser noise is obtained which is independent of the power level of the laser, allowing the noise properties of different laser sources to be more easily compared.

Figure 4-15 shows measurements of the absolute noise spectral density of a hybridly mode-locked laser operating at a wavelength of 1080 nm and a repetition rate of 0.577 GHz. $L(f)$ has been measured at the n = 1 fundamental frequency component of 0.577 GHz, as well as at harmonic components of n = 2, 3, 5, and 10 (n = 10 not shown in Figure 4-15). (The harmonic number, n, used in this section refers to the harmonic Fourier component of the frequency spectrum of the mode-locked laser, as measured by the RFSA, and should not be confused with the harmonic number, N, of a harmonically mode-locked laser, discussed in the previous section). At offset frequencies of 5–10^5 Hz, the noise spectral density increases with harmonic number, indicating that the measured noise is mostly

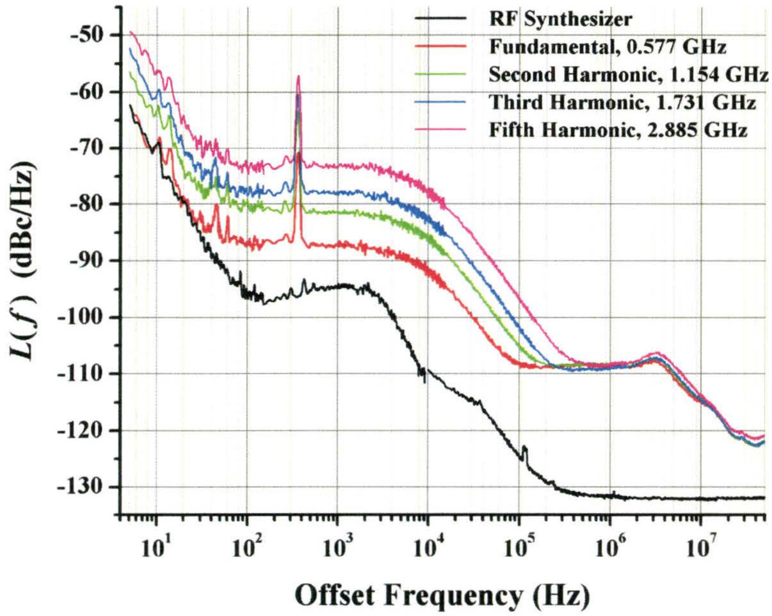

Figure 4-15: SSB noise spectral density of a hybridly mode-locked laser operating at a wavelength of 1080 nm and a repetition rate of 0.577 GHz.

phase noise in nature. As discussed previously, phase noise increases as the square of the harmonic number, causing the relative phase noise level to increase by 6, 9.5, and 14 dB, respectively, for the $n = 2$, 3, and 5 harmonics. This relative increase in the phase noise level as a function of harmonic number is qualitatively observed in the noise traces of Figure 4-15. To determine more quantitatively if the noise level is following an n^2 relationship, $L(f)$ is integrated between 5–10^5 Hz for each laser harmonic. The integration results are shown in Figure 4-16, along with a quadratic fit to the data, revealing that the measured noise is in fact dominated by phase noise at low to intermediate offset frequencies. At offset frequencies larger than 10^5 Hz, the noise spectral density is relatively independent of the harmonic number, indicating that amplitude jitter is the main source of laser noise at high frequencies. At offset frequencies above 3×10^7 Hz, the noise floor of the measurement system is reached. The noise spectral density of the RF synthesizer is obtained by connecting the output of the RF source to the RFSA through a power attenuator, with the RF source operating at the same power level as that used to hybridly mode-lock the laser (typically a few dBm). At offset frequencies below 30 Hz, the phase noise of the laser is dominated by the RF source, indicating that the absolute timing jitter of the mode-locked pulses could be reduced by utilizing an RF synthesizer with improved phase noise

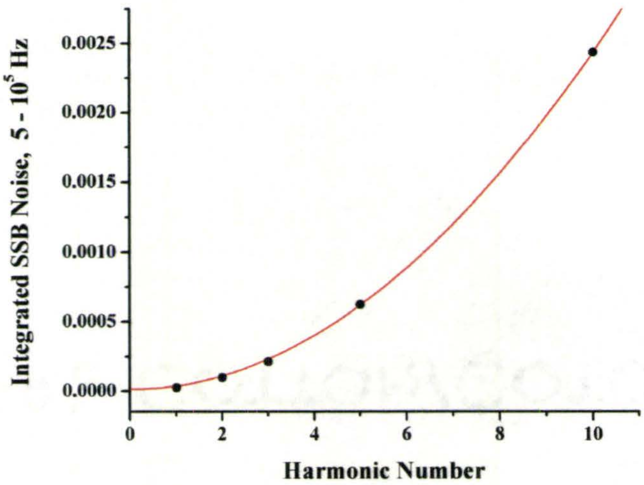

Figure 4-16: SSB noise spectral density of Figure 4-15 integrated over a bandwidth of 5–10^5 Hz as a function of harmonic number. A quadratic fit to the data is shown.

characteristics. To verify this fact, the phase noise characteristics of two different RF synthesizers were measured using the RFSA and were found to exhibit lower noise spectral density (by about 15 dB at some frequencies) over the bandwidth of 5–10^4 Hz compared to the RF source used to hybridly mode-lock the lasers. However, as the phase noise measurements of the RF synthesizers were performed well after the completion of the noise experiments, the reduction in the timing jitter of the mode-locked laser due to the use of a low-noise RF source could not be quantified.

Figure 4-17 compares the noise properties of the 1080 nm mode-locked laser when operated under passive and hybrid mode-locking. For offset frequencies higher than 10^4 Hz, the noise properties of the laser are similar, regardless of the method used to mode-lock the laser. However, below 10^4 Hz, the passively mode-locked laser exhibits significantly higher noise, with a mean decrease in the spectral density of -20 dB/decade. A passively mode-locked laser will typically have very high timing jitter levels due to the absence of a high stability driving source [51]. The free-running nature of the oscillator gives rise to large frequency drifts over long periods of time. Although the frequency-domain noise measurement technique described by von der Linde is generally not applicable to passively mode-locked lasers, since the timing fluctuations of a passively mode-locked laser are cumulative [129], the technique was nevertheless applied to qualitatively determine the ability of the RF source to stabilize the timing fluctuations of the mode-locked lasers. Accurate measurement of the

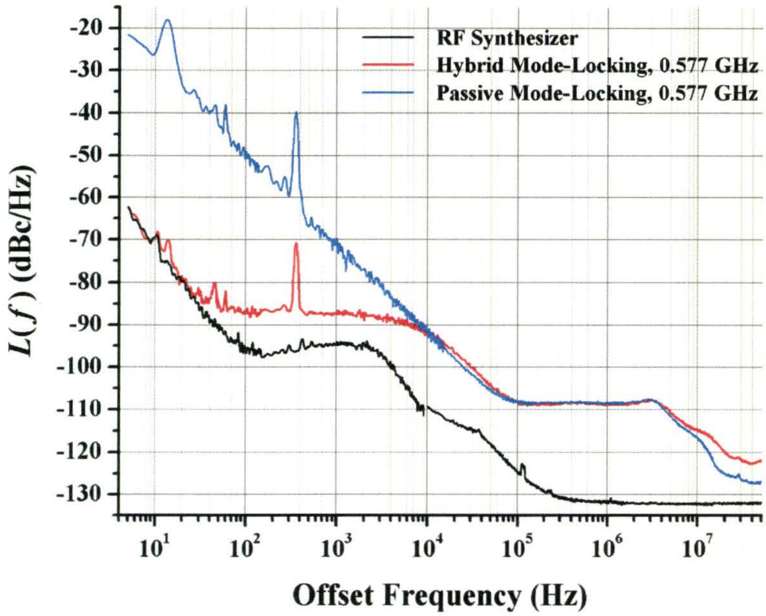

Figure 4-17: SSB noise spectral density of a hybridly and passively mode-locked laser operating at a wavelength of 1080 nm and a repetition rate of 0.577 GHz.

timing jitter of a passively mode-locked laser can be achieved using an optical cross-correlation technique [130].

Figure 4-18 shows measurements of the noise spectral density of a second external-cavity hybridly mode-locked laser operating at a wavelength of 1040 nm and a repetition rate of 0.577 GHz, which is the same as that of the 1080 nm laser. The noise spectral density of the 1040 nm mode-locked laser is dominated by phase noise at offset frequencies below ~4×10^5 Hz, while amplitude noise dominates at larger frequencies.

Figure 4-19 compares the noise characteristics of the 1080 nm and 1040 nm mode-locked lasers at the first-order frequency component of 0.577 GHz. Both lasers are dominated by the phase noise of the RF source at frequencies below ~30 Hz. Above 30 Hz, the 1080 nm laser exhibits a slightly higher white-noise plateau of -87 dBc, which eventually begins to roll-off at a corner frequency of around 10^4 Hz. The white-noise plateau of the 1040 nm laser has a larger corner frequency of 7×10^4 Hz and the amplitude noise of the laser at large offset frequencies is higher compared to the 1080 nm laser. The 1080 nm laser exhibits an interesting narrow-band noise signal located at an offset frequency of 360 Hz. The 3 dB linewidth of the noise spur is around 30 Hz and it was present in all of

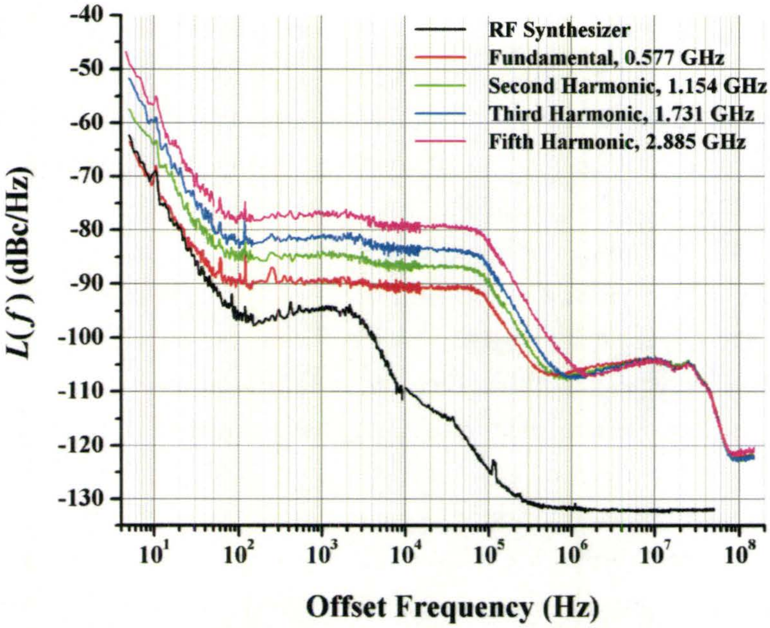

Figure 4-18: SSB noise spectral density of a hybridly mode-locked laser operating at a wavelength of 1040 nm and a repetition rate of 0.577 GHz.

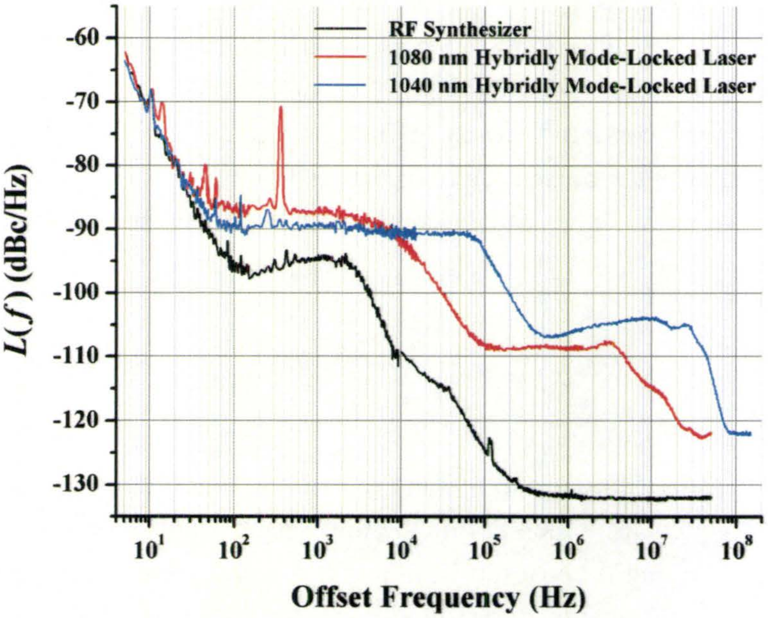

Figure 4-19: SSB noise spectral density of two 0.577 GHz hybridly mode-locked lasers operating at different wavelengths.

the noise measurements of the 1080 nm laser, independent of the method used to mode-lock the laser. The origin of the spur was determined to be due to acoustic modulation of the laser. Initially, the spur was thought to be related to 60 Hz AC line noise. However, in the process of troubleshooting the origin of the spur, it was discovered that speaking near the laser could enhance the magnitude of the spur. The acoustic nature of the noise spur was verified by driving a loudspeaker with a function generator and several different modulation resonances could be excited, with the largest occurring at 360 Hz. The noise spur could be enhanced by pointing the loudspeaker either directly at the laser or at the surface of the optical table. In fact, general background acoustic noise in the laboratory (e.g., people speaking, doors opening/closing, circulation fans) were found to contribute to the overall magnitude of the spur. As shown in Figure 4-15, the 360 Hz spur is present in the higher harmonics with a relative amplitude that increases as n^2, indicating that the spur is phase noise in nature. The cause of the acoustic modulation is believed to be due to the coupling of acoustic noise to the stainless-steel table-top of the optical table assembly. The optical table has characteristic resonance frequencies in the range of 100–500 Hz, with several narrow resonances in the vicinity of 300–400 Hz [131]. Acoustic noise seems to couple from the table-top to the optical mounting assembly that houses the diffraction grating in the external cavity. By softly touching the mounting assembly of the grating to dampen the vibrations, the noise spur could be reduced in amplitude, but not eliminated. The 1040 nm laser utilizes a different and much smaller mounting setup for the external-cavity diffraction grating, which could explain the absence of the spur in the noise spectra of the 1040 nm laser.

The rms timing jitter can be calculated by integrating the phase noise spectral density of the laser [51], [132]

$$\sigma_{rms} = \frac{1}{2\pi f_r}\sqrt{2\int_{f_L}^{f_H} L(f)df} \tag{4.9}$$

where σ_{rms} is the rms timing jitter, f_r is the repetition rate of the laser, and f_L and f_H are the offset frequencies which define the noise bandwidth. Figure 4-20 shows a graph of the rms timing jitter of the 1040 nm and 1080 nm mode-locked lasers as the offset frequency or noise bandwidth of the laser increases. The lower frequency integration limit is 5 Hz. The rms timing jitter of the 1040 nm laser extends to a larger offset frequency on account of its larger phase noise bandwidth (Figure 4-18). For reference, the timing jitter is also calculated for the noise

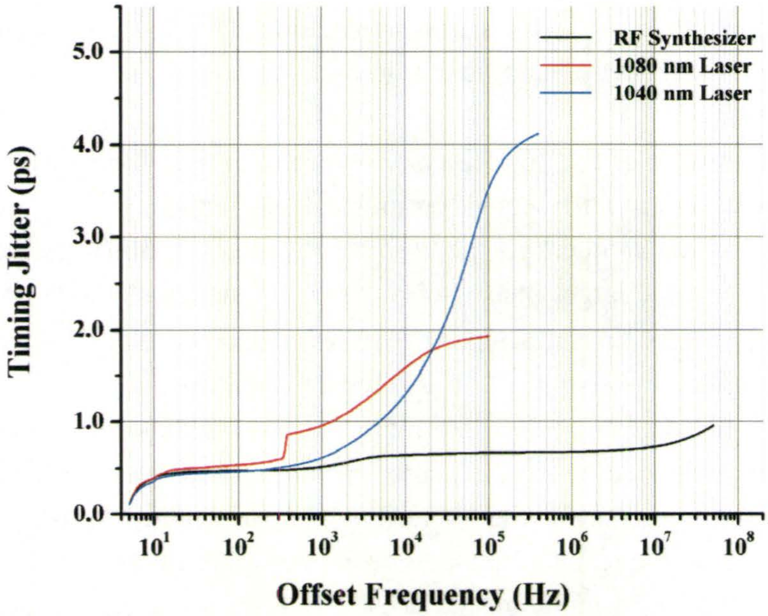

Figure 4-20: RMS timing jitter of the 1040 nm and 1080 nm mode-locked lasers calculated by integrating the SSB noise spectral density of each laser. The relevant integration bandwidths correspond to the phase-noise-dominated region of each laser.

spectrum of the RF source, assuming the measured noise is entirely due to phase noise. It should be noted that subtracting the noise values of the RF source from the laser noise will not yield an estimate for the residual noise of the mode-locked laser. Instead, to obtain a measure of the laser noise independent of the RF synthesizer noise, the homodyne detection technique described earlier should be used. The 360 Hz noise spur is included in the timing jitter calculation for the 1080 nm laser and is found to contribute a value of 0.6 ps rms to the total timing jitter measurement (timing jitter values add as the sum of squares), which is significant considering that overall rms timing jitter of the laser in the bandwidth of 5–10^5 Hz is 1.9 ps rms. The spatial displacement of an optical component in the cavity of a laser that is required to cause a rms jitter of 0.6 ps at 360 Hz can be calculated using [133]

$$\delta L = 2\pi L f_m \sigma_{rms} \tag{4.10}$$

where δL is the change in cavity length, L, required to cause a variation in the timing of the laser in response to a modulation frequency, f_m. Substituting the values above for the 360 Hz noise spur yields δL = 0.35 nm, or a relative change in the cavity length of 10^{-9}. From this calculation, it is evident that extremely small changes in the cavity length can lead to a substantial increase in the timing jitter of the laser.

In the absence of the 360 Hz noise spur, the timing jitters of the 1040 nm and 1080 nm lasers are fairly equal, up to an offset frequency of around 10^4 Hz. Beyond this offset frequency, the 1040 nm laser exhibits greater timing fluctuations due to the larger phase noise corner frequency of the laser, which is located at 7×10^4 Hz. The characteristic features of the phase noise spectra of the mode-locked lasers, consisting of an RF-source-dominated regime at low offset frequencies, a flat or white-noise-like regime at intermediate frequencies, and a corner frequency beyond which the phase noise has a characteristic roll-off, have been investigated theoretically [134]-[136] and experimentally [136], [137]. The phase noise corner frequency is found to be an important figure of merit since the overall timing jitter of a mode-locked laser is mostly due to the integrated noise power in the two decades of frequency surrounding the corner frequency [137]. Therefore, one method of minimizing timing jitter is by moving the phase noise corner frequency closer to the carrier. It has been demonstrated experimentally that the phase noise corner frequency is equal to the linewidth of the oscillating Fabry-Perot longitudinal cavity modes, which comprise the optical pulse [136], [137]. By increasing the cavity length [136], [137] or the Q-factor of the cavity [138], [139], the linewidth of the cavity modes decreases, pushing the phase noise corner frequency to lower offset frequencies, which reduces the integrated timing jitter. The relationship between cavity length and phase noise corner frequency has been used to obtain low-phase-noise harmonically mode-locked lasers [140]. By harmonic mode-locking a laser containing a relatively long cavity length, one can simultaneously achieve the low phase noise that is characteristic of a long-cavity laser, and the high pulse repetition rates that are characteristic of a short-cavity laser. One trade-off associated with harmonic mode-locking is the possibility of inducing supermode noise [141] in the laser output, which can be overcome using a suitable intracavity etalon [139].

Since the 1040 nm and 1080 nm lasers both have the same cavity length, the fact that the 1040 nm laser has a larger phase noise corner frequency could be due to higher loss in the external cavity of the laser, arising from either a lower optical coupling efficiency from the external-cavity into the waveguide of the gain section or from a higher reflection loss at the diffraction grating. A higher cavity loss affects the cavity Q, and therefore, the phase noise corner frequency [138], [139]. However, further work is required to isolate the exact mechanism responsible for the differences in the phase noise corner frequency of the two lasers.

The timing jitters exhibited by the two lasers are comparable to other mode-locked semiconductor lasers. However, the measurements reported here represent the absolute noise of the laser, whereas most of the results reported in the literature focus on the residual phase noise of the laser. Therefore, the measurements reported in this thesis will be inherently larger when comparing absolute to residual phase noise. Derickson *et al.* have reported on the performance of a hybridly mode-locked quantum-well laser operating at a wavelength of ~800 nm and a repetition rate of 5.5 GHz [51]. The absolute and residual rms timing jitter of the laser in the bandwidth of 1.5×10^3–5×10^7 Hz is 1.06 and 0.98 ps, respectively. In comparison, the lasers developed in this thesis have rms jitter values of 4 ps and 1.6 ps, respectively, for the 1040 nm laser (1.5×10^3–4×10^5 Hz) and 1080 nm laser (1.5×10^3–10^5 Hz). Sanders *et al.* have reported on the absolute timing jitter of a two-section quadruple quantum-well laser mode-locked at a repetition rate of 546 MHz [132]. A value of 5.5 ps rms is obtained for a noise bandwidth of 50–10^4 Hz. To demonstrate the reduced timing jitter that can be achieved by harmonic mode-locking with an extended cavity length, Yilmaz *et al.* have reported on the noise properties of a 10 GHz fundamentally mode-locked laser and a 10 GHz harmonically mode-locked laser having a fundamental cavity repetition rate of 147 MHz [140]. The cavity lengths differ by a factor of 7, leading to a reduction in the phase noise corner frequency from 55 MHz in the fundamentally mode-locked laser to 600 kHz in the harmonically mode-locked laser. The corresponding residual rms timing jitter in the bandwidth of 10–5×10^9 Hz was 0.67 ps and 0.24 ps, respectively, for the fundamentally and harmonically mode-locked lasers. In addition to mode-locking with an extended cavity length, the phase noise of a mode-locked semiconductor laser can be minimized using a low-noise RF source [142], [143], a phase-locked loop [144], [145], and by optical synchronization with an external, low-noise optical source [146].

4.7 Mode-Locked Laser Synchronization and Dual-Wavelength Amplification in Yb:Fibre Amplifiers

4.7.1 Paper 5: Short-Pulse Dual-Wavelength System Based on Mode-Locked Diode Lasers with a Single Polarization-Maintaining Yb:Fiber Amplifier

The following manuscript reports on the development of a novel dual-wavelength optical source based on the synchronization and amplification of two external-cavity mode-locked diode lasers. Short picosecond pulses emitted by the synchronized mode-locked lasers, which are separated by about 40 nm, are simultaneously amplified in a polarization-maintaining Yb-doped fibre. The manuscript reports on the design, development, and characterization of a short-pulse dual-wavelength system which could be used as an attractive alternative for generating high-repetition-rate mid-infrared radiation through difference frequency mixing or for use in two-colour pump-probe experiments. Results are presented on the synchronization of the two mode-locked lasers, including the characterization of the relative timing jitter of the two lasers. Numerical simulations of the amplifier gain are also presented. The simulations are used to determine the optimal fibre length and seeding geometry for dual-wavelength amplification in the Yb-doped fibre. I was responsible for the numerical simulations, experimental measurements, data analysis, and the writing of the manuscript. J. Waisman helped with the initial development and benchmarking of the simulator, and Dr. H. Tiedje and Prof. H. Haugen provided extensive feedback on the manuscript. I would also like to acknowledge B. Morasse of CorActive Inc., who helped with the initial benchmarking of the simulator for selected operating conditions.

Accepted for publication in *J. Lightwave Technol.*, Nov. 12, 2008. 1

Short-Pulse Dual-Wavelength System Based on Mode-Locked Diode Lasers with a Single Polarization-Maintaining Yb:Fiber Amplifier

A. J. Budz, *Student Member, IEEE*, J. Waisman, H. F. Tiedje, and H. K. Haugen

***Abstract*—We report on the development of a short-pulse dual-wavelength source consisting of mode-locked diode lasers and a single Yb-doped double-clad fiber amplifier. Two mode-locked external-cavity semiconductor oscillators operating at a repetition rate of 577 MHz with center wavelengths of 1040 nm and 1079 nm are synchronized, producing short pulses which are injected into a Yb-doped polarization-maintaining fiber for amplification. Numerical simulations are used to determine the optimal fiber length and seeding configuration for dual-wavelength amplification in the fiber. Each signal is amplified to an average power of 0.5 W with pulse durations of around 5 ps. Performance issues associated with two-signal amplification in Yb-doped fibers are discussed, as well as perspectives for increasing the wavelength separation of the seed lasers.**

***Index Terms*—Mode-locked lasers, optical fiber amplifiers, optical pulse amplifiers, semiconductor lasers, ytterbium-doped fiber amplifiers (YDFAs).**

I. Introduction

There has been recent interest in the development of ytterbium-doped fiber amplifier (YDFA) systems which utilize a mode-locked semiconductor laser as the seed source [1]-[3]. Such hybrid master-oscillator power-amplifier (MOPA) systems are advantageous since they combine the attractive features of both semiconductor and fiber technologies. Mode-locked diode lasers are capable of readily generating short ps-pulses with broad repetition-rate and wavelength tunability [4], and can exhibit ultralow pulse-to-pulse timing jitter [5]. YDFAs can offer high gain, good efficiency, and excellent beam quality on account of the guided-wave nature of the amplifier [6]. Some of the reported hybrid MOPA systems consisting of a YDFA seeded by a mode-locked semiconductor oscillator include a 30-ps source based on an actively mode-locked diode laser producing amplified average powers of 9.5 W which could be tuned over 45 nm [1]. In a Yb:fiber system based on a passively mode-locked diode oscillator, amplified average powers of up to 0.8 W and pulse durations of 765 fs have been obtained following compression [2]. Also, a multistage YDFA operating in the parabolic-pulse regime has been used to amplify the output of a passively mode-locked vertical-external-cavity surface-emitting diode laser, generating pulses with high average power that were subsequently compressed down to 110 fs [3].

In this paper, we report on the development of a short-pulse dual-wavelength source based on two synchronized mode-locked semiconductor oscillators and a single polarization-maintaining (PM) YDFA. A dual-wavelength hybrid MOPA source could potentially be used for generating high-repetition-rate mid-infrared radiation (MIR) through difference-frequency mixing (DFM), or for two-color pump-probe experiments. Some work involving YDFAs and diode seed lasers for the development of dual-wavelength sources has been reported. Goldberg *et al.* utilized continuous-wave (CW) diode lasers to seed separate Yb-doped and Er-doped fiber amplifiers, generating signals at 1.1 μm and 1.5 μm, which were used to produce MIR at 3.5 μm by DFM in $LiNbO_3$ [7]. Creeden *et al.* utilized two ns-pulsed diode lasers separated by 5.2 nm to generate terahertz radiation at 216 μm using DFM in ZGP by preamplifying the output of each diode laser in separate YDFA chains, followed by simultaneous power-amplification of both signals in a multistage large-mode-area YDFA [8]. In work involving the use of a mode-locked Yb:fiber seed oscillator, Romero-Alvarez *et al.* has recently demonstrated generation of 18-μm radiation by difference-frequency mixing the output of a multistage two-color fiber amplifier in GaSe [9]. In the present paper, we describe the development of a compact, dual-wavelength source consisting of a single YDFA and synchronized semiconductor seed lasers operating at wavelength differences of up to 60 nm. Numerical simulations are conducted to optimize the amplification performance of the dual-wavelength YDFA and to determine the effect of various seeding configurations on amplifier gain and signal-to-noise

Manuscript received July 25, 2008; revised November 7, 2008. This work was supported in part by the Canadian Institute for Photonics Innovations, within the Networks of Centres of Excellence, and in part by the Natural Sciences and Engineering Research Council of Canada.

A. J. Budz is with the Department of Engineering Physics, McMaster University, Hamilton, ON L8S 4L7, Canada (email: budzaj@mcmaster.ca).

J. Waisman was with the Department of Engineering Physics, McMaster University, Hamilton, ON L8S 4L7, Canada.

H. F. Tiedje is with the Brockhouse Institute for Materials Research, McMaster University, Hamilton, ON L8S 4M1, Canada.

H. K. Haugen is with the Department of Engineering Physics and also with the Department of Physics and Astronomy, McMaster University, Hamilton, ON L8S 4L7, Canada

Accepted for publication in *J. Lightwave Technol.*, Nov. 12, 2008.

ratio. In addition, we demonstrate experimentally that good performance can be obtained in a single YDFA for two mode-locked semiconductor seed oscillators separated by approximately 40 nm.

II. Theory

In order to study the amplification of the two seed signals in the fiber we have developed a model of the experimental setup. Due to the small absorption tail of Yb^{3+} which extends out to around 1.1 μm, significant reabsorption of the amplified signal can occur in regions of the fiber that are not pumped, resulting in gain spectra which become highly dependent on the length of the fiber [10]. Modeling the behavior of the amplifier becomes particularly important for the case of multiple input signals of different wavelength, due to the effects of gain competition in the amplifier, and also because of the different seeding geometries that are possible. Simulations are conducted to optimize the performance of the dual-wavelength amplifier under the constraint that the two signals are amplified to the same power level. The model will therefore specify the length of fiber which yields equal gain for the two signal wavelengths and will allow us to study how the different seeding configurations impact the overall performance of the amplifier.

Simulations of the YDFA gain are based on a standard rate equation model for a CW input signal. Approximating the input signals to the amplifier as time-independent is reasonable as the seed lasers are operating at pulse repetition rates of 577 MHz. The period between pulses is much smaller than the excited-state lifetime, causing the pulse train to behave as a quasi-CW signal inside the amplifier. In addition, pulse energies and peak intensities in the fiber are low enough that nonlinear optical effects are minimal (B-integral [11] ~ 1 for the experiments described in this paper). Distortions to the pulse amplitude due to dispersion and self- or cross-phase modulation are minor and can be expected to have a negligible effect on the overall amplifier gain. Since we are mainly interested in simulation results that concern the steady-state characteristics of the amplifier gain, a CW model can provide the relevant information with minimal computational effort.

A. Rate Equations

The equations we use to model the two-signal amplification in the fiber are based on a set of equations which have been used to describe various types of fiber lasers and amplifiers [10], [12]-[14]. Due to the fast thermalization rate of each Yb^{3+} manifold, effective cross-sections are used to describe the optical transitions between manifolds [15], reducing the modeling of the YDFA to a simplified two-level energy structure. The spatially-dependent population and power-propagation rate equations are given by

$$\frac{dN_2}{dt}=\frac{D}{hcA}\sum_{j=1}^{J}\lambda_j^p\left[\sigma_a(\lambda_j^p)N_1-\sigma_e(\lambda_j^p)N_2\right]P_p(\lambda_j^p)$$
$$+\frac{\Gamma}{hcA}\sum_{k=1}^{K}\lambda_k^s\left[\sigma_a(\lambda_k^s)N_1-\sigma_e(\lambda_k^s)N_2\right]P_s^{\pm}(\lambda_k^s)$$
$$+\frac{\Gamma}{hcA}\sum_{l=1}^{L}\lambda_l^{ase}\left[\sigma_a(\lambda_l^{ase})N_1-\sigma_e(\lambda_l^{ase})N_2\right]\cdot\left[P_{ase}^{+}(\lambda_l^{ase})+P_{ase}^{-}(\lambda_l^{ase})\right]-\frac{N_2}{\tau} \tag{1}$$

$$N_1=N_T-N_2 \tag{2}$$

$$\frac{dP_p(\lambda_j^p)}{dz}=D\left[\sigma_e(\lambda_j^p)N_2-\sigma_a(\lambda_j^p)N_1\right]P_p(\lambda_j^p)-\alpha P_p(\lambda_j^p) \tag{3}$$

$$\pm\frac{dP_s^{\pm}(\lambda_k^s)}{dz}=\Gamma\left[\sigma_e(\lambda_k^s)N_2-\sigma_a(\lambda_k^s)N_1\right]P_s^{\pm}(\lambda_k^s)-\alpha P_s^{\pm}(\lambda_k^s) \tag{4}$$

$$\pm\frac{dP_{ase}^{\pm}(\lambda_l^{ase})}{dz}=\Gamma\left[\sigma_e(\lambda_l^{ase})N_2-\sigma_a(\lambda_l^{ase})N_1\right]P_{ase}^{\pm}(\lambda_l^{ase})-\alpha P_{ase}^{\pm}(\lambda_l^{ase})+\Gamma\sigma_e(\lambda_l^{ase})N_2\frac{2hc^2\Delta\lambda}{[\lambda_l^{ase}]^3} \tag{5}$$

where N_T is ytterbium doping density, and N_2, N_1 are the population densities of the upper and lower manifolds, respectively. The pump, signal, and amplified spontaneous emission (ASE) powers are all divided into separate spectral channels. $P_p(\lambda_j^p)$ is the pump power of the j^{th} pump channel, $P_s(\lambda_k^s)$ is the signal power of k^{th} signal channel, and $P_{ase}(\lambda_l^{ase})$ is the ASE power of the l^{th} ASE channel. The pump beam is spectrally divided to account for the fact that the pump laser used in the experiment has a relatively broad bandwidth of around 3 nm near the narrow 975-nm absorption peak of ytterbium. The +(–) sign convention corresponds to forward (backward) propagation with respect to the pump beam. The effective absorption and emission cross-sections of Yb^{3+} are given by σ_a and σ_e, respectively, c is the speed of light in vacuum, α is the background attenuation coefficient of the fiber, and τ is the fluorescence lifetime of the upper laser level. The doped effective area of the fiber is denoted by A and the confinement factors of the pump and signal beams in the doped area are D and Γ, respectively.

Some of the simplifying assumptions used in (1)–(5) are briefly summarized below. The gain medium is assumed to be homogenous, amplified signals are treated as being monochromatic, transverse spatial profiles for signal and ASE beams are Gaussian, the transverse doping profile is uniform, the pump mode profile is considered to be uniform over the area of the inner cladding, and the ytterbium population densities are independent of the radial coordinate of the fiber. (Some of the above assumptions can be modeled more rigorously as described in [12].) In addition, the Γ and α parameters are chosen to be independent of wavelength for simplicity. Since Γ and α will vary by a relatively small amount ($\Delta\Gamma$ ~ 1%) over the range of signal wavelengths used in the experiment (~ 40 nm), spectrally averaged values are

Accepted for publication in *J. Lightwave Technol.*, Nov. 12, 2008.

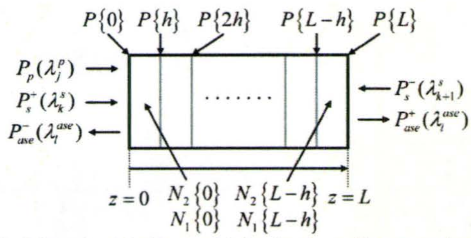

Fig. 1. Schematic of the fiber model showing the seeding conventions used in the simulations.

used to approximate these parameters.

B. Amplifier Configuration

Equations (1)–(5) are numerically solved (see, for example, [14]) by assuming that all population is initially in the lower manifold. The equations are iterated using the finite-difference method to obtain the steady-state population densities and optical powers by spatially dividing the fiber into segments along its axis. A schematic of the fiber model is depicted in Fig. 1. The initial boundary conditions used in solving the equations are the incident pump power at $z = 0$, the incident seed powers at $z = 0$, L, and the fact that the backward and forward ASE must grow from a value of zero at each end of the fiber.

Some of the key simulation parameters used in the numerical model are listed in Table I. These parameters include additional data, such as the numerical aperture (NA) and mode-field diameter (MFD), for the specific Yb-doped double-clad fiber used in the experiment. The fiber has a specified cladding absorption of 2.6 dB/m at 976 nm. The pump beam is divided into 5 spectral channels and has an integrated power of 2.109 W, which is approximately the maximum power that could be launched into the fiber in the experiment. ASE is divided into 11 channels, each of width $\Delta\lambda$ = 10 nm. The effective ytterbium absorption and emission cross-sections are taken from [10].

Using the above model, the gain bandwidth characteristics of the YDFA are investigated first for the parameters given in Table I. The simulation results shown in Fig. 2 indicate how the small-signal gain of the fiber changes for specific wavelengths as a function of the fiber length. For this particular simulation the fiber was seeded with a single signal propagating counterdirectionally to the pump beam with an input power of 0.1 μW. The relatively low seed power is chosen to ensure that the gain of the amplifier is not saturated by the amplified signal. It is clear from Fig. 2 that there exists an optimal length of fiber for maximizing the small-signal gain at a specific wavelength. Also evident in the figure is that for signal wavelengths longer than 1060 nm, the amplifier gain becomes less sensitive to the fiber length. This is of practical significance since operating the amplifier at long wavelengths can simultaneously allow for large gain with nearly complete pump absorption, whereas operation at short wavelengths will result in lower pump absorption when

TABLE I
PARAMETERS USED IN THE NUMERICAL SIMULATIONS

Parameter	Value	Parameter	Value
P_p(972.6 nm)	0.234 W	N_T	8×10^{25} m^{-3}
P_p(973.3 nm)	0.469 W	α	9×10^{-3} m^{-1}
P_p(974.5 nm)	0.703 W	Γ	0.87
P_p(975.5 nm)	0.469 W	D	2.304×10^{-3}
P_p(976.3 nm)	0.234 W	core NA	0.15
λ_1^{ase}	1000 nm	core MFD @ 1060 nm	6 μm
$\lambda_{K=11}^{ase}$	1100 nm	cladding diameter	125 μm
τ	0.8 ms	$\Delta\lambda$	10 nm
A	2.827×10^{-11} m^2	h, step-size	0.001 m

maximizing gain. The dependency of the spectral gain on fiber length is due to the fact that the electronic structure of Yb^{3+} gives rise to a quasi-3-level amplifying transition, exhibiting 3-level-like character (with signal reabsorption) at short wavelengths, and nearly 4-level-like character (with very weak reabsorption) at long wavelengths [10]. A consequence of this behavior is that it is difficult to efficiently amplify multiple input signals in the same fiber that are separated by a substantial difference in wavelength. From Fig. 2 it appears that dual-wavelength amplification would be most effective in the current fiber with a length of around 8 m, where the 1040-, 1060-, and 1080-nm signals have similar gain. It is also important to restrict possible regions of operation to those which yield the largest small-signal gain, as the seed oscillators used in the experiment can only deliver a few hundred microwatts of average power and the amplified signals must compete with the build-up of ASE for the available power in the amplifier.

Two-color simulations are subsequently conducted to determine the optimum fiber length and seeding configuration of the YDFA. The input seeds are separated by 39 nm, which is the largest wavelength separation that could be obtained

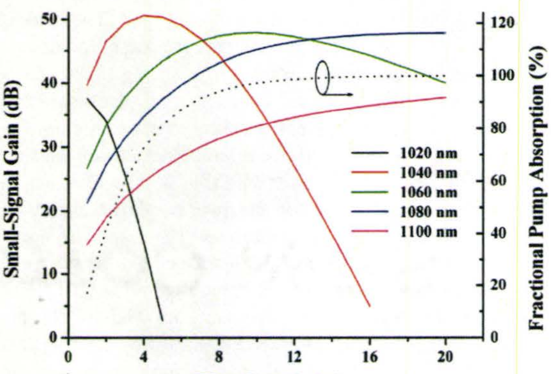

Fig. 2. Variation of amplifier small-signal gain and fractional pump absorption as a function of fiber length.

Accepted for publication in *J. Lightwave Technol.*, Nov. 12, 2008.

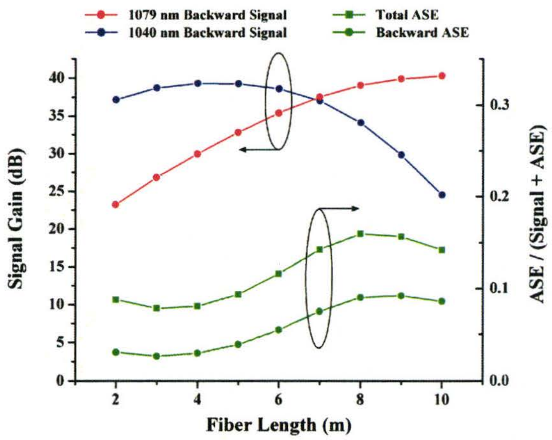

Fig. 3. Simulations to find the optimal fiber length for dual-wavelength amplification in a counterdirectionally-pumped amplifier. The left (right) axis gives the signal gain (noise ratio) at each fiber length. The backward (total) ASE curve represents the noise ratio by taking into account the ASE from the signal output end (both ends) of the fiber.

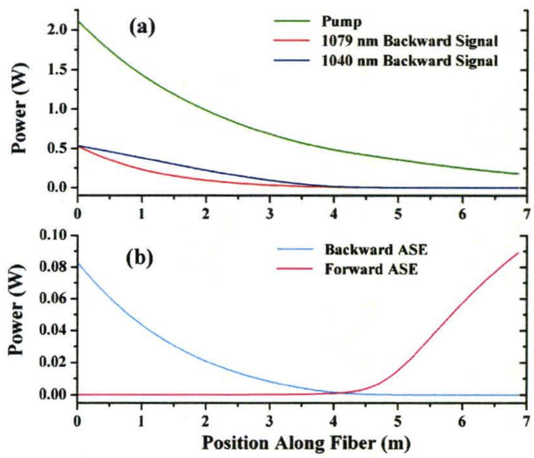

Fig. 4. Power distributions of (a) the amplified signals and pump, and (b) the ASE inside a 6.87-m-long fiber amplifier.

with the synchronized lasers in the experiment. The launched input power of each signal is 100 μW and the signal wavelengths of 1040 and 1079 nm are chosen to correspond to the center wavelengths of the mode-locked seed lasers used in the experiment. Fig. 3 shows the simulation result for the particular case where the two signals are both counter-propagating to the pump light. At a fiber length of 6.87 m, the two amplified signals experience the same net gain of around 37 dB. For fiber lengths longer than 6.87 m, the 1040-nm signal suffers from reabsorption losses due to the limited pump power available at the end of these long fibers. Alternatively, for fiber lengths shorter than 6.87 m, the 1079-nm signal is weaker due to its lower small-signal gain. Also shown in Fig. 3 are the expected ASE levels at each fiber length represented as a ratio of the ASE power to the total output power.

The power distributions of the amplified signals, pump, and ASE are plotted in Fig. 4 for a fiber length of $L = 6.87$ m. The pump power is launched at $z = 0$ and the seed signals are injected into the opposite end of the fiber at $z = L$. The amount of unabsorbed pump power remaining at the end of the fiber is about 8 % of the launched power.

Additional simulations are conducted to investigate the effect of the three other seeding configurations on amplifier performance. A summary of the results obtained for the four possible configurations is given in Table II. The fiber length that results in equal gain for the two amplified signals is nearly identical for all four geometries. The amplified signal gain has a maximum value of 37.3 dB for configuration (A) and a minimum value of 36.6 dB for configuration (D). Noise ratios for the amplified signal beams are highest for the configurations where the two seed signals propagate against each other ((C) and (D)), as ASE levels from both ends of the fiber contribute to the combined signal beam, and lowest for configuration (B), where the two signals propagate with the pump source.

Configuration (A) was deemed optimal for the experiment since it provides the highest gain, has acceptable levels of noise, and is easier to configure than the other three geometries in an experimental setup which consists of free-space optics. The main difficulty associated with configurations (B)–(D) is that one of the signal beams must pass through the same lens which is used to optimize the coupling of the pump beam into the inner cladding. For efficient launching of both pump and signal beams into the same end of the fiber, additional lenses would have to be placed in the beam path of the signal, further complicating the setup. In contrast, configuration (A) requires only two lenses to independently optimize the coupling of both the pump and signal beams, and the two collinear signals can be easily separated following amplification using suitable polarizing optics.

III. Experimental Results

A. Laser Characteristics

A schematic of the experimental setup is shown in Fig. 5. The seed oscillators consist of two external-cavity, mode-locked semiconductor lasers capable of delivering pulses as short as 1 ps over a broad tuning range of 1030–1090 nm [4].

TABLE II
Simulation Results for Different Seeding Configurations

Seeding Geometry	Signal Direction		Optimal Length (m)	Signal Gain (dB)	Noise Ratio
	1040 nm	1079 nm			
A	Backward	Backward	6.87	37.3	0.07
B	Forward	Forward	6.80	36.9	0.05
C	Forward	Backward	6.86	37.2	0.15
D	Backward	Forward	6.75	36.6	0.26

Accepted for publication in *J. Lightwave Technol.*, Nov. 12, 2008.

The lasers are fabricated using the in-house gas-source molecular beam epitaxy facility and contain a single, 6-nm-thick InGaAs quantum-well active region. Each oscillator consists of a two-contact ridge-waveguide device containing integrated gain and saturable absorber sections. Laser 1 has an 80-μm-long absorber and a gain section length of 640 μm. Laser 2 has a 90-μm-long absorber and a gain section length of 800 μm. Both lasers have a lateral ridge width of 2.4 μm. A 600-lines/mm diffraction grating is used as the feedback element in the external cavity of each laser, allowing precise control over the center wavelength of the emitted pulses (within 0.1 nm). Passive mode-locking is initiated by applying a DC reverse bias to the saturable absorber section while driving the gain section with a DC current source.

Synchronization of the two seed lasers is accomplished using an RF modulation technique. The DC bias parameters of each oscillator are first independently optimized to produce short pulses under conditions of passive mode-locking. Tuning the angle of the diffraction grating establishes the center wavelength of each oscillator: laser 1 is set to 1079 nm and laser 2 is set to 1040 nm. Although the operating wavelength of these lasers can be varied by as much as 60 nm, it was difficult to obtain stable, synchronized pulses with sufficient average power to seed the fiber amplifier for wavelength separations greater than 40 nm. Next, the external cavity length of laser 2 is adjusted to match the length of laser 1 such that the pulse repetition rates of the two lasers are equal to within one kHz under free-running conditions. Synchronization is achieved through hybrid mode-locking of the lasers with an RF signal at a frequency that coincides with the free-running mode-locked repetition rate (577 MHz). The RF sinusoid is generated by a frequency synthesizer and amplified by an RF amplifier with a power gain of 17 dB. After passing though a 3-dB power splitter, the RF signal is coupled into the gain section of each laser through a bias-tee.

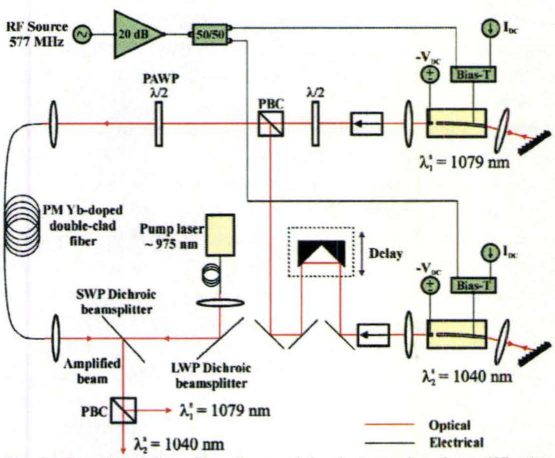

Fig. 5. Experimental configuration used for dual-wavelength amplification of synchronized ultrashort laser pulses. PM: polarization maintaining; PBC: polarizing beamsplitter cube; PAWP: polymer achromatic waveplate; LWP: long-wave pass; SWP: short-wave pass.

A forward RF power of up to 22 dBm incident at each laser is required to achieve a synchronized state due to the fact that there is substantial impedance mismatch between the laser diode and the 50-Ω transmission cable. With a proper impedance-matched network it is expected that the RF drive requirements could be reduced by up to 30 dB [16]. The quality of the synchronization is monitored using a 50-GHz sampling oscilloscope by coupling a fraction of each laser beam into a 20-GHz photodetector. A small amount of RF power is coupled from the output of the signal generator to trigger the oscilloscope. The impulse response of the time-domain measurement system is 20 ps FWHM. Additionally, a 22-GHz RF spectrum analyzer is used to monitor the phase noise characteristics of each laser. Under optimal synchronization conditions each seed laser is capable of generating several hundred microwatts of average power measured at the output of the laser. Pulse durations can vary between 2–8 ps depending on the DC bias parameters and each seed laser can be independently tuned from 1040–1079 nm, producing nearly the same synchronized properties over the entire tuning range. Beyond this range, the lasers can still be synchronized but with significantly reduced average output powers.

An estimate of the relative pulse-to-pulse timing jitter between both seed lasers can be made by cross-correlating the pulses of one laser with the pulses from the second laser using sum frequency mixing in a nonlinear crystal. A delay line present in the beam path of laser 2 permits measurement of the cross-correlation signal. An example of a two-color cross-correlation measurement is shown in Fig. 6 for the seed lasers synchronized at 1079 nm and 1040 nm. The total scan time of the measurement is 210 s. Also shown in the figure are the intensity auto-correlation traces of each seed laser pulse. Excess timing jitter is measured as the broadening of the experimental cross-correlation width compared to a calculated cross-correlation width that is based on the pulsewidth of each laser. From Fig. 6 the relative jitter measured using this technique is 5.1 ps rms, assuming the pulse shapes are Gaussian and the probability density function describing the interlaser jitter is also Gaussian. Additional measurements are performed to confirm the timing jitter results obtained using the cross-correlation. When operated in statistical mode, the sampling oscilloscope can measure the timing jitter between an input signal and the trigger signal. For this measurement, pulses from the 1040-nm laser are coupled into a 20-GHz photodetector, amplified, and connected to the trigger input on the oscilloscope which directly measures the pulses of the 1079-nm laser using a second 20-GHz photodetector. After correcting for the 2-ps internal jitter of the trigger, the relative jitter obtained using this measurement is within 5 % of the cross-correlation result.

Cross-correlation measurements are also made as a function of time to assess the stability of the laser synchronization. Measurements are made at 10 minute intervals for a period of 60 minutes. A maximum deviation of ~100 fs (2 %) is observed in the rms timing jitter values over the course of the

Accepted for publication in *J. Lightwave Technol.*, Nov. 12, 2008.

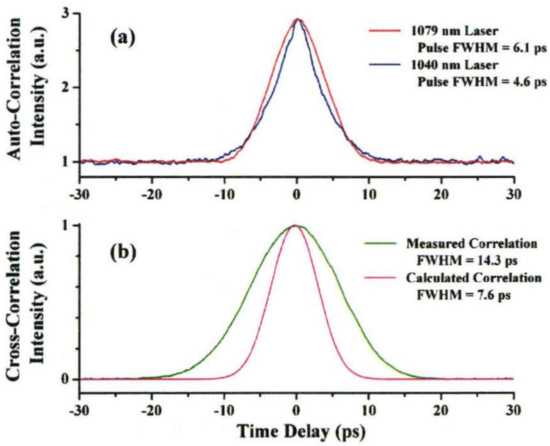

Fig. 6. Auto-correlation (a) and two-color cross-correlation (b) traces of the seed laser pulses. The calculated trace in (b) is based on the deconvolved pulsewidths given in (a). The rms interlaser jitter is estimated to be 5.1 ps.

measurements, indicating good long-term stability of the laser synchronization.

The values obtained for the interlaser timing jitter are typical for RF-synchronized external-cavity mode-locked diode lasers that do not contain feedback electronics to minimize timing fluctuations [17]. Minimizing the interlaser jitter below what is capable with direct RF modulation was not a strict goal of this work and more sophisticated synchronization techniques could be employed to further reduce the interlaser jitter, which would result in more efficient nonlinear optical conversion through DFM of the two beams. Approaches to achieving lower jitter could include driving one or both lasers from an ultrastable reference oscillator and using a phase-locked loop to generate an electronic feedback signal which suppresses the jitter by adjusting the bias of the laser [18] or the external cavity length through piezo-electric means [19]. In addition, optical synchronization methods could be employed to further stabilize the two mode-locked lasers [20], [21].

B. Amplifier Characteristics

The two synchronized pulse trains are injected with orthogonal polarizations into a PM YDFA. The use of a PM fiber as the amplifying medium allows the two signals to be simultaneously amplified in the same fiber and easily separated following amplification using suitable polarizing optics. Moreover, the mechanism responsible for the separation of the signals is largely independent of wavelength, allowing the operating wavelengths of the lasers to be tuned without having to alter the setup (as compared to using dichroic optics for signal separation). In addition, by maintaining the polarization states of both signals during amplification, maximum efficiency can be achieved in nonlinear optical applications.

Polarizing beamsplitter cubes (PBCs) are used to combine the two signals before amplification and to separate them following amplification (Fig. 5). The two-signal beam propagates through a $\lambda/2$ polymer achromatic waveplate (PAWP) which provides easy alignment of the polarization axis of the signals with the slow and fast axis of the PM fiber. The synchronized 1040-nm and 1079-nm input pulses are injected into the core of the PM Yb-doped fiber with each signal having a launched average power of 100 ± 5 μW and a corresponding coupling efficiency of about 40 %. For the power and spectral measurements, the two signals are coupled into the PM fiber with temporally offset pulse trains. This is achieved by adjusting the delay stage of laser 2 while monitoring the pulses in time using the sampling oscilloscope.

The properties of the commercial PM Yb-doped double-clad fiber are given in Table I. Both ends of the fiber are angle-cleaved at 8° to prevent feedback of the signals in the core. The amplifier is pumped counterdirectionally by a diode laser emitting a maximum power of 4 W at a center wavelength of 974.5 nm with a bandwidth of about 3 nm. A dichroic beam-splitter is used to separate the amplified seed signals from the pump beam and 30-dB optical isolators are used to prevent ASE from disturbing the seed lasers.

Power measurements of the amplified pulses are made to compare the experimentally determined optimal fiber length with the simulated optimal length. A thermal power meter placed in between the SWP dichroic beam-splitter and the output PBC is used to measure the direct output power of the amplifier. The percentage contribution of each signal to the amplified beam is obtained by coupling the output of the YDFA (output PBC removed) into an optical spectrum analyzer (OSA) and numerically integrating the measured spectrum. ASE power levels are also obtained through numerical integration of the amplified spectrum. Additional measurement checks are made with the output PBC in place, separating the amplified beam into the two component signals and recording the power level of each signal. Although the modeling predicted a fiber length of 6.87 m, we originally started with a fiber length of 10 m in the YDFA. Amplified spectra were recorded as the fiber was cleaved back in order to determine the position of equal gain for the 1040-nm and 1079-nm signals.

Fig. 7 shows the amplified output power of the YDFA versus absorbed pump power for a fiber length of 6.7 ± 0.1 m. At the maximum value of absorbed pump power, the 1040-nm signal is approximately 4 % larger than the 1079-nm signal, revealing that the fiber was inadvertently cut back slightly shorter than the length required for equal signal powers. Also plotted in Fig. 7 are the simulated power levels of each signal for a fiber length of 6.7 m. In general, good agreement is obtained between the theory and the experimental results. The measured slope efficiency of the two-color amplifier remains quite constant (68 %), despite the fact that the power ratio of the two signals varies with pump power. The amplified power curves shown in Fig. 7 reveal that the shape of the fiber gain spectrum is highly dependent on the pump power, which is characteristic of quasi-3-level systems. At low values of pump power, the upper-state population density at the seed end of

Accepted for publication in *J. Lightwave Technol.*, Nov. 12, 2008.

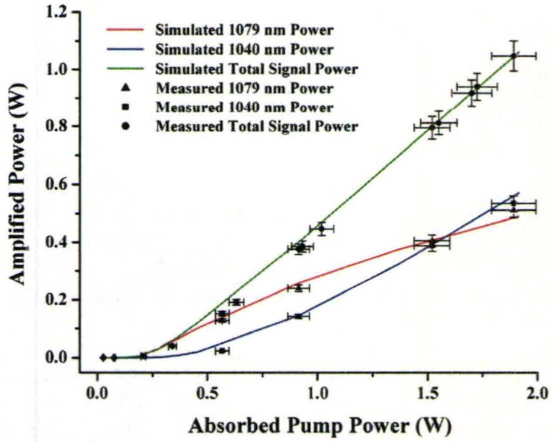

Fig. 7. Dual-wavelength amplification of 1040-nm and 1079-nm ps-pulse-trains operating at a repetition rate of 577 MHz. The simulated curves are based on CW modeling of the YDFA gain. The launched input average power of each signal is 100 ± 5 μW.

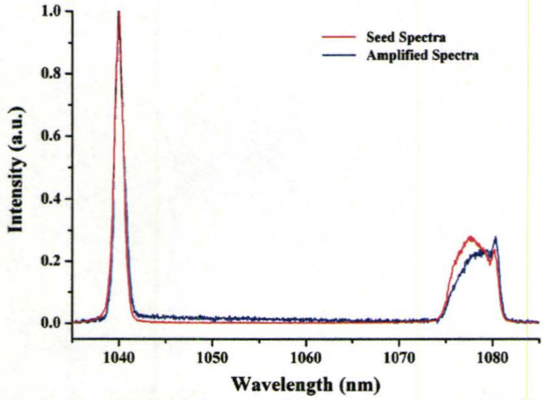

Fig. 8. Normalized optical spectra of the seed laser pulses and the fiber amplified pulses at maximum pump power.

the fiber is quite low and the 1040-nm pulses experience greater reabsorption losses than the 1079-nm pulses.

The spectra of the seed pulses and the fiber amplified pulses are shown in Fig. 8. The amplified pulse spectra are recorded at the maximum value of absorbed pump power and represent the case where the integrated spectral power of the 1040-nm pulses is 4 % larger than the power of the 1079-nm pulses. Amplified linewidths are 1.1 nm and 4.8 nm for the 1040-nm and 1079-nm pulses, respectively. The pulses emitted by the 1079-nm laser are spectrally broader as a result of a larger amount of internal self-phase modulation present in this laser, which could be due to the fact that it was operated at a higher current-density [4]. ASE power levels are around 10 % of the total fiber output. The corresponding auto-correlation and two-color cross-correlation traces of the amplified pulses at maximum pump power are displayed in Fig. 9. Auto-correlation measurements of each signal are made while both pulses propagate through the fiber. Amplified pulse durations are comparable to that of the seed pulses (Fig. 6), owing to the minimal amount of dispersion present in the system, and the two-color cross-correlation trace indicates that the interlaser jitter characteristics of the amplified signals are very similar to that of the seed pulses. Amplified pulses from both lasers are several times the transform limit and external pulse compression could be employed to further reduce the pulsewidths of each signal to below 1 ps, which was demonstrated in our earlier studies of ps-pulse hybrid MOPA systems operating near 1075 nm [2].

The power of signal 1 in the channel of signal 2 is very low, as a result of the high-quality polarizing optics in the setup. Although we were not able to make an exact measurement of the power ratio due to the fact that the power of the 1040-nm signal in the 1079-nm channel was much lower than the power of the background ASE, based on the spectral amplitudes of the two signals and the background ASE, we estimate that the ratio is -30 dB or better, for the YDFA pumped at maximum power.

Further experiments are conducted to investigate the wavelength tuning properties of the YDFA under two-signal seeding conditions. For these measurements, the center wavelength of laser 2 is fixed at 1040 nm while the center wavelength of laser 1 is varied between 1040 – 1079 nm. The length of the fiber in the YDFA is 6.7 ± 0.1 m. At each wavelength of laser 1, the two seed lasers are mode-locked and synchronized, followed by simultaneous amplification of the two pulse trains in the YDFA. The amplifier is pumped at maximum power, the launched input average power of each signal is 100 ± 5 μW, and input pulse durations vary between 4–6 ps over the entire tuning range. Fig. 10 shows the signal gain and ASE noise ratio as the wavelength of laser 1 is

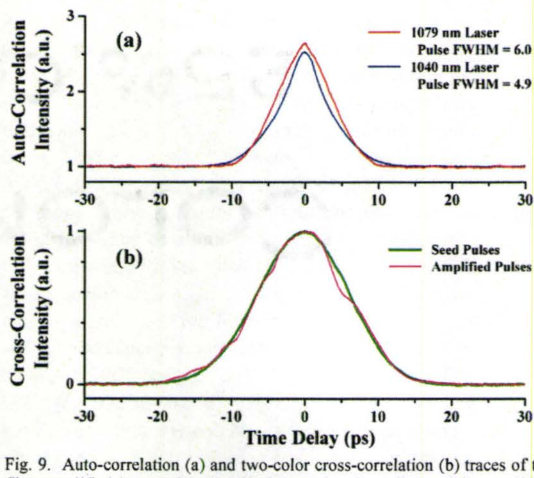

Fig. 9. Auto-correlation (a) and two-color cross-correlation (b) traces of the fiber amplified laser pulses. In (b) the rms interlaser jitter of the amplified pulses is estimated to be the same as that of the seed laser pulses (5.1 ps).

Accepted for publication in *J. Lightwave Technol.*, Nov. 12, 2008.

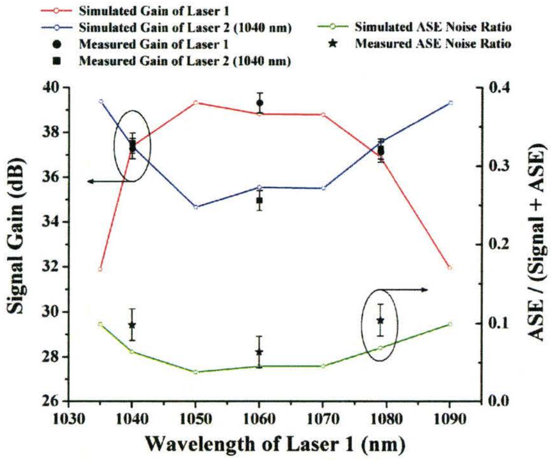

Fig. 10. Measurements and simulations of the two-signal wavelength tuning properties of the YDFA. The pulses emitted by laser 2 are fixed at 1040 nm while the operating wavelength of laser 1 is varied. The left (right) axis gives the signal gain (noise ratio).

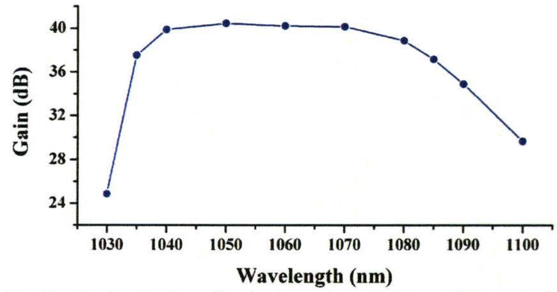

Fig. 11. Simulated gain profile of a 6.87-m-long YDFA amplifying a single seed with an input power of 100 μW.

varied. The laser 2 curve gives the signal gain at 1040 nm as laser 1 is tuned to different wavelengths. Measured gain values have been corrected for coupling losses and represent the gain inside the fiber. Also shown in Fig. 10 are the corresponding numerical simulations of this experiment using a fiber length of 6.7 m. Overall, reasonable agreement between the theory and the experimental results is obtained, further supporting the validity of CW numerical modeling to predict the amplification of the high-repetition-rate pulses from the mode-locked diode lasers. Between the wavelengths of 1040–1079 nm, the two-signal gain profile of the YDFA is relatively flat, with a deviation of around 2 dB about the mean two-signal gain. Simulations were also conducted with laser 1 fixed at 1079 nm and laser 2 varied between 1040–1079 nm. The results are very similar to those displayed in Fig. 10.

Synchronous operation of the seed lasers at wavelength separations larger than 40 nm resulted in low mode-locked average output powers, as discussed previously, and prevented the characterization of the YDFA at signal separations which are more relevant to the generation of MIR. Based on further numerical simulations, however, we expect good amplification of two mode-locked signals separated by 60 nm using the current experimental configuration with a modified seed laser design. Fig. 11 shows a simulated gain profile for the amplification of a single seed with an input power of 100 μW and an amplifier length of 6.87 m. The simulated 3-dB gain bandwidth of the amplifier is 50 nm. Further two-signal simulations indicate that good performance should be possible for two seed lasers operating at 1035 nm and 1095 nm, with each signal having an input average power of 200 μW. The fiber length required for equal signal powers in this case is 6.8 m and the combined amplified power is 0.9 W with a noise ratio of 0.15. Synchronized mode-locked lasers emitting short pulses at 1035 nm and 1095 nm could be easily accomplished by fabricating a modified laser structure in which the indium content of the InGaAs quantum well differs by a few percent from the current design [22]. This would have the effect of moving the spectral gain peak of the long-wavelength laser, thus allowing synchronization of the two mode-locked oscillators at a greater wavelength difference. Beyond a 60-nm separation, simulations reveal that the efficiency of two-color amplification in a single YDFA decreases considerably as a result of the increasing Yb^{3+} absorption below 1035 nm and the reduced emission cross-sections above 1095 nm [10]. These two effects coupled with the relatively low output average power of the seed oscillators results in ASE extracting the majority of amplifier power instead of the amplified signals. It would be necessary to preamplify the input pulse trains for larger signal separations, either using a single-clad PM Yb-doped-fiber or a pair of semiconductor optical amplifiers. Alternatively, separate YDFAs optimized for each signal wavelength could be used for signal separations approaching 100 nm.

IV. Summary

We have presented a dual-wavelength short-pulse optical source based on mode-locked semiconductor seed lasers and a single polarization-maintaining YDFA. Two synchronized pulse trains operating at a repetition rate of 577 MHz and a wavelength separation of approximately 40 nm have been amplified to a combined average power of 1.1 W. Numerical simulations based on a CW model for the fiber gain were used to predict and optimize the performance of the YDFA under two-signal seeding conditions. The simulations revealed that optimal amplifier performance (high gain and good signal-to-ASE ratio) is obtained for seeding configurations where the two signals are co-propagating. In general, good agreement between the simulations and experimental results was achieved. We have demonstrated that good performance can be obtained in a single YDFA for signal separations of 40 nm and further extensions of the current work should be possible using mode-locked semiconductor seed oscillators separated by 60 nm. In addition, the current system could be scaled in power using a stronger pump laser or a second stage of amplification. For higher intensity systems aimed at dual-beam nonlinear optical conversion applications, a second delay stage could be introduced at the output of the fiber amplifier to control the relative timing of the two pulse trains. The dual-wavelength system presented here combines the attractive features of both the semiconductor-seed-oscillator and Yb:fiber amplifier, and provides a compact source for two-color pump-probe experiments. With a sufficient extension of the wavelength separation of the two oscillators, this system could represent a promising approach for generating high-repetition-rate MIR through DFM.

ACKNOWLEDGMENT

The authors would like to thank S. Golin for her help with configuring and characterizing the 1040-nm mode-locked oscillator. The authors would also like to thank B. Morasse, D. Strickland, and M. Piché for helpful discussions.

REFERENCES

[1] B. Adhimoolam, M. G. Hekelaar, P. Gross, I. D. Lindsay, and K.-J. Boller, "Wavelength-tunable short-pulse diode-laser fiber-amplifier system around 1.06 um," *IEEE Photon. Technol. Lett.*, vol. 18, pp. 838-840, Apr. 2006.
[2] A. J. Budz, A. S. Logan, D. Strickland, and H. K. Haugen, "Ultrashort pulses from a mode-locked diode-oscillator Yb-fiber-amplifier system," *IEEE Photon. Technol. Lett.*, vol. 19, pp. 94-96, Jan. 2007.
[3] P. Dupriez *et al.*, "High-power, high repetition rate picosecond and femtosecond sources based on Yb-doped fiber amplification of VECSELs," *Opt. Express*, vol. 14, pp. 9611-9616, Oct. 2006.
[4] A. J. Budz and H. K. Haugen, "Wavelength and repetition-rate tunable mode-locked semiconductor-seed-source for Yb-fiber-amplifier systems," *IEEE Photon. Technol. Lett.*, vol. 19, pp. 1412-1414, Oct. 2007.
[5] S. Gee *et al.*, "Self-stabilization of an actively mode-locked semiconductor-based fiber-ring laser for ultralow jitter," *IEEE Photon. Technol. Lett.*, vol. 19, pp. 498-500, Apr. 2007.
[6] J. Limpert *et al.*, "High-average-power femtosecond fiber chirped-pulse amplification system," *Opt. Lett.*, vol. 28, pp. 1984-1986, Oct. 2003.
[7] L. Goldberg, J. Koplow, D. G. Lancaster, R. F. Curl, and F. K. Tittel, "Mid-infrared difference-frequency generation source pumped by a 1.1-1.5-μm dual-wavelength fiber amplifier for trace-gas detection," *Opt. Lett.*, vol. 23, pp. 1517-1519, Oct. 1998.
[8] D. Creeden *et al.*, "Compact fiber-pumped terahertz source based on difference frequency mixing in ZGP," *IEEE J. Select. Topics Quantum Electron.*, vol. 13, pp. 732-737, May/June 2007.
[9] R. Romero-Alvarez, R. Pettus, Z. Wu, and D. Strickland, "Two-color fiber amplifier for short-pulse, mid-infrared generation," *Opt. Lett.*, vol. 33, pp. 1065-1067, May. 2008.
[10] R. Paschotta, J. Nilsson, A. C. Tropper, and D. C. Hanna, "Ytterbium-doped fiber amplifiers," *IEEE J. Quantum Electron.*, vol. 33, pp. 1049-1056, Jul. 1997.
[11] Y. -H. Chuang, L. Zheng, and D. D. Meyerhofer, "Propagation of light pulses in a chirped-pulse-amplification laser," *IEEE J. Quantum Electron.*, vol. 29, pp. 270-280, Jan. 1993.
[12] C. R. Giles and E. Desurvire, "Modeling erbium-doped fiber amplifiers," *J. Lightwave Technol.*, vol. 9, pp. 271-283, Feb. 1991.
[13] Y. Wang and H. Po, "Dynamic characteristics of double-clad fiber amplifiers for high-power pulse amplification," *J. Lightwave Technol.*, vol. 21, pp. 2262-2270, Oct. 2003.
[14] M. Eichhorn, "Numerical modeling of Tm-doped double-clad fluoride fiber amplifiers," *IEEE J. Quantum Electron.*, vol. 41, pp. 1574-1581, Dec. 2005.
[15] E. Desurvire, *Erbium-Doped Fiber Amplifiers: Principles and Applications*, New York: Wiely, 1994.
[16] S. Arahira, N. Mineo, K. Tachibana, and Y. Ogawa, "40 GHz hybrid modelocked laser diode module operated at ultra-low RF power with impedance-matching circuit," *Electron. Lett.*, vol. 39, pp. 287-289, Feb. 2003.
[17] P. J. Delfyett, "Hybrid mode-locked diode lasers for synchronous optical network applications," *Proceedings of the SPIE*, vol. 2116, pp. 8-13, May 1994.
[18] J. B. Georges *et al.*, "Stable picosecond pulse generation at 46 GHz by modelocking of a semiconductor laser operating in an optoelectronic phaselocked loop," *Electron. Lett.*, vol. 30, pp. 69-71, Jan. 1994.
[19] D. J. Jones *et al.*, "Ultralow-jitter, 1550-nm mode-locked semiconductor laser synchronized to a visible optical frequency standard," *Opt. Lett.*, vol. 28, pp. 813-815, May. 2003.
[20] S. Arahira and Y. Ogawa, "480-GHz subharmonic synchronous mode locking in a short-cavity colliding-pulse mode-locked laser diode," *IEEE Photon. Technol. Lett.*, vol. 14, pp. 537-539, Apr. 2002.
[21] M. J. Brennan, H. F. Tiedje, and H. K. Haugen, "Passively modelocked semiconductor laser synchronization and pulse cross-correlation with Ti:sapphire laser," *Electron. Lett.*, vol. 38, pp. 713-714, July 2002.
[22] F. Bugge *et al.*, "Effect of growth conditions and strain compensation on indium incorporation for diode lasers emitting above 1050 nm," *J. Cryst. Growth*, vol. 221, pp. 496-502, Dec. 2000.

The procedure used to synchronize the two mode-locked lasers will be discussed in greater detail. As stated in the manuscript, the DC bias parameters of both lasers are independently optimized to produce short picosecond pulses under conditions of passive mode-locking. The external-cavity length of laser #2 is finely adjusted such that the pulse repetition rates of both lasers are equal to less than one kilohertz under free-running conditions. The DC bias parameters and external-cavity coupling of laser #2 may need to be re-adjusted following the modification to the cavity length. Laser #1 is then hybridly mode-locked using the RF source. The magnitude and frequency of the RF source is configured to optimize the hybrid mode-locking of laser #1. This typically requires a reduction in the gain section current by a few milliamps as the amplitude of the RF sinusoid is increased. Also, the frequency of the RF source usually needs to be larger than the free-running frequency to induce hybrid mode-locking. The DC and RF bias parameters are then optimized to produce stable pulses with minimal noise side-bands, as measured by the sampling oscilloscope and the RFSA. For the synchronization experiments, the oscilloscope is triggered using a signal from the RF source. Under conditions of hybrid mode-locking, the repetition rate of the laser can typically be tuned by adjusting the frequency of RF source. The frequency pulling range is usually on the order of 10–30 kHz. This fact can be utilized to synchronize the two lasers. By adjusting the frequency of the RF source, the repetition rate of laser #1 is pulled to match that of laser #2. An alternative method to induce synchronization involves adjusting the cavity length of laser #2 without modifying the frequency of the RF source. The cavity length of the laser is modified until stable pulses with minimal noise are observed on the oscilloscope and RFSA. The latter synchronization method is typically used, followed by slight adjustments of the DC bias parameters of laser #2 to optimize the duration of the generated pulses. Once the sampling oscilloscope indicates that the two lasers are synchronized, an optical cross-correlation measurement may be performed to characterize the quality of the synchronization. Typical rms inter-laser timing jitter levels are on the order of 5 ps. Based on the noise measurements, a relative jitter of 5 ps rms is not surprising considering that absolute rms timing jitter of each laser is on the order of a few picoseconds. It is expected that by employing methods to reduce the absolute phase noise of the mode-locked lasers, the relative jitter can be improved as well. As discussed in the manuscript, additional methods of minimizing the relative jitter include the use of a phase-locked loop [144], [145] and optical synchronization [121], [146].

Details on the calculation procedure used to solve Equations (1)–(5) of the preceding manuscript will be summarized. The equations were coded using Matlab and numerically solved using the finite-difference method. The fibre is spatially-divided longitudinally using a typical step-size of dz = 0.001 m. The boundary conditions at each end of the fibre are given by the incident pump and seed powers, and by the fact that the forward and backward propagating ASE must grow from an initial value of zero. Initially, all population is assumed to be in the ground manifold $\{N_1(z) = N_T, N_2(z) = 0\}$ at $t = 0$. The power propagation Equations (3)–(5) are then solved to obtain the power values at each segment of the fibre. With the power values of the pump, signal, and ASE known at each longitudinal segment, the change in the population density of each manifold can be calculated using Equations (1)–(2). The time differential is then incremented by dt and the calculation procedure begins again by solving the power propagation equations using the new values of $N_1(z)$ and $N_2(z)$. The simulation process repeats until a convergence criterion is satisfied for the signal power. Convergence is typically achieved after a simulation time, t_o, which is on the order of the fluorescence lifetime of the excited manifold (0.8 ms). Therefore, for a temporal step-size of $dt = 10^{-6}$ s, the simulation process may require 1000 iterations. The overall computation time using a standard computer is usually less than one minute for a given set of operating parameters.

The modeling approach described in the manuscript is sufficient for studying the steady-state characteristics of the amplifier gain for the high-repetition-rate low-peak-power pulses generated by the mode-locked diode lasers. For seed pulses of low repetition frequency (on the order of a few tens of kHz) or high peak intensity, the modeling approach would need to be modified. For low-repetition-rate pulses with low peak power, a time-dependent model [147], [148] can be adopted to account for the depletion of the amplifier gain due to the build-up of ASE in the interval between the pulses. In addition, the above time-dependent models can account for distortions to the pulse temporal profile due to time-dependent gain saturation. When the intensity of the pulse propagating through the fibre becomes large enough such that spectral broadening due to SPM is significant, then a full time-dependent spectrally-resolved nonlinear modeling approach [149], [150] should be used. Other effects such as dispersion should be included for ultrashort pulses and in particular, if the fibre is sufficiently long. In general, if one is interested in studying the detailed modifications to the temporal and spectral characteristics of the amplified pulse due to fibre gain, dispersion, and nonlinearity, then a full time-dependent modeling approach should be adopted.

During the experimental work on the dual-wavelength system, amplification measurements were conducted on two different commercially-available single-mode Yb-doped double-clad fibres. The first fibre (LAS-Yb-10-PM-01, CorActive) exhibited a significant degradation mechanism, which manifested itself as a reduction in the output power over time. This rendered it practically useless for the intended experiment and prompted the use of a second fibre (Yb1200-6/125DC-PM, Liekki), which was advertized as offering low photodegradation. Prior to switching to the low-degradation-fibre, measurements were made on the CorActive fibre in order to gain an understanding of the degradation mechanism. Amplified power measurements were made for three different fibre lengths: 2, 4, and 6 m. In each case, a gradual decline in the output power was observed over time, with shorter fibres exhibiting a greater rate of degradation. A reduction in the output power of a factor of 10 was typical for a few hours of continuous operation.

The photodegradation mechanism is believed to be consistent with photodarkening, which is a phenomenon that leads to an increase in the core background loss of the fibre. Photodarkening has been observed in a variety of RE-doped silica fibres [151] and with the recent development of high-power Yb:fibre amplifier systems, there are now several reports of photodarkening occurring in fibres doped with ytterbium [151]-[158]. Photodarkening manifests itself as an increase in the excess loss of the core when the fibre is operated at elevated power levels. The absorption spectrum of the induced loss has a peak in the visible spectrum and a long-wavelength tail that extends into the near infrared [151], [152], [154], [156]-[158]. Therefore, photodarkening can lead to a reduction in the power of both the pump and signal beams, limiting the overall output power and conversion efficiency of the amplifier. Several research groups have reported that the rate of degradation is proportional to the power level in the fibre, or more specifically, to the population density of the excited Yb energy state [152], [153], [156]. Photodarkening is therefore expected to be more severe for fibre amplifiers rather than fibre lasers, and particularly for amplifiers based on single-clad fibres or high-power double-clad fibres. The temporal characteristics of photodarkening are such that the rate of degradation is initially large, followed by a slow decline to a steady-state value. The temporal decay characteristics of the output power can be typically represented using a stretched-exponential function, with a $1/e$ decay constant on the order of minutes to hours, depending on the inversion density of the Yb ions [152]-[154], [156], [158]. Experiments have also revealed that photodarkening is more pronounced in highly doped fibres, suggesting that the clustering of Yb ions may be contributing to the overall effect [152]. It is believed that the induced loss is due the creation of colour centers in the glass core, though the underlying physical process responsible for the creation of the colour centers is currently not fully known and research in this area is on-going (e.g., [156], [157], [158]). One possible explanation for the mechanism responsible for inducing photodarkening is as follows [152], [158]: clusters of excited Yb ions co-operatively emit light in the UV spectral region, which photo-ionize precursors in the glass, leading to the generation of colour centers. There have been several reports on methods to mitigate photodarkening in Yb-doped fibres. One approach involves co-doping the core with Al [152], which reduces the tendency for Yb ions to cluster, thereby reducing the level of co-operative luminescence. A second method of mitigating photodarkening involves working with phosphate fibres, which have demonstrated a higher resistance to photodarkening than silica fibres [158]. It should be noted that not all Yb-doped silica fibres are susceptible to photodarkening, implying that the fabrication process and the quality of the glass are important parameters. Clearly, more research is required to elucidate the mechanisms responsible for photodarkening in Yb-doped silica fibres.

The level of photodegradation that was observed with the CorActive Yb-doped fibre is consistent with photodarkening. The fact that a higher rate of degradation was observed with shorter fibres also makes qualitative sense since the spatially-averaged inversion density is larger in a shorter fibre. The proportionality between the magnitude of the excess loss and the excited-state population density of Yb ions implies that the excess loss should be spatially distributed both transversely and longitudinally along the fibre. This property has not been investigated in the literature. In fact, a rather interesting experiment could consist of purposely inducing photodarkening in a fibre, dividing the fibre into sections to determine the localized magnitude of the excess loss, and correlating the measured distributed loss with a numerical model based on the spatially-dependent population density of the Yb ions. The experimental measurements could be conducted as a function of time to determine the time-dependent spatial-evolution of the excess loss. Such experiments could provide further insight into the dynamics of photodarkening and in particular, the exact correlation between the magnitude of the induced loss and the fractional population density of excited Yb ions.

Chapter 5 Conclusions and Future Work

5.1 Summary

In this thesis, the development of an ultrashort-pulse semiconductor-based optical source operating in the 1 μm wavelength region was presented. Mode-locking of an external-cavity semiconductor laser provides a practical method of generating wavelength-tunable short picosecond and sub-picosecond pulses. Amplifying strategies based on both semiconductor and Yb:fibre technologies were investigated as a means of scaling the average power level of the mode-locked pulses. Noise characteristics as well as the synchronization properties of two mode-locked semiconductor lasers were discussed. In addition, simulations were conducted to investigate the steady-state gain characteristics of a Yb:fibre amplifier operated under dual-wavelength signal amplification. In connection with the simulations, preliminary results were presented on the development of a novel dual-wavelength source consisting of mode-locked diode lasers and a single Yb:fibre amplifier. The results obtained for this thesis have been broken down into several smaller sections, representing a natural progression from the design and characterization of a master mode-locked oscillator to the development of a short-pulse laser system comprising optical amplifiers. Results specific to each of the individual components will be summarized below.

Mode-locked semiconductor lasers have been fabricated at wavelengths corresponding to the spectral region where Yb:fibre amplifiers provide gain. Pulses ranging in duration from 1 to 10 ps have been generated over a wavelength range of 1030–1090 nm, which corresponds to a significant fraction of the Yb^{3+} gain bandwidth. In addition, the lasers are capable of being mode-locked at harmonics of the cavity round-trip frequency, allowing tuning of the pulse repetition rate from 500 MHz to over 5 GHz. Typical average output powers range from 0.2 to 2 mW. Noise measurements on two independently mode-locked lasers revealed that the lasers are dominated by phase or timing jitter in the noise bandwidth of 5–10^5 Hz, while amplitude noise dominates at higher frequencies. Integration of the laser noise over the phase noise bandwidth yields absolute rms timing jitters of a few picoseconds. The absolute phase jitter of each optical source is dominated at low frequencies by the noise of the RF synthesizer, suggesting that the overall timing jitter of each laser could be improved by utilizing a low-noise RF source. Synchronization of two mode-locked lasers separated by a wavelength difference of 40 nm was achieved using a RF modulation technique, resulting in a relative timing jitter of 5 ps rms. Compression of the mode-locked laser pulses using a modified grating-pair configuration has produced pulse durations as low as 500 fs. The results obtained with the 1070 nm lasers represent the first experimental demonstration of short-pulse generation using electrically-pumped long-wavelength InGaAs-GaAs devices.

Semiconductor optical amplifiers consisting of narrow-stripe and flared-waveguide designs have been fabricated using the same material structure as the mode-locked oscillators. Narrow-stripe devices with a length of 800 μm have produced amplified average signal powers of 13 mW with excellent signal-to-ASE ratios. Pulse amplification with a 2°, 1700-μm-long flared-waveguide device has produced amplified average signal powers of 50 mW and ASE levels of around 10–20 % of the total SOA output. Small-signal gains for both SOA designs are in the region of 25–30 dB.

Fibre amplifiers consisting of a single-mode double-clad Yb-doped fibre have been constructed to investigate the feasibility of using a short-pulse semiconductor laser as a seed-source. Amplified average signal powers of up to 1.4 W have been obtained with very low ASE contamination (typically 1–3 %). Small-signal power gains are on the order of 40–50 dB. The development of the hybrid MOPA source consisting of a passively mode-locked diode laser and a Yb-doped fibre amplifier was one of the first reports on the performance characteristics of a Yb:fibre system seeded with a short-pulse semiconductor source.

Numerical simulations based on a cw rate-equation model for the amplifier gain were conducted to investigate the performance characteristics of a Yb:fibre amplifier when operated under dual-wavelength signal amplification. The simulations were used to predict and optimize the performance of the fibre amplifier for two mode-locked semiconductor-seed-oscillators operating at wavelengths of 1040 and 1079 nm. Experimental measurements on the dual-wavelength system were found to be in good agreement with the simulation results. Each signal was amplified to an average power of ~0.5 W, yielding a combined signal average power of ~1 W. The dual-wavelength system exhibited good performance over the 40 nm wavelength separation of the two oscillators and further simulations reveal that good performance should be possible for a wavelength difference of 60 nm, indicating that the system could be an attractive source of mid-infrared radiation at 19 μm based on difference frequency mixing. To the best of the author's knowledge, the results given in Paper 5 represent the first report on simulating the performance characteristics of a Yb:fibre amplifier when operated under dual-wavelength amplification. There has been a very recent report on the development of a dual-wavelength Q-switched Yb:fibre laser generating 100-ns-pulses at wavelengths of 1040 and 1070 nm [159]. Numerical simulations were used to study the Q-switching behavior of the dual-wavelength oscillator for fixed wavelengths of 1040 and 1070 nm.

The mode-locked semiconductor oscillators developed in this thesis have demonstrated good overall performance in terms of the relevant pulse properties. The design of the oscillator consisting of a curved-waveguide device with integrated gain and saturable absorber sections permits mode-locking in a simple, linear external cavity. In general, the oscillators are quite versatile, displaying good flexibility with respect to the ability to vary the properties of the generated pulses, such as the duration, wavelength, repetition frequency, and average power. However, one limitation of the mode-locked oscillators is the low pulse energy, which is typical of a pulsed semiconductor laser, and is a consequence of the low saturation energy of the gain medium. Therefore, from an application standpoint, it is necessary to combine post-amplification methods with most short-pulse semiconductor oscillators.

Of the amplifiers studied in this thesis, the performance of the Yb:fibre system is superior to that of the SOAs in almost all respects. The fibre amplifier can deliver much higher average power with lower ASE and excellent amplified beam quality. It is unlikely that the SOAs could be scaled to the level of average power that has been achieved with fibre-based systems, even with improved waveguide geometries. The SOAs should rather be regarded as effective pre-amplifiers. Depending on the application, it could be attractive to combine a mode-locked semiconductor-seed-oscillator with an SOA pre-amplifier, followed by a much higher gain fibre-based LMA power-amplifier. The SOA would be complimentary to using a fibre pre-amplifier, but without the added dispersion. Based on the present devices, the narrow-stripe SOAs would offer better performance in terms of minimizing the level of ASE that is injected into the power amplifier stage. However, there are a number of approaches to reduce the ASE level of a flared-SOA, as discussed in Section 4.3.2, and with an optimized waveguide geometry for the device, the flared SOAs would be better suited to seed a high-power LMA fibre amplifier. From the perspective of size, efficiency, and potential for integration, the SOAs are more attractive than fibre-based amplifiers. Indeed, the integration aspect of a semiconductor MOPA source is an interesting research topic in itself. Compact multi-watt cw diode laser systems have been developed by monolithically integrating a semiconductor master oscillator and flared amplifier into a single semiconductor chip [160]-[162]. Such an integration approach is not feasible, however, with a mode-locked master oscillator, unless an integrated optical isolator can be fabricated to prevent the back-travelling ASE from interfering with the recovery dynamics of the saturable absorber. Integrated optical isolator technology is currently insufficient for mode-locked lasers [163].

The present fibre-based laser system can provide amplified output average powers of 1.4 W, pulse energies of around 3 nJ, and peak powers of 500 W. Following pulse compression, peak powers of around 1.5 kW can be achieved. This level of peak power should be sufficient for a variety of nonlinear optical applications, including two-photon fluorescence microscopy [122]. Furthermore, there are a number of approaches to scale the power level of the system if warranted by an application. The achievable output power of the current system is limited by the magnitude of the pump laser. It is expected that the present system should maintain good overall performance up to several watts of output average power. Beyond this range, the system could be combined with a LMA power-amplifier, or a semiconductor pre-amplifier could be combined with a LMA fibre power-amplifier, to reach signal levels of tens to hundreds of watts of average power. Indeed, such multi-stage Yb-fibre systems have recently been demonstrated using a gain-switched semiconductor-seed-source [164] and a passively mode-locked VECSEL-seed-source [23]. The higher power levels afforded by a cascaded amplifier approach present a wider range of possibilities, including efficient nonlinear frequency conversion into the visible spectrum and materials processing applications. The generation of terahertz radiation was recently demonstrated using a novel compact optical source consisting of a multi-stage Yb:fibre system in combination with ns-pulsed diode-seed-lasers [165].

One final note concerning the development of hybrid MOPA sources based on mode-locked semiconductor oscillators and fibre amplifiers: mode-locked semiconductor lasers are inherently high-repetition-rate sources, whereas solid-state fibre amplifiers are more suited to the amplification of kHz repetition rate pulses. This is a direct consequence of the longer fluorescence lifetime of the doped fibre medium (~1 ms) compared to the semiconductor gain medium (~1 ns). From the perspective of optimizing the energy gain per pulse and therefore, pulse peak power, it would be advantageous for the oscillator to operate at lower repetition rates. Mode-locked semiconductor lasers typically operate at repetition rates above 100 MHz, owing to the short spontaneous emission lifetime, and it would therefore be necessary to reduce the pulse repetition rate using external methods. One approach reported on by Kim *et al.* involves sending the mode-locked pulses from the oscillator through a 'pulse picker' SOA that is electrically driven in synchronization with the optical pulse train [21]. A forward electrical bias provides gain for some pulses, while other pulses experience absorption due to the application of a reverse bias to the device, leading to a reduction in the effective repetition rate of the pulse train from 285 MHz to 95 MHz. Such an approach could be extended to achieve repetition rates in the tens of kHz regime. Alternatively, a gain-switched diode laser operating directly in the kHz regime might be attractive for some applications. However, gain-switched devices tend to generate pulses with much larger durations (several tens to hundreds of picoseconds) and higher timing jitter, making them less attractive when compared to mode-locked sources.

5.2 Future Work

Some topics of future research have already been alluded to in earlier chapters, but will be repeated here for completeness. There are a number of directions along which future work can proceed. Some of the suggested areas are an extension of the work already completed, while other areas represent a substantial new undertaking.

5.2.1 Mode-Locked Semiconductor Oscillators

Further improvements to the mode-locked wavelength tuning range could be achieved using an asymmetric quantum-well active region for the oscillator. For the incorporation of two or more wells, a strain compensation scheme would need to be introduced into the active region of the laser. As discussed in Section 2.2.3, strain compensation could be implemented using GaAsP barriers [64]. Extending the wavelength tuning range of the oscillator could also be attractive for enhancing the wavelength separation of the dual-wavelength system, which would allow for the generation of wavelengths in the 20 μm range using difference frequency generation in a nonlinear crystal. Alternatively, the active region of the oscillator could be tailored to produce mode-locked pulses at a slightly longer wavelength than that achieved with the current devices, allowing the two synchronized oscillators to be separated by a greater wavelength difference. This could be achieved using an active region containing a single quantum-well with a modified indium percentage [64]. Strain compensation may also be necessary depending on the required wavelength shift and indium content of the well material.

A more substantial research initiative could involve investigating mode-locked diode lasers containing quantum-dot active regions. There have been several recent reports on the performance characteristics of mode-locked quantum-dot lasers [43], [45], [46], [47]. One of the shortest pulses generated directly from a semiconductor laser was achieved using a mode-locked quantum dot laser. A pulse duration of 390 fs was obtained without any form of pulse compression using a passively mode-locked two-section quantum-dot laser operating at 1260 nm [45]. Compared to a quantum-well laser, a semiconductor quantum-dot laser is expected to deliver improved performance, such as reduced threshold current, lower temperature sensitivity, and a reduced linewidth enhancement factor [166], [167]. Of the proposed advantages, a reduction in the linewidth enhancement factor is probably the most promising and could allow for the generation of mode-locked pulses with significantly reduced chirp.

5.2.2 SOAs

Flared-SOAs with an improved waveguide geometry have been designed and the appropriate photolithographic masks have been developed. However, due to the advances made with the fibre-based amplifier system, devices based on the improved SOA design were never fabricated. Characterization of these devices thus represents an area of potential future work. Modifications to the flared SOA consist of an improved photolithographic mask for the oxide deposition, which should increase the maximum drive current, and separate biasing electrodes have been created for the narrow-stripe and flared regions. A schematic of the two-contact monolithic flared amplifier is shown in Figure 5-1. Independently biased narrow-stripe and flared regions will provide control over the gain of each section, allowing the pulse energy to build in the narrow-stripe section to a point where it can begin to saturate the gain of the flared section. Therefore, the narrow-

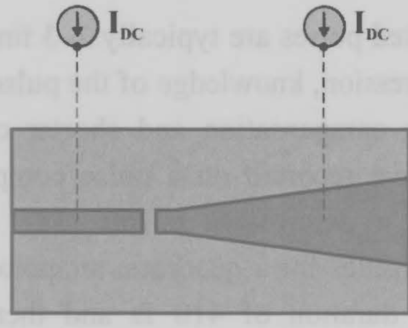

Figure 5-1: Schematic of a two-section monolithic SOA consisting of independently biased narrow-stripe and flared regions.

stripe region can be viewed as a pre-amplifier for the higher-gain flared section. The two-section SOA is expected to deliver higher output power with lower ASE, as compared to the present flared-SOAs. Experiments should be conducted to determine the level of performance that can be achieved using the two-section SOA and in particular, if it can function as an effective pre-amplifier for a LMA fibre power-amplifier. Similar experiments should also be conducted to assess the performance that can be achieved using a narrow-stripe pre-amplifier and a fibre power-amplifier.

5.2.3 Chirp Measurement and Compensation

One remaining characteristic of the mode-locked pulses that has yet to be accurately determined is the functional dependence of the pulse chirp. Accurate measurement of the pulse chirp would yield valuable information to assist with modeling endeavors and higher-order pulse compression. In this thesis, the large uncertainty in the chirp of the mode-locked pulses was one of the limiting factors in being able to predict the distortions to the pulse spectrum following various SPM processes. Approaches to measure the chirp or time-dependent phase of the pulse could include various frequency-resolved optical gating (FROG) techniques [109]. However, to have sufficient power to make a practical FROG measurement, pulses generated by the oscillator would probably require amplification, similar to the approach reported by Delfyett *et al.* [168], which would effectively result in a measurement of chirp of the amplified pulses. Another method of chirp measurement is based on a cross-correlation technique [67], but would require the synchronization of the mode-locked diode laser to an ultrafast laser emitting much shorter pulses than the diode system.

Since the mode-locked pulses are typically 2–3 times above the transform limit following pulse compression, knowledge of the pulse chirp could also allow for higher-order dispersion compensation and shorter compressed pulses. For example, Delfyett *et al.* have reported on a pulse compressor providing cubic phase compensation using a deformable mirror [18]. A standard diffraction grating compressor (compensates for a quadratic temporal phase) is first used to compress the pulses to a duration of 410 fs and then a cubic phase pulse compressor is used to provide higher-order dispersion compensation, resulting in a final pulse duration of 290 fs.

5.2.4 Parabolic-Pulse Amplification

An interesting regime of pulse propagation can be achieved in a Yb:fibre amplifier in which SPM is dominant. It has been shown that under the conditions of normal dispersion, nonlinearity (SPM), and gain, a propagating pulse will asymptotically evolve into a similariton, which is a pulse characterized by a parabolic intensity profile with a perfectly linear chirp [169]-[171]. Perhaps more interesting is that a similariton can be achieved regardless of the initial shape or width of the pulse [170], [171]. The initial parameters of the pulse only affect the propagation distance required to reach the similariton regime. Shorter pulses will typically converge faster to a similariton, for a given value of the input pulse energy [169]-[171]. Once the pulse has evolved into a similariton, it will continue to propagate along the fibre as a similariton but with spectral and temporal widths that increase exponentially with distance (to a limit) [171]. This regime of pulse propagation in a fibre amplifier is sometimes referred to in the literature as parabolic-pulse amplification. One of the attractive features of parabolic pulse-amplification is that as the pulse is amplified, the spectrum of the pulse broadens with an entirely linear chirp. Following amplification, the linear chirp can be efficiently removed using standard dispersion compensation techniques, allowing for very short and high-quality compressed pulses. This approach has been used to realize fibre amplified pulses with sub-100-fs pulse durations [99], [169].

Parabolic-pulse amplification would be interesting to investigate using the laser system developed in this thesis. A second stage of amplification would be required since very little SPM is generated in the current Yb:fibre amplifier. However, since certain applications may require that the system be scaled in power using a second stage of amplification, a parabolic-pulse approach could be adopted, which would be particularly attractive for converting the chirp of pulses to the more ideal linear chirp.

5.2.5 Dual-Wavelength Source

Preliminary work has been presented on the development of a dual-wavelength source. There are several areas of the system that could be improved and since most of the suggested improvements have already been discussed in earlier sections and particularly in Paper 5, they will only be briefly summarized here. Based on the numerical simulations, a single Yb:fibre amplifier should be able to support the amplification of two mode-locked semiconductor oscillators separated by about 60 nm. This would allow for the generation of mid-infrared radiation at ~19 μm. To achieve a 60 nm separation, a diode laser based on a modified active region would need to be designed and fabricated. The design approaches discussed previously in Section 5.2.1 would be sufficient. Following the improvements to the wavelength span of the system, difference frequency mixing using a configuration similar to that described in [172] should be attempted. This may require an improvement in the noise properties of the laser synchronization, using either a phase-locked loop or an optical synchronization approach, which would yield higher efficiencies for the difference frequency mixing. Finally, it could be interesting to extend the wavelength span of the dual-wavelength system by optically synchronizing the 1070 nm mode-locked laser to a mode-locked diode laser operating at a wavelength of 980 nm, which was previously developed in our research group [67]. Such an approach would allow for broader wavelength tunability of the system, which could be useful for potential two-colour pump-probe applications, and would provide access to a broader range of wavelengths in the mid-infrared, but would also require that two separate amplifiers be optimized for each oscillator wavelength.

5.3 Concluding Remarks

When I joined the ultrafast research group within the Department of Engineering Physics, a relatively new research initiative was underway to develop a broadly-tunable mode-locked semiconductor laser source. One of the intended applications of the laser was as an excitation source for two-photon fluorescence microscopy. The laser system at the time was based on a mode-locked diode oscillator and narrow-stripe SOA operating at a wavelength of 980 nm with maximum output average power and pulse energy of 15 mW and 20 pJ, respectively. Through refinements to the system, it was deemed necessary to shift the operating wavelength of the oscillator to take advantage of the recent advances in the development of Yb:fibre amplifiers. The present laser system, based on a long-wavelength InGaAs-GaAs mode-locked semiconductor oscillator and a Yb:fibre amplifier, can provide the level of peak power required for nonlinear optical applications, such as two-photon microscopy. Further optimization of the system combined with additional stages of amplification present a wider range of interesting possibilities, including efficient nonlinear frequency conversion and materials processing applications. The laser system also presents new perspectives in terms of the development of a mid-infrared radiation source based on mode-locked semiconductor oscillators. Continued development of mode-locked semiconductor laser systems will allow for more widespread use of these systems in many technological areas and will present new and interesting applications for ultrashort-pulse lasers.

Appendix A

Additional Research Contributions

Other Publications

H. E. Ruda, J. C. Polanyi, J. S. Y. Yang, Z. Wu, U. Philipose, T. Xu, S. Yang, K. L. Kavanagh, J. Q. Liu, L. Yang, Y. Wang, K. Robbie, J. Yang, K. Kaminska, D. G. Cooke, F. A. Hegmann, A. J. Budz, and H. K. Haugen, "Developing 1D nanostructure arrays for future nanophotonics", *Nanoscale Res. Lett.*, vol. 1, pp. 99-119, 2006.

Conference and Meeting Contributions

M. J. Brennan, J. N. Milgram, A. J. Budz, P. Mascher, and H. K. Haugen, "Generation and amplification of wavelength tunable short optical pulses from asymmetric quantum well semiconductor devices," *Conference on Lasers and Electro-Optics* (*CLEO*), Baltimore, USA, May 2003, paper CThM10.

M. J. Brennan, A. J. Budz, J. N. Milgram, P. Mascher, and H. K. Haugen, "Wavelength tunable ultra-short optical pulses from asymmetric quantum well semiconductor devices," *Canadian Association of Physicists* (*CAP*) *Annual Congress*, Charlottetown, Canada, June 2003, paper MO-POS-78.

M. J. Brennan, A. J. Budz, J. N. Milgram, P. Mascher, and H. K. Haugen, "Generation and amplification of wavelength tunable short optical pulses from asymmetric quantum well semiconductor devices," *Canadian Institute for Photonic Innovations* (*CIPI*) *Annual Meeting*, Edmonton, Canada, June 2003.

A. J. Budz, M. J. Brennan, and H. K. Haugen, "Generation and amplification of ultra-short optical pulses from a mode-locked long-wavelength (1075 nm – 1085 nm) InGaAs/GaAs quantum well laser," *Conference on Lasers and Electro-Optics* (*CLEO*), San Francisco, USA, May 2004, paper CTuP6.

A. J. Budz and H. K. Haugen, "Generation and amplification of ultra-short optical pulses from a mode-locked long-wavelength (1075 nm – 1085 nm) InGaAs/GaAs quantum well laser," *Canadian Institute for Photonic Innovations* (*CIPI*) *Annual Meeting*, Hamilton, Canada, May 2005.

A. J. Budz and H. K. Haugen, "Amplification of picosecond optical pulses at 1080 nm using an InGaAs/GaAs quantum well SOA," *Optical Amplifiers and their Applications* (*OAA*), Budapest, Hungary, August 2005, paper ME11.

A. J. Budz, A. S. Logan, D. Strickland, and H. K. Haugen, "Ultrashort pulse generation at 1075 nm with a mode-locked semiconductor laser and a ytterbium-doped fiber amplifier," *Conference on Lasers and Electro-Optics* (*CLEO*), Long Beach, USA, May 2006, paper JWB40.

A. J. Budz, A. S. Logan, D. Strickland, and H. K. Haugen, "Ultrashort pulse generation at 1075 nm with a mode-locked semiconductor laser and a ytterbium-doped fiber amplifier," *Canadian Institute for Photonic Innovations* (*CIPI*) *Annual Meeting*, Quebec City, Canada, June 2006.

A. J. Budz and H. K. Haugen, "Yb-fiber-amplification of harmonically mode-locked semiconductor-laser-pulses," *Canadian Institute for Photonic Innovations* (*CIPI*) *Annual Meeting*, Ottawa, Canada, May 2007.

J. Waisman, A. J. Budz, and H. K. Haugen, "Simulation of Yb-doped fiber amplification," *Canadian Institute for Photonic Innovations* (*CIPI*) *Annual Meeting*, Ottawa, Canada, May 2007.

J. Waisman, A. J. Budz, and H. K. Haugen, "Simulation of Yb-doped fiber amplification," *Photonics North*, Ottawa, Canada, June 2007.

A. J. Budz and H. K. Haugen, "Yb-fiber-amplification of harmonically mode-locked semiconductor-laser-pulses", *Conference on Lasers and Electro-Optics* (*CLEO*)-*Europe*, Munich, Germany, June 2007, paper CJ-8-TUE.

A. J. Budz, J. Waisman, and H. K. Haugen, "Short-pulse dual-wavelength system based on mode-locked diode lasers with a polarization-maintaining Yb:fiber amplifier," *Canadian Institute for Photonic Innovations* (*CIPI*) *Annual Meeting*, Banff, Canada, May 2008.

Appendix B

Processing of Semiconductor Devices

The semiconductor structures used in the mode-locked oscillators and semiconductor optical amplifiers were grown using gas-source MBE. A discussion on the growth of the semiconductor structures using MBE and an overview of the McMaster MBE system can be found in [57]. The structures were processed into ridge-waveguide devices using standard photolithography techniques in a cleanroom environment. Details on the specific processing steps have been previously described in [57]. A brief summary of the processing steps will be given below.

Wafer Cleaning

A standard UV ozone cleaning is followed by an oxide etch using buffered HF (BHF).

Ridge Definition

An etch-mask (1000 Å SiO_2) is deposited using plasma-enhanced chemical vapor deposition (PE-CVD). Positive photoresist is deposited on the wafer surface and using the appropriate photolithographic mask, the ridge-waveguides are defined in the photoresist. BHF is used to etch away portions of the SiO_2 to define the ridges in the SiO_2 etch-mask. Semiconductor etchants are then used to remove the top two semiconducting *p*-doped layers to create the ridges. The remaining photoresist and SiO_2 etch-mask are removed using acetone and BHF.

Deposition of Isolation Dielectric

An isolation dielectric (1000 Å SiO_2) is deposited using the PE-CVD system.

Via Formation

Photoresist is deposited on the wafer surface and a small stripe on top of each ridge is exposed in the photoresist using photolithography. After developing the exposed photoresist, the underlying oxide layer is removed using BHF. The small stripe in the oxide layer running on top of and along each ridge is known as the via: it is the region through which current is injected into the device. The remaining photoresist is removed.

Metallization Patterning
Photoresist is deposited and developed to form a metallization mask. Photoresist is removed over top of and along the length of each ridge, leaving behind sections of photoresist alongside each ridge.

Metallization *p*-Contact
An electron-beam evaporation system is used to deposit the *p*-contact metal layers consisting of titanium, platinum, and gold. After the contact deposition, the remaining sections of photoresist are removed using acetone, lifting away the overlying metallic contact layers on either side of each ridge. The ridges are now electrically isolated from each other.

Substrate Lapping
The substrate is thinned and polished to a thickness of approximately 120 μm.

Metallization *n*-Contact
The *n*-contact layer consisting of nickel, germanium, and gold is deposited using the electron beam evaporation system.

Annealing and Cleaving
Annealing at 400°C for 30 s, followed by cleaving of the sample into the desired cavity lengths.

Mounting of Devices for AR Deposition
The cleaved laser/SOA bars are mounted for AR deposition. A schematic of the mounting setup is shown in Figure B-1. Each bar is positioned such that the facet to be coated is facing up. To ensure that the AR dielectric is deposited only on the

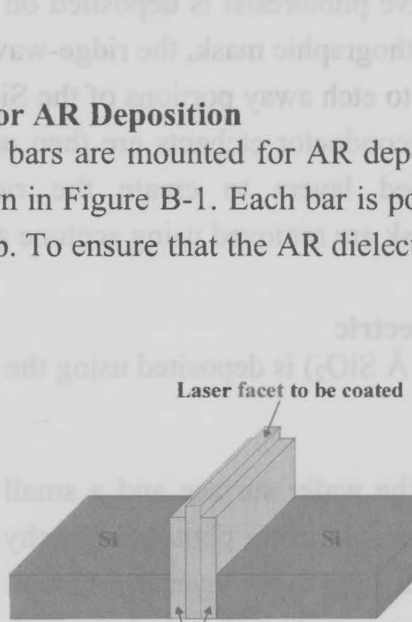

Figure B-1: Schematic of the mounting setup used for depositing an anti-reflection coating on the facet of a laser or SOA.

facet of each device and not on the *p*- or *n*-contact surfaces, the bars are sandwiched between sacrificial laser bars and pieces of silicon. The sacrificial bars are cleaved slightly shorter than the cavity length of the devices to be coated and the pieces of silicon are typically 300 μm thick.

Appendix C

Permission for Reproduction of Published Work

Papers 1, 3, and 4 were previously published in *IEEE Photonics Technology Letters* and Paper 2 was published in the *Journal of Lightwave Technology*. Paper 5 has been accepted for publication in the *Journal of Lightwave Technology*. The IEEE has granted me permission to reproduce these articles in my thesis. I hereby grant an irrevocable, nonexclusive licence to McMaster University and the National Library of Canada to reproduce the material as part of the thesis.

Permission from the IEEE

Dear Andrew Budz :

This is in response to your letter below, in which you have requested permission to reprint, in your upcoming thesis/dissertation, your described IEEE copyrighted material, we are happy to grant this permission.

In regards to distributing paper copies of your thesis or placing it on the university's website, please be sure that the following copyright/credit notice appears in the credits with the appropriate details filled in:

© [Year] IEEE. Reprinted, with permission, from (complete publication information).

Additionally, if your thesis is to appear on the university's website, the following message should be displayed at the beginning of the credits or in an appropriate and prominent place on the website:

This material is posted here with permission of the IEEE. Such permission of the IEEE does not in any way imply IEEE endorsement of any of the McMaster University's (or the National Library of Canada's) products or services. Internal or personal use of this material is permitted. However, permission to reprint/republish this material for advertising or promotional purposes or for creating new collective works for resale or redistribution must be obtained from the IEEE by writing to pubs-permissions@ieee.org.

By choosing to view this material, you agree to all

provisions of the copyright laws protecting it.
Please be advised that wherever a copyright notice from another organization is displayed beneath a figure, a photo, a videotape or a Powerpoint presentation, you must get permission from that organization, as IEEE would not be the copyright holder.

Sincerely,

Jacqueline Hansson
IEEE Intellectual Property Rights Coordinator
IEEE Intellectual Property Rights Office
445 Hoes Lane
Piscataway, NJ 08855-1331 USA
+1 732 562 3828 (phone)
+1 732 562 1746(fax)
e-mail: j.hansson@ieee.org

IEEE Fostering technological innovation
and excellence for the benefit of humanity.

----- Forwarded by William Hagen/PUBS/STAFF/US/IEEE on 10/14/2008 02:08 PM

From
"A.J. Budz"
<budzaj@univmail.cis.mcmaster.ca>
To
"w.hagen@ieee.org" <w.hagen@ieee.org>
cc

10/14/2008
12:27 PM Subject permission for reproduction of published work

Dear Sir/Madam,

I am completing a Ph.D. thesis at McMaster University entitled, "Ultrashort-Pulse Laser Systems Based on External-Cavity Mode-Locked InGaAs-GaAs Semiconductor Oscillators and Semiconductor or Yb:Fibre Amplifiers". I would like your permission to reprint the following journal articles in my thesis:

M. J. Brennan, A. J. Budz, B. J. Robinson, P. Mascher, and H. K. Haugen, "Ultrashort optical pulse generation with a mode-locked long-wavelength (1075-1085 nm) InGaAs-GaAs semiconductor laser," IEEE Photon. Technol. Lett., vol. 16, pp. 1798-1800, Aug. 2004.

A. J. Budz, A. S. Logan, D. Strickland, and H. K. Haugen, "Ultrashort pulses from a mode-locked diode-oscillator Yb-fiber-amplifier system," IEEE Photon. Technol. Lett., vol. 19, pp. 94-96, Jan. 2007.

A. J. Budz and H. K. Haugen, "Wavelength and repetition-rate tunable mode-locked semiconductor-seed-source for Yb-fiber-amplifier systems," IEEE Photon. Technol. Lett., vol. 19, pp. 1412-1414, Oct. 2007.

A. J. Budz and H. K. Haugen, "Ultrashort pulse amplification at 1080 nm with a long-wavelength InGaAs-GaAs flared amplifier," J. Lightwave Technol., vol. 25, pp. 3766-3769, Dec. 2007.

Also, the following manuscript which was submitted to J. Lightwave Technol., but has not yet been accepted:

A. J. Budz, J. Waisman, H. F. Tiedje, and H. K. Haugen, "Short-pulse dual-wavelength system based on mode-locked diode lasers with a single polarization-maintaining Yb:fiber amplifier," submitted to J. Lightwave Technol., July 2008.

Please note that I am a co-author of the above articles.

I am also requesting that you grant irrevocable, nonexclusive licence to McMaster University and to the National Library of Canada to reproduce this material as part of the thesis. Proper acknowledgement of your copyright of the reprinted material (including title, authors, date, and publisher) will be given in the thesis.

If these arrangements meet with your approval, please let me know.

Thank-you very much,

Andrew Budz
Department of Engineering Physics
McMaster University
Hamilton, ON
L8S 4L7 Canada
(905) 525-9140 x24324
budzaj@mcmaster.ca

References

[1] A. Lago, A. T. Obeidat, A. E. Kaplan, J. B. Khurgin, P. L. Shkolnikov, and M. D. Stern, "Two-photon-induced fluorescence of biological markers based on optical fibers," *Opt. Lett.*, vol. 20, pp. 2054-2056, 1995.

[2] J. Sytsma, J. M. Vroom, C. J. de Grauw, and H. C. Gerritsen, "Time-gated fluorescence lifetime imaging and microvolume spectroscopy using two-photon excitation," *J. Microscopy*, vol. 191, pp. 39-51, 1998.

[3] R. P. Haugland, *Handbook of fluorescent probes and research products*, Molecular Probes, 2002.

[4] J. Limpert, T. Clausnitzer, A. Liem, T. Schreiber, H.-J. Fuchs, H. Zellmer, E.-B. Kley, and A. Tünnermann, "High-average-power femtosecond fiber chirped-pulse amplification system," *Opt. Lett.*, vol. 28, pp. 1984-1986, 2003.

[5] P. Vasil'ev, *Ultrafast diode lasers*. Norwood, MA: Artech House Inc., 1995, pp. 95-149.

[6] P.-T. Ho, L. A. Glasser, E. P. Ippen, and H. A. Haus, "Picosecond pulse generation with a cw GaAlAs laser diode, " *Appl. Phys. Lett*, vol. 33, pp. 241-242, 1978.

[7] A. Olsson and C. L. Tang, "Active mode locking of linear and ring external-cavity semiconductor lasers," *IEEE J. Quantum. Electron.*, vol. 17, pp. 1977-1978, 1981.

[8] P. P. Vasil'ev, V. N. Morozov, and A. B. Sergeev, "Bandwidth-limited picosecond pulses from an injection GaAlAs DH laser with an external dispersive cavity," *IEEE J. Quantum. Electron.*, vol. 21, pp. 576-581, 1985.

[9] M. Hofmann, W. Weise, W. Elsäßer, and E. O. Göbel, "High spectral tuning range of a mode-locked InGaAs/InGaAsP MWQ laser diode due to light hole gain contribution," *IEEE Photon. Technol. Lett.*, vol. 6, pp. 1306-1308, 1994.

[10] E. P. Ippen, D. J. Eilenberger, and R. W. Dixon, "Picosecond pulse generation by passive mode locking of diode lasers, " *Appl. Phys. Lett*, vol. 37, pp. 267-269, 1980.

[11] Y. Silberberg, P. W. Smith, D. J. Eilenberger, D. A. B. Miller, A. C. Gossard and W. Wiegmann, "Passive mode locking of a semiconductor diode laser," *Optics Letters*, vol. 9, pp. 507-509, 1984.

[12] Y. K. Chen, M. C. Wu, T. Tanbun-Ek, R. A. Logan, and M. A. Chin, "Subpicosecond monolithic colliding-pulse mode-locked multiple quantum well lasers," *Appl. Phys. Lett*, vol. 58, pp. 1253-1255, 1991.

[13] P. B. Hanson , G. Raybon, U. Koren, P. P. Iannone, B. I. Miller, G. M. Young, M. A. Newkirk, and C. A. Burrus, "InGaAsP monolithic extended-cavity lasers with integrated saturable absorbers for active, passive, and hybrid mode locking at 8.4 GHz," *Appl. Phys. Lett*, vol. 62, pp. 1445-1447, 1993.

[14] D. Kunimatsu, S. Arahira, Y. Kato, and Y. Ogawa, "Passively mode-locked laser diodes with bandgap-wavelength detuned saturable absorbers," *IEEE Photon. Tech. Lett.*, vol. 11 pp. 1363-1365, 1999.

[15] S. Hoogland, A. Garnache, I. Sagnes, J. S. Roberts, and A. C. Tropper, "10-GHz train of sub-500-fs optical soliton-like pulses from a surface-emitting semiconductor laser," *IEEE Photon. Tech. Lett.*, vol. 17, pp. 267-269, 2005.

[16] G. Eisenstein, R. S Tucker, J. M. Wiesenfeld, P. B. Hansen, G. Raybon, B. C. Johnson, T. J. Bridges, F. G. Storz, and C. A. Burrus, "Gain recovery time of traveling-wave semiconductor optical amplifiers," *Appl. Phys. Lett.*, vol. 54, pp. 454-456, 1989.

[17] P. J. Delfyett, C.-H. Lee, G. A. Alphonse, and J. C. Connolly, "High peak power picosecond pulse generation from AlGaAs external cavity mode-locked semiconductor laser and traveling-wave amplifier," *Appl. Phys. Lett.*, vol. 57, pp. 971-973, 1990.

[18] P. J. Delfyett, L. T. Florez, N. Stoffel, T. Gmitter, N. C. Andreadakis, Y. Silberberg, J. P. Heritage, G. A. Alphonse, "High-power ultrafast laser diodes," *IEEE J. Quantum. Electron.*, vol. 28, pp. 2203-2219, 1992.

[19] A. Mar, R. Helkey, J. Bowers, D. Mehuys, and D. Welch, "Mode-locked operation of a master oscillator power amplifier," *IEEE Photon. Technol. Lett.*, vol. 6, pp. 1067-1069, 1994.

[20] Y. Xiong, S. Murphy, J. L. Carlsten, and K. Repasky, "Design and characteristics of a tapered amplifier diode system by seeding with continuous-wave and mode-locked external cavity diode laser," *Optical Engineering*, vol. 45, pp. 124205, 2006.

[21] K. Kim, S. Lee, and P. J. Delfyett, "1.4kW high peak power generation from an all semiconductor mode-locked master oscillator power amplifier system based on eXtreme Chirped Pulse Amplification (X-CPA)," *Opt. Express*, vol. 13, pp. 4600-4606, 2005.

[22] B. Adhimoolam, M. G. Hekelaar, P. Groß, I. D. Lindsay, and K.-J. Boller, "Wavelength-tunable short-pulse diode-laser fiber-amplifier system around 1.06 um," *IEEE Photon. Technol. Lett.*, vol. 18, pp. 838-840, 2006.

[23] P. Dupriez, C. Finot, A. Malinowski, J. K. Sahu, J. Nilsson, D. J. Richardson, K. G. Wilcox, H. D. Foreman, and A. C. Tropper, "High-power, high repetition rate picosecond and femtosecond sources based on Yb-doped fiber amplification of VECSELs," *Opt. Express*, vol. 14, pp. 9611-9616, Oct. 2006.

[24] D. J. Derickson, R. J. Helkey, A. Mar, J. R. Karin, J. G. Wasserbauer, J. E. Bowers, "Short Pulse Generation Using Multisegment Mode-Locked Semiconductor Lasers," *IEEE J. Quantum. Electron.*, vol. 28, pp. 2186-2201, 1992.

[25] E. A. Avrutin, J. H. Marsh, and E. L. Portnoi, "Monolithic and mulit-Gigahertz mode-locked semiconductor lasers: constructions, experiments, models, and applications," *IEE Proc. Optoelectron*, vol. 147, pp. 251-278, 2000.

[26] K. A. Williams, M. G. Thompson, and I. H. White, "Long-wavelength monolithic mode-locked diode lasers," *New J. Phys.*, vol. 6, pp. 179, 2004.

[27] P. Vasil'ev, *Ultrafast diode lasers*. Norwood, MA: Artech House Inc., 1995, pp. 53-149.

[28] G. J. Aspen, J. E. Carroll, and R. G. Plumb, "The effect of cavity length on picosecond pulse generation with highly RF modulated AlGaAs double heterostructure lasers," *Appl. Phys. Lett.*, vol. 39, pp. 860-861, 1981.

[29] R. A. Elliot, H. DeXiu, R.K. DeFreez, J. M. Hunt, and P. G. Rickman, "Picosecond optical pulse generation by impulse train current modulation of a semiconductor laser," *Appl. Phys. Lett.*, vol. 42, pp. 1012-1014, 1983.

[30] R. Nagarajan, T. Kamiya, A. Kasukawa, and H. Okamoto, "Observation of ultrashort (< 4 ps) gain-switched optical pulses from long-wavelength multiple quantum well lasers," *Appl. Phys. Lett.*, vol. 55, pp. 1273-1275, 1989.

[31] Y. Matsui, M. D. Pelusi, and A. Suzuki, "Generation of 20-fs optical pulses from a gain-switched laser diode by a four-stage soliton compression technique," *IEEE Photon. Tech. Lett.*, vol. 11, pp. 1217-1219, 1999.

[32] Y. Arakawa, A. Larsson, J. Paslaski and A. Yariv, "Active Q-switching in a GaAs/GaAlAs multiquantum well laser with an intracavity loss modulator," *Appl. Phys. Lett.*, vol. 48, pp. 561-563, 1986.

[33] B. J. Thedrez, S. E. Saddow, Y. Q. Liu, C. Wood, R. Wilson and C. H. Lee, "Experimental and theoretical investigation of large output power Q-switched AlGaAs semiconductor lasers," *IEEE Photon. Tech. Lett.*, vol. 5, pp. 19-22, 1993.

[34] D. R. Dykaar, K. Berthold, A. F. J. Levi, T. Tanbun-Ek and R. A. Logan, "Large-signal picosecond response of InGaAs/InP quantum well lasers with an intracavity loss modulator," *Appl. Phys. Lett.*, vol. 56, pp. 1629-1631, 1990.

[35] P. Vasil'ev, *Ultrafast diode lasers*. Norwood, MA: Artech House Inc., 1995, pp. 69.

[36] R. S. Tucker, U. Koren, G. Raybon, C. A. Burrus, B. I. Miller, T. L. Koch, and G. Eisenstein, "40 GHz active mode-locking in a 1.5 um monolithic extended-cavity laser," *Electron. Lett.*, vol. 25, pp. 621-622, 1989.

[37] G. Raybon, P. B. Hanson, U. Koren, B. I. Miller, M. G. Young, M. Newkirk, P. P. Iannone, C. A. Burrus, J. C. Centanni, and M. Zirngibl, "Two contact, 1 cm long, monolithic extended cavity laser actively mode-locked at 4.4 GHz," *Electron. Lett.*, vol. 28, pp. 2220-2221, 1992.

[38] S. W. Corzine, J. E. Bowers, G. Przybylek, U. Koren, B. I. Miller and C. E. Soccolich, "Actively mode-locked GaInAsP laser with subpicosecond output," *Appl. Phys. Lett.*, vol. 52, pp. 348-350, 1988.

[39] P. Vasil'ev, *Ultrafast diode lasers*. Norwood, MA: Artech House Inc., 1995, pp. 115-117.

[40] A. E. Siegman, *Lasers*. Mill Valey, CA: University Science Books, 1986, pp. 1109-1128.

[41] A. V. Uskov, J. R. Karin, R. Nagarajan, and J. E. Bowers, "Dynamics of carrier heating and sweepout in waveguide saturable absorbers," *IEEE J. Sel. Top. Quantum Electron.*, vol. 1, pp. 552-561, 1995.

[42] U. Keller, K. J. Weingarten, F. X. Kärtner, D. Kopf, B. Braun, I. D. Jung, R. Fluck, C. Hönninger, N. Matuschek, and J. Aus der Au, "Semiconductor saturable absorber mirrors (SESAMs) for femtosecond to nanosecond pulse generation in solid-state lasers," *IEEE J. Sel. Top. Quantum Electron.*, vol. 2, pp. 435-453, 1996.

[43] M. G. Thompson, A. Rae, R. L. Sellin, C. Marinelli, R. V. Penty, I. H. White, A. R. Kovosh, S. S. Mikhrin, D. A. Livshits, I. L. Krestnikov, "Subpicosecond high-power mode-locking using flared waveguide monolithic quantum-dot lasers," *Appl. Phys. Lett*, vol. 88, pp. 133119, 2006.

[44] J. P. van der Ziel, W. T. Tsang, R. A. Logan, R. M. Mikulyak, and W. M. Augustyniak, "Subpicosecond pulses from passively mode locked GaAs buried optical guide semiconductor lasers," *Appl. Phys. Lett*, vol. 39, pp. 525-527, 1981.

[45] E. U. Rafailov, M. A. Cataluna, W. Sibbett, N. D. Il'inskaya, Y. M. Zadiranov, A. E. Zhukov, V. M. Ustinov, D. A. Livshits, A. R. Kovsh, and N. N. Ledentsov, "High-power picosecond and femtosecond pulse generation from a two-section mode-locked quantum-dot laser," *Appl. Phys. Lett*, vol. 87, pp. 081107, 2005.

[46] M. Kuntz, G. Fiol, M. Lämmlin, D. Bimberg, M. G. Thompson, K. T. Tan, C. Marinelli, R. V. Penty, I. H. White, V. M. Ustinov, A. E. Zhukov, and Y. M. Shernyakov, "35 GHz mode-locking of 1.3 μm quantum dot lasers," *Appl. Phys. Lett*, vol. 85, pp. 843-845, 2004.

[47] M. T. Todaro, J-P. Tourrenc, S. P. Hegarty, C. Kelleher, B. Corbett, G. Huyet, and J. McInerney, "Simultaneous achievement of narrow pulse width and low pulse-to-pulse timing jitter in 1.3 μm passively mode-locked quantum-dot lasers," *Optics Letters*, vol. 31, pp. 3107-3109, 2006.

[48] A. E. Siegman, *Lasers*. Mill Valey, CA: University Science Books, 1986, pp. 1073-1074.

[49] S. Arahira, Y. Matsui, and Y. Ogawa, "Mode-locking at very high repetition rates more than terahertz in passively mode-locked distributed-bragg-reflector laser diodes," *IEEE J. Quantum. Electron.*, vol. 32, pp. 1211-1224, 1996.

[50] D. A. Yanson, M. W. Street, S. D. McDougall, I. G. Thayne, J. H. Marsh, and E. A. Avrutin, "Ultrafast harmonic mode-locking of monolithic compound-cavity laser diodes incorporating photonic bandgap reflectors," *IEEE J. Quantum. Electron.*, vol. 38, pp. 1-11, 2002.

[51] D. J. Derickson, P. A. Morton, J. E Bowers, and R. L Thornton, " Comparison of timing jitter in external and monolithic cavity mode-locked semiconductor lasers," *Appl. Phys. Lett*, vol. 59, pp. 3372-3374, 1991.

[52] P. J. Delfyett, C.-H. Lee, L. T. Florez, N. G. Stoffel, T. J. Gmitter, N. C. Andreadakis, G. A. Alphonse, J. C. Connolly, "Generation of subpicosecond high-power optical pulses from a hybrid mode-locked semiconductor laser," *Opt. Lett.*, vol. 15, pp. 1371-1373, 1990.

[53] J. Yu, M. Schell, M. Schulze, and D. Bimberg, "Generation of 290 fs pulses at 1.3 mm by hybrid mode-locking of a semiconductor laser and optimization of the time-bandwidth product," *Appl. Phys. Lett.*, vol. 65, pp. 2395-2397, 1994.

[54] A. Takada, K. Sato, M. Saruwatari, and M. Yamamoto, "Pulse width tunable subpicosecond pulse generation from an actively modelocked monolithic MQW laser/MQW electroabsorption modulator," *Electron. Lett.*, vol. 30, pp. 898-900, 1994.

[55] K. Yvind, D. Larsson, L. J. Christiansen, C. Angelo, L. K. Oxenløwe, J. Mørk, D. Birkedal, J. M. Hvam, and J. Hanberg, "Low-jitter and high-power 40-GHz all-active mode-locked lasers," *IEEE Photon. Tech. Lett.*, vol. 16 pp. 975-977, 2004.

[56] P. S. Zory Jr., *Quantum well lasers*, San Diego CA: Academic Press Inc., 1993.

[57] S. G. Wallace, "InGaAsP/GaAs quantum well lasers: material properties, laser design and fabrication, ultrashort-pulse external-cavity operation," Ph.D. thesis, McMaster University, 2000.

[58] S. Adachi, "Material Parameters of $In_{1-x}Ga_xAs_yP_{1-y}$ and related binaries," *J. Appl. Phys.*, vol. 53, pp. 8775-8792, 1982.

[59] J. W. Matthews and A. E. Blakeslee, "Defects in epitaxial multilayers I – misfit dislocations," *J. Cryst. Growth*, vol. 27, pp. 118-125, 1974.

[60] Y. Arakawa and A. Yariv, "Quantum well lasers-gain, spectra, dynamics," *IEEE J. Quantum. Electron.*, vol. 22, pp. 1887-1899, 1986.

[61] C-F. Lin, B-L. Lee and P-C. Lin, "Broad-band superluminescent diodes fabricated on a substrate with asymmetric dual quantum wells," *IEEE Photon. Tech. Lett.*, vol. 8, pp. 1456-1458, 1996.

[62] M. J. Hamp and D. T. Cassidy, "Critical design parameters for engineering broadly tunable asymmetric multiple-quantum-well lasers," *IEEE J. Quantum. Electron.*, vol. 36, pp. 978-983, 2000.

[63] S. C. Woodworth, D. T. Cassidy and M. J. Hamp, "Experimental analysis of a broadly tunable InGaAsP laser with compositionally varied quantum wells," *IEEE J. Quantum. Electron.*, vol. 39, pp. 426-430, 2003.

[64] F. Bugge, U. Zeimer, S. Gramlich, I. Rechenberg, J. Sebastian, G. Erbert and M. Weyers, "Effect of growth conditions and strain compensation on indium incorporation for diode lasers emitting above 1050 nm," *J. Cryst. Growth.*, vol. 221, pp. 496-502, 2000.

[65] P. Vasil'ev, *Ultrafast diode lasers*. Norwood, MA: Artech House Inc., 1995, pp. 98.

[66] M. Schell, A. G. Weber, E. Scholl, and D. Bimberg, "Fundamental limits of sub-ps pulse generation by active mode locking of semiconductor lasers: the spectral gain width and the facet reflectivities," *IEEE J. Quantum. Electron.*, vol. 27, pp. 1661-1668, 1991.

[67] M. J. Brennan, "Broadly tunable ultrashort pulse generation with mode-locked semiconductor lasers," Ph.D. thesis, McMaster University, 2004.

[68] J. Roscoe, "Development of InGaAsp/GaAs diode lasers for ultrashort pulse generation," M. Eng. thesis, McMaster University, 1999.

[69] P.-A. Besse, J.-S. Gu, and H. Melchior, "Relfectivity minimization of semiconductor laser amplifiers with coated and angled facets considering two-dimensional beam profiles," *IEEE J. Quantum. Electron.*, vol. 27, pp. 1830-1836, 1991.

[70] P. Sewell, M. Reed, T. M. Benson, P. C.Kendall, "Full vector analysis of two-dimensional angled and coated optical waveguide facets," *IEEE J. Quantum. Electron.*, vol. 33, pp. 2311-2318, 1997.

[71] Z. Wang, B. Mikkelsen, B. Pedersen, K. E. Stubkjaer, and D. S. Olesen, "Coupling between angled-facet amplifiers and tapered lens-ended fibers," *J. Lightwave Technol.*, vol. 9, pp. 49-55, 1991.

[72] A. J. Collar, G. D. Henshall, J. Farré, B. Mikkelsen, Z. Wang, L. Eskildsen, D. S. Olesen, and K. E. Stubkjaer, "Low residual reflectivity of angled-facet semiconductor laser amplifiers," *IEEE Photon. Tech. Lett.*, vol. 2, pp. 553-555, 1990.

[73] M. J. Brennan, J. N. Milgram, P. Mascher, and H. K. Haugen, "Wavelength tunable ultrashort pulse generation from a passively mode-locked asymmetric-quantum-well semiconductor laser," *Appl. Phys. Lett.*, vol. 81, pp. 2502-2504, 2002.

[74] M. Reed, T. M. Benso, P. C. Kendall, P. Sewell, "Antireflection-coated angled facet design," *IEE Proc.-Optoelectron.*, vol. 143, pp. 214-220, 1996.

[75] M. J. Connelly. *Semiconductor optical amplifiers*. New York, NY: Kluwer Academic Publishers, 2004.

[76] J. Mark and J. Mørk, "Subpicosecond gain dynamics in InGaAsp optical amplifiers: experiment and theory," *Appl. Phys. Lett.*, vol. 61, pp. 2281-2283, 1992.

[77] G. Eisenstein, P. B. Hansen, J. M. Wiesenfeld, R. S Tucker, and G. Raybon, "Amplification of high repetition rate picosecond pulses using an InGaAsP traveling-wave optical amplifier," *Appl. Phys. Lett.*, vol. 53, pp. 1539-1541, 1988.

[78] G. Eisenstein, U. Koren, G. Raybon, T. L. Koch, J. M. Wiesenfeld, M. Wegener, R. S Tucker, and B. I. Miller, "Large- and small-signal gain characteristics of 1.5 μm multiple quantum well optical amplifiers," *Appl. Phys. Lett.*, vol. 56, pp. 1201-1203, 1990.

[79] L. Zhang, I. Kang, A. Bhardwaj, N. Sauer, S. Cabot, J. Jaques, and D. T. Neilson, "Reduced recovery time semiconductor optical amplifier using p-type-doped multiple quantum wells," *IEEE Photon. Tech. Lett.*, vol. 18, pp. 2323-2325, 2006.

[80] A. E. Siegman, *Lasers*. Mill Valey, CA: University Science Books, 1986, pp. 362-375.

[81] C.-H. Lee and P. J. Delfyett, "Limits on amplification of picosecond pulses by using semiconductor laser traveling-wave amplifiers," *IEEE J. Quantum. Electron.*, vol. 27, pp. 1110-1114, 1991.

[82] N. A. Olsson and G. P. Agrawal, "Spectral shift and distortion due to self-phase modulation of picosecond pulses in 1.5 μm optical amplifiers," *Appl. Phys. Lett.*, vol. 55, pp. 13-15, 1989.

[83] C. H. Henry, "Theory of the linewidth of semiconductor lasers," *IEEE J. Quantum. Electron.*, vol. 18, pp. 259-264, 1982.

[84] G. P. Agrawal and N. A. Olsson, "Self-phase modulation and spectral broadening of optical pulses in asemiconductor laser amplifiers," *IEEE J. Quantum. Electron.*, vol. 25, pp. 2297-2306, 1989.

[85] J. M. Wiesenfeld, G. Eisenstein, R. S. Tucker, G. Raybon, and P. B. Hansen, "Distortionless picosecond pulse amplification and gain compression in a traveling-wave InGaAsP optical amplifier," *Appl. Phys. Lett.*, vol. 53, pp. 1239-1241, 1988.

[86] L. A. Coldren and S. W. Corzine, *Diode lasers and photonic integrated circuits*, New York, NY: John Wiley & Sons Inc., 1995, pg. 360.

[87] L. Goldberg, D. Mehuys, M. R. Surette, and D. C. Hall, "High-power, near-diffraction-limited large-area traveling-wave semiconductor amplifiers," *IEEE J. Quantum. Electron.*, vol. 29, pp. 2028-2043, 1993.

[88] G. Bendelli, K. Komori, and S. Arai, "Gain saturation and propagation characteristics of index-guided tapered-waveguide traveling-wave semiconductor laser amplifiers (TTW-SLA's)," *IEEE J. Quantum. Electron.*, vol. 28, pp. 447-458, 1992.

[89] H. Ghafouri-Shiraz, P. W. Tan, and T. Aruga, "Picosecond pulse amplification in tapered-waveguide laser-diode amplifiers," *IEEE J. Sel. Top. Quantum Electron.*, vol. 3, pp. 210-217, 1997.

[90] R. J. Lang, A. Hardy, R. Parke, D. Mehuys, S. O'Brien, J. Major, and D. Welch, "Numerical analysis of flared semiconductor laser amplifiers," *IEEE J. Quantum. Electron.*, vol. 29, pp. 2044-2051, 1993.

[91] S. Gee, G. Alphonse, J. Connolly, and P. J. Delfyett, "High-power mode-locked external cavity semiconductor laser using inverse bow-tie semiconductor optical amplifiers," *IEEE J. Sel. Top. Quantum Electron.*, vol. 4, pp. 209-215, 1998.

[92] J. E. Townsend, S. B. Poole, and D. N. Payne, "Solution-doping technique for fabrication of rare-earth-doped optical fibres," *Electron. Lett.*, vol. 23, pp. 329-331, 1987.

[93] G. P. Agrawal, *Nonlinear fiber optics*, San Diego, CA: Academic Press Inc., 1995, pp. 473.

[94] E. Desurvire, *Erbium-Doped Fiber Amplifiers: Principles and Applications*, New York: Wiely, 1994.

[95] D. B. S. Soh, S. Yoo, J. Nilsson, J. K. Sahu, K. Oh, S. Baek, Y. Jeong, C. Codemard, P. Dupriez, J. Kim, and V. Philippov, "Neodymium-doped cladding-pumped aluminosilicate fiber laser tunable in the 0.9-μm wavelength range," *IEEE J. Quantum. Electron.*, vol. 40, pp. 1275-1282, 2004.

[96] J. Nilsson, W. A. Clarkson, R. Selvas, J. K. Sahu, P. W. Turner, S.-U. Alam, and A. B. Grudinin, "High-power wavelength-tunable cladding-pumped rare-earth-doped silica fiber lasers," *Opt. Fiber Technol.*, vol. 10, pp. 5-30, 2004.

[97] R. Paschotta, J. Nilsson, A. C. Tropper, and D. C. Hanna, "Ytterbium-doped fiber amplifiers," *IEEE J. Quantum Electron.*, vol. 33, pp. 1049-1056, 1997.

[98] M. Eichhorn, "Numerical modeling of Tm-doped double-clad fluoride fiber amplifiers," *IEEE J. Quantum Electron.*, vol. 41, pp. 1574-1581, 2005.

[99] J. Limpert, F. Röser, T. Schreiber, and A. Tünnermann, "High-power ultrafast fiber laser systems," *IEEE J. Sel. Top. Quantum Electron.*, vol. 12, pp. 233-244, 2006.

[100] H. M. Pask, R. J. Carman, D. C. Hanna, A. C. Tropper, C. J. Mackechine, P. R. Barber, and J. M. Dawes, "Ytterbium-doped silica fiber lasers: versatile sources for the 1-1.2 μm region," *IEEE J. Sel. Top. Quantum Electron.*, vol. 1, pp. 2-13, 1995.

[101] L. Goldberg, J. P. Koplow, and D. A. Kliner, "Highly efficient 4-W Yb-doped fiber amplifier pumped by a broad-stripe laser diode," *Opt. Lett.*, vol. 24, pp. 673-675, 1999.

[102] X. Zou and H. Toratani, "Evaluation of spectroscopic properties of Yb^{3+} -doped glasses," *Phys. Rev. B*, vol. 52, pp. 15889-15897, 1995.

[103] J. Limpert, T. Schreiber, S. Nolte, H. Zellmer, A. Tünnermann, R. Iliew, F. Lederer, J. Broeng, G. Vienne, A. Petersson, and C. Jakobsen, "High-power air-clad large-mode-area photonic crystal fiber laser", *Opt. Express*, vol. 11, pp. 818-823, 2003.

[104] J. Limpert, A. Liem, M. Reich, T. Schreiber, S. Nolte, H. Zellmer, A. Tünnermann, J. Broeng, A. Petersson, and C. Jakobsen, "Low-nonlinearity single-transverse-mode ytterbium-doped photonic crystal fiber amplifier", *Opt. Express*, vol. 12, pp. 1313-1319, 2004.

[105] P. Laperle, C. Paré, H. Zheng, A. Croteau, and Y. Taillon, "Yb-doped LMA triple-clad fiber laser," *Proc. SPIE*, vol. 6343, 63430X, 2006.

[106] P. Laperle, C. Paré, H. Zheng, and A. Croteau, "Yb-doped LMA triple-clad fiber for power amplifiers," *Proc. SPIE*, vol. 6453, 645308, 2007.

[107] New Focus Catalogue, 2005.

[108] J.-C. Diels and W. Rudolph, *Ultrashort laser pulse phenomena*, San Diego, CA: Academic Press Inc., Chapter 8, 1996.

[109] R. Trebino, *Frequency-resolved optical gating: the measurement of ultrashort laser pulses*, Norwell, MA: Kluwer Academic Publishers, 2000.

[110] P. F. Curley, G. Darpentigny, G. Cheriaux, J. P. Chambaret, A. Antonetti, "High dynamic range autocorrelation studies of a femtosecond Ti:sapphire oscillator and its relevance to the optimization of chirped pulse amplification systems," *Opt. Comm.*, vol. 120, pp. 71-77, 1995.

[111] J. P. Curtis and J. E. Carroll, "Autocorrelation systems for the measurement of picosecond pulses from injection lasers," *Int. J. Electron.*, vol. 60, pp. 87-111, 1986.

[112] G. P. Agrawal, *Nonlinear fiber optics*, San Diego, CA: Academic Press Inc., 1995, pp. 64-67.

[113] O. E. Martinez, "3000 times grating compressor with positive group velocity dispersion: application to fiber compensation in 1.3-1.6 μm region," *IEEE J. Quantum Electron.*, vol. 23, pp. 59-64, 1987.

[114] G. P. Agrawal, "Effect of gain dispersion on ultrashort pulse amplification in semiconductor laser amplifiers," *IEEE J. Quantum Electron.*, vol. 27, pp. 1843-1849, 1991.

[115] D. B. Malins, A. Gomez-Iglesias, S. J. White, W. Sibbett, A. Miller, and E. U. Rafailov, "Ultrafast electroabsorption dynamics in an InAs quantum dot saturable absorber at 1.3 μm," *Appl. Phys. Lett.*, vol. 89, pp. 17111, 2006.

[116] J. N. Milgram, M. J. Brennan, H. F. Tiedje, and H. K. Haugen, "Picosecond pulses from mode-locked quantum well semiconductor lasers," *Opto-Canada: SPIE Regional Meeting on Optoelectronics, Photonics, and Imaging*, SPIE vol. TD01, pp. 21-23, 2002

[117] T. Saitoh, H. Itoh, Y. Noguchi, S. Sudo, and T. Mukai, "Pulse energy gain saturation in subpico- and picosecond pulse amplification by a traveling-wave semiconductor laser amplifier," *IEEE Photon. Tech. Lett.*, vol. 1, pp. 297-299, 1989.

[118] L. Goldberg, D. Mehuys, and D. Welch, "High power mode-locked compound laser using a tapered semiconductor amplifier," *IEEE Photon. Technol. Lett.*, vol. 6, pp. 1070-1072, 1994.

[119] G. P. Agrawal, *Nonlinear fiber optics*, San Diego, CA: Academic Press Inc., 1995.

[120] M. Schell, J. Yu, M. Tsuchiya, and T. Kamiya, "Chirp of passively and actively mode-locked semiconductor lasers," *Appl. Phys. Lett.*, vol. 67, pp. 1797-1799, 1995.

[121] M. J. Brennan, H. F. Tiedje, and H. K. Haugen, "Passively modelocked semiconductor laser synchronization and pulse cross-correlation with Ti:sapphire laser," *Electron. Lett.*, vol. 38, pp. 713-714, July 2002.

[122] A. S. Logan, "Investigation of the feasibility of mode-locked semiconductor devices as excitation sources for two-photon fluorescence," M.A.Sc. thesis, McMaster University, 2005.

[123] S. Sanders, A. Yariv, J. Paslaski, J. E. Ungar, and H. A. Zarem, "Passive mode locking of a two-section multiple quantum well laser at harmonics of the cavity round-trip frequency", *Appl. Phys. Lett.*, vol. 58, pp. 681-683, 1991.

[124] B. Ortaç, A. Hideur, G. Martel, and M. Brunel, "2-GHz passive harmonically mode-locked Yb-doped double-clad fiber laser," *Appl. Phys. B.*, vol. 81, pp. 507-509, 2005.

[125] X. Han, J. Wu, and H. Zeng, "Controllable harmonic mode locking and multiple pulsing in a Ti:sapphire laser," *Opt. Express*, vol. 16, pp. 3686-3692, 2008.

[126] T. Schrans, S. Sanders, and A. Yariv, "Broad-band wavelength tunable picosecond pulses from cw passively mode-locked two-section multiple quantum-well lasers," *IEEE Photon. Technol. Lett.*, vol. 4, pp. 323-326, 1992.

[127] D. von der Linde, "Characterization of the noise in continuously operating mode-locked lasers," *Appl. Phys. B.*, vol. 39, pp. 201-217, 1986.

[128] D. J. Derickson, A. Mar, and J. E. Bowers, "Residual and absolute timing jitter in actively mode-locked semiconductor lasers," *Electron. Lett.*, vol. 26, pp. 2026-2028, 1990.

[129] D. Eliyahu, R. A. Salvatore, and A. Yariv, "Effect of noise on the power spectrum of passively mode-locked lasers," *J. Opt. Soc. Am. B*, vol. 14, pp. 167-174, 1997.

[130] L. A. Jiang, M. E. Grein, H. A. Haus, E. P. Ippen, "Noise of mode-locked semiconductor lasers," *IEEE J. Sel. Top. Quantum Electron.*, vol. 7, pp. 159-167, 2001.

[131] Newport Catalogue, 2007.

[132] S. Sanders, T. Schrans, A. Yariv, J. Paslaski, J. E. Ungar, and H. A. Zarem, "Timing jitter and pulse energy fluctuations in a passively mode-locked two-section quantum-well laser coupled to an external cavity," *Appl. Phys. Lett.*, vol. 59, pp. 1275-1277, 1991.

[133] G. T. Harvey, M. S. Heutmaker, P. R. Smith, M. C. Nuss, U. Keller, and J. A. Valdmanis, "Timing jitter and pump-induced amplitude modulation in the colliding-pulse mode-locked (CPM) laser," *IEEE J. Quantum Electron.*, vol. 27, pp. 295-301, 1991.

[134] D. R. Hjelme and A. R. Mickelson, "Theory of timing jitter in actively mode-locked lasers," *IEEE J. Quantum Electron.*, vol. 28, pp. 1594-1606, 1992.

[135] F. Rana and R. Ram, "Noise and timing jitter in active and hybrid mode-locked semiconductor lasers," presented at the Conf. Lasers and Electro-Optics, 2001, paper CMB2.

[136] T. Yilmaz, C. M. Depriest, A. Braun, J. H. Abeles, and P. J. Delfyett, "Noise in fundamental and harmonic modelocked semiconductor lasers: experiments and simulations," *IEEE J. Quantum Electron.*, vol. 39, pp. 838-849, 2003.

[137] T. Yilmaz, C. M. DePriest, P. J. Delfyett, A. Braun, and J. Abeles, "Measurement of residual phase noise and longitudinal-mode linewidth in a hybridly mode-locked external cavity semiconductor laser," *Opt. Lett.*, vol. 27, pp. 872-874, 2002.

[138] C. M. DePriest, T. Yilmaz, P. J. Delfyett, S. Etemad, A. Braun, and A. J. Abeles, "Ultralow noise and supermode suppression in an actively mode-locked external-cavity semiconductor diode ring laser," *Opt. Lett.*, vol. 27, pp. 719-721, 2002.

[139] T. Yilmaz, C. M. DePriest, P. J. Delfyett, S. Etemad, A. Braun, and J. H. Abeles, "Supermode suppression to below -130 dBc/Hz in a 10 GHz harmonically mode-locked external sigma cavity semiconductor laser," *Opt. Express*, vol. 11, pp. 1090-1095, 2003.

[140] T. Yilmaz, C. M. DePriest, and P. J. Delfyett, "Complete noise characterization of external cavity semiconductor laser hybridly modelocked at 10 GHz," *Electron. Lett.*, vol. 37, pp. 1338-1339, 2001.

[141] F. Rana H. L. Lee, R. J. Ram, M. E. Grein, L. A. Jiang, E. P. Ippen, and H. H. Haus, "Characterization of the noise and correlations in harmonically mode-locked lasers," *J. Opt. Soc. Am. B*, vol. 19, pp. 2609-2621, 2002.

[142] D. Burns, A. Finch, W. Sleat, and W. Sibbett, "Noise characterization of a mode-locked InGaAsP Semiconductor diode laser," *IEEE J. Quantum Electron.*, vol. 26, pp. 1860-1863, 1990.

[143] F. Quinlan, S. Gee, S. Ozharar, and P. J. Delfyett, "Ultralow-jitter and –amplitude-noise semiconductor-based actively mode-locked laser," *Opt. Lett.*, vol. 31, pp. 2870-2872, 2006.

[144] J. B. Georges L. Buckman, D. Vassilovski, J. Park, M.-H. Kiang, O. Solgaard, and K. L. Lau, "Stable picosecond pulse generation at 46 GHz by modelocking of a semiconductor laser operating in an optoelectronic phaselocked loop," *Electron. Lett.*, vol. 30, pp. 69-71, 1994.

[145] D. J. Jones, K. W. Holman, M. Notcutt, J. Ye, J. Chandalia, L. A. Jiang, E. P. Ippen, and H. Yokoyama, "Ultralow-jitter, 1550-nm mode-locked semiconductor laser synchronized to a visible optical frequency standard," *Opt. Lett.*, vol. 28, pp. 813-815, 2003.

[146] S. Arahira and Y. Ogawa, "480-GHz subharmonic synchronous mode locking in a short-cavity colliding-pulse mode-locked laser diode," *IEEE Photon. Technol. Lett.*, vol. 14, pp. 537-539, 2002.

[147] Y. Wang and H. Po, "Dynamic characteristics of double-clad fiber amplifiers for high-power pulse amplification," *J. Lightwave Technol.,* vol. 21, pp. 2262-2270, 2003.

[148] M. Eichhorn, "Numerical modeling of Tm-doped double-clad fluoride fiber amplifiers," *IEEE J. Quantum Electron.*, vol. 41, pp. 1574-1581, 2005.

[149] J. Waisman, "Simulation of ytterbium doped fiber amplification," M.A. Sc. thesis, McMaster Univ., 2007.

[150] E. Yahel, O. Hess, and A. A. Hardy, "Ultrashort-pulse high-power Yb^{3+}-doped fiber amplifiers," *IEEE J. Quantum Electron.*, vol. 43, pp. 824-832, 2007.

[151] J. J. Koponen, M. J. Söderlund, H. J. Hoffman, and S. K. T. Tammela, "Measuring photodarkening from single-mode ytterbium doped silica fibers," *Opt. Express*, vol. 14, pp. 11539-11544, 2006.

[152] B. Morasse, S. Chatigny, É. Gagnon, C. Hovington, J.-P. Martin, and J.-P. de Sandro, "Low photodarkening single cladding ytterbium fibre amplifier," *Proc. SPIE*, vol. 6453, 64531E, 2007.

[153] S. Jetschke, S. Unger, U. Röpke, and J. Kirchhof, "Photodarkening in Yb doped fibers: experimental evidence of equilibrium states depending on the pump power," *Opt. Express*, vol. 15, pp. 14838-14843, 2007.

[154] I. Manek-Hönninger, J. Boullet, T. Cardinal, F. Guillen, S. Ermeneux, M. Podgorski, R. B. Doua, and F. Salin, "Photodarkening and photobleaching of an ytterbium-doped silica double-clad LMA fiber," *Opt. Express*, vol. 15, pp. 1606-1611, 2007.

[155] M. Engholm, L. Norin, and D. Åberg, "Strong UV absorption and visible luminescence in ytterbium-doped aluminosilicate glass under UV excitation," *Opt. Lett.*, vol. 32, pp. 3352-3354, 2007

[156] S. Yoo, C. Basu, A. J. Boyland, C. Sones, J. Nilsson, J. K. Sahu, and D. Payne, "Photodarkening in Yb-doped aluminosilicate fibers induced by 488 nm irradiation," *Opt. Lett.*, vol. 32, pp. 1626-1628, 2007

[157] M. Engholm and L. Norin, "Preventing photodarkening in ytterbium-doped high power fiber lasers; correlation to the UV-transparency of the core glass," *Opt. Express*, vol. 16, pp. 1260-1268, 2008.

[158] Y, W. Lee, S. Sinha, M. J. F. Digonnet, R. L. Byer, and S. Jiang, "Measurement of high photodarkening resistance in heavily Yb^{3+} -doped phosphate fibers," *Electron. Lett.*, vol. 44, pp. 14-16, 2008.

[159] L. Pan, I. Utkin, and R. Fedosejevs, "Two-wavelength passively Q-switched ytterbium doped fiber laser," *Opt. Express*, vol. 16, pp. 11858-11870, 2008.

[160] D. F. Welch, R. Parke, D. Mehuys, A. Hardy, R. Lang, S. O'Brien, and S. Scifres, "1.1 W cw, diffraction-limited operation of a monolithically integrated flared-amplifier master oscillator power amplifier," *Electron. Lett.*, vol. 28, pp. 2011-2013, 1992.

[161] S. O'Brien, D. F. Welch, R. A. Parke, D. Mehuys, K. Dzurko, R. Lang, R. Warrts, and S. Scifres, "Operating characteristics of a high-power monolithically integrated flared amplifier master oscillator power amplifier," *IEEE J. Quantum Electron.*, vol. 29, pp. 2052-2057, 1993.

[162] S. O'Brien, R. Lang, R. Parke, J. Major, D. F. Welch, and D. Mehuys, "2.2-W continuous-wave diffraction-limited monolithically integrated master oscillator power amplifier at 854 nm," *IEEE Photon. Technol. Lett.*, vol. 9, pp. 440-442, 1997.

[163] J. S. Yang, J. W. Roh, S. H. Ok, D. H. Woo, Y. T. Byun, W. Y. Lee, T. Mizumoto, and S. Lee, "An integrated optical waveguide isolator based on multimode interference by wafer direct bonding," *IEEE Trans. Magn.*, vol. 41, pp. 3520-3522, Oct. 2005.

[164] P. Dupriez, A. Piper, A. Malinowski, J. K. Sahu, M. Ibsen, B. C. Thomsen, Y. Jeong, L. M. B. Hickey, M. N. Zervas, J. Nilsson, and D. J. Richardson, "High average power, high repetition rate, picosecond pulsed fiber master oscillator power amplifier source seeded by a gain-switched laser diode at 1060 nm," *IEEE Photon. Technol. Lett.*, vol. 18, pp. 1013-1015, 2006.

[165] D. Creeden, J. C. McCarthy, P. A. Ketteridge, T. Southward, P. G. Schunemann, J. J. Komiak, W. Dove, and E. P. Chicklis, "Compact fiber-pumped terahertz source based on difference frequency mixing in ZGP," *IEEE J. Select. Topics Quantum Electron.*, vol. 13, pp. 732-737, 2007.

[166] D. Bimberg, "Quantum dots for lasers, amplifiers, and computing," *J. Phys. D: Appl. Phys.*, vol. 38, pp. 2055-2058, 2005.

[167] D. Bimberg, N. Kirstaedter, N. N. Ledentsov, Zh. I. Alferov, P. S. Kop'ev, and V. M. Ustinov, "InGaAs-GaAs quantum-dot lasers," *IEEE J. Select. Topics Quantum Electron.*, vol. 3, pp. 196-205, 2007.

[168] P. J. Delfyett, H. Shi, S. Gee, I. Nitta, J. C. Connolly, and G. A. Alphonse, "Joint time-frequency measurements of mode-locked semiconductor diode lasers and dynamics using frequency-resolved optical gating," *IEEE J. Quantum Electron.*, vol. 35, pp. 487-500, 1999.

[169] M. E. Fermann, V. I. Kruglov, B. C. Thomsen, J. M. Dudley, and J. D. Harvey, "self-similar propagation and amplification of parabolic pulses in optical fibres," *Phys. Rev. Lett.*, vol. 84, pp. 6010-6013, 2000.

[170] V. I. Kruglov, A. C. Peacock, J. D. Harvey, and J. M. Dudley, "Self-similar propagation of parabolic pulses in normal-dispersion fiber amplifiers," *J. Opt. Soc. Am. B*, vol. 19, pp. 461-469, 2002.

[171] C. Finot, F. Parmigiani, P. Petropoulos, and D. J. Richardson, "Parabolic pulse evolution in normally dispersive fiber amplifiers preceding the similariton formation regime," *Opt. Express*, vol. 14, pp. 3161-3170, 2006.

[172] R. Romero-Alvarez, R. Pettus, Z. Wu, and D. Strickland, "Two-color fiber amplifier for short-pulse, mid-infrared generation," *Opt. Lett.*, vol. 33, pp. 1065-1067, 2008.